REPUBLIQUE DU CAMEROUN
Paix-Travail-Patrie

UNIVERSITE DE YAOUNDE I
FACULTE DES SCIENCES

CENTRE DE RECHERCHE ET FORMATION DOCTORALE SCIENCES, TECHNOLOGIES ET GEOSCIENCES

REPUBLIC OF CAMEROON
Peace -Work-Fatherland

UNIVERSITY OF YAOUNDE I
FACULTY OF SCIENCE

POSTGRADUATE SCHOOL OF SCIENCES, TECHNOLOGY AND GEOSCIENCES

UNITE OF FORMATION AND PHD RESEARCH FOR GEOSCIENCES AND APPLICATIONS

UNITE DE FORMATION DE RECHERCHE DOCTORALE EN GEOSCIENCES ET APPLICATIONS

DEPARTMENT OF EARTH SCIENCES
DEPARTEMENT DES SCIENCES DE LA TERRE

LABORATORY OF SUPERFICIAL FORMATIONS AND APPLICATIONS
LABORATOIRE DE FORMATIONS SUPPERFICIELLES ET APPLICATIONS

UNRAVELLING THE DEEP-WATER TURBIDITE SYSTEMS ARCHITECTURE IN THE KRIBI-CAMPO SUB-BASIN, OFFSHORE CAMEROON: IMPLICATIONS ON HYDROCARBON PROSPECTIVITY

A THESIS SUMMITTED IN PARTIAL FULFILLMENT OF THE REQUIREMENTS FOR THE DEGREE OF DOCTOR OF PHILISOPHY IN EARTH SCIENCES

Option: Geosciences of Surface Processes and Applications

Specialty: Mining Geology and Petroleum Resources

By

SECKE BEKONGA GOUOTT Boris

Master in Geology

Registration number: **10X0350**

Co-supervised by

MBIDA YEM
Associate Professor
University of Yaoundé I

YENE ATANGANA Joseph Quentin
Professor
University of Yaoundé I

Academic year 2024-2025

RÉPUBLIQUE DU CAMERON
Paix – Travail – Patrie
.....
UNIVERSITÉ DE YAOUNDÉ I
.....
CENTRE DE RECHERCHE ET DE FORMATION DOCTORALE EN SCIENCES, TECHNOLOGIE ET GÉOSCIENCES
.....
BP : 812 Yaoundé
Email: crfd_stg@uy1.uninet.cm
secretariat@uy1reseachstg.cm
Site web: www.uy1researchstg.cm

REPUBLIC OF CAMEROON
Peace – Work –Fatherland
.....
THE UNIVERSITY OF YAOUNDE I
.....
POSTGRADUATE SCHOOL OF SCIENCES, TECHNOLOGY AND GEOSCIENCES
.....
P.O Box 812 Yaoundé
Email: crfd_stg@uy1.uninet.cm
secretariat@uy1reseachstg.cm
Web site: www.uy1researchstg.cm

ATTESTATION DE CORRECTION DE THÈSE DE DOCTORAT/Ph.D

****

Spécialité : **GEOSCIENCES DES FORMATIONS SUPERFICIELLES ET APPLICATIONS**

Option : **GEOLOGIE MINIERE ET RESSOURCES PETROLIERES**

Nom du candidat : **SECKE BEKONGA GOUOTT Boris**

Matricule : **10X0350**

Titre de la thèse : **UNRAVELLING THE DEEP-WATER TURBIDITE SYSTEMS ARCHITECTURE IN THE KRIBI-CAMPO SUB-BASIN, OFFSHORE CAMEROON: IMPLICATIONS ON HYDROCARBON PROSPECTIVITY**

Date de soutenance : **Mardi le 22 Avril 2025**

Nous, membres du jury après avoir lu le document qui nous a été présenté ce jour, attestons que le candidat a effectué toutes les corrections, conformément aux observations et suggestions formulées lors de la soutenance.

En foi de quoi, la présente **Attestation de correction**, lui est délivrée, pour servir et faire valoir ce que de droit. /

Fait à Yaoundé, le 19 JUIN 2025

Président

Examinateurs

Prof. Elias SAMANKASSOU

Nguetchoua Gabriel
Professeur

REPUBLIQUE DU CAMEROUN
Paix-Travail-Patrie

UNIVERSITE DE YAOUNDE I
FACULTE DES SCIENCES

CENTRE DE RECHERCHE ET FORMATION DOCTORALE SCIENCES, TECHNOLOGIES ET GEOSCIENCES

REPUBLIC OF CAMEROON
Peace -Work-Fatherland

UNIVERSITY OF YAOUNDE I
FACULTY OF SCIENCE

POSTGRADUATE SCHOOL OF SCIENCES, TECHNOLOGY AND GEOSCIENCES

UNITE OF FORMATION AND PHD RESEARCH FOR GEOSCIENCES AND APPLICATIONS

UNITE DE FORMATION DE RECHERCHE DOCTORALE EN GEOSCIENCES ET APPLICATIONS

DEPARTMENT OF EARTH SCIENCES
DEPARTEMENT DES SCIENCES DE LA TERRE

LABORATORY OF SUPERFICIAL FORMATIONS AND APPLICATIONS
LABORATOIRE DE FORMATIONS SUPPERFICIELLES ET APPLICATIONS

UNRAVELLING THE DEEP-WATER TURBIDITE SYSTEMS ARCHITECTURE IN THE KRIBI-CAMPO SUB-BASIN, OFFSHORE CAMEROON: IMPLICATIONS ON HYDROCARBON PROSPECTIVITY

A THESIS SUMMITTED IN PARTIAL FULFILLMENT OF THE REQUIREMENTS FOR THE DEGREE OF DOCTOR OF PHILISOPHY IN EARTH SCIENCES

Option: Geosciences of Surface Processes and Applications

Specialty: Mining Geology and Petroleum Resources

By

SECKE BEKONGA GOUOTT Boris

Master in Geology

Registration number: **10X0350**

Co-supervised by

MBIDA YEM
Associate Professor
University of Yaoundé I

YENE ATANGANA Joseph Quentin
Professor
University of Yaoundé I

Academic year 2024-2025

Dedication

TO

MY MOTHER

VICTORINE GOUOTT BEKONGA

MY FATHER

MARTIN DIVAE BEKONGA

MY BELOVED WIFE

MARIE DIANE TONYE SECKE AND

MY CHILDREN

OVIEREYA MICHELE SECKE

ELIAS RAPHAEL SECKE

Acknowledgements

To God be the glory and adoration for a successful completion of the thesis.

I would like to express my immense gratitude to my supervisors, Prof. Mbida Yem for accepting me for the PhD program. I am thankful to him not only for initiating me into research, but also for his corrections and advice during the course of this PhD work. Prof. Joseph Quentin Yene Atangana is greatly acknowledged for his supervision of my thesis, for always reviewing my manuscripts and for many discussions about future possibilities and research directions.

By agreeing to supervise a part of my thesis, Professor Elias Samankassou, at the University of Geneva, Switzerland has given this work a decisive direction. I would like to thank him for sharing his ideas with me, for the relevance of his remarks and for the discussions we had during the course of this work. Professor Elias Samankassou is also thanked for funding my trip to the EGU at Vienna in Austria, Swiss geosciences meeting at the University of Lausanne and Swiss Sedimentologist meeting at the University of Fribourg.

The Head of Department of Earth Sciences, of the Faculty of Science, University of Yaoundé I, Prof. Dieudonné Bisso, for his good management.

I give thanks to all academic staff of Department of Earth Sciences at the University of Yaoundé I Prs. Paul Désiré Ndjigui, Rose Yongue Fouateu, Ndam Ngoupayou, Charles Nkoumbou, Simon Ngos III, Monick Abossolo Angue, Jean-Pierre Tchouankoué, Vincent Laurent Onana, Emile Ekomane, Sylvestre Ganno, Marie Louise Ngo Bidjeck, Gabriel Nguetchoua and Cecile Mbesse for their academic and moral support.

I would like to express my gratitude to Dr. Joseph Victor Hell, General Manager of the Institute of Geological and Mining Researches (Cameroon) and Dr. Jean Paul Sep Nlomgan, Head of the Center of Geological and Mining Researches (Garoua, Cameroon) for giving me the opportunity to achieve this work.

My collaborators over the years: Dr. Ovie Emmanuel Eruteya**,** at the University of Geneva, Switzerland is acknowledged for the excellent collaboration. Without the help of Ovie in obtaining the Swiss Government Excellence PhD Fellowship at the University of Geneva, this work would not have been possible. I would like to thank him most sincerely for his guidance, his determination to see my thesis through, and his constant presence and encouragement during the difficult moments of my stay in Geneva. Most importantly, I am grateful to him for connecting me with many of his academic and industry contacts. I owe all the credit and success of this work to you, Ovie, and I know that you had to sacrifice many hours of your rest to help me. Thank you for helping me to finish the race. Dr. Yakufu Niyazi, Postdoc fellow at the University of Western Australia instructed me from year 2 and I thank him for his involvement and giving me great support, excellent guidance and advise for exciting topics such as channels, pockmarks and fluid flow. He offered me the greatest support and kindness whenever I was in need. He is as a brother, friend and educator.

I would like to acknowledge the Swiss Government Excellence for awarding him a scholarship ESKAS No. 2022.0697, at the University of Geneva for its support.

This work was carried out thanks to the support and collaboration of National Hydrocarbon Corporation of Cameroon (NHC-Yaoundé). I would particularly like to thank its Chief Executive Office Director, Mr Adolphe Moudiki, for granting me a year's academic training and, above all, for providing me with all the necessary logistical resources.

I would also like to thank Dr. Serge Edouard Angoua Biouele and Eric Nkoa, respectively Exploration Manager and Head Department of Geosciences NHC, for their comments and suggestions. Eric Nkoa is my first Petrel software trainer who was always on hand to help when any technical problem or interpretation questions arose.

Prof. Bineli Betsi at the Botswana International University of Science and Technology is acknowledged for his support and encouragement during my thesis.

I appreciate the support and understanding of my family during the PhD period. The moral, financial, and spiritual support of my parents Martin Divae Bekonga and Victorine Gouott Bekonga is greatly acknowledged. The remarkable and unquantifiable emotional, moral support of my wife Marie Diane is appreciated. Oviereya Michele and Elias Raphael are commendable for their patience and understanding during the PhD. I love you all. To the rest of my family (Armand, Yves, Zoher, Arielle, Henri, Diane, Obiege), I am very grateful for your prayers and support. Thank you very much.

Finally, I am very thankful to all my friends who have always been close and supportive, sponsoring with ideas, consoling me during bad times; to those who direct and indirectly have blessed me during the course of this work, Adrien, Eric, Arnold, Charles, Ibrahim, Ferdinand, William, Claudine, Michel, Armel, Raphael, Consantin, Magloire, Thierry.

To all my friends in Geneva: Thierry, Perince, Achille, Réné, Bintou, Patrick; to the "flatmates": Claire, Delphine, thank you for the discussions, for the moments of sharing, for the support. All those who in the course of this research helped me in one way or the other and whose names are not mentioned in this thesis, in Cameroon or abroad, for their moral and financial support. I express my sincere gratitude.

Abstract

In this study, analyses of a high-resolution, three-dimensional seismic reflection dataset and well-log data were combined to describe stratigraphic architecture, morphological evolution of turbidite systems and evaluate their reservoirs potentials in the deep-water of Kribi-Campo sub-basin. The results revealed a submarine channel system and submarine fans with good quality reservoirs that developed during the Late Cretaceous. The submarine channel system consisting of an early and a late-stage channel. Morphologically, the submarine channel system has a NE-SW trend and is U-shaped in cross-section with a length of 56 km within the study area. The early-stage channel has a relatively straight morphology and varies in width and depth from 3 to 5 km and 89–197 m, respectively. However, the late stage of the channel is characterized by a narrower (1–3 km) and shallower (41–103 m) incision, with sinuous morphology carved into the early channel infill. The submarine fan is characterized by a high amplitude seismic facies exhibiting a stacked pattern with parallel and continuous reflectors. The stacked fan-shaped morphology is up to 500 m thick, extends over an area of 600 km^2 and oriented NE-SW, near the Kribi High. Analysis of the fan architecture reveals the presence of well-defined internal structures such as overbank, a sinuous distributary channel and an elongated depositional lobe whose beds are made up of sand, silt and mud. The changing interaction of differential local tectonic, relative sea level, source sediment supply and change in slope gradient are the major control on the geometry and internal characteristics of the submarine channel system and submarine fans. Six potential reservoir intervals with thickness ranging between 27 and 105.7 m were delineated from analysis of well logs within turbidite systems. Lithological analysis of these reservoir intervals indicates a heterogeneous reservoir matrix comprising sand, limestone, and dolomite. These major reservoir encountered have porosity ranging from 15.5 to 21.3%, permeability ranging between 5.65 and 75.09 md and a water saturation of 34.5 to 74.2%, while hydrocarbon saturation is between 65.5 and 25.8%. As a result, the reservoirs have good porosity, low to moderate hydrocarbon saturation and, overall, good reservoir quality. However, both wells were water-bearing with non-mobile hydrocarbon residuals and did not contain commercial quantities of hydrocarbons. The results from this study is crucial information for successful hydrocarbon exploration in deep-water environments.

Keywords: *Seismic geomorphology, Submarine channel, Submarine fans, Petrophysical properties, Kribi-Campo sub-basin.*

Résumé

Dans cette étude l'analyse des données de sismique réflexion 3D et de diagraphies de puits ont été combiné pour décrire l'architecture stratigraphique, l'évolution morphologique des systèmes de turbidites et évaluer leurs potentiels réservoirs en eaux profondes dans le sous-bassin de Kribi-Campo. Les résultats ont révélé l'existence d'un système de chenaux sous-marins et une série d'éventails sous-marins qui se sont développés au cours du Crétacé supérieur. Le système de chenaux sous-marins se compose de deux stades de chenaux. D'un point de vue morphologique, le système de chenaux sous-marin a une orientation NE-SW et une section en forme de U, d'une longueur de 56 km dans la zone d'étude. Le premier stade de chenal présente une morphologie relativement rectiligne et varie en largeur et en profondeur de 3 à 5 km et de 89 à 197 m, respectivement. Cependant, le second stade du chenal est caractérisé par une incision plus étroite (1-3 km) et moins profonde (41-103 m), avec une morphologie sinueuse creusée dans le remplissage du premier chenal. L'éventail sous-marin est caractérisé par un faciès sismique de grande amplitude présentant un motif empilé avec des réflecteurs parallèles et continus. La morphologie empilée de l'éventail a une épaisseur allant jusqu'à 500 m, s'étend sur une superficie de 600 km^2 et est orientée NE-SW, près du Horst de Kribi. L'analyse de l'architecture stratigraphique de l'éventail révèle la présence de structures internes bien définies, telles que des berges, un chenal de distribution sinueux et un lobe de dépôt allongé dont les lits sont constitués de sable, limons et boue. L'interaction changeante de la tectonique locale, le niveau relatif de la mer, l'apport de sédiments et le changement de gradient de pente sont les principaux facteurs de contrôle de la géométrie et des caractéristiques internes du système de chenaux et de l'éventail sous-marin. Six intervalles potentiels de réservoirs d'une épaisseur comprise entre 27 et 105,7 m ont été délimités à partir de l'analyse des diagraphies de puits dans les systèmes de turbidites. L'analyse lithologique de ces réservoirs indique une matrice de réservoir hétérogène comprenant du sable, du calcaire et de la dolomie. Ces principaux réservoirs ont une porosité comprise entre 15,5 et 21,3 %, une perméabilité comprise entre 5,65 et 75,09 mD et une saturation en eau comprise entre 34,5 et 74,2 %, tandis que la saturation en hydrocarbures est comprise entre 65,5 et 25,8 %. Par conséquent, les réservoirs présentent une bonne porosité, une saturation en hydrocarbures faible à modérée et dans l'ensemble, une bonne qualité de réservoir. Cependant, les puits sont remplis d'eau avec des résidus d'hydrocarbures non mobiles et ne contiennent pas de quantités commerciales d'hydrocarbures. Les résultats de cette étude constituent des informations cruciales pour la réussite de l'exploration des hydrocarbures dans les eaux profondes.

Mots-clés : *Géomorphologie sismique, Chenal sous-marin, Eventail sous-marin, Propriétés pétrophysiques, Kribi-Campo sous-bassin.*

Table of contents

List of Figures

List of Tables

List of abbreviations

API: American Petroleum Institute
AVO: amplitude versus offset
BVW: Bulk Water Volume
CCS: Carbon Capture and Storage
CGG: General Company of Geophysics
CM-1: Campo Marine 1
CMP: Common Midpoint
CVLs: Continuous velocity logs
DMO: Dip-Moveout
DT: Sonic
ECL: Exploration Consultants Limited
GR: Gamma Ray
HFK: Potassium
HTHO: Thorium
IP: Interactive Petrophysics
K: Permeability
KC: Kribi-Campo
KFZ: Kribi Fracture Zone
MD: Major depth
MTDs: Mass-transport deposits
MWD: Measured while drilling
NHC: National Hydrocarbon Corporation
NMO: Normal Moveout
NPHI: Neutron porosity
NTG: Net to gross
PSDM: Pre-stack depth migration
PSTM: Pre-stack time migrated
RHOB: Bulk density
RMS: Root Mean Square
SEG: Society of Exploration Geophysicists
SF: Seismic facies
SNR: Signal-to-noise ratios
SPT: Simon Petroleum Technology
SU: Seismic unit
Sw: water saturation
TD: Total Depth
TWT: Two-way travel time
Vsh: Volume of shale
WL: Wireline

Introduction

Research Context

Deep-water turbidite systems are important submarine features formed by the erosion, diversion, and deposition of turbidity currents and other sediment loads and flows (Shepard, 1981; Peakall and Sumner, 2015; Chiang et al., 2020; Tek et al., 2021). Submarine channels are a vital component of ancient and modern deep-water settings and play an essential role in transporting sediments into the deep sea (Stow and Mayall, 2000; Normark and Carlson, 2003; Posamentier and Kolla, 2003; Mayall et al., 2006; Posamentier and Walker, 2006; Shanmugam, 2006; Gamboa et al., 2012; Chima et al., 2019). Deep-water sediments within these channels record paleoclimatic and oceanographic information and are crucial in understanding the geological evolution of sedimentary basins (Marsset et al., 2009; Jobe et al., 2015; Picot et al., 2016; Hansen et al., 2017; Niyazi et al., 2018; Chima et al., 2020). Deep-water sediments transported by submarine channels are a potential host for significant hydrocarbon accumulations (Mayall et al., 2006; Wynn et al., 2007; Di Celma et al., 2010; Jobe et al., 2015).

Previous studies have focused on the origin, depositional processes and factors controlling the emplacement, composition, and morphological evolution of submarine channels (Kane et al., 2008; Babonneau et al., 2010; Covault et al., 2014; Li and Gong, 2016; Sylvester and Covault, 2016; Li et al., 2020). Also, the increased availability of marine geophysical data has significantly improved the understanding of the architecture, morphometry and processes leading to submarine channel development (Abreu et al., 2003; Deptuck et al., 2003, 2007; Kolla et al., 2007; Sylvester et al., 2011; Mitchell et al., 2021). High-resolution 3D seismic reflection data has been used in many studies to investigate the geomorphologic character of deep-water systems, and their implication for hydrocarbon exploration in the offshore settings (Deptuck et al., 2007; McHargue et al., 2011; Jobe et al., 2011; Qin et al., 2016; Covault et al., 2019; Mitchell et al., 2021).

Turbidites systems in the deep offshore West Africa (e.g., Niger Delta, Congo, and Gabon) are well studied using high-quality seismic reflection and borehole datasets provided by hydrocarbon exploration companies operating in these regions (Abreu et al., 2003; Le et al., 2014; Jolly et al., 2015; Huang, 2018; Chima et al., 2019, 2020; Chen et al., 2021). These turbidite systems include channel levee systems, terraces, intraslope fans and lobes, and are important for hydrocarbon exploration. Submarine channel systems form major repositories for coarse-grained sediment (reservoirs) deposited along channel axes and for fine-grained sands and silts deposited on levees (seals/traps). These are the primary targets of interest during hydrocarbon exploration (Mayall et al., 2006). In addition, hydrocarbon reservoirs (e.g.,

Okume, Oveng, Ebano and Ceiba oil fields) in similar geological settings within the offshore West African Basins, have been found in the Santonian-Maastrichtian turbidite sediments in offshore of Equatorial Guinea (Dailly et al., 2002; Sterling, 2010). Along the Cameroonian margin, various Miocene channels, and fan systems across the Douala/Kribi-Campo Basin are also proven to be hydrocarbon-rich (SPT/Simon Petroleum and Technology, 1995; Loule et al., 2018).

Many submarine channels and fans occur in the Late Cretaceous and Tertiary in the Kribi-Campo sub-basin (Le, 2012, 2021; Loule et al., 2018). During the Late Cretaceous in the study area, there are relatively low sinuosity channel systems and several distinctive large compound channel systems (Loule et al., 2018). These compound geobodies formed from the superposition of separate channel-fill phases having individual channels which have similar widths to the low sinuosity channels (1000–1500 m). These two types of channels are controlled by the local tectonics (Loule et al., 2018). Also, in the Early Pliocene, deep-water channels occurring in the study area are characterized by high amplitude reflections with bi-directional downlap on the base of the Pliocene (Le, 2021). These Pliocene channels flowed from east to west in the High Gradient Slope (HGS). The occurrence of striated unconformity at the base of the Pliocene sequence, overlain by the channels suggests a period of slope failure and high sedimentation rate which is possibly the result of a major tectonic uplift event or significant climatic changes (Le, 2021).

The Kribi/Campo sub-basin hosts the South Sanaga and Kribi oil fields in deep-water turbidite sediments (Pauken et al., 1991; Pauken, 1992; Nguene et al., 1992; Ackerman et al., 1993; Tamfu et al., 1995; Brownfield and Charpentier, 2006; Ndonwie Mahbou, 2007). In contrast to the well-studied submarine channels, fans and their implications for hydrocarbon exploration in the West African basins (e.g., Niger Delta, Congo, and Gabon), those in the Kribi/Campo sub-basin are poorly understood in terms of their architectural elements, morphological variations and factors controlling the distribution of turbidity sands (see Iboum Kissaaka et al., 2016; Loule et al., 2018; Yugye et al., 2021).

Research Aims and Objectives

The overarching goal of this research is to investigate the architectural and morphological evolution of deep-water turbidite systems (channels and fans) in the Kribi-Campo sub-basin and its implication for deep-water hydrocarbon prospectivity. Alongside evaluating the reservoir potential within these turbidite systems. The Kribi-Campo sub-basin is well suited for this research as evidence of turbidite systems is documented. Importantly,

features are well-imaged in the high-resolution subsurface geophysical dataset available from this basin.

The aims of the research were achieved by answering the following research questions:

- What are the geometries and spatio-temporal distribution of the turbidites systems in the study area?
- What are the factors that control the sedimentation of turbidite systems?
- What are the depositional architectural characteristics of the reservoirs encountered? channel sands vs submarine fans? And how do they control or influence the reservoir quality in terms of petrophysical properties?
- What are the implications of the evolution and spatiotemporal distribution of the depositional elements on deep-water hydrocarbon prospectivity in the study area?

Research Objectives

- Describe seismic stratigraphic architecture of the Late Cretaceous succession;
- Describe and analyze the geometry and internal configuration of a newly mapped well-developed Late Cretaceous submarine channel system in the study area;
- Access the fan internal architecture, lobe stacking pattern, and channel morphology of the Late Cretaceous (Campanian) in the study area;
- Provide a detailed petrophysical analysis of the reservoir intervals within systems (channels and fans) in the study area;
- Develop a conceptual model reconstructing turbidites systems in the Late Cretaceous succession;
- Understand the implication of the submarine fans and channels on deep-water hydrocarbon exploration and production.

All these objectives have been addressed in the following four chapters (from Chapter 4 to Chapter 6) by using an integrated workflow to interpret the available 3D seismic dataset and borehole data provided by the National Hydrocarbon Company (NHC) Cameroon.

Thesis outline

This thesis is presented in an alternative format consisting of seven chapters.

Chapter One presents the background of the research, focusing on the synthesis of work on deep-water processes and depositional environment.

Chapter Two presents the geological settings of the Kribi-campo sub-Basin. It highlights the location, tectonostratigraphic evolution and Petroleum system of the study area.

Chapter Three presents the subsurface geophysical datasets analysed, as well as methodological workflow adopted to achieve the objectives of the thesis.

Chapters Four to Six consists of papers based on findings from the research. Chapter four and five have been already published and chapter six has been submitted for publication.

Chapter Seven is a discussion of the factors controlling the submarine channels, and fans and provides the conceptual model of these turbidite systems. It also focus on the reservoir quality within turbidite systems.

Chapter 1: Literature Review

This chapter explores key aspects of sedimentation in marine environments, with a particular emphasis on the processes governing exchanges between deep and shallow marine settings, as well as the concept of stratigraphic architecture within turbidite systems.

1.1. Deepwater processes

1.1.1. Turbidity flows

Turbidites are sediments formed as a result of turbidity currents and by density flows. Turbidity currents are sediment gravity flows in which particles are mainly suspended by fluid turbulence (Fig. 1) (Kneller and Buckee, 2000). These sediment gravity flows can be generated by different mechanisms, such as failures on the 30 shelf and slope, or river flood (i.e. hyperpycnal flows) (e.g., Piper et al., 1988; Piper and Savoye, 1993). Turbidity currents can be classified as low- and high-density types based on the near-bed sediment concentration (Fig. 1). Low-density turbidity currents are characterised by fully turbulent near-bed conditions with low sediment concentration, associated with relatively low sediment fallout rates and the development of traction structures such as ripple cross-lamination and planar lamination (Fig. 1) (Mulder and Alexander, 2001; Talling et al., 2012). In comparison, turbidities deposited from high-density flows (from high sediments concentrations) typically form thick-bedded successions containing medium to coarse-grained sands, while turbidities resulting from low sediments concentrations are made up of largely clay, silt and fine to medium-grained sand-size particles that are supported in suspension entirely by turbulence mentioned by (Boggs, 2006).

1.1.2. Debris flows

Debris flows are sediment gravity flows in which particles are predominantly supported by the matrix strength (Iverson, 1997; Talling et al., 2012). Debris flow deposits form many of the same features of that turbidite sands express and also form in mass by abrupt freezing (Talling et al., 2012). Debris are therefore, usually ungraded, structureless, and poorly sorted because of the absence of grain segregation during deposition (Talling et al., 2012). These range from low-sinuosity channel fills, narrow elongate lobes, and sheets and are characterized seismically by contorted, chaotic, low-amplitude reflection patterns (Posamentier & Kola, 2003). Where the flows are unconfined, divergent striation patterns probably reflect the flow direction and behavior. Debris flow can extend at least as far basin ward as turbidites, and individual debris-flow units can reach 80 m thick and commonly are marked by steep edges (Posamentier & Kola, 2003).

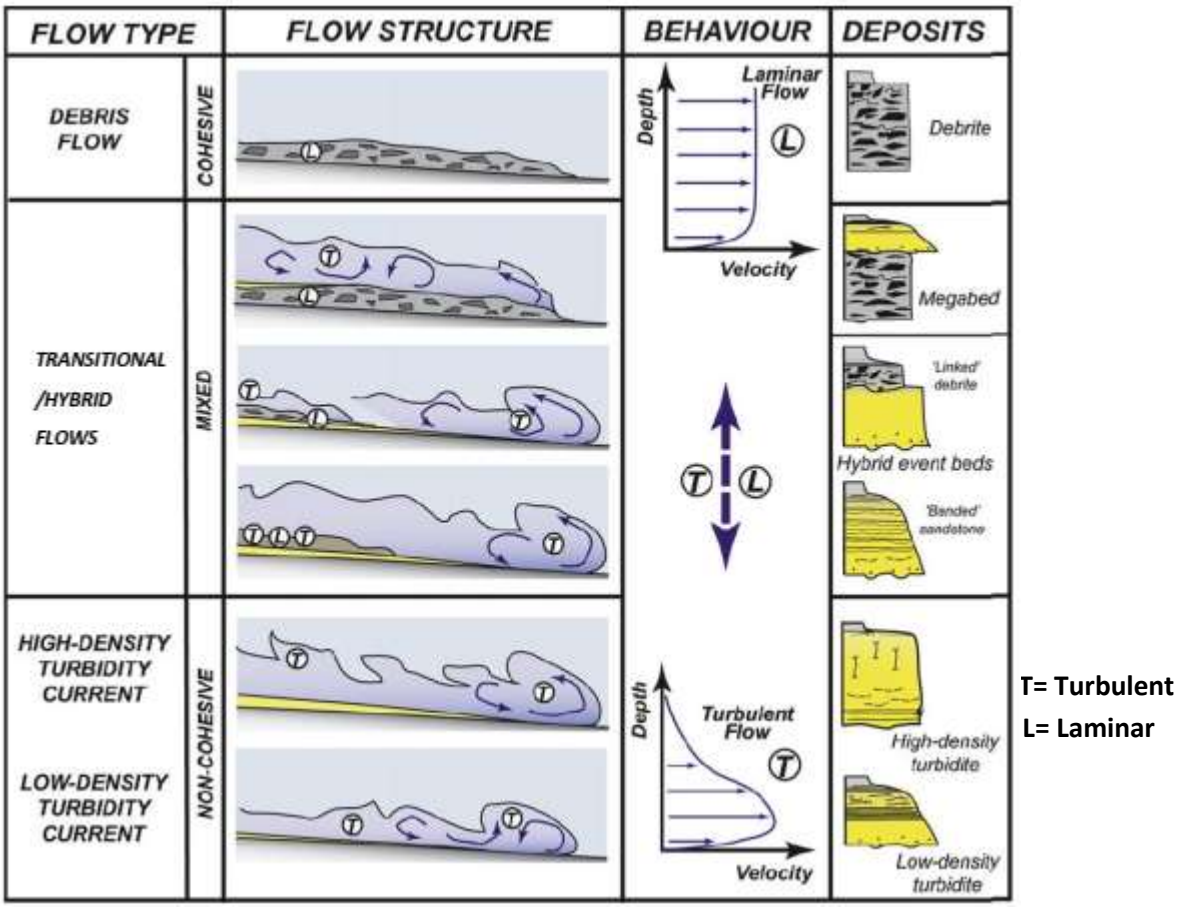

Figure 1. Deep-water sediment gravity flow processes and resultant sedimentary products (Haughton et al., 2009). Composite/Co-genetic flows are similar to transitional flows.

1.1.3. Mass-transport deposits

Mass-transport deposits (MTDs) comprise sediment packages emplaced during a single event of slope failure. In turn, the term mass-transport complex is used where multiple slope failures have coalesced into a larger unit or package (Posamentier and Walker, 2006; Gamberi et al., 2011). Mass-transport deposits are ubiquitous features on submarine slopes, and in all geological settings, including rift and transform margins, convergent and passive continental margins (Hunerbach et al., 2004). They occur at all water depths, especially in areas where soft sediments predominate (Morgan et al., 2009). Large MTDs usually cover tenths to hundreds of kilometres, they are formed by shelf break or mid-slope failure, in contrast to smaller scale MTDs formed by collapse of canyon walls or elevated gradients on the flanks of salt diapirs (Posamentier and Walker, 2006).

1.2. Deep-water depositional environments

1.2.1. Submarine Channels

Submarine channels are long-term conduits for sediments transport from the continental shelf to the basin floor (Mutti and Normark, 1991; Abreu et al., 2003). Depending on their spatial and temporal setting, they can be straight or sinuous and involve variable amounts of confinement (Wynn et al., 2007; Gee et al., 2007; Janocko et al., 2013). Flow confinement is a keyway in which flow efficiency is maintained (Kneller, 2003), enabling channels to develop run-out lengths up to 4000 km (Chough and Hesse, 1976). Sediment gravity flows are focused down deep-marine channels and can enhance confinement through erosion of the channel thalweg or aggradation in overbank levees (Pirmez et al., 2000; Kneller, 2003; Georgiopoulou and Cartwright, 2013). The equilibrium profile of a deep-marine channel is similar to that of a fluvial channel; both tend to erode up-dip and deposit down-dip developing an overall concave-up geometry and reducing gradient down-dip (Fig. 2; Ferry et al., 2005; Georgiopoulou and Cartwright, 2013). In channels with negative accommodation (i.e., when the slope profile lies above the equilibrium profile), flows will be incisional in nature, eroding the substrate and increasing flow confinement. When the slope profile lies beneath the equilibrium profile, channels will be in a setting of surplus accommodation, where they can become depositional, resulting in channel aggradation (Kneller, 2003). Aggradational channels maintain their overall aspect ratio by depositing in overbank areas as well as along the channel thalweg, creating depositional features known as levees. These levees build up on either side of the aggrading channel and thus, confinement is created and maintained (Fig. 3; Kane et al., 2007; Kane and Hodgson, 2011). As levees develop and channel walls become steeper, slope instabilities often cause sliding and slumping from the channel walls to the base of the channel. This leads to a significant alteration of the channel geomorphology by widening at the sides and partially filling the channel base (Mayall et al., 2006). If the slope profile matches the equilibrium profile, the channel is said to be in a state of equilibrium (Pirmez et al., 2000). Under these conditions, channels will neither erode nor aggrade, and all sediment will be bypassed to deposit in the deeper basin (Hodgson et al., 2016; Stevenson et al., 2015).

Overall channel morphology is dictated by repeated cut-fill cycles whereby the channel's geomorphic surface at any one time can differ significantly from the stratigraphic surface preserved in the rock record (McCaffrey et al., 2002; Sylvester et al., 2011). Through this process of incision, deposition, and re-incision, terraces can be developed and preserved

and have been documented in several modern and ancient settings (Janocko et al., 2013; Hansen et al., 2015; Hansen et al., 2017).

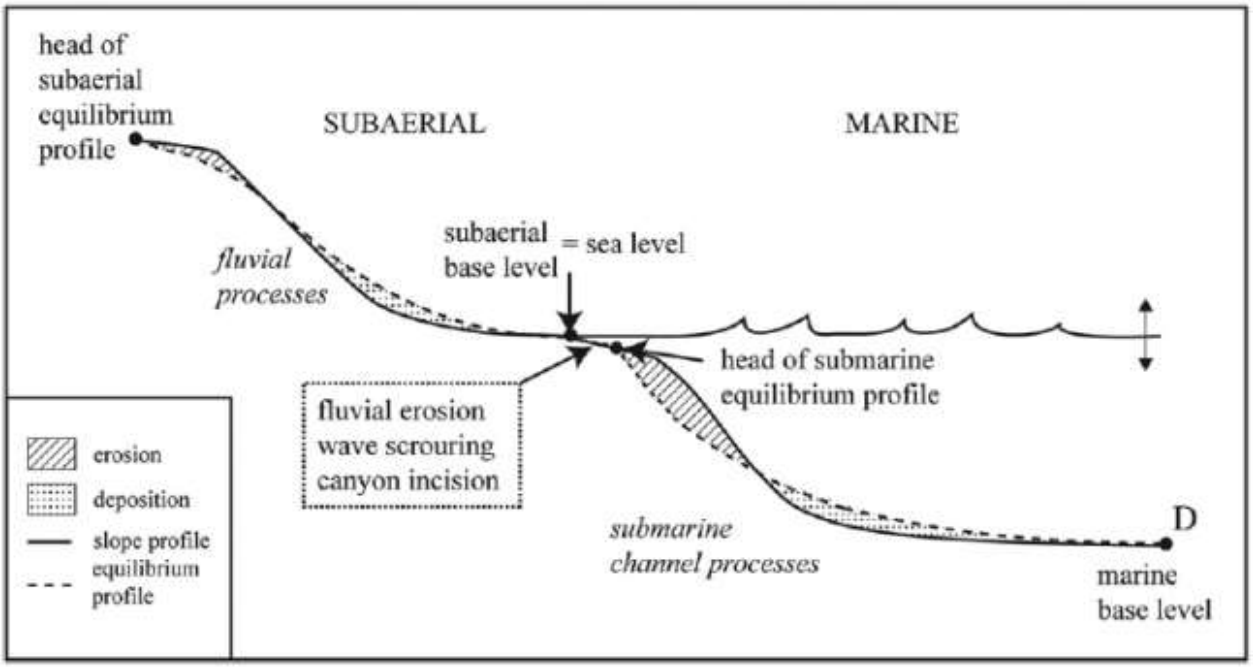

Figure 2. Schematic illustration of subaerial and submarine equilibrium profile in relation to actual slope profile and predicted zones of erosion and deposition (Georgiopoulou and Cartwright, 2013).

Terraces are topographically flat areas located above active submarine channels but confined to inside the channel-belt (Babonneau et al., 2004). They may be formed by overspill of sediments from the channel thalweg, or by the collapse of external levee deposits into the channel-belt (Fig. 4; Hansen et al., 2015). Depositional terraces are developmentally and architecturally similar to internal levees (Kane et al., 2007; Fig. 3). However, internal levees only tend to develop when the channel is deep enough to limit overspill to the uppermost fraction of the flow, and where there is enough space in the channel belt for the flow to gradually decelerate and leave characteristic wedge-shaped deposits (Hansen et al., 2015, 2017).

Deep-marine channels appear very similar in appearance to sub-aerial fluvial channels in terms of their planform and geometry. However this similarity is mostly superficial as the processes that establish them are fundamentally different (Peakall et al., 2000). Riverine flows are approximately one thousand times denser than their surrounding air whereas the density difference between a sediment gravity flow and its ambient water is almost purely dependent upon the sediment concentration of the flow.

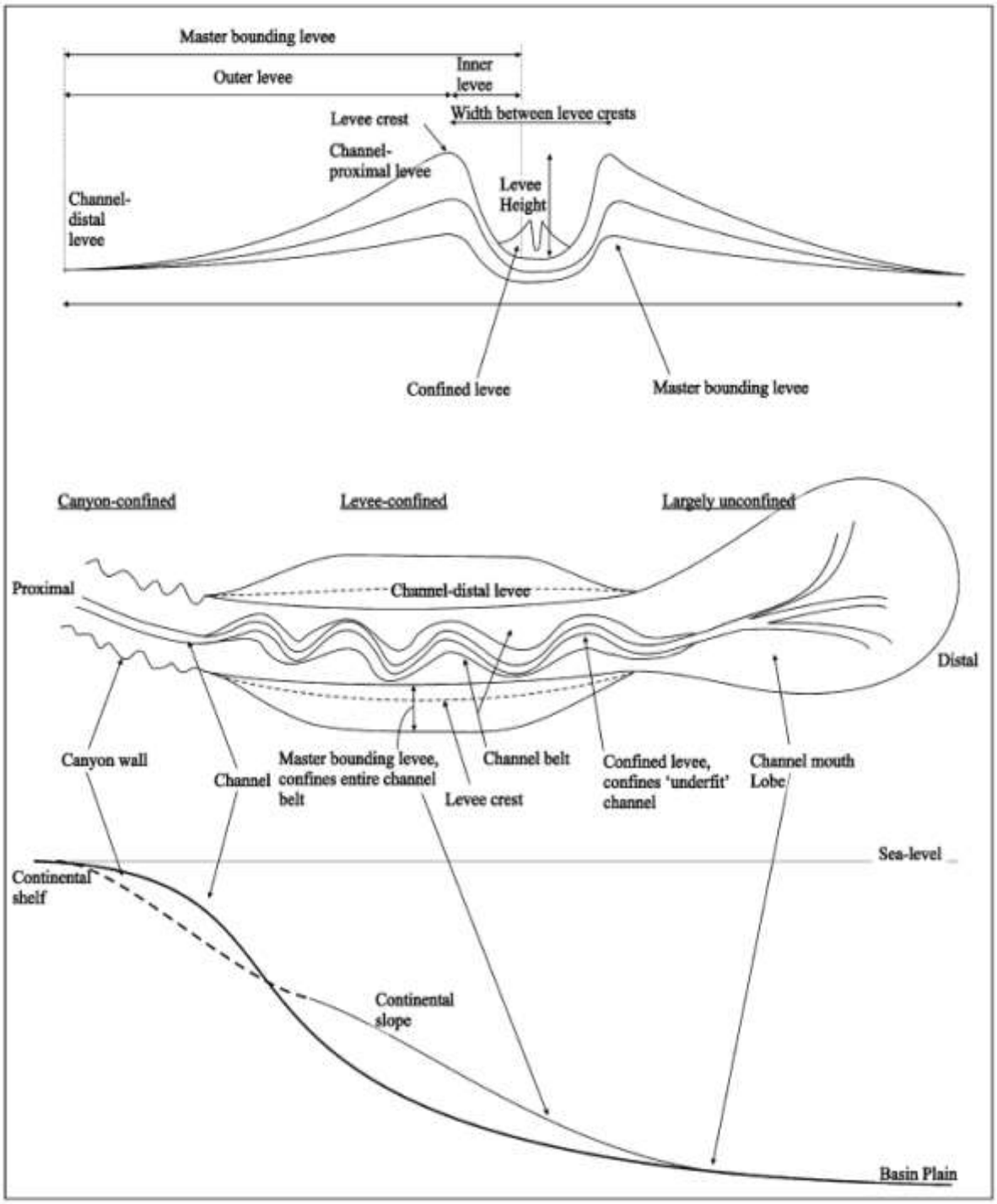

Figure 3. Schematic diagram illustrating the key architectural elements of a classical deep-marine channel-levee system (Kane et al., 2007)

Despite these physical differences, sinuosity is common in both settings and despite channel bend cut-offs reportedly being less common in deep-marine channels than in meandering fluvial systems, they have been documented and observed (Peakall et al., 2000; Babonneau et al., 2004; Babonneau et al., 2010).

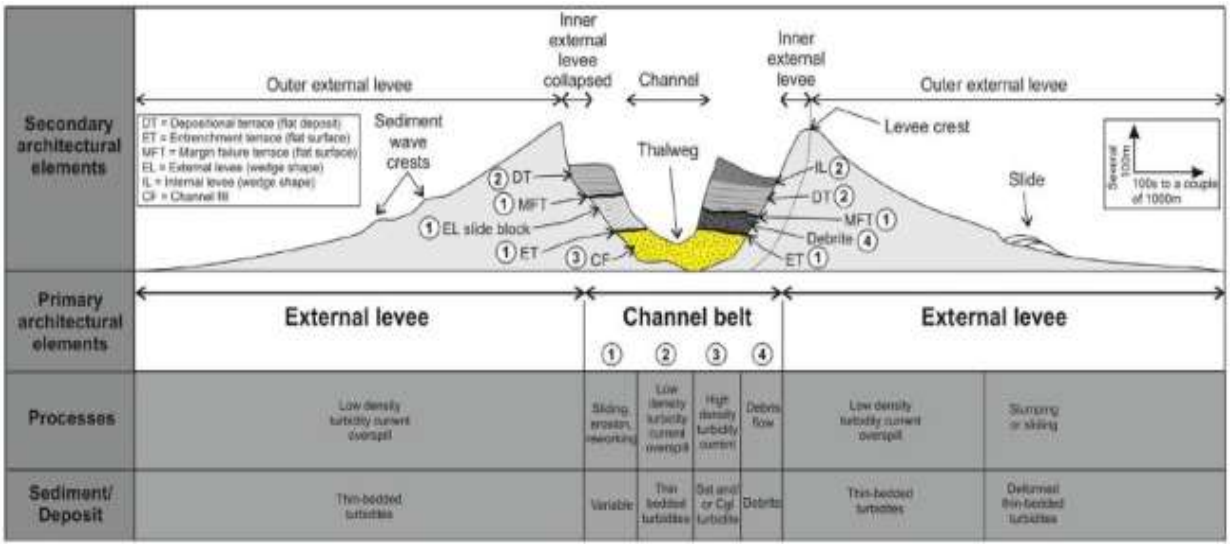

Figure 4. Schematic of a typical channel-levee cross-section showing the range of potential facies and facies associations (Hansen et al., 2015).

- **Submarine Channel Hierarchy**

Gardner and Borer (2000) proposed a model to explain observed depositional geometries and stacking patterns of deep-water deposits based on hierarchical concepts (Fig. 5). This Deepwater Hierarchy and comprises: Submarine Fan Conduit Complex, Submarine Fan Conduit, Channel System Complex and Single-Story Channel. The deep-water stratigraphic hierarchy is based on the principles of sequence stratigraphy, which is the recognition of genetically-related strata packages and their bounding surfaces (Mitchum, 1977). In the constricted salt province of the Gulf of Mexico and the West Africa continental slopes sheet sand and channel-levee systems are vertically inter-layered. This is caused by changes in the gradient of micro-basins or the locally scoured and uplifted basin surface and fluctuating rates of sediment supply as the basin fills and sediment spills into the next basin downslope. The four elements that fill the confined basins are: leveed channel sands; amalgamated channel sands; amalgamated and layered sheet sands; and slumps, debris flows, and marine shales (Steffens, 1993). In (Fig. 5) the black color is the organic rich siltstone, and white color is inter-bedded sandstone and siltstone with beds thinning from channel margin. Also the yellow color is heterolithic channel fill with rip-up clasts and red structure less sandstone with horizontal laminated cap and last one the red line is the erosional surface.

1.2.2. Submarine lobes

Submarine lobes are the dominant architectural expression of sediments deposition in the deep-marine environment (Mutti and Normark, 1987). They are convex-up deposits of sediment

gravity flows and tend to form in intraslope and basin floor settings, down-dip of submarine channel mouths (Etienne et al., 2012).

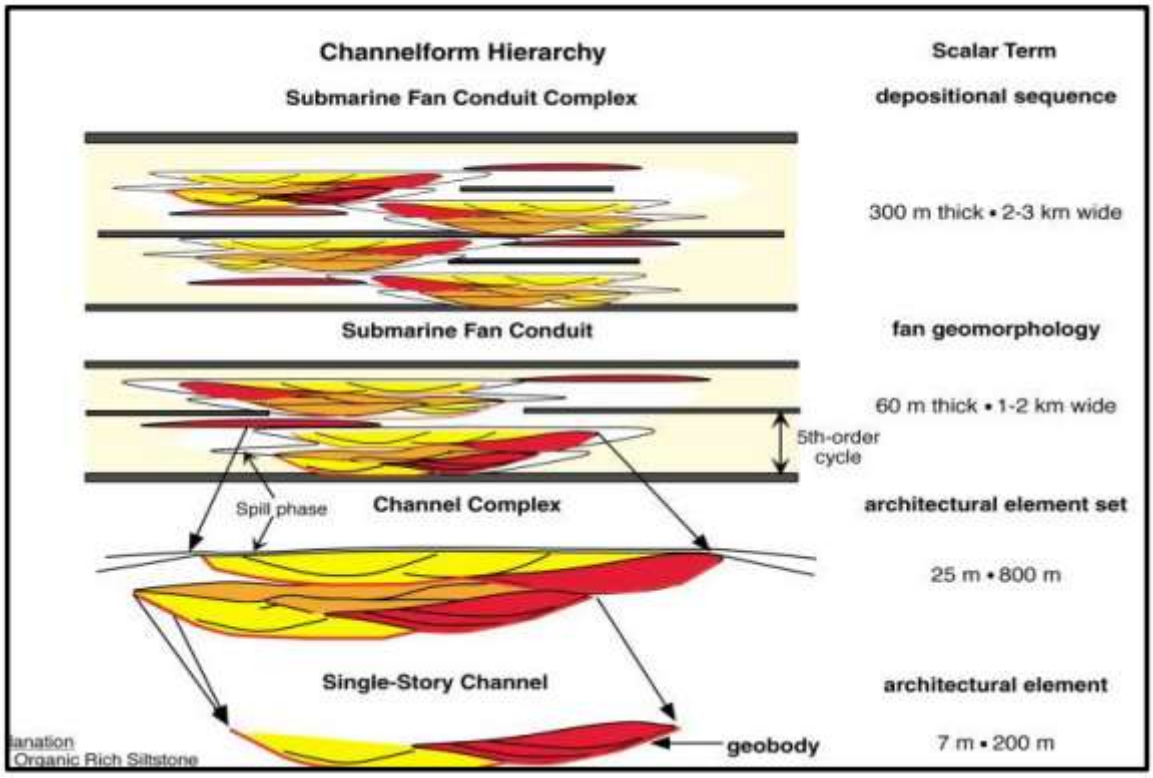

Figure 5. Channel form hierarchy (Gardner and Borer 2000).

Beyond channel mouths, flows become relatively unconfined and spread out in an approximately radial fashion, creating their lobate shape (Fig. 6, Kneller, 1995; Kane et al., 2017). As flows spread, they progressively lose energy, depositing sand-rich high density turbidites in proximal locations, and mud-dominated low density turbidites and hybrid beds in distal lobe environment (Fig. 6, Kane et al., 2017; Fonnesu et al., 2018). Three main lobe sub-environments have been identified through outcrop-based studies using facies associations. These include: 1) the lobe axis, which is found towards the centre of the lobe and is generally characterised by structureless, thick, amalgamated, sand-rich high density turbidites (Terlaky et al., 2016); 2) the lobe off-axis, which features more common low density turbidites composed of mudstone interbedded with structured sandstone (Prélat et al., 2009); and 3) the lobe fringe, which represents the outermost deposits of the lobe and contains the highest proportion of thin-bedded mud-rich low density turbidites and hybrid beds (Fig. 6, Hansen et al., 2019). Small distributary channels that expand in an arborescent style from the main feeder channel across the top surface of lobe deposits commonly convey sediment to distal parts of submarine lobes (Fig. 6; Normark et al., 1979; Posamentier and Walker, 2006).

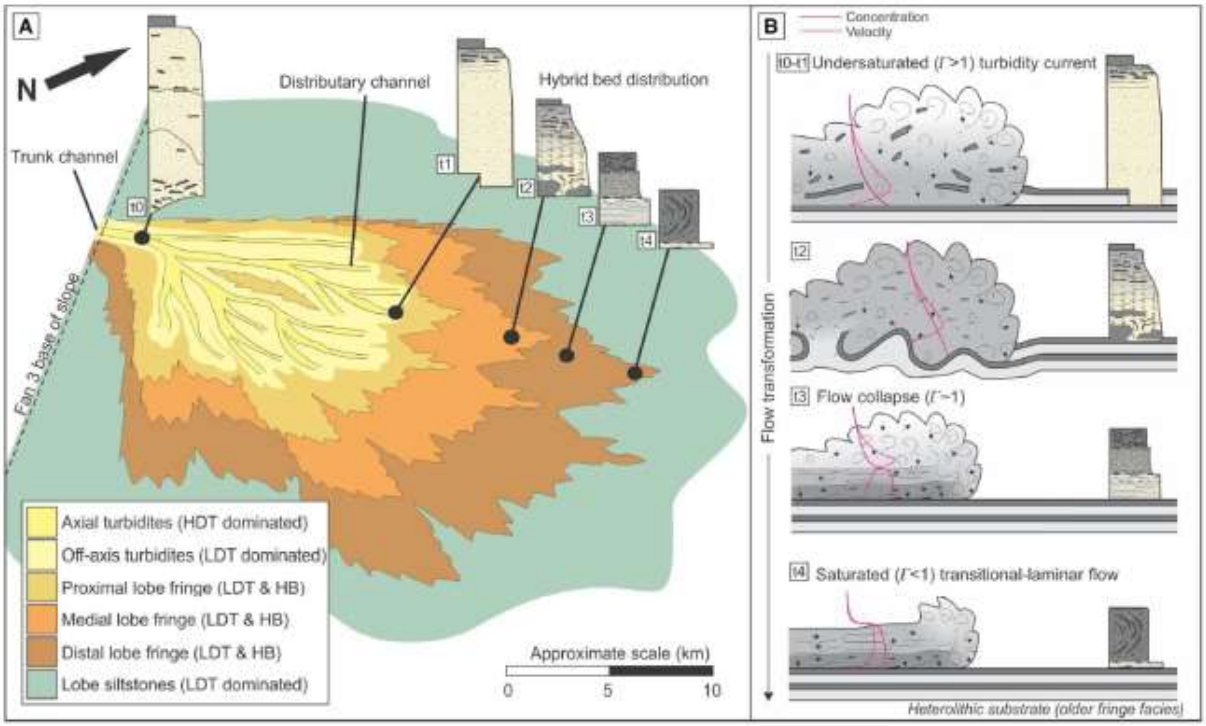

Figure 6. a) Schematic representation of a submarine lobe (Fan 3, Karoo Basin, South Africa), its associated sub-environments. b) Distribution of different types of hybrid event beds are indicated (Kane et al., 2017).

Like channels, lobe development is system specific and strongly influenced by underlying seafloor topography (Piper and Normark, 1983). The total volume of sediments accumulation within lobe deposit is determined by available accommodation space, which is variably dependent upon the sea-surface level, seafloor topography, and changes in sediment supply rates (Kneller et al., 2016). Basin topography has a substantial effect on the routing of sediment gravity flows and subsequent architecture of associated lobe deposits (Booth et al., 2003). This topography can be generated by mud or salt diapirism (Gee and Gawthorpe, 2006; Doughty-Jones et al., 2017), tectonic events (Hodgson and Haughton, 2004; McArthur et al., 2019), and depositional and erosional relief (Normark et al., 1979; Ortiz-Karpf et al., 2015). Flow interaction with this topography can result in highly heterogeneous and complex onlap geometries as flows can be redirected, transform, or run up-topography to variable degrees (Fig. 7, Soutter et al., 2019). A relatively restricted basin may confine flows to the point where lobe deposits are generally thick and amalgamated, stacking aggradationally (Marini et al., 2015). In relatively unconfined settings, lobes spread out laterally, preferentially depositing within topographic lows adjacent to preceding lobe deposits; stacking compensationally (Fig. 8, Prélat et al., 2009, 2010; Marini et al., 2015). Over an extended period of sedimentation, lobes grow and build basin-wards in a progradational fashion (Morris et al., 2014). When sediment supply

begins to wane, the system will retreat, resulting in complex lobe stacking geometries (Prélat and Hodgson, 2013). A deep-marine lobe will cease development once sediment supply has been cut-off either by internal (e.g., up-dip avulsion event) or external (e.g., sea-level rise and reduced sediment input) means and subsequently be overlain by hemipelagic deposits (Prélat et al., 2010).

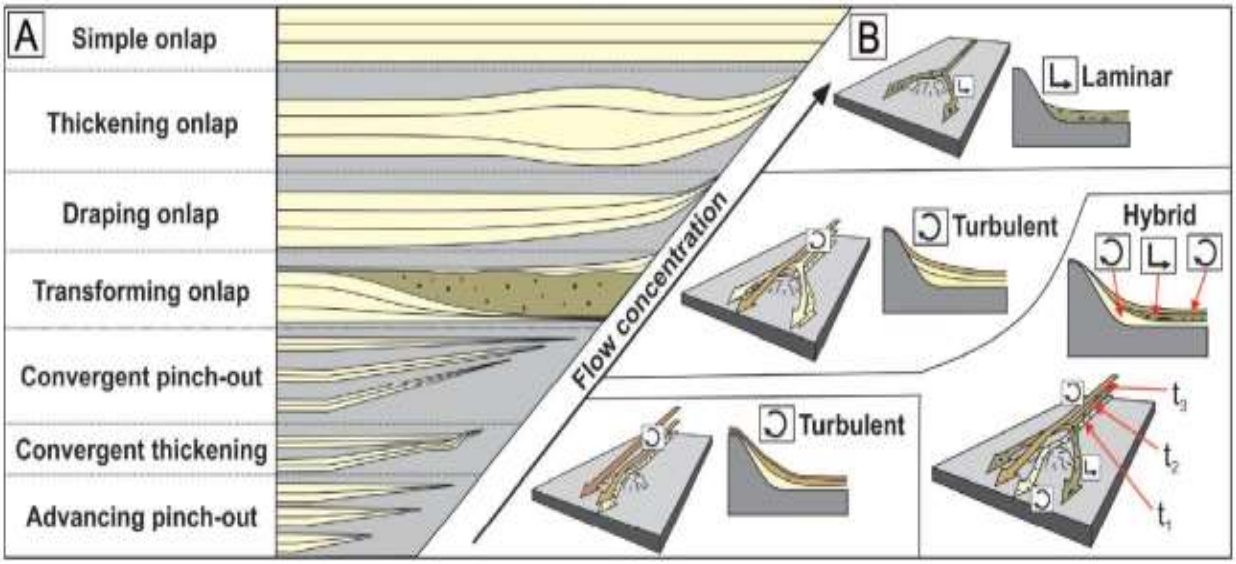

Figure 7. Styles of onlap termination, and relationship between flow concentration and onlap geometry (Soutter et al., 2019).

- **Lobe Hierarchy**

Like submarine channels, several hierarchical schemes have been developed to aid characterisation of submarine lobe systems (Gervais et al., 2006; Deptuck et al., 2008; Prélat et al., 2009). The terminology of Prélat et al. (2009) is used in this thesis because it is well-defined and has been widely used in previous studies (Collins et al., 2015). Their outcrop work established a four-level hierarchical scheme for lobe deposits based upon the internal stratigraphy of 'Fan 3', a basin floor lobe succession in the Karoo Basin, South Africa (Fig. 9). The fundamental building block of this scheme is the 'bed' which represents a single flow event. Owing to excellent outcrop exposure within the Karoo Basin these beds can often be traced laterally for hundreds of metres and have been observed to have an average thickness of 0.5 m (Prélat et al., 2009). One or more beds may stack into amalgamated 1-3 m thick 'lobe elements' which are bounded by laterally extensive siltstones that are <0.02 m thick ('interlobe elements'). Lobe elements are sand-prone and may be laterally traced for several kilometres (Prélat et al., 2009). One or more lobe elements may stack to form a 4-10 m thick 'lobe', bounded by 0.2-2 m thick units of thin interbedded siltstone and very fine-grained sandstone

('interlobes') (Prélat et al., 2009). Genetically related lobes stack into 30-60 m thick 'lobe complexes' bounded by 2-20 m thick hemipelagic mudstones ('interlobe complexes'). Whilst exact width and thickness values for these measurements will vary from system to system, they provide a means to visualise the scaling of this hierarchical scheme.

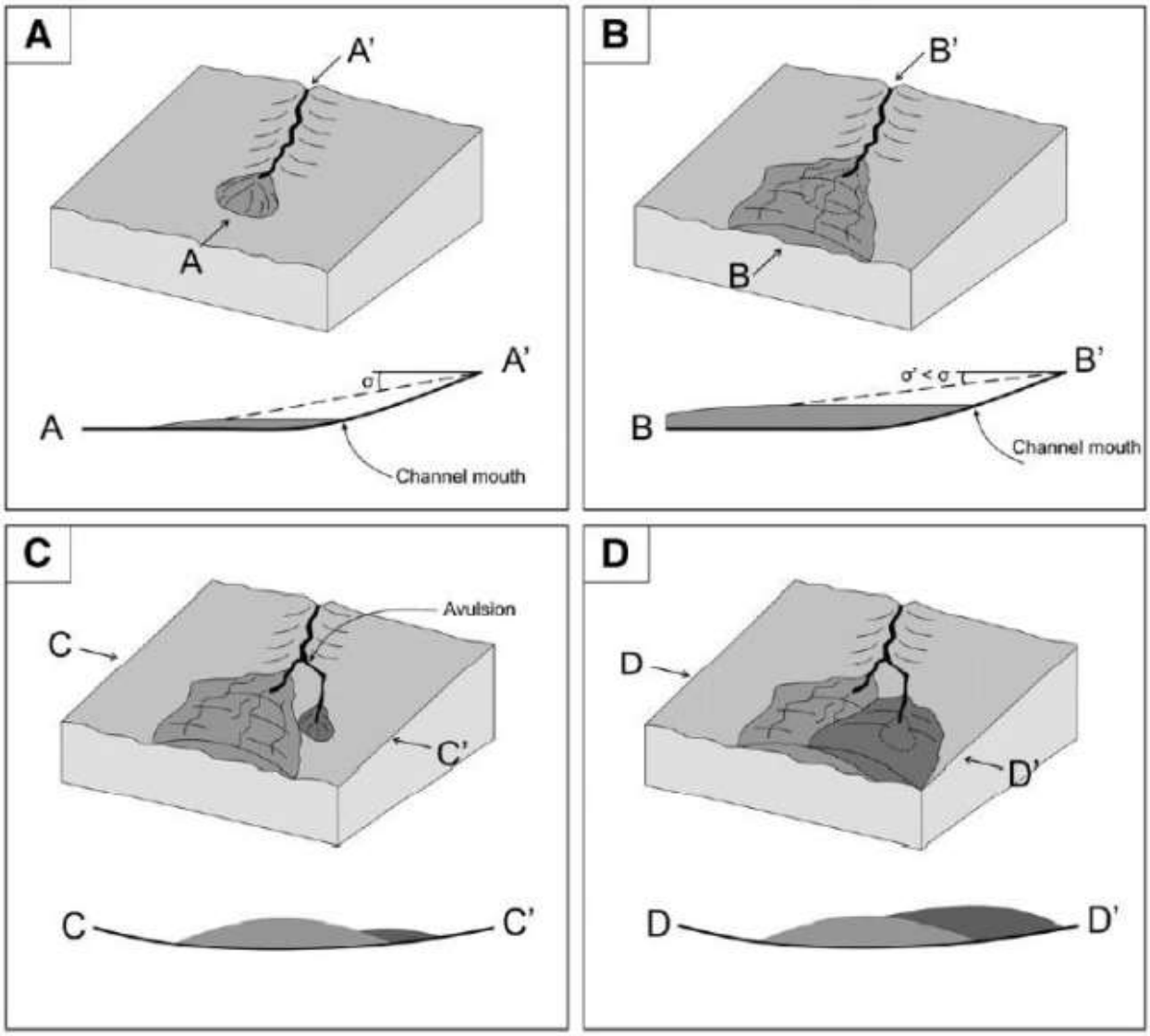

Figure 8. Submarine lobe initiation and development (Prélat et al., 2010). (A) Lobe initiation. (B) Lobe Growth. Gradient between top of channel and top of lobe reduced. (C) Avulsion event. System seeks lowest topography. (D) New lobe growth.

The origin of interlobe components is dependent on whether they formed by external or internal mechanisms (Fig. 10). If externally controlled, it is inferred that interlobes are the result of a waning of sediments supply to the system and an extended period of deposition by hemipelagic fallout (Prélat et al., 2009). If controlled internally, they represent the marginal expression of other laterally deposited lobes (Prélat et al., 2009).

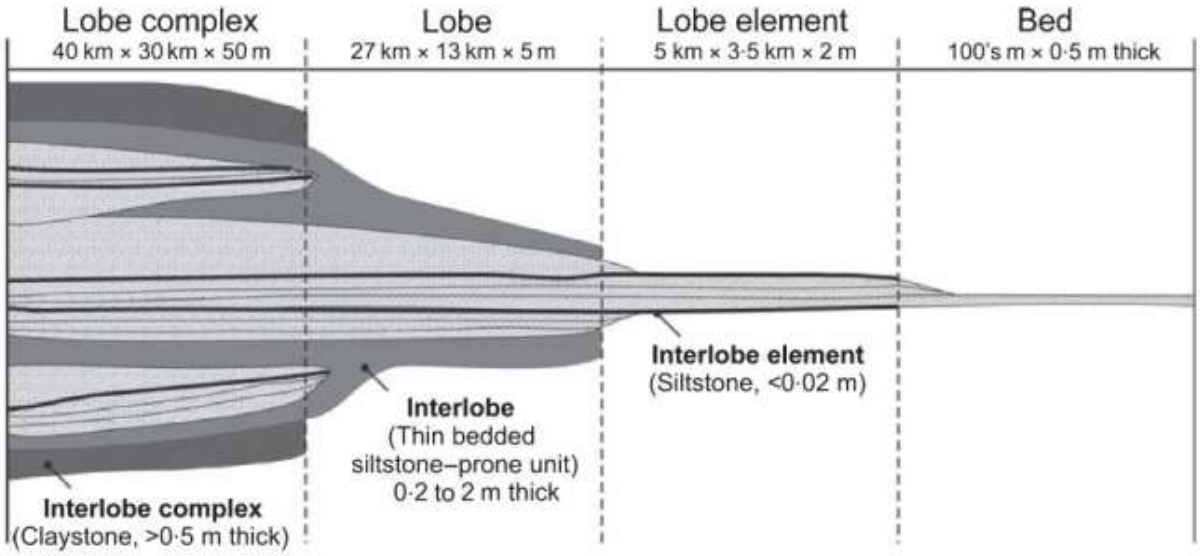

Figure 9. Hierarchical scheme for the Fan 3 lobe complex in the Karoo Basin (Prélat et al., 2009). Four main elements are presented: Beds stack into lobe elements, which make up lobes, which in turn are the building blocks of lobe complexes. The sand-rich lobe components are separated by mud-rich 'interlobe' components.

Interlobe complexes are more likely an externally triggered response to a reduction, or termination, of sediments supply to the deep basin (Fig. 10; Prélat et al., 2009). Interlobes (Fig. 9) are suggested to be the result of compensational stacking, having been locally observed to pass laterally into larger sandstone units (Prélat and Hodgson, 2013). This interpretation is supported by recent work by Boulesteix et al. (2019), which has highlighted that many deep-marine mudstones intervals associated with submarine lobes are the product of sediment gravity flows, rather than hemipelagic fallout.

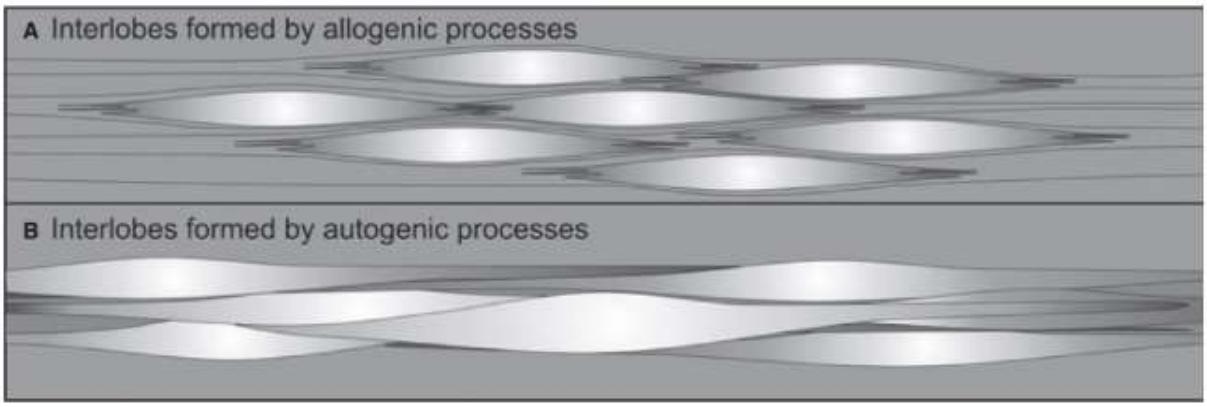

Figure 10. Schematic cross-section through a lobe complex of external (allogenic) vs. internal (autogenic) interlobe formation (Prélat et al., 2009). Note compensational stacking of lobes. a) If interlobes are interpreted as externally derived, they are deemed to be regional drapes that

bound lobe deposits at their tops and bases, representative of a period of reduced flow-derived sediment supply to the system. b) If interlobes are formed by internal processes, they represent the marginal or distal fringes of other offset lobes.

In conclusion, this chapter has presented a comprehensive overview of the fundamental sedimentary processes namely turbidity flows, debris flows, and mass-transport deposits that shape deep-water environments. It has also outlined the key depositional settings, particularly submarine channels and lobes, which play a critical role in the development of deep-marine stratigraphic architectures. This foundational understanding is essential for interpreting sedimentary records and guiding further analysis in subsequent chapters.

Chapter 2: Geological Setting of the Kribi-Campo Sub-Basin

This chapter provides a review of previous scientific research conducted in the Kribi-Campo sub-basin, along with a summary of internal reports made available by the National Hydrocarbon Corporation (NHC). It covers the location of the study area, the tectonic framework, the stratigraphic evolution of the Kribi-Campo sub-basin, and an overview of its petroleum system.

2.1. Location of the study area

The study area is located along the continental slope of the Kribi-Campo sub-basin approximately 25 km to the coast of Cameroon (Fig. 11). It is situated in water depths ranging from 20 to 2000 m (Fig. 11). The Douala/Kribi-Campo Basin is one of a series of continental shelf basins extending in West Africa from the edge of the Niger delta in Cameroon to the Walvis ridge near the Angola–Namibia border (Brownfield and Charpentier, 2006; Ntamak-Nida et al., 2008). The basin is divided into two sub-basins, namely the Douala sub-basin in the northern part and the Kribi-Campo sub-basin in the south (Fig. 11). The Kribi-Campo sub-basin extends over 6150 km^2 offshore and 45 km^2 in a triangular onshore area (Ntamak-Nida et al., 2010). This sub-basin is limited to the south by the Campo high, which formed as a rift basin that deepened to the northeast (Meyers et al., 1996), and it separates the Kribi-Campo sub-basin and Equatorial Guinea Rio Muni Basin. Its northern limit corresponds to the Kribi Fracture Zone, which stops the extension of the Douala sub-basin. At the east, the Precambrian basement outcrops occur close to the shoreline (Nguene et al., 1992; Ntamak-Nida et al., 2010). The offshore part of the basin, which was investigated in this study, covers an area of approximately 1500 km^2, between 2°20′ and 3°00′N, and 9°00 and 9°50′E (Fig. 11).

2.2. Tectonic framework and stratigraphic evolution

Like most sedimentary basins in the South Atlantic, the tectono-stratigraphic evolution of the Kribi-Campo sub-basin can be divided into four broad stages: a pre-rift stage (Late Proterozoic to Late Jurassic), syn-rift stage (Late Jurassic to Early Cretaceous), transitional stage (mid-late Aptian), and post-rift stage (Late Cretaceous to Holocene) (Pauken, 1992, Lawrence et al., 2002, Brownfield and Charpentier, 2006) (Fig. 12).

Pre-rift stage (Precambrian)

The eastern boundary of the Douala/Kribi-Campo sub-basin is represented by the present-day coastline where a series of north-south en echelon faults form a boundary with the Pre-Cambrian metamorphic basement which is exposed at the surface (Nguene et al., 1992).

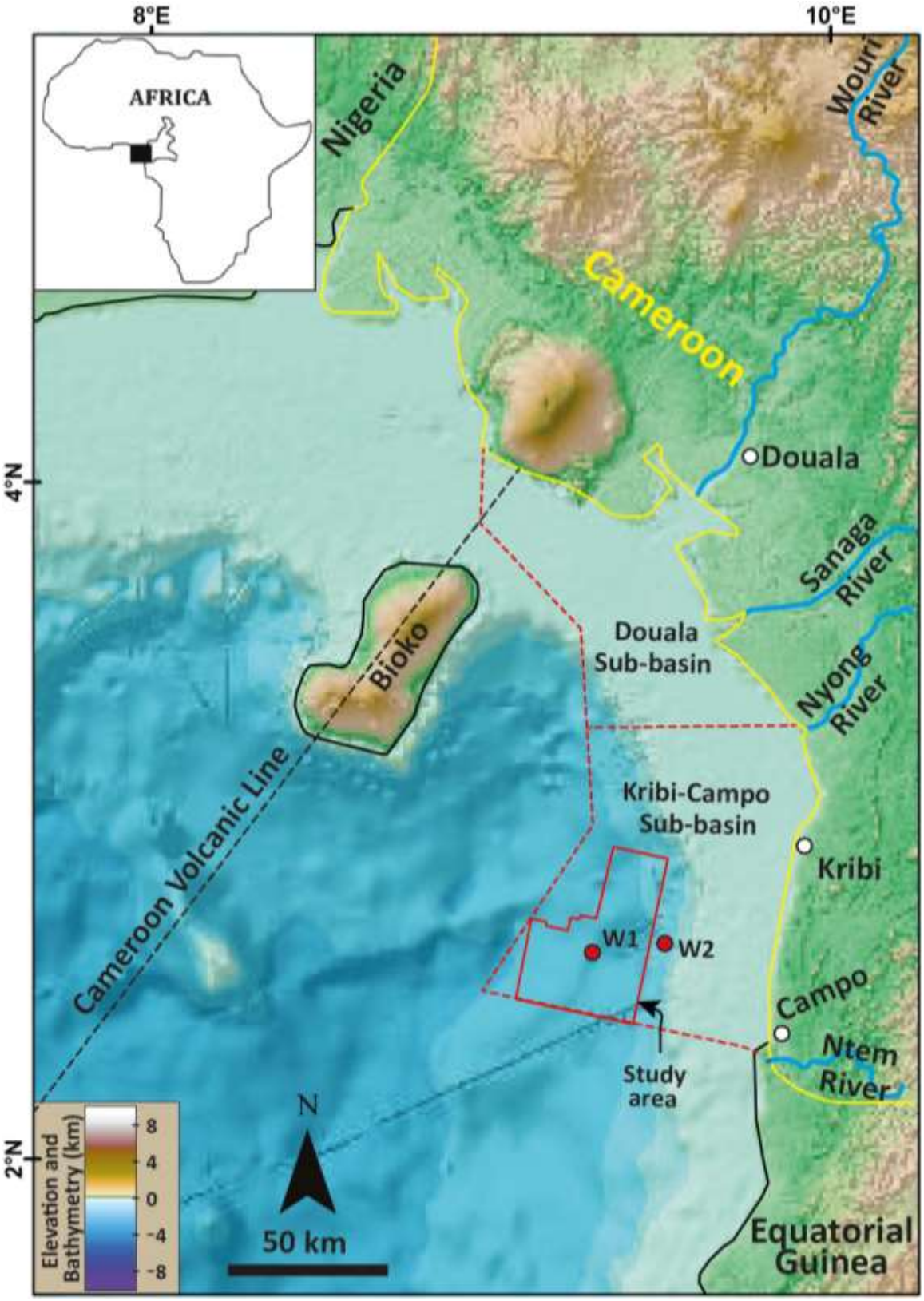

Figure 11. Superimposed relief and bathymetric map of Cameroon, showing the location of the study area. Insert map on the left-hand corner of the map shows the location of Cameroon in the Gulf of Guinea. The 3D block, which we studied is outlined in red box, while the red circles with black outlines labelled W1 and W2, represent well locations.

This basement of high-grade gneisses and granites continues westwards, where it underlies the Douala/Kribi-Campo sub-basin up to the boundary with the NE-SW trending Kribi Fracture Zone. The initial pre-rift sedimentary sequence deposited in the Douala/Kribi-Campo basin is interpreted as a continental succession laid down in a N-S trending intracratonic depocentre referred to as the Afro-Brazilian Depression (Fusion Oil & Gaz NL, 2002). The Jurassic age sequence is interpreted to extend across the Gabon and Douala/Kribi-Campo basins. However, true continental and lacustrine sediments have not been proved by drilling (Pre-Lower Aptian) in Douala but are likely to exist with depth. By analogy with the Gabon basin, where drilling has proven a succession of scattered aeolian deposits, redbeds, fluvial and lacustrine deposits, then it is reasonable to assume that these types of sediments are preserved along the Kribi-Campo High, are yet to be reached by drilling.

Syn-rift stage (Barremian-Aptian)

In Late Jurassic- to Early Cretaceous (Barremian) time, the South American and African continental plates began to separate with the opening and 'unzipping' propagation of these plates from south to north from the Walvis Ridge/Rio Grande Rise to the Benue Trough (Fusion Oil & Gaz NL, 2002). The 'unzipping' or rifting was compartmentalised by major transfer structures with their own unique extensional and subsidence histories for each compartment. This is reflected in a series of syn-rift depocentres of different ages with the South Gabon Basin being Neocomian-Barremian in age and the North Gabon and Douala/Kribi-Campo Basins being Barremian-Aptian in age (Ntamak Nida et al., 2008, 2010; Sterling, 2010; Le et al., 2014).

The early rift phase was characterised by extensional fault blocks (i.e., horst and graben structures) that remain parallel to the present-day coastline and average 5 km in width with the main faults sub-parallel to the coastline and displacements of up to 2 km. The horst fault blocks underwent erosion in which sediments then accumulated in the neighbouring grabens that formed deep narrow lakes of thick muddy lacustrine, deltaic facies and freshwater shales.

In the Douala/Kribi-Campo Basin, the only syn-rift deposits of Aptian age that have been discovered are those found east of the town of Douala and which consist of fluvial-lacustrine sequence overlying a narrow band of attenuated continental basement. Evidence in the offshore of Aptian age syn-rift deposits (e.g., below the Cameroon coastal plain and shelf along the Kribi-Campo High Trend) is based solely on seismic data because wells drilled to date have Total Depth (TD) only in younger post rift sediments.

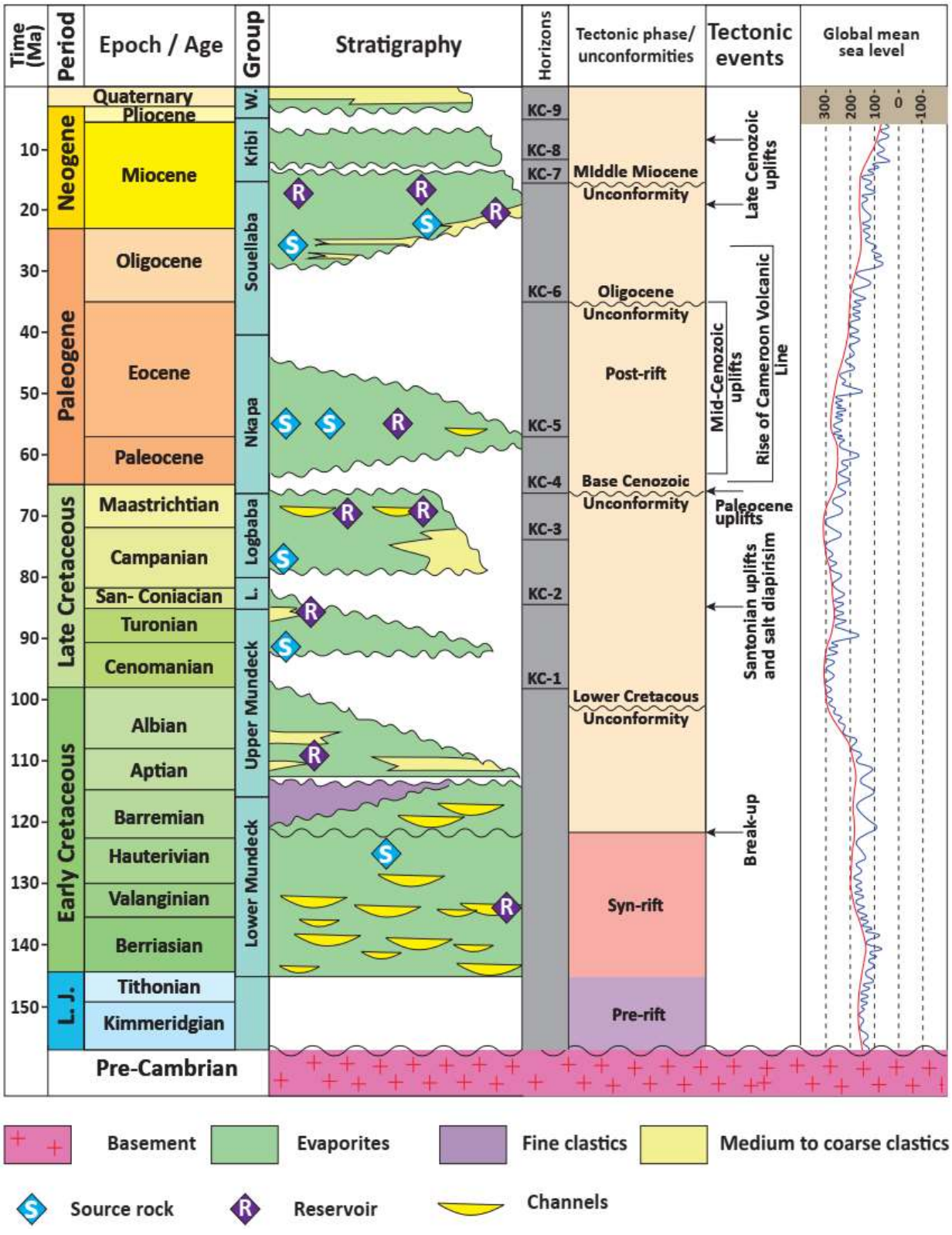

Figure 12. Stratigraphic column of the Kribi-Campo Sub-basin showing the tectono-sedimentary phases and global mean sea level (Modified from Pauken, 1992; Lawrence et al., 2002; CGG Robertson, 2015; Iboum Kissaaka et al., 2016).

Any preserved syn-rift sequence in the study area will be restricted to the southeastern corner, between the Kribi Fracture Zone and Kribi-Campo High. The late syn-rift phase (Late Barremian to Early Aptian) was characterised by transpressional uplift within the Douala/Kribi-Campo sub-basin with subsidence shifting whereby rift structures were infilled and draped by calcareous organic shales and marls of shallow saline lakes to fluvial-deltaic clastics, lagoonal to restricted marine sediments (Gibbs, 2003; Meyer et al. 1996).

In the study area, the syn-rift sediments are part of the Lower Mundeck Formation (Ntamak Nida et al., 2010; Sterling, 2010; Le et al., 2014).

Transition stage (mid-late Aptian)

Syn-rift basin development and deposition was soon followed by a transitional phase of post rift thermal subsidence and marine sedimentation in Late Aptian-Coniacian. A thick succession of intercalated salt, sandstone and dark shale with turbiditic clastics and carbonate rocks became the dominate form of rock types deposited in Douala sub-basin. Turner (1999) described it best with his documented work on neighbouring Rio Muni basin of Equatorial Guinea to the south of study area. He interprets an unconformity bounded Late Aptian-Coniacian early drift sequence that separates a Barremian-Aptian syn-rift sequence from a Santonian-Recent post-rift sequence. A combination of an end-rift to early post-rift uplift of the basin margin coupled with a rapidly subsiding deep offshore bathymetry led to a gravitational collapse of the basin margin with the translation of thick rafts of shelf carbonates down the slope during the Cenomanian (Fusion Oil & Gaz NL, 2002). As Turner (1999) indicated in his paper, this is particularly evident to the south of study area along the Rio Muni High.

Fusion Oil & Gaz NL (2002) stated that in the Kribi-Campo High and study area, any gravity sliding of early post-rift sediments is interpreted to have been initiated as early as the Cenomanian, resulting from a combination of salt withdrawal and the existence of tectonically-induced high relief along the cratonic margin (Fusion Oil & Gaz NL, 2002). The translation of thick rafted blocks has yet to be unequivocally proven in the Douala/Kribi-Campo Basin, that is, little physical evidence exists for a Late Cretaceous allochthonous rafts in the study area vicinity that are observed in the Rio Muni High basin area to the south. However, in reviewing previously published work (Pauken, 1992, Meyers et al., 1996, Coward, 1999) and Sterling's own proprietary work there does appear to be reasonably good seismic and well (Kribi Marine-1) evidence to explain the salt presence and quite possibly an Albian sediment 'raft block' in

study area as being allochthonous in nature and hence a rafted segment not too dissimilar in formation from that seen in Rio Muni Basin to the south.

In addition, other observations made from both seismic and wells drilled (and cored) is the presence of a series of Aptian-Albian tilted fault blocks along the Kribi-Campo High which are thought to be the consequence of a second phase of rifting. An alternative interpretation of these tilted fault blocks is a zone of gravity sliding (Fusion Oil & Gaz NL, 2002). For all practical purposes, Sterling (2010) does not possess a sufficient database of closely spaced, high quality seismic and well data to arrive at a firm independent interpretation for this transitional to early drift sequence present in the Kribi-Campo High and study area. However, the 2D and 3D data that it does have plus the support of published papers gives Sterling some confidence that gravitational slide (raft) blocks are present in the eastern area of study area.

In regard to the multi-well appraisal drilling programmes (including extensive cores) carried out on the Kribi-Campo High in the 1980's, this has shown the individual Aptian-Albian sandstone sequences encountered to show good correlation between wells drilled in separate sealing fault blocks. This has been proven through recorded dynamic reservoir pressure and fluid data in Kribi wells. This indicates that the faults were either syndepositional to the emplacement of sandstone sequences (i.e., syntectonic clastic wedge) or the faults were post-depositional. Cores taken in this area are interpreted to be composed of high-density gravity flow clastics and turbidites.

Post-rift stage (Albian - present)

A major regional drift unconformity developed across the Douala/Kribi-campo Basin in the Early Senonian marking the complete cessation of lithospheric extension and the onset of continental divergence (or 'drifting') with the development of the passive margin. The unconformity is characterised by the discordant erosion of Early Cretaceous sequences along the uplifted eastern margin of the Douala/Kribi-Campo Basin as well as south of the Kribi Fracture Zone where the foot-wall was subject to in excess of 1 km of uplift. Formation of the drift unconformity is bracketed between 92 and 86 Ma and it is conjectured that a minimum of 660 m or eroded section occurred (Turner, 1999; Fusion, 2002).

Following the end Santonian uplift event, the basin returned to rapid thermal sag subsidence (SPT/Simon Petroleum and Technology, 1995). As a result, a thick succession of Campanian-Maastrichtian sediments (Logbaba Formation) drapes the underlying structures and

lie slightly unconformably over the Santonian (Logbadjeck Formation). The rapid subsidence caused a significant phase of halokinesis along the margin of the Kribi-Campo High (Nguene et al., 1992; SPT/Simon Petroleum and Technology, 1995). This Santonian tectonic event with its associated uplift led to the deposition of thick late Cretaceous clastics characterized by slope and basin floor fans containing multiple channel complexes (Sterling, 2010; Le, 2012, 2021). A series of eustatic lowstands during the Campanian-Maastrichtian and the Santonian uplift facilitated the episodic transport of major clastic sequences across the relatively narrow shelf into the deeper basin to the west (i.e., in the study area) (Fig. 12). Sterling (2010) estimated that an excess of 1500–2000 m of Senonian deep-water clastic sediments were deposited in the study area during this phase of post-rift sedimentation. Sag subsidence during the Campanian led to basin deepening and the widespread development of basinal sediments. Continued halokinesis in the south of the basin may have led to complex turbidite sand distribution. Eustatic sea-level fall during the Maastrichtian (Nguene et al., 1992; Seiglie and Baker, 1984) resulted in the progressive westward progradation of the shelf. Sand appears to have been fed to the basin by the palaeo-Ntem, palaeo-Sanaga and palaeo-Nyong Rivers, with sand rich aprons developed were these rivers debouched into the basin (SPT/Simon Petroleum and Technology, 1995). During the Early Tertiary, relative sea-level fall resulted in slumping and collapse of shelf-slope sediments and deposition of mounds on the Kribi-Campo sub-basin floor (Iboum Kissaaka et al., 2016 and Le, 2021). An intra-Miocene unconformity marks an incision surface, with the development of canyons cutting down into underlying sediments. In the more proximal settings (i.e., east of Kribi-Campo High), there are multiple submarine incisions several kilometres wide and some amalgamated cut-and-fill submarine channel complexes downslope and parallel to present-day shelf-break in most of the Paleocene section (Wornardt et al., 1999; Le, 2012; Iboum Kissaaka et al., 2016). The late Eocene-early Oligocene tectonic event facilitated a relative sea-level fall, responsible for the widespread erosion and non-deposition in the deep-water of the basin (Wornardt et al., 1999; Helm, 2009; Mvondo, 2010; Iboum Kissaaka et al., 2016; Ngo et al., 2018; Le, 2021) (Fig. 12). Following this period of non-deposition, a thick Miocene-Pliocene clastic wedge originating from a combination of multiple continental paleo-river drainage systems (e.g., Proto-Sanaga, proto-Nyong and proto-Ntem River systems), prograded across the narrow shelf area (Sterling, 2010; Le, 2012). Sediments prograded down the steeply dipping fault margin into the offshore Kribi-Campo sub-basin and deposited a thick sequence of sand-rich turbiditic channels (Sterling, 2010; Le, 2012).

In summary, the Mesozoic-Cenozoic stratigraphy of the Kribi-Campo sub-Basin can be divided into nine formations, namely the Lower Mundeck (Barremian-Aptian), Upper Mundeck (Albian-Turonian), Logbadjeck (Turonian-Campanian), Logbaba (Campanian-Maastrichtian), N'Kapa (Palaeocene-Eocene), Souellaba (Oligocene to Lower Miocene), Kribi (Upper Miocene), Matanda and Wouri (Pliocene to recent) (Fig. 12).

2.3 Structural setting of the Kribi-Campo sub-Basin

The Cameroon Douala/Kribi-Campo Basin is the northernmost basin of a string of en-echelon set of West African basins (extending 4000kms) that developed from the Walvis Ridge in the south to the Cameroon Volcanic Ridge in the north. These basins formed as the consequence of right lateral shear conditions (Coward et al., 1999) during the opening of the South Atlantic (115 Ma) in Early Cretaceous (Wilson et al., 2003). Rifting began in the Late Jurassic and lasted until the onset of seafloor spreading in Albian-Cenomanian time (Pauken, 1992). This was followed by thermal sag, and the basin is classified as an Atlantic–type marginal sag basin (Clifford, 1986).

Two major fracture zones were formed by continental extension: the Kribi Fracture Zone (KFZ) to the southeast; and an unnamed fracture zone to the northwest (Meyers et al., 1996). Only the KFZ actually intersects the study area, associated with development of a structural high to the southeast. The structure can be correlated with similar uplifted highs on the margin of the continental shelf, first described by Pauken (1992). This eroded high consists of a thick syn-rift sequence (Lower Cretaceous) overlain by post-rift sediments (Upper Cretaceous). Inversion of the older syn-rift section has been documented on many margins of West Africa (Dailly, 2000, Brownfield and Charpentier, 2006). According to Le, (2012); the Kribi High associated with the KFZ to the southeast is the main control on basin profile, forming the basin boundary to the southeast in the Upper Cretaceous.

Most of N120 faults die out within the syn-rift sequence, and terminate at, or close to, the fracture zone, The observations of both N30 and N120 fault sets in the syn-rift sequence (Lower Cretaceous), suggests that both fault sets may be related to a rifting stage during basin opening, and are related to evolution of the fracture zone. Similar normal fault characteristics have been documented in the Niger Delta (Briggs et al., 2009), Rio-Muni Basin (Dailly, 2000), and the Gabon Basin (Mbina Mounguengui and Guiraud, 2009). The development of fault-related folds in the Upper Cretaceous could be related to re-activation of the N30 faults associated with regional tectonic uplift during Senonian (post-rift) time. Furthermore, the reactivation of some of these structures (e.g., Kribi and Campo Fracture Zones, Kribi Campo

High etc) through Cretaceous and Tertiary times also affected and helped to focus the entry and deposition of gravity flow deposits of coarse-grained clastics that are in some cases the primary reservoir targets in the study area (Sterling, 2010).

2.4 Cenozoic breakup of Africa and Southern America and palaeogeography of the Kribi-Campo sub-Basin.

The basin was formed during the break-up of North America, Africa, and South America, with continental separation gradually propagating south to north from the Late Jurassic to Late Cretaceous time. The Kribi-Campo sub-basin was one of the latest basins to open in the Late Cretaceous (Late Albian to Turonian), coeval with opening of the Gulf of Guinea, and forming a continuous restricted seaway from the Walvis Ridge to North Africa (Fig. 13) (Tissot et al., 1980). By the end of the Turonian, the Atlantic Ocean had developed, with fully oxic marine conditions (Fig. 13).

The basin was initially a rift branch of the proto-Atlantic, which includes the Rio-Muni, North Gabon (West Africa), and Sergipe-Angolas (Brazil) (de Matos, 1992a, Davison, 1997). During the later passive margin phase, the basin experienced several additional regional tectonic events resulting in inversion and folding in the Santonian, and gravity sliding during Early/Mid/Late Tertiary time (Brownfield and Charpentier, 2006; Le, 2012, 2021). These events are marked by major unconformities including the Albian-Aptian break up unconformity (115 Ma), Middle Cretaceous (Santonian - ~ 85 Ma), Late Cretaceous (K/T boundary - ~ 70 Ma), and Mid-Oligocene (~30 Ma), Mid-Miocene (~15 Ma), and Late Tertiary event (~5.3 Ma) (Lawrence et al., 2002; Iboum Kissaaka et al., 2016; Le, 2021; Mienlam Essi et al., 2021; Yugye et al., 2021) (Fig. 12).

2.5 Petroleum system of the study area

Exploration in the Kribi-Campo Sub-basin began in 1969, the first well to be drilled (Mobil) in the Kribi-Campo sub-basin in which the Ntem licence block lies was the Kribi Marine-1 which TD'd and penetrated over 1000m of Aptian age salt. Following this, there was a 10-yr drilling hiatus until 1979, when Mobil/Total consortium drilled the Sanaga Sud A-1 discovery of gas-condensate within the Aptian-Albian-aged Mundeck Formation, that exploration accelerated with the drilling of 11 discoveries in the Cretaceous, two with secondary Tertiary reservoirs.

This exploration phase was primarily focused on the shallow water Kribi-Campo Sub-basin, targeting Cretaceous tilted fault-block plays, which also extend onshore, where oil is currently produced from the overlying Cretaceous Logbadjeck Formation in the Mvia Field.

Despite the early success, production was not established until 1997 in the Ebome Field. Today, more than 1 million bbls of oil is produced annually from the Kribi-Campo Sub-basin (Loule et al., 2018).

2.5.1 Source rocks

Source rocks have been identified from several stratigraphic levels including the:

- aptian/albian (Mundeck Formation); the main rocks are the marine (transgressive) oil-prone source rocks preserved in the Upper Mundeck Formation, which correlate with the organic rich Albian-Turonian interval formed during the Atlantic marine anoxic event. They contain rocks with 15 kg Hydrocarbons/tonne yield and an average of 7kg/tonne. They have fair- to-good TOC and the HI > 300; gas-prone values of HI also occur with the Lower Mundeck Formation exhibiting the highest HI (400-700). (Pauken, 1992; SPT, 1995).
- upper Cretaceous (Logbaba Formation); the Logbaba shales have low- to fair TOC values but very low HI values (> 100) and the kerogen presents large components of land plant and burnt material with poor gas-prone potential (SPT, 1995).
- oligocene/Miocene (Souellaba Formation); the best marine oil-prone rocks to the south of the basin in the Miocene deposits, while towards the north, the TOC increases, kerogen becomes humid and the rocks become gas-prone. TOC values of 2.5% and HI of 400 is observed. The Lower Souellaba prodelta mixed oil and gas prone sediment are the major source rocks (SPT, 1995).
- potential Paleocene/Eocene (N'kapa Formation); the N'kapa too has some fair TOC (2%) with very low HI (> 100). However, possible good source rocks are expected to be good towards the basin ward setting (SPT, 1995).

All the oil properties indicate that oils originate from terrigenous dominated source rocks deposited in a marine environment. Abundant oil seeps exist at the basin margins.

2.5.2 Reservoir rocks

The main reservoir units in the Kribi-Campo sub-Basin can be grouped as:

- Lower Mundeck Formation

It is characterized by sharp based blocky packages sand up to 150m separated by muddy intervals and discrete sands (Fig. 14). The reservoirs are lacustrine to fluviatile sands. The porosities range from 15% to 25% and locally exceed 30%. The permeabilities range between 15 mD to 420 mD (SPT, 1995; ECL, 2001).

- Logbadjeck Formation

The reservoirs are mainly deepwater sands in channel/fan deposits lying above the Senonian unconformity (Fig. 14). The poro-perm data are that of the Logbaba and porosities of 15% and permeabilities of 250mD are observed (SPT, 1995; ECL, 2001).

- Logbaba Formation

Offshore to the west, initial shelf, submarine fans develop with turbidites present. A local restricted separate fan system is developed at Kribi area shallow marine clastics occur close to the basin edge and proximal to the topography on the Senonian unconformity (Fig. 14). The reservoirs are mainly deepwater marine sands in slope and base-of-slope settings. The porosities range from 6% to 23% and the permeabilities averages 50mD (SPT, 1995; ECL, 2001).

- Souellaba Formation

The best reservoirs are reworked transgressive shoreline sands and the deep-water sands in the slopes, base-of-slopes and basin floor fan settings (Fig. 14). The sands are thin with good reservoir qualities. The porosities of 30% and the permeabilities of 225 mD (SPT, 1995; ECL, 2001).

- Matanda Formation

In terms of reservoirs, the best ones are developed at the basin centre, where good reservoir shoreline and inner shelf sandstones and formed. Limited data exist in terms of reservoir quality, but, they are probably relatively good (Fig. 14, SPT, 1995).

2.5.3 Seals

In the Kribi-campo sub-basin, the seal is present in the Logbadjeck, Logbaba, N'kapa and Souellaba formations. Shales from across the different stratigraphic levels provide the seals. The turbidites are sealed by intraformational slope/basin shales and the shelf sandstones are sealed by intraformational shelf mudstones (SPT, 1995).

2.5.4 Play Types

Within the entire of the Kribi-Campo sub-basin, six main play types are recognized (ECL, 2001; Sterling, 2010). These are: (1) tilted fault blocks on the Kribi Campo High, (2) inner shelf fluvio-deltaic to turbidite channelised sands in combination traps (3) pinch out of clastic sequences against the flanks of the high, (4) salt induced structures, (5) slope apron submarine canyon and/or channel complex and (6) basin floor submarine fans, channels and crevasse splays. Fig. 15 illustrates the mix of these play types by prospect name.

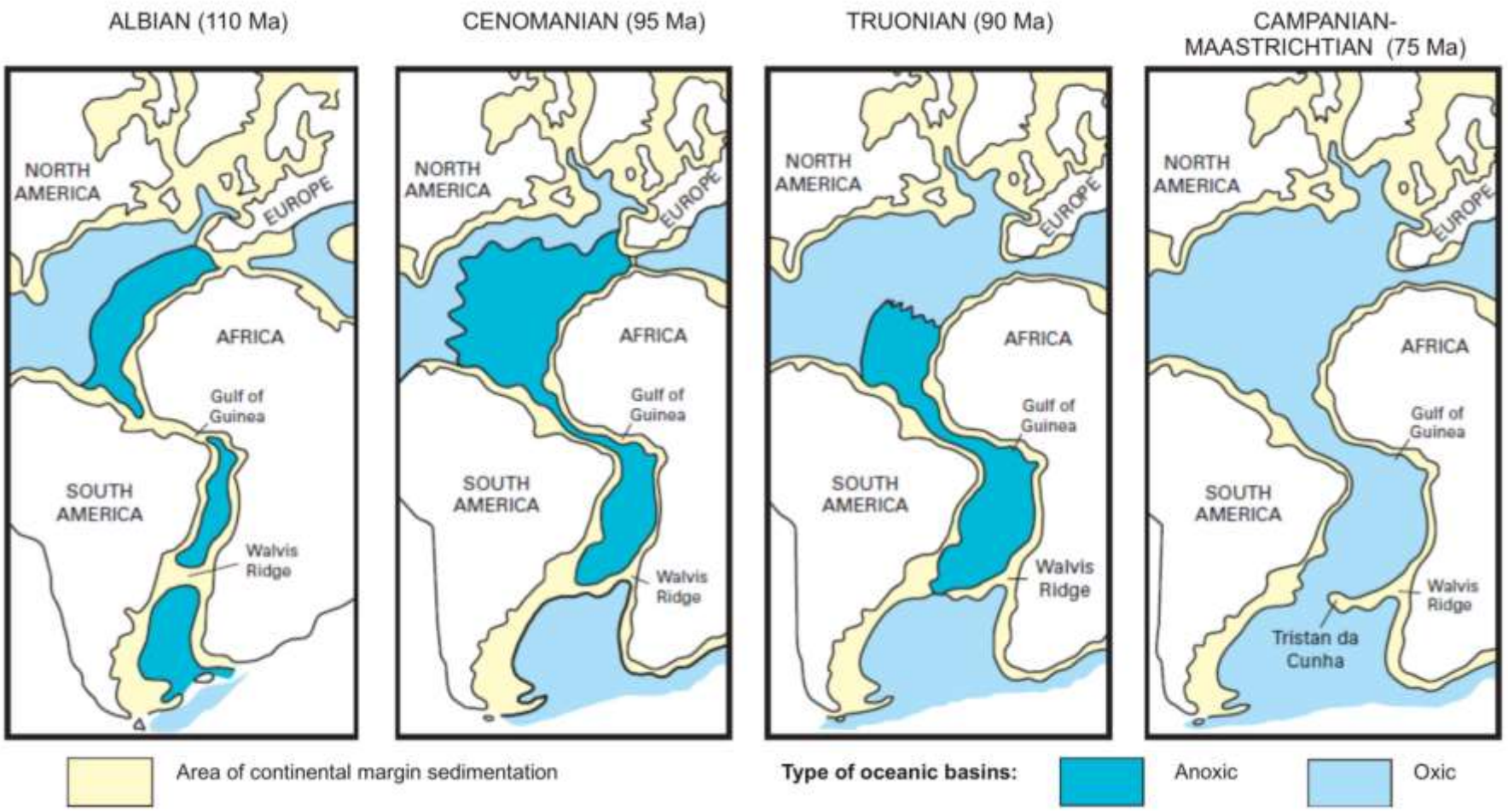

Figure 13. Paleogeographic maps of the Cretaceous breakup of Africa and South America, showing the distribution of restricted seaways (anoxic) to fully open marine (oxic) environments through the Cretaceous in the Atlantic basins. Oxygen content of oxic water is probably less than present concentrations in normal oceans (after Brownfield and Charpentier (2006), adapted from Tissot and others (1980).

The tilted fault blocks on the Kribi-Campo High have been the focus of drilling and development in this southern part of the Douala sub-basin. Aptian-Albian fluvial lacustrine, fan delta and turbiditic sandstones are the primary reservoirs within these fault blocks that are sealed by the combination of an erosional unconformity (Santonian age) and overlying Tertiary shales and mudstones (SPT, 1995). Campanian-Maastrichtian fluvio-deltaic to turbiditic sandstones have been successfully tested for oil/gas within the Kribi-Campo High area (Kribi L-1, Kribi Y-1 and Kribi D-1). The trapping mechanism is not certain but is likely to be structural rollover features that have formed as a consequence of reactivation of underlying faults that define the tilted fault block plays of Aptian-Albian sequences (SPT, 1995; ECL, 2001).

A third play type that is more envisaged versus confirmed is the pinch out of Late Cretaceous and Tertiary sequences against the outboard flanks of the Kribi-Campo High which lies along the eastern margin of the study area. No wells have drilled this play type but the expectation that these are likely to exist have been supported by Sterling mapping in study area (Sterling, 2010).

It has been noted earlier that the Kribi Marine-1 well intersected some +1000 m of Aptian salt in what appears on seismic to be a salt diapir situated on the northwestern edge of the Kribi-Campo High (SPT, 1995). The diapir is also very near to the northeastern extension of the Kribi Fracture Zone (KFZ) and may have resulted to fault movements along the KFZ. The exploration target and play type were Cretaceous and Tertiary sands, which if present would form a combination trap of 3-way dip closure against a salt side seal. Other yet drilled salt diapir features may be present in the area. Sterling has identified a “salt type feature” in the southeastern corner of the study area and may represent a salt raft and potential 4th play type that is very near to the Sterling’s Faraday Prospect (Sterling, 2010). The fifth play type that has been tested within 6 km of the study area’s eastern border is Perenco’s operated CM-1A well (2003) in the neighbouring Ebodje block. The well was to test a seismically defined submarine canyon feeder system located on the steep, westerly dipping Kribi Campo High. The well was P&A’d with oil shows in high density gravity flow units that were deposited within a submarine canyon in a steep slope apron depositional environment (Sterling, 2010).

The sixth recognised play type in the study area is Cretaceous and Tertiary aged basin floor submarine fans, channels and crevasse splays that are preserved outboard of the Kribi-Campo High into the deep-water basin proper (Sterling, 2010).

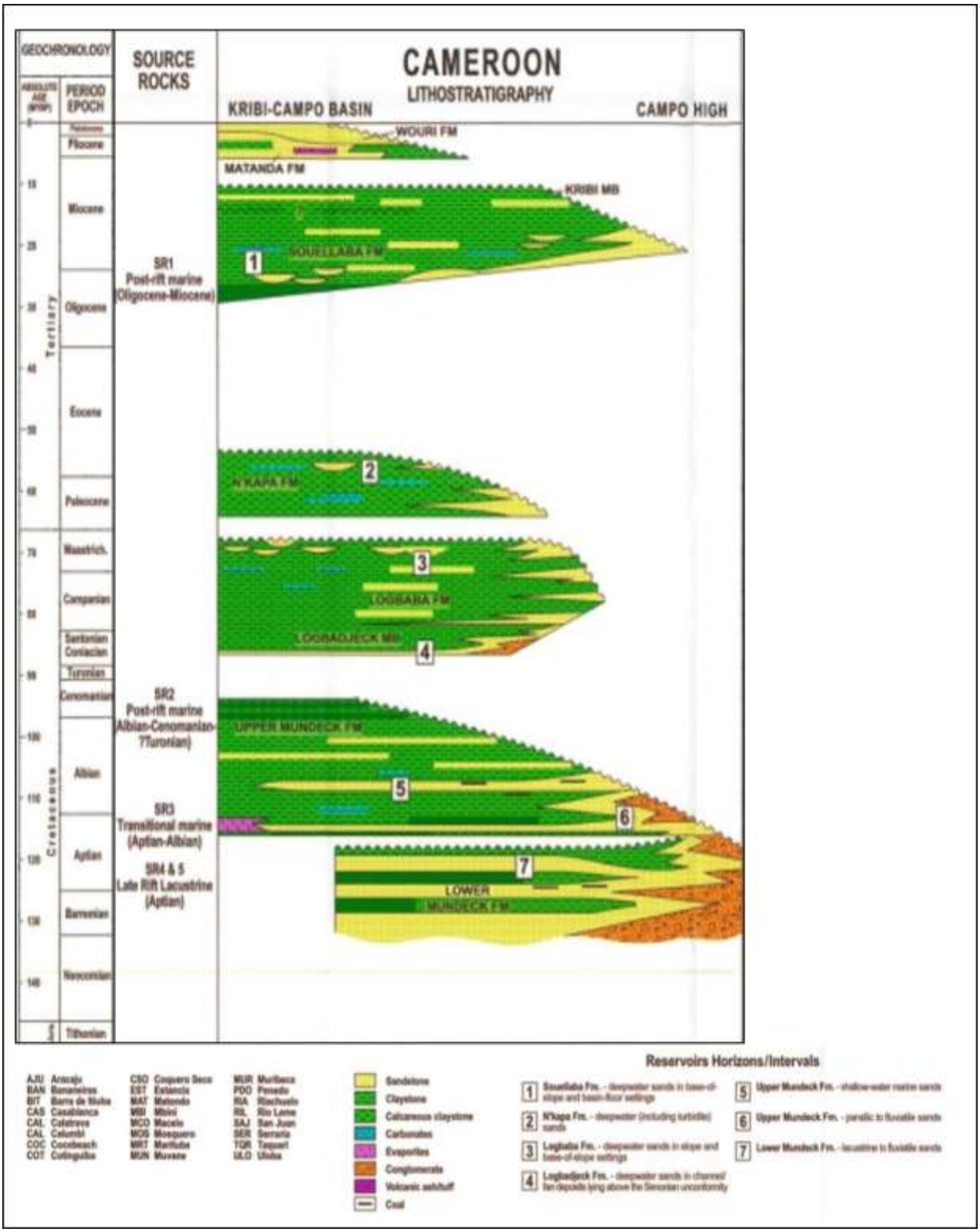

Figure 14. Reservoir rocks in the Kribi-campo sub-basin (ECL, 2001).

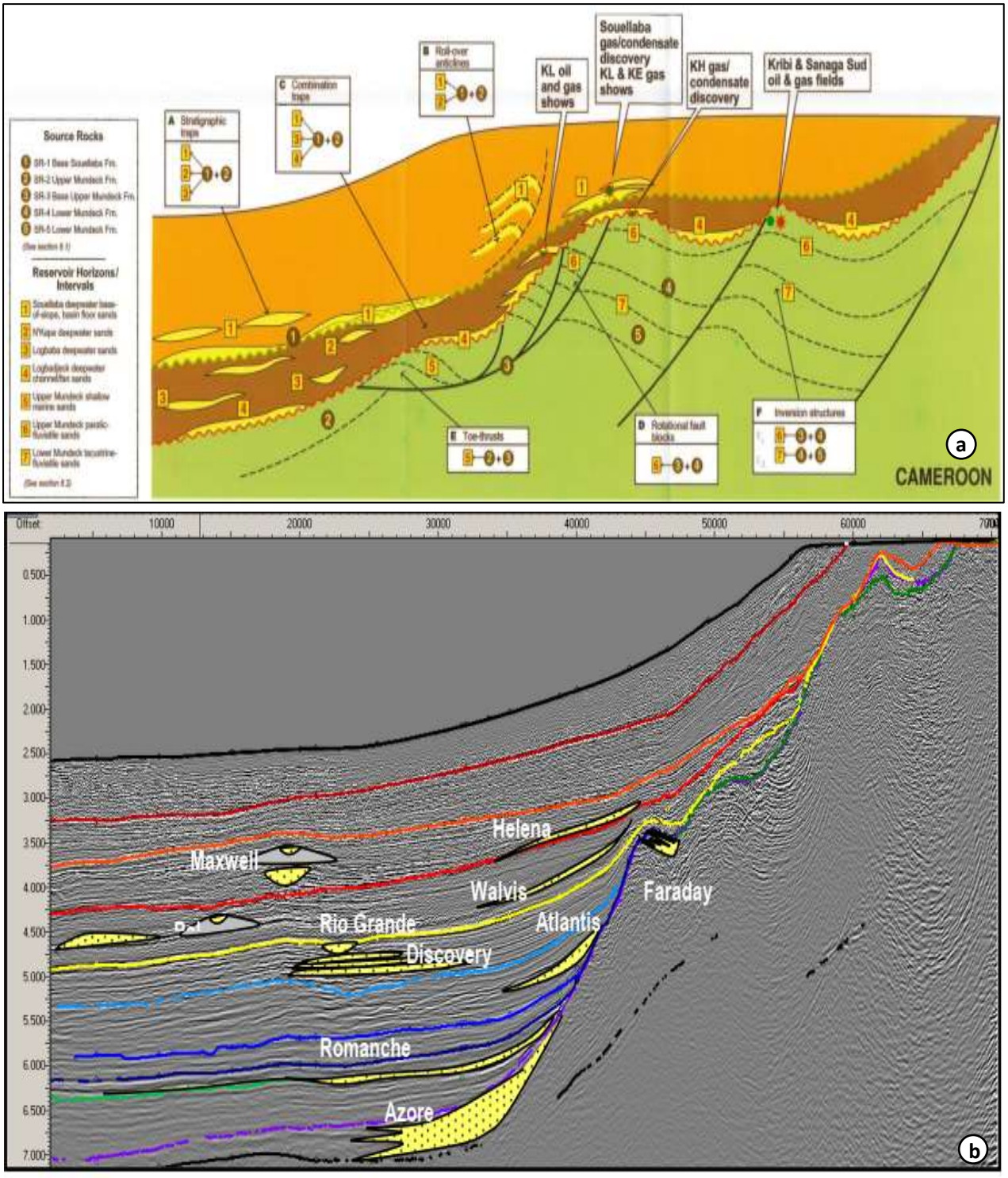

Figure 15. a) Cross section illustrating the stratigraphic and structural play types b) 3D seismic line through study area showing play types (ECL, 2001; Sterling, 2010).

Table 1. Identifies the specific stratigraphic and structural play types that have been identified to date (Sterling, 2010).

TRAP TYPES		
Stratigraphic elements	Structural elements	Age
Submarine canyons		
Debris flow, Channels, Levees		Miocene
Channel complexes		
Channel belt	**Wrench related closure**	Palaeogene, Cretaceous
Channel-Levee	**Compaction drape**	Maastrictian & Palaeocene & Mio
Submarine Fan Complex		
Slope Fan Lobe	**Fault assisted**	Tertiary, Cretaceous
Meandering channel belt	**Fault block**	Cretaceous Senonian-Campanian
Distal Fan Lobe		Cretaceous (Maast-Camp, Albian-Cen)
Pinch-out or Remnant		Aptian and Albian

The Kribi-Campo sub-basin is located along the West African passive margin, in the southern part of the Gulf of Guinea. Its formation is closely linked to the opening of the South Atlantic. Located on a continental margin oriented NNE-SSW, this sub-basin is crossed by two oceanic fracture zones: the Kribi fracture zone, which separates it from the Douala sub-basin, and the Campo fracture zone, which structures the high Campo that forms the boundary with the Rio Muni basin in Equatorial Guinea. Its stratigraphy comprises nine formations: Lower Mundeck, Upper Mundeck, Logbadjeck, Logbaba, N'Kappa, Souellaba, Kribi, Matanda and Wouri. Six main play types are recognized Kribi-Campo sub-basin such as tilted fault blocks on the Kribi Campo High, inner shelf fluvio-deltaic to turbidite channelised sands in combination traps, pinch out of clastic sequences against the flanks of the high, salt induced structures, slope apron submarine canyon and/or channel complex and basin floor submarine fans, channels and crevasse splays.

Chapter 3: Materials and Methods

This chapter summarizes the materials and methodology used to answer the research questions presented in the introduction section. A review of techniques of seismic surveying and well log are provided below and methods used in this research are outlined.

3.1 Seismic data acquisition

Seismic waves are created by a controlled source and propagate through the subsurface (Kearey et al., 2002). Some waves will return to the surface after refraction or reflection at geological boundaries at the subsurface. Instruments distributed along the surface detect the ground motion caused by these returning waves and hence measure the arrival times of the waves at different ranges from the source (Fig. 16). Arrival times may be converted to depth values providing information on the subsurface geological interfaces (Kearey et al., 2002). Body waves generated at seismic source include compressional (P-primary wave) and shear waves (S-waves). Body waves propagate through the interval volume of an elastic solid, P-waves travel in the direction of wave travel while shear waves propagate by a pure shear strain in a direction perpendicular to the direction of wave travel (Sheriff and Geldart, 1995; Kearey et al., 2002).

Seismic sources include dynamite, vibroseis, mini-sosie (or wacker), shotguns, electrical sparkers, boomers, weight drops and hammers, air guns and water guns (Fig. 17). The choice of seismic source is dependent on the environment in which the survey is done (land or offshore), the desire to obtain the sufficient energy across the broadest possible frequency, the necessity to obtain a repeatable source waveform, and environmental issues. The main goal of any survey is to reduce the noise ratio compared to the signal produced from the geological interfaces (Sheriff and Geldart, 1995; Kearey et al., 2002). In marine reflection seismic surveys the energy source is typically an array of air guns (a single gun in the case of a vertical seismic profile) with receivers in various combinations towed by a vessel at the sea surface (Fig. 16). Marine seismic reflection surveys are mostly concerned with Pwave reflections, as fluids do not transmit S-waves (Sheriff and Geldart, 1995; Kearey et al., 2002).

Fundamental to the seismic reflection method is the property of a layer termed acoustic impedance (Z), which can be defined as: $\boldsymbol{Z = \rho V}$ **(Eq. 1)**

Where ρ is the density of the rock or sediment and V is the velocity of a P-wave through the rock or sediment. Contrasts in acoustic impedance determines the reflection coefficient at normal incidence (Sheriff and Geldart, 1995; Kearey et al., 2002).

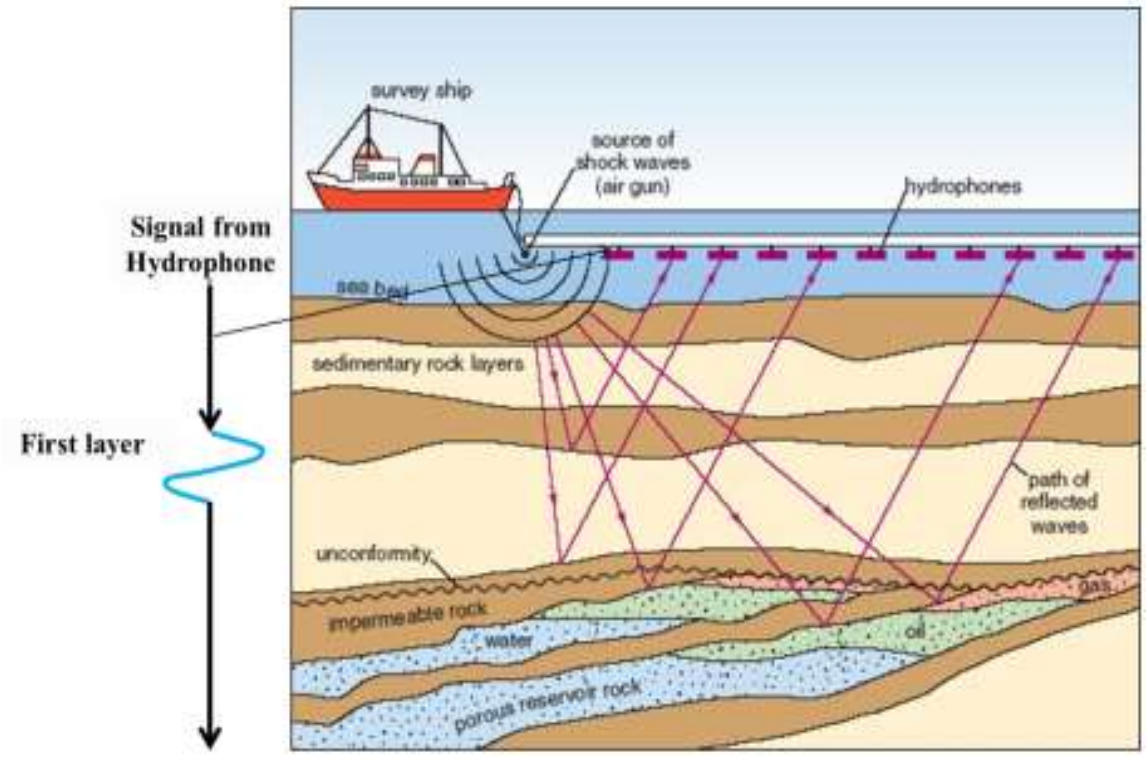

Figure 16. The principles and techniques of seismic reflection survey in offshore area (Modified from http://www.epa.gov/esd/cmb/GeophysicsWebsite).

The velocity of a P-wave through an isotropic, homogenous solid is controlled by the elastic constants and density of the material (Sheriff and Geldart, 1995). Rocks and sediments are rarely isotropic or homogenous, and as such the velocity of wave will vary depending on composition, porosity, and fluid content, which may all vary in the three dimensions (Sheriff and Geldart, 1995; Kearey et al., 2002).

3.1.1 3D seismic survey

Seismic surveys are achieved through the design of appropriate line geometry for source and geophone locations. The general practice is to lay out geophones and source set in a rectangular grid, called dip lines and strike lines (2D) or inlines and crosslines (3D) (Stone, 1994). A *dip line* follows (at least approximately) the line of steepest descent down the structure; it minimizes the problem of reflections originating out of the plane of section. A *strike line* follows (at least approximately) a contour line on the structure (Stone, 1994). Initial knowledge of the structure could be derived from surface geology, or regional geology, or satellite imagery, or previous geophysical surveys such as gravity and magnetics (Weimer and Davis, 1996; Vermeer, 2000).

Figure 17. Examples of seismic acquisition sources a) Vibroseis in a set b) Weight dropping and sledge hammer c) geophones d) weight dropping e) Air gun used for marine survey

For example, if the structural trend of the prospect area trends northwest-southeast, the dip lines will be in NE-SW and while strike lines NW-SE. A simple rectangular grid will suffice for simple structures such as anticlines, faults and simple stratigraphic sequences. For complex structures such as salt dome or a patch reef, an additional number of radial lines will be required to map the flanks of the structure. Planning the survey layout may include planning for both surface and sub-surface factors potentially affecting the seismic processing algorithm, particularly structural local dips and local topography (Stone, 1994).

The layout of 3-D lines involves a greater volume of work that 2-D seismic although their principles are the same. Most surveys are planned using workstations. These allow the planner to superimpose the survey on a topographic map so that operational problems can be integrated into the planning process. Marine streamer 3-Ds and oblong land 3-Ds have longer offsets in a defined azimuth (Weimer and Davis, 1996; Vermeer, 2000). The choice of this azimuth will depend on the structure and processing methods to be applied. If the long offsets are parallel to dip, then the NMO correction will vary according to dip, and may be difficult to achieve accurately. This problem is mitigated by the use of DMO or pre-stack depth migration.

If the long offsets are parallel to strike, then there will be no variation in stacking velocity as a function of dip and the processing becomes simpler (Weimer and Davis, 1996; Vermeer, 2000). However, this method may require closer CMP spacing in the cross-line direction, which may be expensive to achieve (Vermeer, 2000). In addition, the acquisition parameters can sometimes be designed to obliterate certain kind of multiples before the data is processed. These will be discussed further in the next section.

3.1.2 Seismic Processing

The main goal of seismic processing is to obtain the most precise representation of the subsurface information inferred from the seismic. It is central to the seismic prospecting technique, hence, the reason why it is ambiguous and extremely time consuming. The goal of seismic processing is to produce higher signal-to-noise ratios (SNR) than raw seismic data. A typical processing flowchart and algorithm is provided in Fig. 18. The readers can refer to seismic processing technique of Sheriff and Geldart (1995) and Yilmaz (2001) for further details.

3.1.3 Seismic interpretation

The main approaches to seismic interpretation include structural and stratigraphic analyses (Kearey et al., 2002) (Fig. 19). The former reflect studies of reflector geometry on the basis of reflection times with the sole goal of searching for structural traps containing hydrocarbons. On the contrary, seismic stratigraphy study of depositional facies and stratigraphy from seismic data utilizing its unique properties that allow direct application of geologic concepts based on physical stratigraphy (Mitchum Jr et al., 1977a; Vail and Mitchum, 1977). Furthermore, sequence stratigraphy is a methodology that provides a framework for the elements of any depositional setting (channel, fans); it facilitates paleogeographic reconstructions and the prediction of facies and lithologies away from control points (Catuneanu et al., 2011).

Mitchum Jr et al. (1977a) defined that seismic stratigraphy study consists of two approaches: seismic sequence analysis and seismic facies analysis. Seismic sequence is a depositional sequence interpreted from seismic data, genetically related strata, bounded by surfaces at the top and base (unconformities or their correlative conformities) marked by reflection terminations (Fig. 20); lap-out (onlap, downlap and toplap), truncation (erosional and structural) and concordance (no termination) (Mitchum Jr et al., 1977a; Vail and Mitchum, 1977). Whereas, seismic facies analysis is the description and geologic interpretation

(sedimentary processes, depositional environments, sediment source, geological setting, etc.) of seismic reflection parameters, including reflection configuration (Fig. 20), continuity, amplitude, frequency, interval velocity, external form and areal association of seismic facies units (Mitchum Jr et al., 1977a).

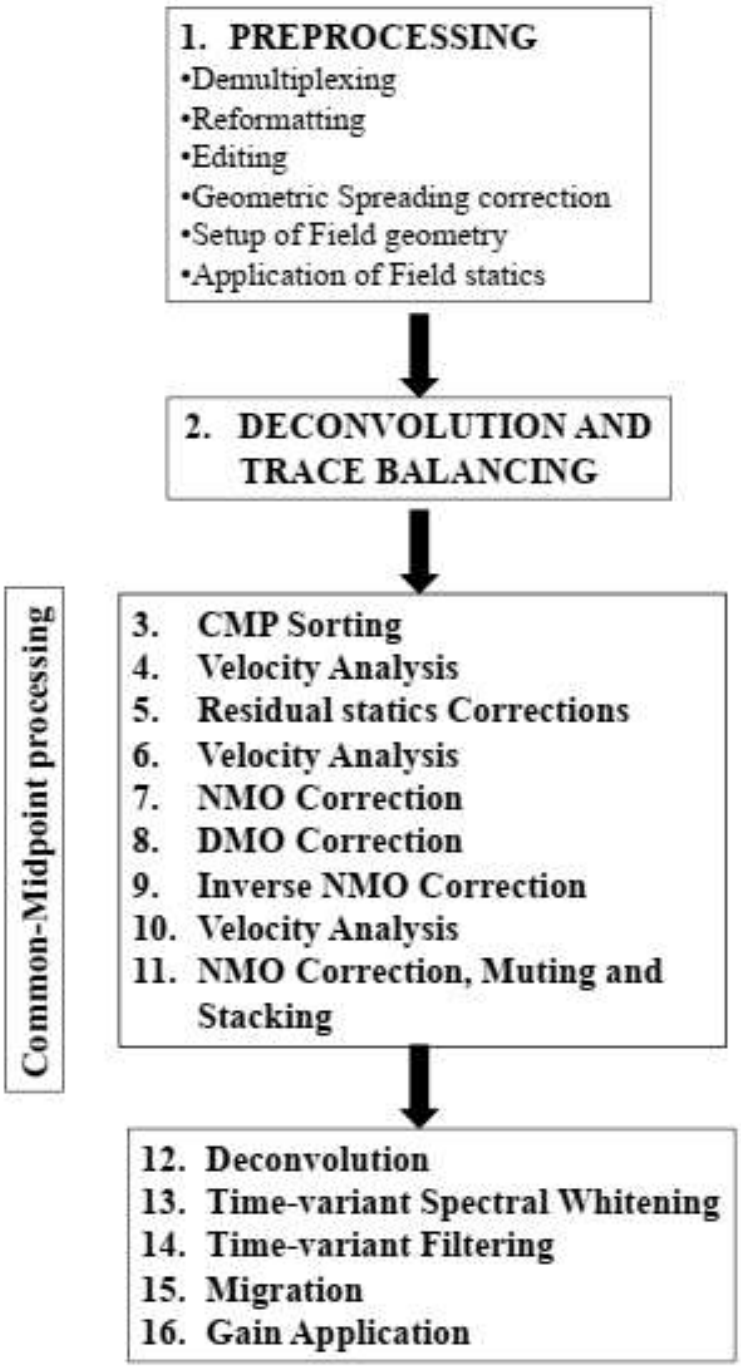

Figure 18. Flow chart for conventional seismic processing (Yilmaz, 2001).

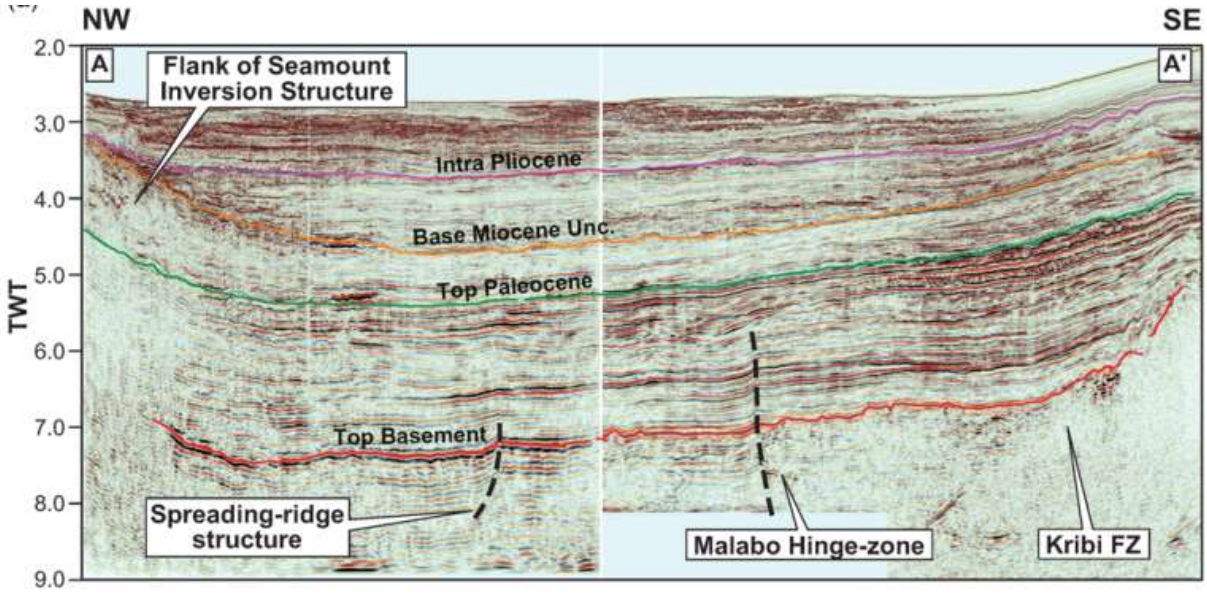

Figure 19. Example of structural and stratigraphic seismic interpretation. The seismic section was interpreted from a section of the dataset Douala/Kribi-Campo and Rio Muni basin (Lawrence et al., 2016).

Two dimensional (2-D) seismic data provide a cross-section beneath the Earth's surface unlike 3-D data, which images the subsurface geology as a volume in x, y, z direction. Seismic profiles are usually displayed with vertical (z) axis in two way travel time [TWTT (s/ms)] or depth (m) and horizontal (x, y) axis in metres (m) or kilometres (km). Two-way travel time (TWTT) can be converted to depth using appropriate P-wave velocities (Brown, 2005a).

3.2. Well logs

When drilling wells, information from the borehole is collected by different logging tools during, or after drilling operations. This data is called measured while drilling (MWD) or wireline (WL) data. A well log is defined as a continuous recording of a geophysical parameter along a borehole (Rider and Kennedy, 2011). Some of the most important well logs are the gamma ray log, sonic, density, neutron porosity and the resistivity log.

- **The gamma ray log**

This log measures the natural gamma radioactivity from uranium, thorium and potassium in a formation, where the output is the total count rate of these. The GR does not distinguish between the individual elements (Rider & Kennedy, 2011). Metamorphic, igneous and sedimentary rocks contain traces of gamma-emitting elements. When it comes to sedimentary rocks, shale exhibit the highest radioactivity. Because of this, the gamma log is often called the "shale log", even though it is not equivalent to the amount of shale content. (Rider and Kennedy,

2011). The gamma ray is commonly used for correlation of different strata, like picking well tops while drilling. It is also helpful in identifying lithology, stratigraphic surfaces, facies and sequences. The unit for the GR log is the API, defined as 1/200 of the difference between two reference units. An average shale usually represents 100 API units, while sandstones and carbonates normally have low API (10-40 API) compared to shales (Rider and Kennedy, 2011). The gamma ray is considered as the most useful logging tool in sequence stratigraphic analysis, as it can be used to assess the relative proportions of sand and mud within a succession. In general, muddy sediments indicate deeper marine deposition than sandy successions. Lower energy in deeper marine environment causes smaller grains to be deposited, contra shallower marine environment with more energy and capacity to accumulate coarser grains (Nichols, 2009). A trend with decreasing values upwards on a gamma-ray log can indicate increase in sand content and be interpreted as a shallowing-up succession. An increase in the reading indicates a higher mud content. This can be used as evidence for a flooding surface (Nichols, 2009). Trends in sand and mud content on gamma logs within flooding surfaces can be used to identify patterns which can be recognized as either progradation, retrogradation or aggradation through the succession. The gamma ray log can also be used to distinguish between sand-filled channel successions and mud-rich floodplain. River channels are characterized by sharp increases in sand content (low gamma log value) at the base followed by a trend with increasing gamma log values, meaning more mud-rich material. The GR can also be important to help identify fluvial facies which can be indicators of sequence boundaries. Maximum flooding surfaces may also be picked up on more sophisticated gamma logs, the spectral gamma logs, which could read a characteristic increase in the potassium content indicating a concentration of glauconite (Nichols, 2009).

- **The density log**

Density logs reads the bulk density of formations, including the density of the rock and potential fluids enclosed in the pores. By emitting gamma radiation into the formation, the density log measures the induced radiation. The attenuation and re-emitting of gamma rays is a function of the electron density (electrons/cm^3) of the formation, which is closely related to density, measured by g/cm^3. (Rider and Kennedy, 2011). The density log can calculate the hydrocarbon volume and density. It can also model seismic response by calculating acoustic impedance (density multiplied with sonic log). When combined with the neutron log, it is a good indicator of general lithology (Rider and Kennedy, 2011).

- **The neutron log**

This log measures how a formation reacts to neutron bombardment. A source emits high energy neutrons into the formation, and a receiver measures the numbers of low energy neutrons that are reemitted back. Since emitted neutrons strongly respond on hydrogen in the formation, the returning amount of neutrons strongly depend on the hydrogen content. In high porosity rocks, the neutrons are slowed quickly down and absorbed. This causes the count rate to be low. In low porosity rocks, the emitted neutrons travel further, making the count rate higher (Rider and Kennedy, 2011).

Hydrogen appears in all formation fluids (water, oil and gas), but not in all minerals. Because of this, the response from the neutron log could be correlated with porosity (Rider & Kennedy, 2011). The neutron log output scale is given in neutron porosity units. This is an indication of the hydrogen index for the formation, and is given as percentage or fraction. Typical values for sandstones is between 0 - 30 %, and for shales, values between 25 – 75 % is normal. The neutron log is often plotted with the highest values to the left and lowest to the right (Rider and Kennedy, 2011)

- **The sonic log**

The sonic measures the formation's capacity to transmit sound waves by measuring the time it takes for a sound wave to travel a known distance within the formation. The sonic logging tool consists of one or two transmitters and several receivers where the distance between them is known. (Rider and Kennedy, 2011). The sonic log measures the velocity, but it is frequently expressed as slowness, with unit μs/ft. Typical values for formations in the subsurface range from 50-150 μs/ft, corresponding to velocity of 6000-2000 m/s. The main use of sonic log is seismic investigations by contribute to depth conversions, velocity modelling and performing well-to-seismic tie. By combining the sonic log with the density log, an acoustic impedance log can be established, which can be used to create a synthetic seismogram. (Rider and Kennedy, 2011).

- **Check-Shot Survey**

The check-shot survey, also known as well velocity shooting, is conducted to measure the true average velocity needed for converting recorded reflection times to depths of geologic formations. With a source firing at the surface, it records the first arrivals of direct waves (the first breaks) by deploying geophones in the well, placed at different depths, usually at irregular and at large intervals. The energy source is placed as close as possible to the well-head of a

vertical well (without any risk to the well), so that the ray path travels straight down to geophones measuring the true vertical velocity. In the case of a deviated well, the source to receiver travel path becomes slant and needs a simple correction of cosine factor for conversion of drilled depth to true vertical depth to provide the true velocity. The receiver depth spacing in the well is chosen with the geophones placed preferably close to the major litho-boundaries to provide the formation velocities accurately. The spacing is commonly irregular and random, typically 75–150 m (Brewer, 2002), depending on a trade-off between precise velocity measurements at more depth points and the additional cost incurred because of required increase in rig-time.

Direct travel times of seismic waves from the surface (source) to the geophones in the well provide accurate measurement of true average velocities at the receiver depth points. A graph, plotted with first arrival time recorded at the geophone versus its depth (T-D curve), provides the true average velocity function, which is the key requisite for crucial conversion of seismic times to geologic depths. The check-shot data, besides being useful for time-depth conversion, also plays a significant role in correcting sonic velocities which are used for preparing synthetic seismograms or continuous velocity logs (CVLs) to calibrate seismic. Constrained by check-shot, the corrected sonic velocities offer accurate estimation of interval velocities for thin formations which is not doable in check-shot survey due to time and cost constraints.

3.3 Dataset utilised in this study

The datasets analyzed in this study consist of a high-resolution 3D seismic reflection survey and borehole data from the Kribi-Campo Sub-basin offshore Cameroon (Fig. 11; Table 2).

Table 2. Datasets with their different file format and type.

Data		**File Format**	**Type**
Seismic		SEGY	Volume
Borehole	**Well logs**	LAS	Well
	Well tops	ASCII (*.*)	Well tops
	Checkshots	ASCII (*.*)	Well velocity

3.3.1. Seismic data

The 3D seismic survey is a pre-stack time migrated (PSTM) dataset that covers an area of about 1500 km^2 in water depths ranging between 600 m and 2000 m (Fig. 21). It was acquired

using 10 streamers, with a 12.5 m group interval. The separation between the streamers was 100 m, with a spatial resolution of 25 × 25 m. It includes 1581 in-lines and 2051 crosslines with lines spacing of 25 m and a seismic recording sampling interval of 2 ms two-way travel time (TWT). The seismic survey was processed as a zero-phase at the seabed and displayed using the Society of Exploration Geophysicists (SEG) normal polarity (Brown, 2004).

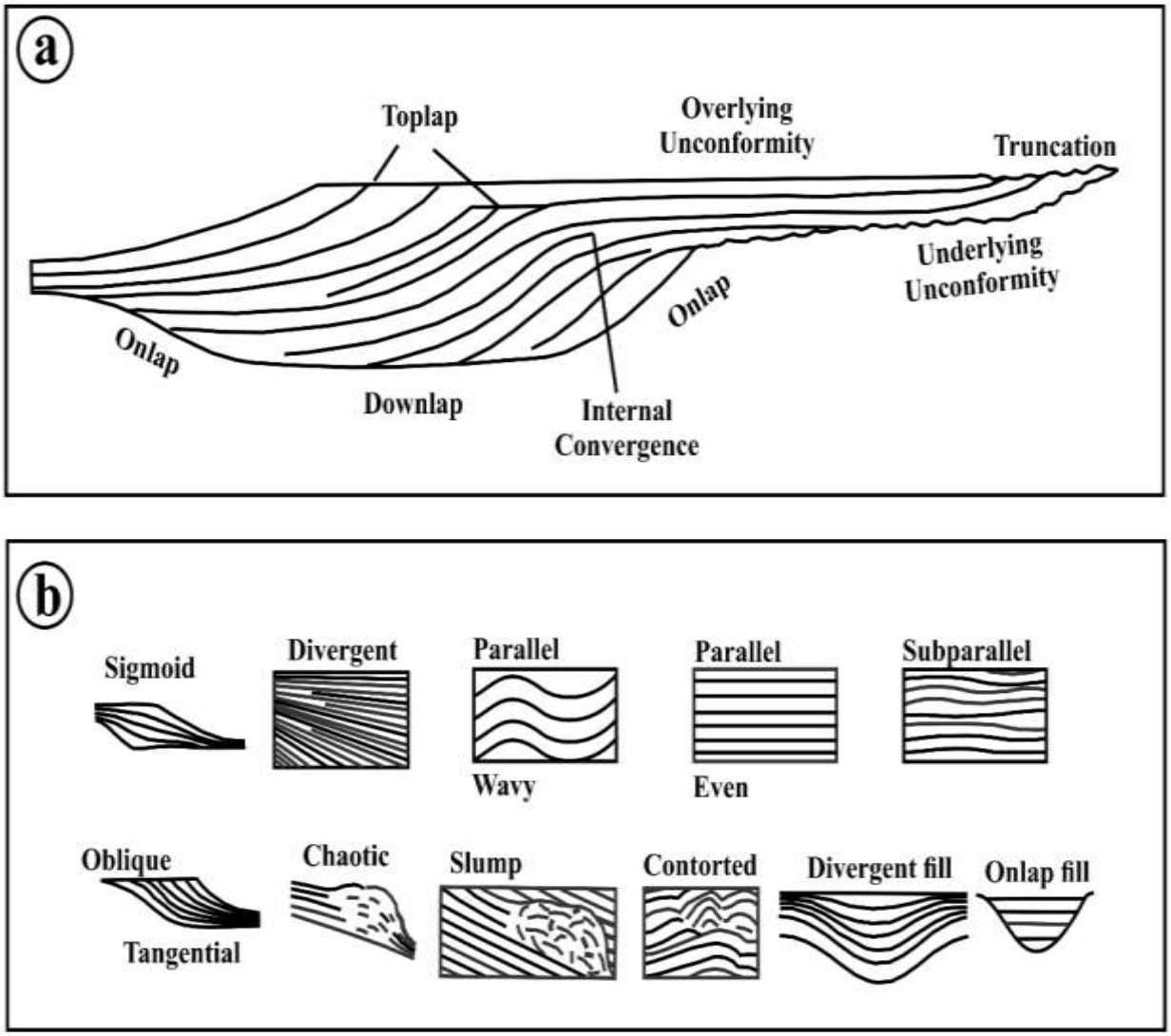

Figure 20. a) Seismic stratigraphic reflection terminations within idealized seismic sequences, and b) Seismic reflection configurations (Mitchum Jr et al., 1977a).

Hence, a positive event represents a downward increase in acoustic impedance (red, yellow, or orange reflection on seismic sections), and a negative event represents a downward decrease in acoustic impedance (blue reflection on seismic profiles). The seismic dataset reaches 6.6 s TWT. The dominant frequency of the data is 17 Hz for the Late Cretaceous and 45 Hz in the Cenozoic resulting in a vertical resolution ($\lambda/4$) of ~28 m and ~10 m, respectively (Le, 2012, 2021), with an average velocity of 2400 m/s derived from the check-shot data in the

interval of interest (4000–5000 ms). Further details on the processing algorithm are provided in Table 3.

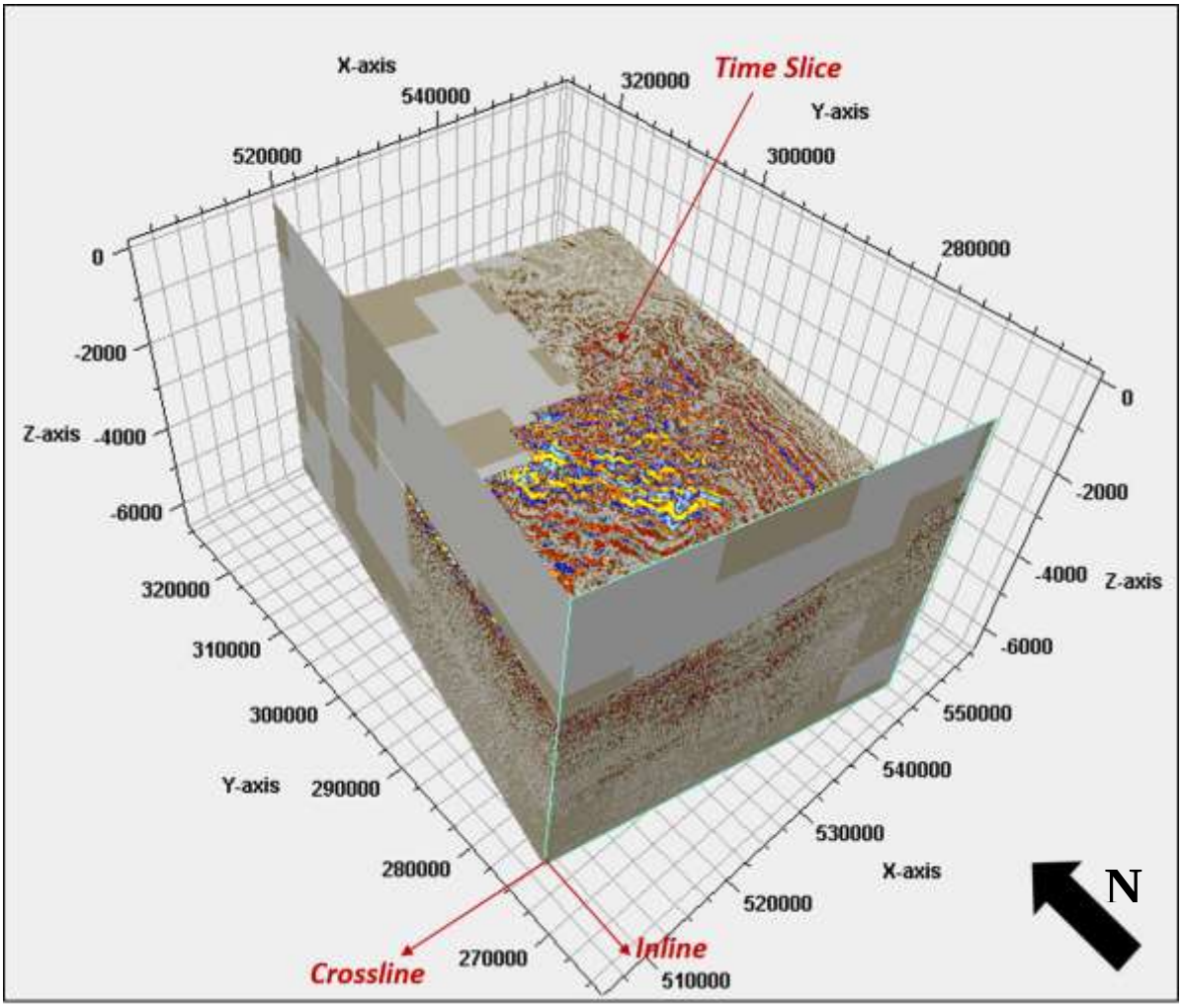

Figure 21. Seismic cube through the study area. Also shown in the figure are examples of an inline, crossline, and time slice. The interpreted seismic cube covers ~1500 km^2 in Kribi-Campo sub-basin, offshore Cameroon.

3.3.2. Boreholes data

The study integrates well log data from two wells W1 and W2 from the southern part of the Kribi/Campo sub-basin (Fig. 11). Formations tops of the two wells and the checkshots data for the well W1 were used to correlate the seismic and borehole data. Well data from the W1 wellbore were used to constrain the lithology and ages of the different horizons and sedimentary intervals interpreted. These two wells were analyzed to assess the reservoir quality and hydrocarbon potential of the clastic reservoir rocks of the Logbaba Formation. The well data were made available by the National Hydrocarbon Corporation (NHC), Republic of Cameroon.

Table 3. Acquisition parameters for the 3D seismic data (Sterling, 2010).

NTEM 3D PGS 2003	**Area (approx.)**	**1500 sqkm (full fold)**
	Operator	Amerada Hess
	Contractor	PGS
	Vessel	M/V Ramform Victory
	Type	Towed Cable
	Vintage	Q1 2003
	In-line orientation	11.7° / 191.7°
Production	Prime production (sail line km)	3304
	Infill production (sail line km)	622
Source	Number of sources	2
	Separation	50m
	SP Interval	25m flip flop
	Depth (nominal)	6m
	Array volume (cu in)	3090
	Pressure (psi)	2500
Streamer	Number of cables	10
	Streamer separation	100m
	Channels / cable	408
	Group interval	12.5m
	Streamer Length (nominal)	5100m
	Depth (nominal)	6m
CDPs	Bin size (natural)	6.25 x 25m
	Fold (nominal)	51
	Data density (traces/sqkm)	326,400
Data	Record length	8.196s
	Sample Interval	.002s
	Tape format	SEGD

The available well logs from W1 and W2 consist of conventional well log data including Gamma ray (GR), shallow, medium and deep resistivity logs (P16H, P28H and P40H respectively), density (RHOB), neutron (NPHI) and sonic (DT) (Table 4). The two wells drilled between 2013 and 2014 with a total depth of 4090 m and 4747 m respectively for W2 and W1 wells, below the seafloor corresponding to a stratigraphic interval ranging between Albian to Recent. The distance between the two wells is 22 km and these wells were selected because of penetrated the Late Cretaceous reservoir of the Logbaba Formation. Table 5. Shows well top of formation data provide the well to seismic correlation for geological age control.

Table 4. List of available well log data of the Logbaba Formation in the studied wells from Kribi-Campo sub-Basin.

Well name	**Top (m)**	**Bottom (m)**	**thickness (m)**	**Available well logs**
Well-W1	3947	4736	789	GR-DCAV-P16H-P28H-P40H-DT-RHOB-TNPH-DRHO
Well-W2	3215	4051	836	GR_ARC-DCAV-P16H-P28H-P40H-DTCO-RHOB-TNPH-DRHO-HFK-HTHO

Table 5. Formations tops of well log data studied in the Kribi-Campo sub-Basin.

	W1	**W2**
Formation Tops	MD(m)	MD(m)
Seabed	1570.5	712.87
Late Miocene	2210	----------
Middle Miocene	2369	----------
Lower Miocene	2648.4	1845
Eocene MFS	3025	2040
Paleocene	3530	2450
Maastrichtian	3814	3215
Campanian	3947	3645
Total Depth	4747	4090

3.4 Methods utilised in this study

In following chapter of this thesis, specific methodologies pertinent to that specific research theme are detailed. Seismic well tie, seismic stratigraphy, attribute analysis, seismic geomorphology are employed for analysis of the seismic data. Petrophysical analysis is the main methods employed for analysis the well log data. The interpretation of the seismic data and well log data have primarily used the Schlumberger™ Petrel and Interactive petrophysics software respectively. These software were used in the laboratories of the National Hydrocarbon Corporation (NHC), Yaoundé, Cameroon, and also in the University of Geneva.

3.4.1. Seismic well tie analysis

The first step was to accomplish the seismic to well calibration after loading the seismic survey and well data. To do this calibration, it was needed to develop a synthetic seismogram. The development of synthetic seismogram was based on four main steps in this project: sonic log calibration, seismic wavelet extraction, synthetic seismogram generation and integrated seismic well tie.

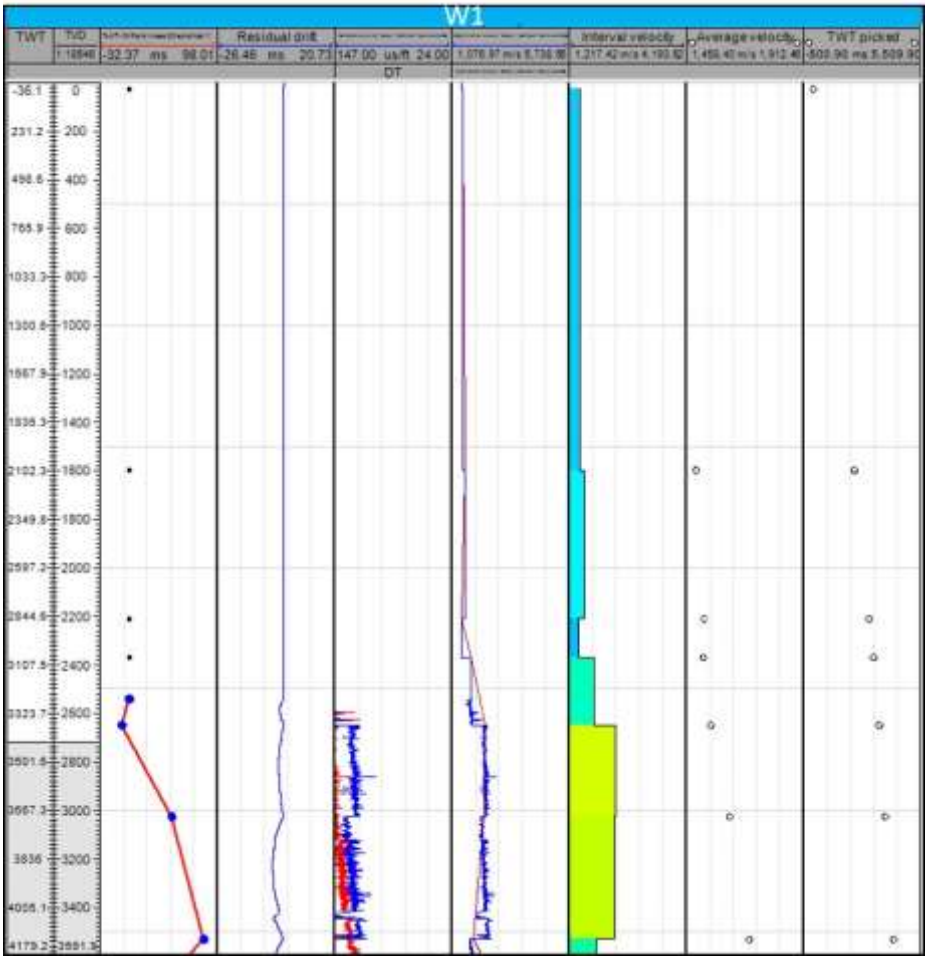

Figure 22. Sonic log calibration.

The spike values were removed from the sonic log using despiking tool prior to sonic calibration (Fig. 22). Sonic calibration was performed by adjusting the sonic values between checkshot points. This process was continued until the integrated sonic times coincided with those from the checkshot. The aim of sonic calibration method was to make a relationship between well depth and time for the well shown in Fig. 22.

After developing the sonic calibration, the wavelet extraction is necessary in prior to the synthetic seismogram generation. In Fig. 23, a wavelet was extracted directly from the seismic close to well. The wavelet displayed a positive zero phase, and the dominant frequency was in range of 17 to 45 Hz. Thus, the extracted wavelet demonstrated a good percentage of predictability which was above 60. It means that there is a good relationship between the seismic around the well and the reflection coefficient, considering Inline-crossline positions, the lag time and wavelet phase.

If the sonic log is correctly calibrated, and the best wavelet is extracted, the synthetic seismogram can be constructed. It is necessary to use the convolutional model to construct the synthetic seismogram. A basic assumption of this model for stacked seismic trace can be written as a convolution between a wavelet and reflection series:

$$y(t) = w(t) * f(t) \qquad (2)$$

Where $y(t)$, $w(t)$ and $f(t)$ denote recorded seismic signal, input signal and impulse response of the Earth, respectively.

The density and sonic logs are necessary for calculation of the acoustic impedances of various layers used to estimate the reflection coefficient on that interface. The equation of the reflection coefficient is described as a function of acoustic impedance:

$$RC = (AIi - AIi\text{-}1) = (AIi + AIi\text{-}1) \qquad (3)$$

Where *RC* and *AIi* are reflection coefficient and acoustic impedance, respectively.

In this study, output of the synthetic seismogram showed a very good match with seismic data in the area close to the well (Fig. 23). It means that the well data is almost perfectly tied to the geological markers. Good match between seismic data and synthetic seismogram is necessary for proper correlation of the stratigraphy in the well.

3.4.2 Seismic stratigraphy

The approach used here consists of the seismic interpretation of ten horizons (KC-1 to KC-9, and the seafloor). These seismic horizons were tied to the well W1 using the checkshot data for the geological age correlation (e.g., Albian to Pliocene).

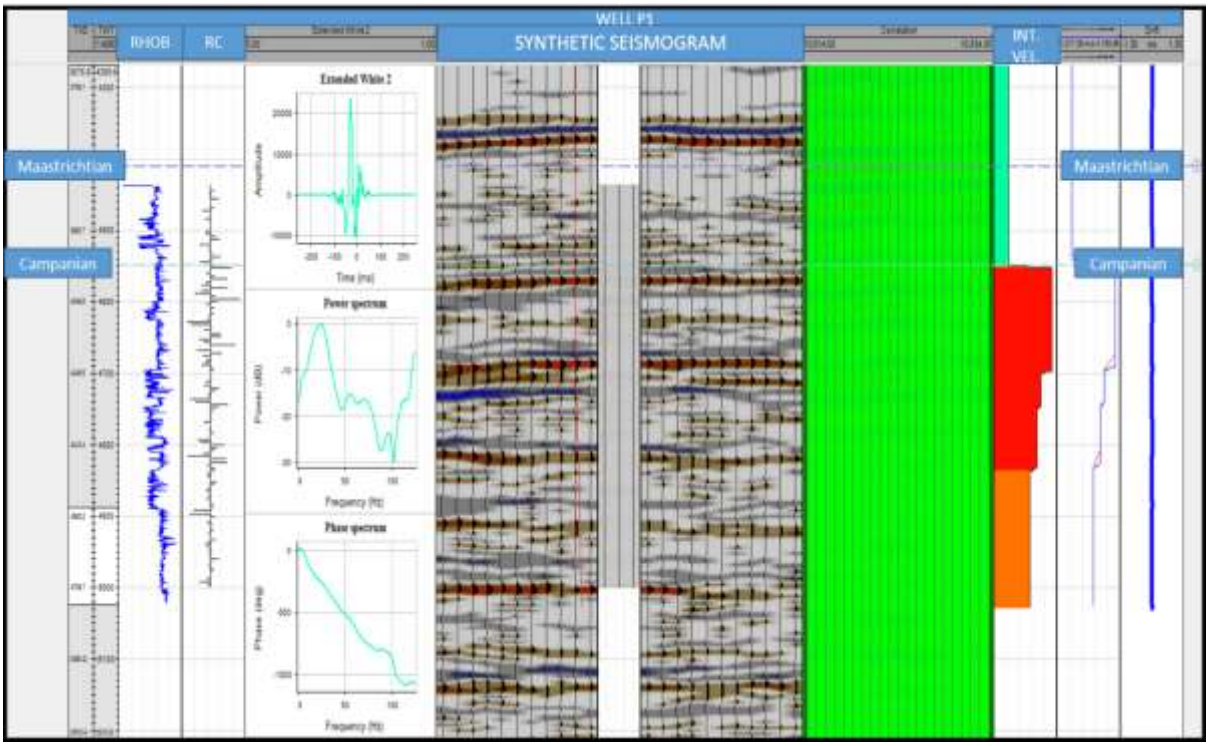

Figure 23. Synthetic seismogram generated by the checkshot and sonic log data in well W1. Wavelet is generated from the seismic data, indicating a good relation between seismic and well data.

The interval of interest was divided into two main seismic units based on the characteristics (amplitude, frequency, and continuity) of the seismic reflections and the recognition of reflection termination patterns such as onlap, erosional truncations, seismic facies/configuration, and vertical stacking patterns (Mitchum et al., 1977).

In the present study, submarine channel systems and submarine fans were identified based on seismic criteria and 3D geomorphology in both cross sections and plan-view maps (e.g., Posamentier and Kolla, 2003; Loule et al., 2018).

3.4.3 Seismic attribute analysis

Seismic attributes such as RMS (Root Mean Square) amplitude and variance, were extracted along the horizons to illuminate and visualize the channels, fans as well as to characterize geological anomalies that are isolated from background features by means of an amplitude response (Taner, 2001).

- **RMS amplitude Root-mean square**

The RMS amplitude maps are mathematically computed by squaring individual traces over a defined time window (Brown, 2004; Omosanya and Alves, 2013). They boost high amplitudes

in an interpreted interval, allowing the amplitude reflections related to sands or other high-density materials within channels to be discriminated from their associated low amplitude chaotic facies (Brown, 2004; Omosanya and Alves, 2013; Chima et al., 2019) (Fig. 24).
In this thesis, RMS amplitude maps were extracted from the time and stratal slices to illuminate and visualise the channels, submarine fans.

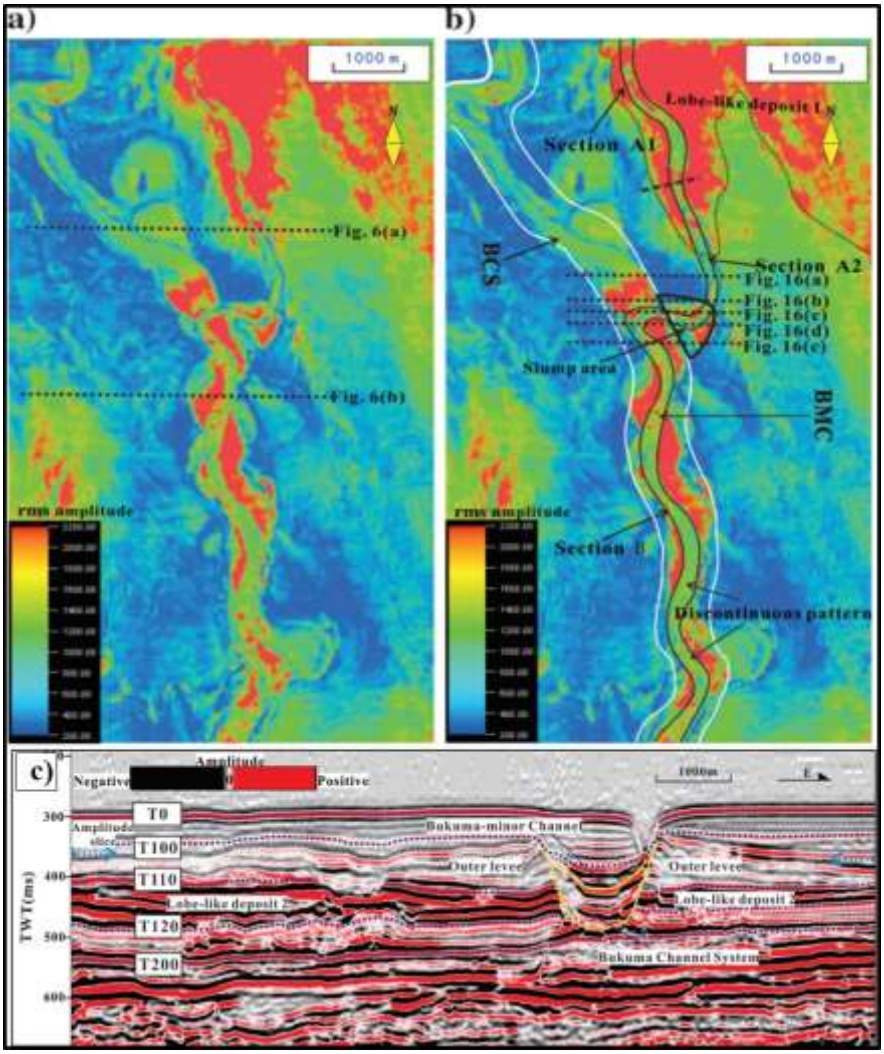

Figure 24. (a) Uninterpreted rms amplitude map of a time slice extracted from 340 ms below the seafloor. (b) Interpreted rms map illustrating the extension and the division of Bukuma-minor channel on southern Niger Delta slope (c) The interpreted seismic profile across the target channel in section B (Zhao et al., 2018).

- **Variance or Coherence**

Variance is the direct measurement of the dissimilarity of seismic traces. Variance maps convert a volume of continuity into a volume of discontinuity, highlighting structural and stratigraphic boundaries (Brown, 2004; Niyazi et al., 2020, 2021). High coherence areas are

typically shown as white to light grey and may indicate slow rates of deposition. Low or non-coherence areas are shown as dark grey or black (Fig. 25). Similar traces are mapped as high coherence coefficients while discontinuities have low coefficients (Bahorich and Farmer, 1995). Sharp discontinuities may result from fracturing, faulting, diagenesis, erosion, fluvial systems, or changes in the rate of deposition (Bahorich and Farmer, 1995). Coherence provides an accurate first estimation of subtle changes in a waveform of a seismic trace over an entire cube. It is a useful reconnaissance mapping tool because it gives an unbiased view of the features in the seismic volume without any prior interpretation. In addition to faults, channels and fans (Fig. 25), it has been successfully utilized in the visualisation of mud volcanoes, salt intrusions, MTDs and polygonal faults (Eruteya et al., 2016; Niyazi et al., 2021). For this study, variance was used to map depositional elements as channels and fans.

3.4.4 Quantitative seismic geomorphology

Plan-view images of the depositional elements and depositional systems (on a large-scale) were provided by 3D seismic data, in which the morphology of these things could be extracted from a seismic cube. Analyses of such images could significantly enhance predictions of the spatial and temporal distributions of subsurface lithology (reservoirs, sources, and seals), compartmentalization, and stratigraphic trapping capabilities, as well as contribute to an enhanced understanding of process sedimentology and sequence stratigraphy (Davies et al., 2006; Posamentier et al., 2007).

Seismic geomorphology, based on the interpretation of plan-view seismic images, is rapidly developing on several fronts, which include (a) understanding the development of seascapes and landscapes in clastic and carbonate settings; (b) advances in workflow directed toward lithological prediction through the integration of seismic stratigraphy and seismic geomorphology; (c) revising and improving sequence stratigraphic models; and (d) development of new and increasingly sophisticated analytical techniques (Posamentier et al., 2007).

Quick scan interpretation of a 3D seismic volume is commonly used to derive stratigraphic settings and seismic features. Posamentier et al. (2007) described how a detailed analysis could be performed in the following sequence: (1) horizon picking and subsequent illumination; (2) amplitude extraction along specific horizons; (3) horizon slicing or stratal slicing, whereby the volume is flattened on a key horizon, and amplitude extractions are subsequently made from time slices parallel to the key horizon; (4) proportional horizon slicing, in which an interval is bound between two mapped horizons and then is unproportionally sliced

between the two horizons; (5) interval attribute analysis, whereby an interval that brackets the interesting seismic feature is defined and then characterized seismically; (6) vox-body picking; (7) extraction of horizon-based attributes, such as dip magnitude, dip azimuth, curvature, and roughness and (8) extraction of volume-based attributes, such as phase, coherence, and impedance.

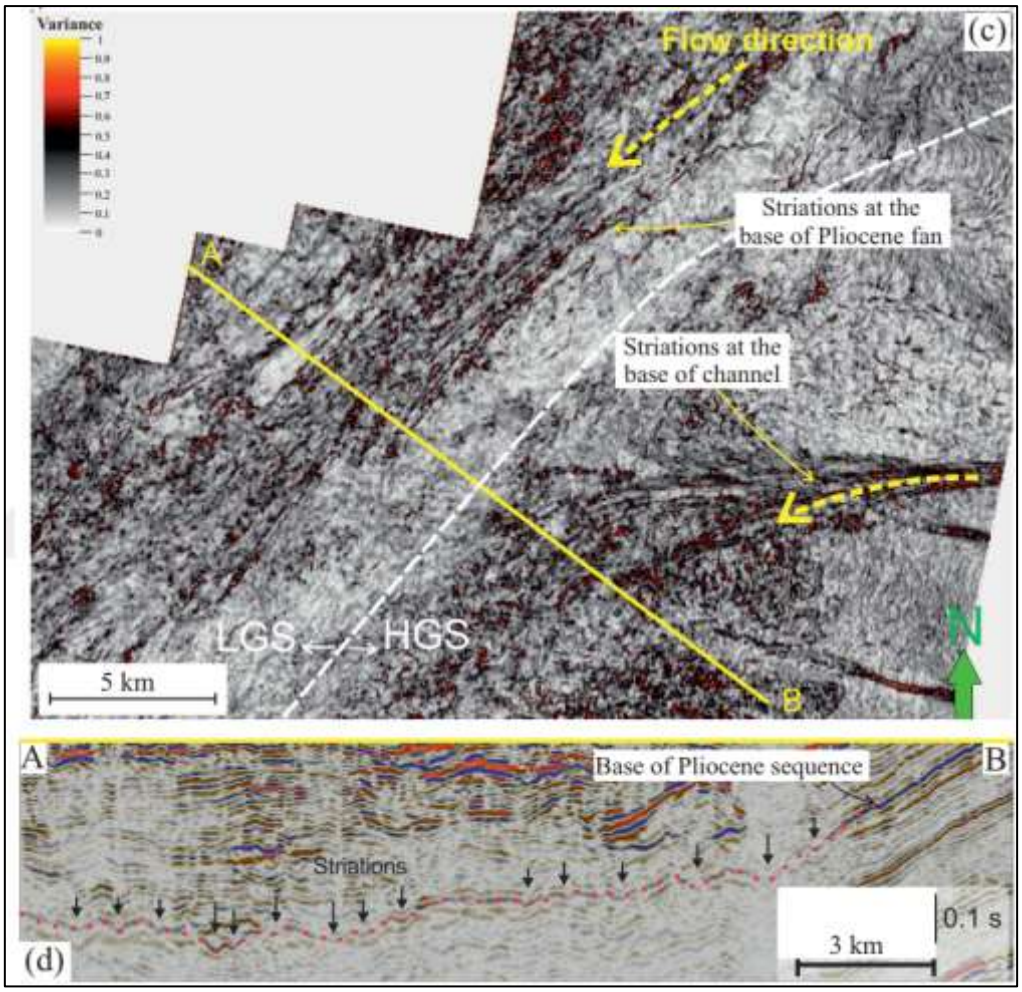

Figure 25. (c) Variance map of base of Pliocene sequence showing a series of striations at the base of a fan derived from NE and a W-flowing channel in. Striations are associated with the pattern of the Pliocene fan and at the base of E - W trending channel. (d) Striations are shown on seismic cross-section (Le et al., 2021).

Furthermore, the quantitative analysis of the seismic geomorphology of submarine channels was performed following the methodologies proposed by Deptuck et al. (2007), Gamboa and Alves (2015), Qin et al. (2016), Hansen et al. (2017), Harishidayat et al. (2018) and Zhao et al. (2018). Morphometric parameters such as width (defined as the distance between the banks of the channel system), depth (defined as the depth of the channel from their overspill points to their bases), and depth of the channel thalweg (defined as a middle point of

the channel walls and the lowest point of the erosional surface), were measured in cross-sectional seismic profiles (Fig. 26). These seismic profiles are perpendicular to the channel axis and are located at an interval of 1 km (average). The zero point was defined as the northernmost limit of the channel. The thalweg depth (in s TWT) was converted to depth (in m) using the time-depth relationship produced from checkshot data available of Well W1 (Fig. 27). Furthermore, the channel gradient was calculated based on changes in thalweg depth along the axis of the channel. For this purpose, the thalweg depth was measured on each profile along the channel. Subsequently, the paleo-topography on which the channel developed was divided into windows with different average gradient segments depending on the magnitude of the thalweg depth variations on the profiles.

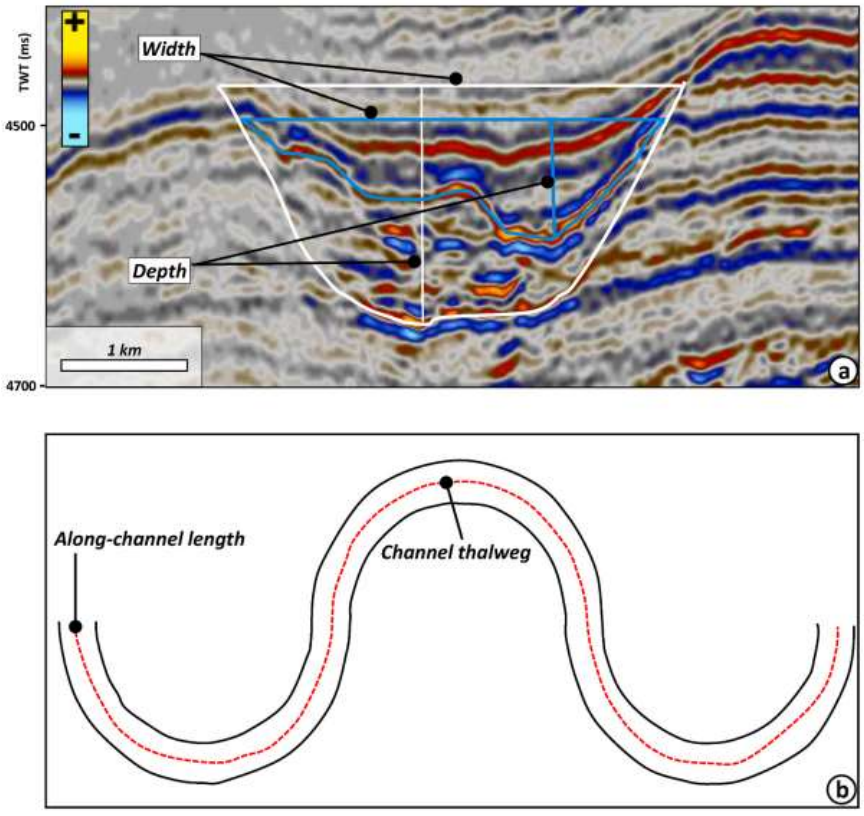

Figure 26. a) A seismic cross section showing the definition of width and depth as used in this paper. The distances between two intersection points on the top surface and the left/right boundary are defined as the width, the vertical distance between the thalweg and the top surface as the depth. b) Schematic diagram showing the definition of the along channel length and channel Thalweg.

Vertical and horizontal distances (the vertical distance must be converted into depth profiles) between the starting and ending points of these windows were measured. Then final

gradients were measured based on the arc tangent function (Deptuck et al., 2007; Gamboa and Alves, 2015; Qin et al., 2016; Harishidayat et al., 2018; Zhao et al., 2018).

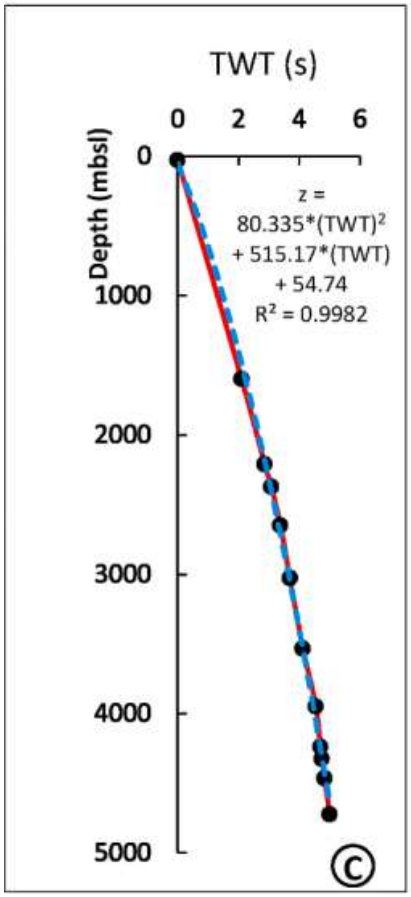

Figure 27. Depth conversion scheme

3.4.5 Petrophysical analysis

The well log data were interpreted qualitatively and quantitatively to derive the petrophysical properties of the reservoir intervals. This was achieved using the Senergy LR company Interactive Petrophysics (IP) software. The software consists of separate modules for reliable interpretation of all petrophysical and lithological features, including environmental corrections and statistical analyses using several equations, empirical relationships and charts (Schlumberger, 1989; Hakimi et al., 2017; Chongwain et al., 2018 and 2019; Hu et al., 2020; Radwan et al., 2021; Elmahdy et al. 2023).

3.4.5.1 Lithological and reservoir identification

The lithological and mineralogical components of the clastic rocks of the Logbaba Formation were identified using Schlumberger charts such as neutron-density, neutron-gamma, neutron-sonic and M-N cross plots (Schlumberger, 1989). The potassium vs thorium cross-plot

allows to identify the clay mineralogy in the reservoir formation (Tiyan and Ayers, 2010). The impact of these identified clay minerals on the reservoir quality was also analyzed.

The well log analysis was used to delineate reservoir sands characterized by cylindrical or blocky gamma-ray shapes, which are utilized to understand the depositional environment of reservoir sands in this study (Fig. 28). Following the methodology adopted from Shier (2004), the gamma ray logs of the two wells were standardized. Subsequently, the gamma ray logs were used to identify the reservoir units and establish a clay (shale) cut-off value of 60 API for W1 and W2. Also, this was used to establish the sand baseline and the reservoir units which were discriminated based on the lower gamma ray readings (Chongwain et al., 2018 and 2019). Also, reservoirs were identified using gamma ray and resistivity log signatures. Intervals with high resistivity are hydrocarbon while low resistivity areas are aquifer intervals. In this study, zones with resistivity values greater than 4 Ω m are identified as hydrocarbon (Chongwain et al., 2018 and 2019). The resistivity (P40H), neutron (TNPH) and bulk density (RHOB) logs were used together to discriminate the types of hydrocarbons (oil or gas) present in the reservoirs.

In addition, the well logs were analyzed to determine the reservoir thickness, net-gross (NTG), volume of shale (V_{sh}), effective porosity ($Ø_{eff}$) and hydrocarbon saturation (1- S_w). These parameters were also used to assess the hydrocarbon potential of the study area.

3.4.5.2 Fraction shale volume

The shale content (V_{Sh}) in the reservoirs was calculated from the gamma ray logs. The first step is to determine the gamma index using (Eq. 4).

$$\boldsymbol{I_{GR} = \frac{GRlog - GRmin}{GRmax - GRmin}} \qquad (\mathbf{4})$$

Where I_{GR} = gamma ray index, GR_{log} = gamma ray reading of formation, GR_{min} = minimum gamma ray (clean carbonate), GR_{max} = maximum gamma ray (shale). After obtaining the gamma index, the volume of shale was then calculated according to formula (5). Given that the Logbaba Formation is Cretaceous age (Nguene et al., 1992; SPT, 1995; Lawrence et al., 2002; Brownfield and Charpentier, 2006), the volume of shale (V_{sh}) was estimated using the Larionov (1969) Cretaceous Eqs. (4) and (5) (Asquith and Krygowski, 2004).

$$\boldsymbol{V_{sh} = 0.33(2^{2 \times I_{GR}} - 1)} \qquad (\mathbf{5})$$

Determining the shale volume (Vsh) holds significance within petrophysical assessment due to its impact on reservoir porosity and permeability (Balaky et al., 2023).

Shape	Smooth	Environments	Serrated	Environments
Cylinder Represents uniform deposition		Aeolian dunes Tidal sands Fluvial Channels		Deltaic distributaries Turbidite channels Proximal deep-sea fans
Bell Shape Fining upwards sequences		Tidal sands Alluvial sands Braided streams Fluvial channels Point bars		Lacustrine sands Deltaic distributaries Turbidite channels Proximal deep-sea fans
Funnel Shape Coarsening upwards sequences		Barrier bars Beaches Crevasse splays		Distributary mouth bars Delta marine fringe Distal deep-sea fans

Figure 28. Gamma ray log shape and depositional environments

3.4.5.3 Porosity estimation

The porosity logs and density porosity model, which capture the empirical relationship between the measured bulk density (ρ_b), porosity (∅), matrix (ρ_{ma}), and fluid (ρ_f) densities, were used to calculate the void ratios (total and effective porosities) of the identified reservoir units, while integrating the clay volume effect was used to calculate formation fractional porosity (Eq. 6) (Chongwain et al., 2018).

$$\emptyset = \frac{\left(\boldsymbol{\rho_{ma} - \rho_b - V_{cl} \times (\rho_{ma} - \rho_{cl})}\right)}{\boldsymbol{\rho_{ma} - \rho_f \times S_{xo} - \rho_{HyAp} \times (1 - S_{xo})}} \qquad (6)$$

Where ρ_{ma} is the matrix density, ρ_b is the bulk density, ρ_{cl} is the density wet clay, ρ_f is the mud filtrate density, ρ_{HyAp} is the apparent hydrocarbon density, V_{cl} is the volume of wet clay, and S_{xo} is the water saturation of the fushed zone.

3.4.5.4 Water saturation and hydrocarbon saturation estimation

The modified Simandoux equation was used to estimate the water saturation (Sw) values, using (Eq. 7) below (Bardon and Pied, 1969):

$$\frac{\boldsymbol{1}}{\boldsymbol{R_t}} = \frac{\emptyset^{\boldsymbol{m}} \times \boldsymbol{S_w^n}}{\boldsymbol{a \times R_w \times (1 - V_{sh})}} + \frac{\boldsymbol{V_{sh} \times S_w}}{\boldsymbol{R_{sh}}} \qquad (7)$$

Where S_w is the effective water saturation, R_w is the water resistivity, R_t is the true formation resistivity, a is the tortuosity factor, m is the cementation factor, ∅ is the formation porosity, V_{sh} is the volume of wet clay, and R_{sh} is the clay resistivity. The hydrocarbon saturation for the reservoir zone was then calculated using Eq. 8 below. The hydrocarbon saturation (Sh) was obtained by subtracting the value obtained for the 100% water saturation (Rider, 1996):

$$\boldsymbol{S_h = 1 - S_w \; or \; S_h = 100 - S_w}(\%) \qquad (8)$$

Where, S_h = Hydrocarbon Saturation; S_w=Water Saturation.

The reservoir net-pay values were evaluated using 40% shale volume (V_{sh}), 12% effective porosity ($\emptyset_{eff}$), and 65% water saturation (S_w) cutoff values (Sterling et al., 2010; Chongwain et al., 2018). These values are generally chosen based on published literature and on detailed petrophysical analysis, but also on parameters used for similar reservoirs in the same area with comparable petrophysical properties (Jumat et al., 2018; Radwan et al., 2021).

Finally, using the comparison table provided by Fertl and Vercellino (1978), the bulk water volume (BVW), which is a product porosity (∅) and water saturation (S_w) (Eq. 9), was

utilised to estimate the grain size of the reservoir formation. The bulk volume of water (BVW) is further used for differentiating between reservoir/non-reservoir intervals to estimate the net pay thickness (Dewan, 1983; Asquith, 1985).

$$\boldsymbol{BVW = S_w \times \emptyset} \qquad (\mathbf{9})$$

3.4.5.5 Permeability estimation

Since core data was not available in this study, the permeability equation of Morris and Biggs (1967) was used to calculate the permeability from well log data. This equation is as follows:

$$\boldsymbol{K = a\,Phi^b / Swi^c} \qquad (\mathbf{10})$$

where: K = permeability (md); Phi = effective porosity; Swi = irreducible water saturation; a = 62,500; b = 6; and c = 2.

In summary, this chapter has outlined the methodological framework adopted in this study, which integrates seismic and borehole data to address the central questions posed by the thesis. Specifically, the research seeks to determine the geometries and spatio-temporal distribution of turbidite systems within the study area, and to identify the key factors controlling their sedimentation in the Kribi-Campo sub-basin. The integrated approach presented here is expected to provide valuable insights and contribute significantly to answering these fundamental questions in the chapters that follow

Chapter 4: Seismic geomorphology of a Late Cretaceous submarine channel system in the Kribi/Campo sub-basin, offshore Cameroon

The tectono-stratigraphic framework of the Late Cretaceous mega-sequence is the focus of this chapter. The interpretation was carried out using 3D seismic data. Key seismic horizons are defined and seismic facies analysis undertaken of the post-rift Late Cretaceous deposits. The study emphasises on internal architecture, geometry and morphometry analysis of submarine channel.

4.1. Seismic interpretation

The interpreted ten horizons (KC-1 to KC-9 and the seafloor) were used to describe the seismic stratigraphic framework of the study area (Fig. 29). All horizons are pre-fixed with 'KC' (abbreviation for the Kribi-Campo sub-Basin) and then numbered in order of descending stratigraphic age. KC-1 to KC-9 horizons correspond to the Top Albian, Santonian, Campanian, Maastrichtian, Paleocene, Eocene, lower Miocene, middle Miocene, late Miocene, respectively.

- **KC-1: Lower Cretaceous unconformity**

KC-1 is picked along an angular unconformity below the present-day shelf that is represented by a high-amplitude trough. The surface marks a significant hiatus in sedimentation with tilted Albian-Aptian units below and Tertiary-Late Cretaceous sediments above. Because of the diachronous nature of the surface, we refer to this surface as the Lower Cretaceous Unconformity. The origin of the unconformity is attributed to progressive phases of oblique inversion of the rift basin around the KFZ. In a few localised areas, inversion has coincided with production of negative relief, probably around the releasing bends of the reactivated strike slip systems transecting the basin. Here, the unconformities are less angular and more of the Cretaceous succession not penetrated in the well database may be present.

- **KC-2: Santonian**

KC-2 is a weak-to strong positive amplitude reflection. The surface is identified by downlap above and a change from dominantly high amplitudes below to an overlying lower amplitude seismic facies above. This surface extends across the whole area, but onlaps onto the Kribi High**.**

- **KC- 3: Late Cretaceous unconformity**

The horizon (KC- 3) is picked on a high-amplitude peak on the lower to middle slope. The surface represents an unconformity which progressively shows greater truncation of underlying units toward the upper slope. From the few available wells that penetrate this surface we tentatively infer an age of Campanian. But, given that all unconformities are diachronous in

nature it may be more appropriate to refer to this horizon as the Late Cretaceous unconformity. This surface onlaps an older Lower Cretaceous Unconformity (Horizon KC-1) below the shelf further increasing the hiatus in sedimentation shoreward.

- **KC-4: Maastrichtian**

The horizon KC-4 is picked on a high amplitude peak near the base of the Tertiary. On the basin floor at the more distal end of the depositional system (i.e., around W1), the surface marks the base of the largely low-amplitude Tertiary package. This is in contrast to the underlying Cretaceous units which, in cross-section, appear more channelized and possess higher gross amplitudes. The change in amplitude across this surface is less abrupt toward the upper slope and shelf and the surface appears to climb up through stratigraphy. Within the context of available well data this surface could either represent the Base Tertiary Unconformity

- **KC-5: Paleocene**

The horizon is recognized as a week to strong positive amplitude reflection, disrupted by polygonal faults and extending across the whole study area. The surface marks a change from low amplitude reflection below to higher amplitude reflections above.

- **KC-6: Eocene**

The horizon is characterized by a strong negative reflection disrupted by polygonal faults in the southern area. Surface erosion is clearly observed by offset stacked channels to the north and channels to the south.

- **KC-7 to KC-9: Miocene Horizons**

The Tertiary sedimentary succession in the Kribi-Campo sub-Basin is expressed by a series of south-westward prograding clinoforms, slope channel-systems and basin-floor turbidite fans above a Tertiary unconformity base. The seismic expression of the key seismic packages (depositional sequences) within the Tertiary succession changes seaward across the palaeo-shelf (top of clinoform), palaeo-shoreface (slope of clinoform) to the basin floor (seaward of clinoform). Each clinoform set comprises a sequence of truncated, prograding and downlapping reflectors. The reflectors at the top and upper slope of the clinoforms are typically moderate-to high amplitude and are deformed by seaward-dipping planar to listric normal faults formed during gravitational collapse of the palaeo-upper slope. Because of the nature of seaward migration of the upper slope during the Tertiary the age of faulting growth youngs seaward. Onlapping the base of, or overstepping, the clinoforms are relatively thin packages of largely

continuous low to moderate amplitude reflectors transected by moderate to high-amplitude channels and fans.

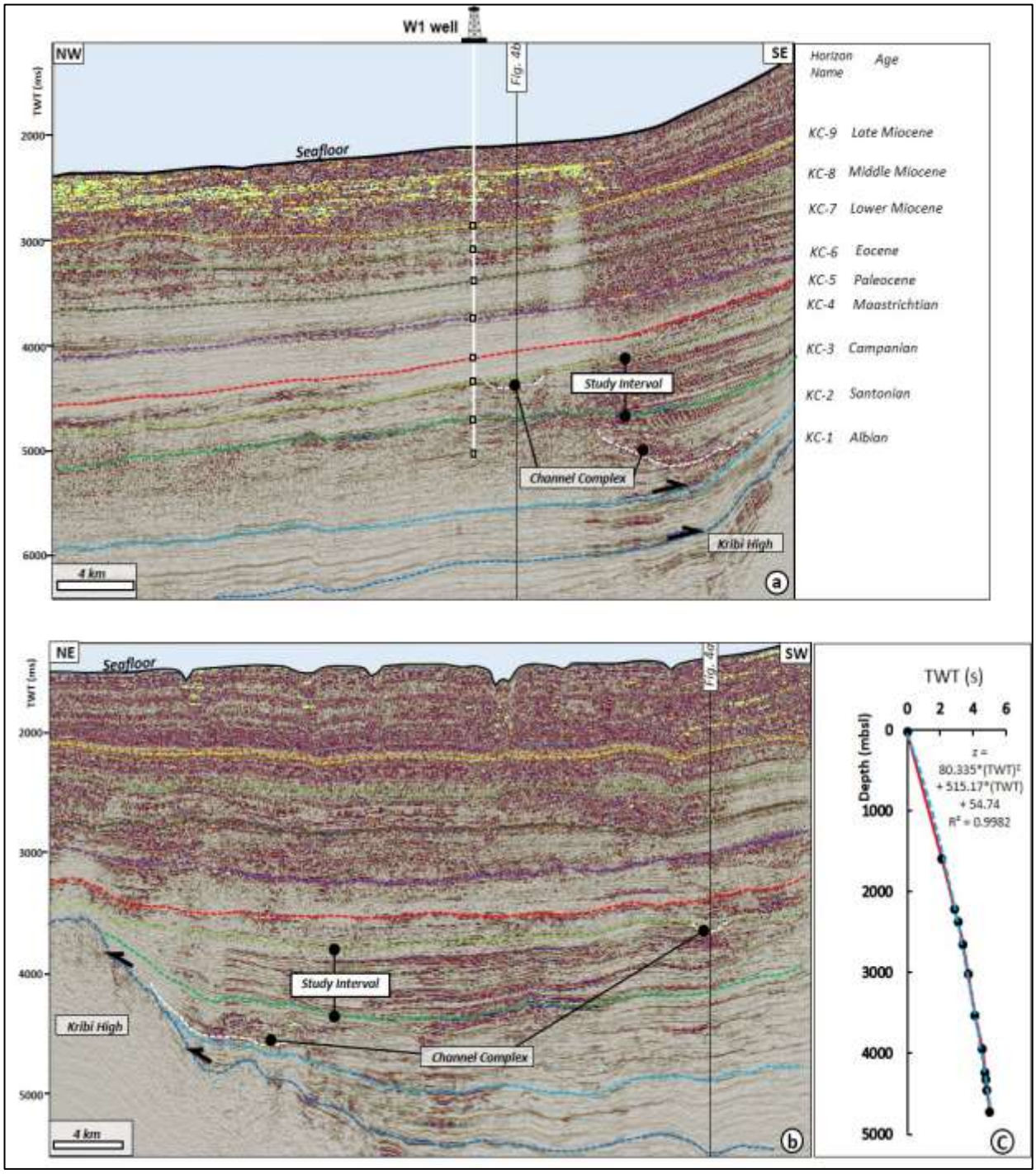

Figure 29. a) Seismic line through W1 well showing the entire basin successions and channel complex deposits identified within the dataset. Ten Horizon name (KC-1 to KC-9 and the seafloor) are identified in the study area based on Le (2012); Iboum Kissaaka et al. (2016) and Loule et al. (2018). b) Seismic section, taken perpendicular to regional dip, showing the channel complex deposits within the study interval. c) Depth conversion scheme.

The parallel, low-amplitude, units outside of the channels and fans are pervasively deformed by strata-bound arrays of small, densely-spaced normal fault systems formally known as "Polygonal Fault Systems". Worldwide, these faults systems are confined to very fine-grained hemipelagic sediments deposited in deep water settings. The horizons, KC-7, KC-8 and KC-9, all mark moderate-to-high amplitude peaks within the Tertiary succession and are likely to be candidate sequence boundaries or maximum flooding surfaces. W1 is the only well available for the study with a comprehensive breakdown of interpreted ages for this interval and we infer the ages of horizons KC-7 to KC-9 as follows; KC-7: Lower Miocene KC-8: Middle Miocene, and KC-9: Late Miocene.

- **Seafloor**

The shallowest principal trough in the seismic survey represents the seafloor. The horizon is picked with high confidence across the upper and lower slope. On the shelf, the trough representing the seafloor is absent. A manual interpretation atop the shallowest reflectors was generated to complete the seafloor surface.

4.2. Seismic stratigraphy of the study interval

The interval of interest in the study area is bounded by the KC-3 and KC-4 horizons at the base and top, respectively. This interval is characterized by distinctive seismic facies of the Campanian-Maastrichtian Logbaba Formation (Fig. 29). The KC-3 is located at approximately 4900 ms TWT and is characterised by a high-amplitude positive reflection with good continuity (Fig. 29). This horizon is characterised by onlap above the Kribi High area and defines the base of the stack of high to bright amplitude reflection laterally migrating westward. This probably corresponds to a turbidite fan system which extends from the east to the southern half of the study area (Fig. 30). Based on its seismic characteristics and according to Le (2012); the surface KC-3 corresponds to an unconformity in the study area which progressively shows greater truncation of underlying sequences toward the upper slope (Fig. 29). The isochore map shows values ranging from − 3700 ms upstream to − 5100 ms downstream (Fig. 31a). These two extreme values correspond respectively to a high and low topographic area on either side of the study area (Fig. 31a). It is separated by a steep slope on the east that decreases towards the seabed. The horizon KC-4 is located at approximately 4600 ms TWT and is also a positive reflection with high amplitude. The horizon is characterized by downlaps onto an erosional surface and separates the overlying high to moderate frequency, low to moderate amplitude reflection packages from the underlying low to moderate frequency, and high to moderate amplitude reflection packages (Fig. 30).

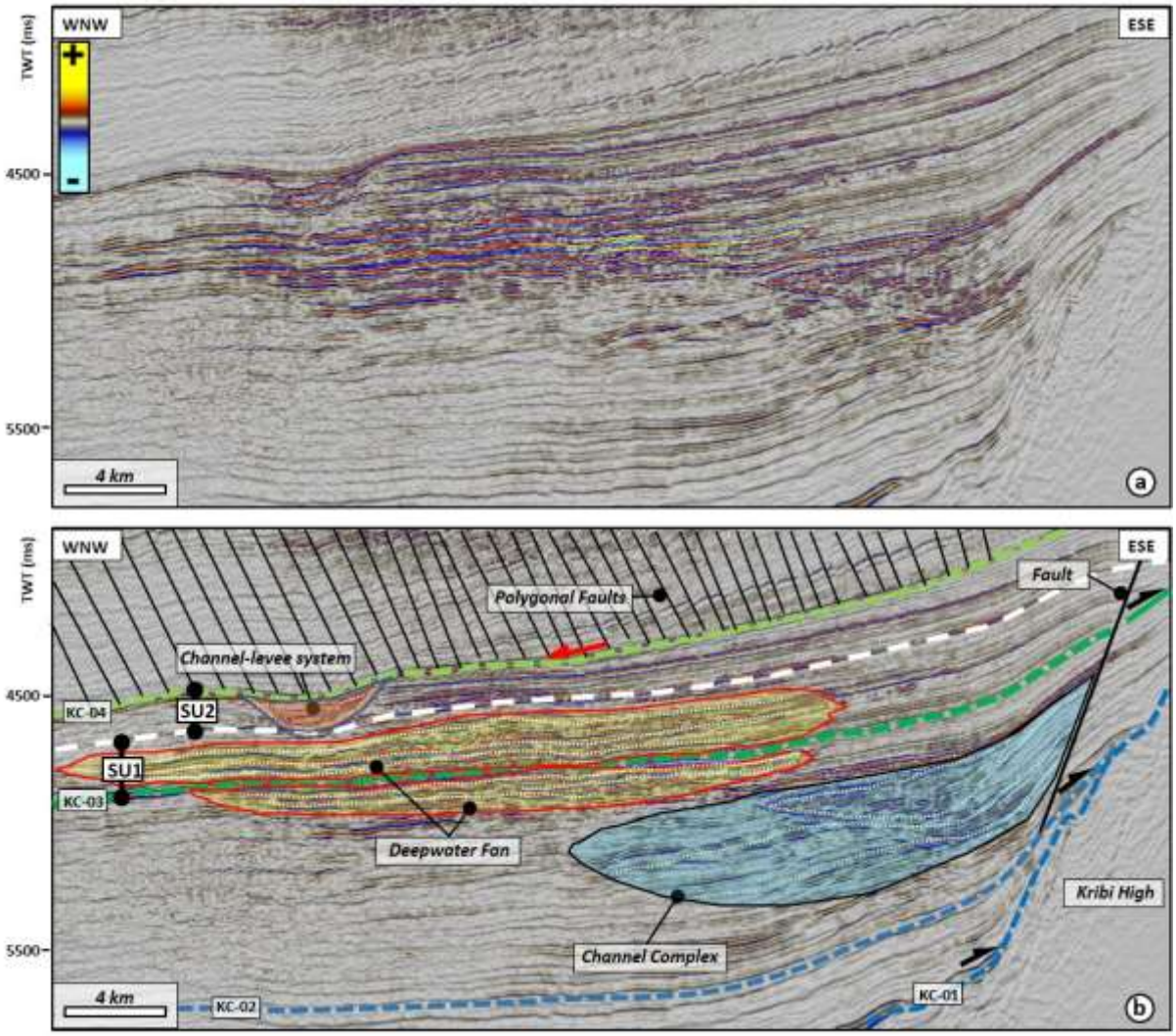

Figure 30. Along the slope seismic profile showing. a) Uninterpreted and (b) The interpreted seismic stratigraphy of the slope. The submarine channel system is located within unit (SU2) and deep-water fan is located within (SU1) in the study interval.

The isochore map shows values ranging from − 3200 ms to − 4800 ms, respectively, at two downstream and upstream ends of the sub-basin (Fig. 31b). The contours lines of this map have a preferred NE-SW direction (Fig. 31b). The surface KC-4 is incised by a NE-SW trending channel and covers the Kribi High in the east (Fig. 29a and b). On the basin floor at the more distal end of the large incision (i.e., around W1), the surface marks the base of the relatively low-amplitude Tertiary package (Fig. 29a). This contrasts with the underlying Cretaceous sequences which in cross-section are more channelized and display higher amplitudes (Fig. 30). The thickest area reaches 1560 m (Vp = 2400 m/s) in the east, and the average thickness of the unit is 1080 m (Fig. 31c). The interval of interest in this study (Campanian-Maastrichtian succession) has been divided into two seismic sub-units: seismic sub-unit 1 (SU1) and seismic

sub-unit (SU2) based on the differences in the internal seismic reflection configurations (Fig. 30). SU1 consists of sub parallel and aggradational reflections (Fig. 30). SU1 is generally characterized by low amplitudes reflections with limited occurrence of high amplitude reflections and displays maximum thickness in the east (Fig. 30). The high amplitude seismic facies display an aggradational pattern with parallel and continuous reflections having a fan-shaped geometry (Table 6, Fig. 30). SU2 forms the uppermost sub-unit in the Late Cretaceous, and consists of low to high amplitude, sub-parallel and continuous reflectors. A large incision occurs within this unit, which is interpreted as a submarine channel, characterized by high-amplitude reflections at its base (Table 6, Fig. 30).

4.3. Late Cretaceous submarine channel

4.3.1. Channel infill: distribution of seismic facies and interpretation

Five seismic facies (SF1 to SF5) were identified in the study interval and can be interpreted to represent five specific depositional settings in the area of interest (Table 6). SF1 consists of high amplitude, chaotic reflections confined within a U-shaped erosional surface in cross section (Fig. 32b and c). In plan-view, SF1 is expressed as a more linear morphology compared to SF2 (Fig. 34). It occurs at the basal lags of the early-stage channel. This facies is interpreted as coarse-grained sediments deposited in the submarine channel axis (Mayall et al., 2006; Gee et al., 2007) (Fig. 34). SF2 consists of low-amplitude, discontinuous to chaotic reflections, with a U- shaped external geometry (41–103 m depth, 1–3 km wide) in cross section (Fig. 32). SF2 is narrow and has a sinuous morphology in map-view (Fig. 34). This facies is interpreted as clay-prone channel fills that may record earlier channel bypassing (of coarse-grained sediments) and later abandonment (deposition of fine-grained sediments). SF3 is composed of low-amplitude, discontinuous to continuous seismic reflections and occurs in the background unit that encompasses the submarine channel (Fig. 32b and c; Table 5). It occurs in the entire seismic volume on the map-view outside the submarine channel system (Fig. 34). SF3 can be interpreted as hemipelagic sediments (Fig. 34); SF3 is similar to those of hemipelagic sediments as observed in other studies (e. g., Su et al., 2015; Gong et al., 2016). SF4 is comprised of high-to low-amplitude, convergent reflections that show a broadly wedge-shaped geometry in cross section (Fig. 32b and c). This facies is widely recognized elsewhere and interpreted to represent levees deposits (Table 6) formed of fine-grained sediments from the overbanking of turbidity currents (e.g., Posamentier and Kolla, 2003; Deptuck et al., 2003; Catterall et al., 2010; Janocko et al., 2013).

Table 6. Description and interpretation of the seismic facies observed in the submarine channel system within the study interval.

Seismic facies	Seismic profile	Schematic	Description	Plan/Map view	Interpretation
SF1	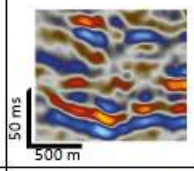		Chaotic, high amplitude, discontinuous reflections, basal lags usually confined within a V- or U- shaped erosional surface	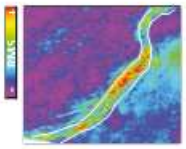	Coarse-grained channel fill
SF2	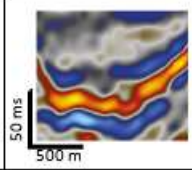	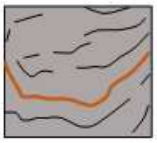	Low to high amplitude, discontinuous to chaotic reflections, with a U- or V-shaped external geometry	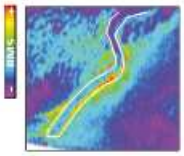	Fine-grained Channel fill
SF3	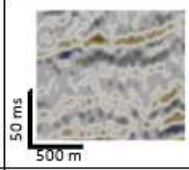		Semi transparent, low amplitude, semi-continuous to continuous reflections	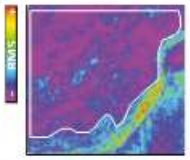	Mass-transport deposits
SF4	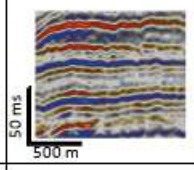	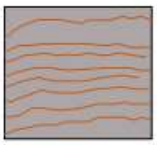	high- to low-amplitude, continuous, parallel to subparallel reflections	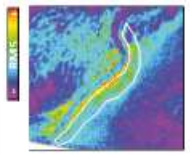	Levee deposits
SF5	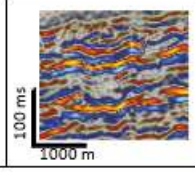		High amplitude seismic facies displaying an aggradational pattern with parallel and good continuity reflectors	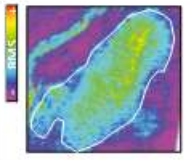	Turbidites fan system

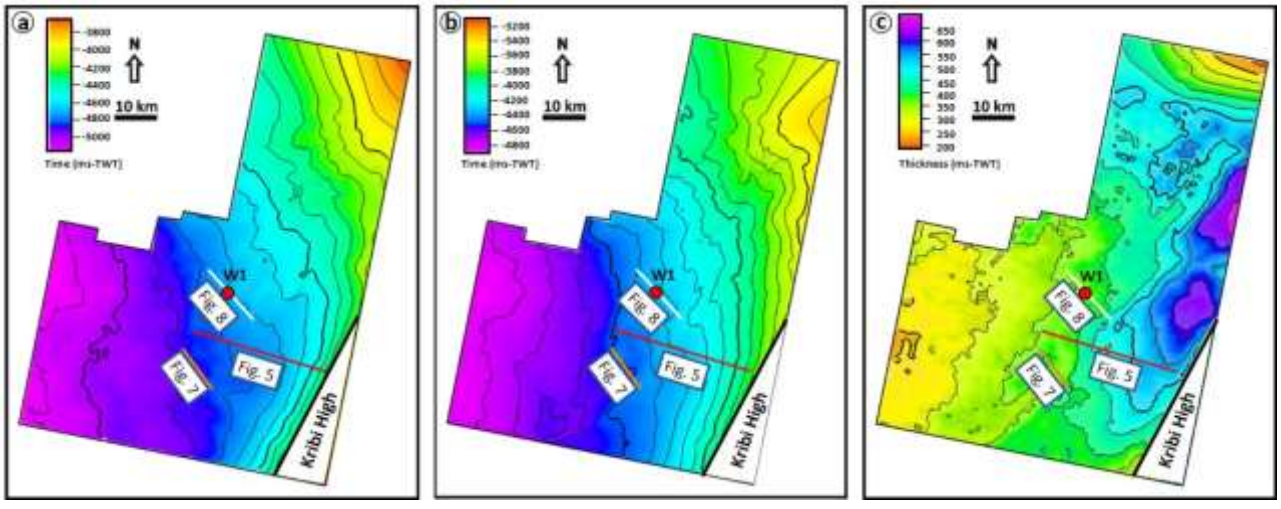

Figure 31. a) Isochronal map of the KC 03 horizon. b) Isochronal map of the KC 04 horizon. c) Isopach map of Late Cretaceous between KC 03 and KC 04.

SF5 is characterized by high-amplitude reflection displaying an aggradational pattern in cross-section (Table 6) and it is located below the submarine channel system in sub-unit SU1 (Fig. 30b). In map view, it occurs in the SE part of the study area (Fig. 34c and d). This facies correspond to the sand body which can be interpreted to fan deposits, and it is like those observed and described by Twichell et al. (2009).

4.3.2. Internal architecture and geometry of the submarine channel

The submarine channel observed in unit SU2 is U-shaped in cross section (Fig. 32). It has two vertically stacked channels that developed at different stages. The late-stage channel lies completely within the early-stage channel, and both exhibit distinct seismic reflection characteristics (Fig. 32b and c). The early-stage of the channel is characterized by seismic facies SF1 and SF2. Seismic facies SF1 is mainly located along the thalweg of the early-stage of the channel. It occurs at the base of submarine channel analyzed in this study (Fig. 32b and c). Seismic reflection characteristics of this facies is like those of the channel axial deposits described by Deptuck et al. (2003), Mayall et al. (2006) and Catterall et al. (2010). SF2 is usually confined at the flanks of the channel (Fig. 32b and c). Specifically, the late-stage channel is embedded in this facies (Fig. 32b and c). The late-stage of the channel is dominated by the SF2. In addition, SF1 and SF2 are within the channel system, while SF3 and SF4 are located outside the system (Fig. 32b and c). SF3, mainly occurs in SU2, and it confined to the left side of the submarine channel (Fig. 32b and c). SF4 is seen outside of the early channel belt and occurs only locally (Fig. 32; Table 6). These reflections typically dip away from the channel axis and decrease in amplitude away from the channel axis (Fig. 32b). To analyze the evolutionary history and infilling of the submarine channel system, SU2 was divided into four intervals (Figs. 32a and 33). The well-log in the vicinity of the submarine channel system indicates that the thickness between the top and base of the channel is approximately 90 m (Fig. 33a). The gamma-ray is characterized by sharp-based (between 3900 m and 3850 m), finning upward pattern (between 3850 m and 3810 m). The basal coarse-grained lags of the early-stage channel in well W1 show a large kick in GR and display a serrate GR log motif with some blocky/bell-shaped intervals (Well W1 in Fig. 33a). The late-stage channel fills are mainly characterized by a serrate GR motif with some low-amplitude bell-shaped GR intervals (Fig. 33a). The well-log patterns of this submarine channel consist of clay interbedded with thin layers of sands (Fig. 33a). The early-stage channel is visible on all the maps and is characterized by relatively linear morphology (Fig. 34). The channel is 56 km long and 3–5 km wide (Fig. 34), with an incision depth of 89–197 m (Fig. 35). In contrast, at the late-stage, the channel

could only be imaged in the upper two slices, showing that it incises the infillings of the early-stage channel (Fig. 34a and b). The RMS and variance values also characterize the channel fills in the horizon slices. The high RMS amplitudes and low variance occur within the submarine channel axis. The channel also locally incises areas of high RMS amplitudes and low variances, characterized by lobate geometry outside the channel axis (Fig. 34). The low RMS values and high variances are observed in the northeast part of the channel while the high RMS values and low variances are observed in the southwest part of the channel (Fig. 34d). This high amplitude RMS channel fill observed in the horizon slice corresponds in cross section to seismic facies SF1 and the low amplitude RMS fill corresponds to seismic facies SF2. The late-stage channel is narrower and has a sinuous morphology, embedded in the early-stage channel (Fig. 34). The dimension of the late-stage channel is 1–3 km wide, 56 km long (Fig. 34), and vary in depth from 41 to 103 m (Fig. 35).

4.3.3. Morphometric analysis of the submarine channel

There is a significant morphological variation along the submarine channel system (Figs. 36 and 37). In the northeastern portion, near the sediment source area, the channel morphology varies considerably with smaller width and depth when compared to the southwestern portion where the channel is characterized by significantly greater width and depth (Fig. 35). The depth profile of the early channel thalweg shows an exponential trend and can be divided into three intervals (1, 2 and 3) that correspond to three segments (x, y, and z) based on the channel gradient variations (Fig. 36a; Table 7). The gradient for the early-stage channel is 2.64° in the first segment, and decreases to 2.02° in the mid segment y, which spans between 12 km and 33 km along channel axis (Fig. 36a). In the rest of the channel, segment z, the channel slope decreases dramatically, and reaches its lowest value of 0.40° (Fig. 36a). The channel width also displays three intervals. It varies between 3224 m and 4677 m for the early-stage channel to 1094 m and 2865 m for the late-stage channel in the first 12 km interval (Fig. 36b; Table 7). In interval 2, channel width increased to a maximum value of 5573 m at 17 km for the early channel to 3802 m at 18 km for the late-stage channel.

This increasing trend is followed by a decrease in the width of the late channel to its lowest value of 2993 m at 27 km. In the interval 2, between 27 and 32 km the channel shows an increase in width with slight variation. In interval 3, between 33 and 44 km, the width of the early-stage channel varies from 3830 m to 4260 m. The width of this late-stage channel has a decreasing trend and varies between 3300 m and 1115 m (Fig. 36b).

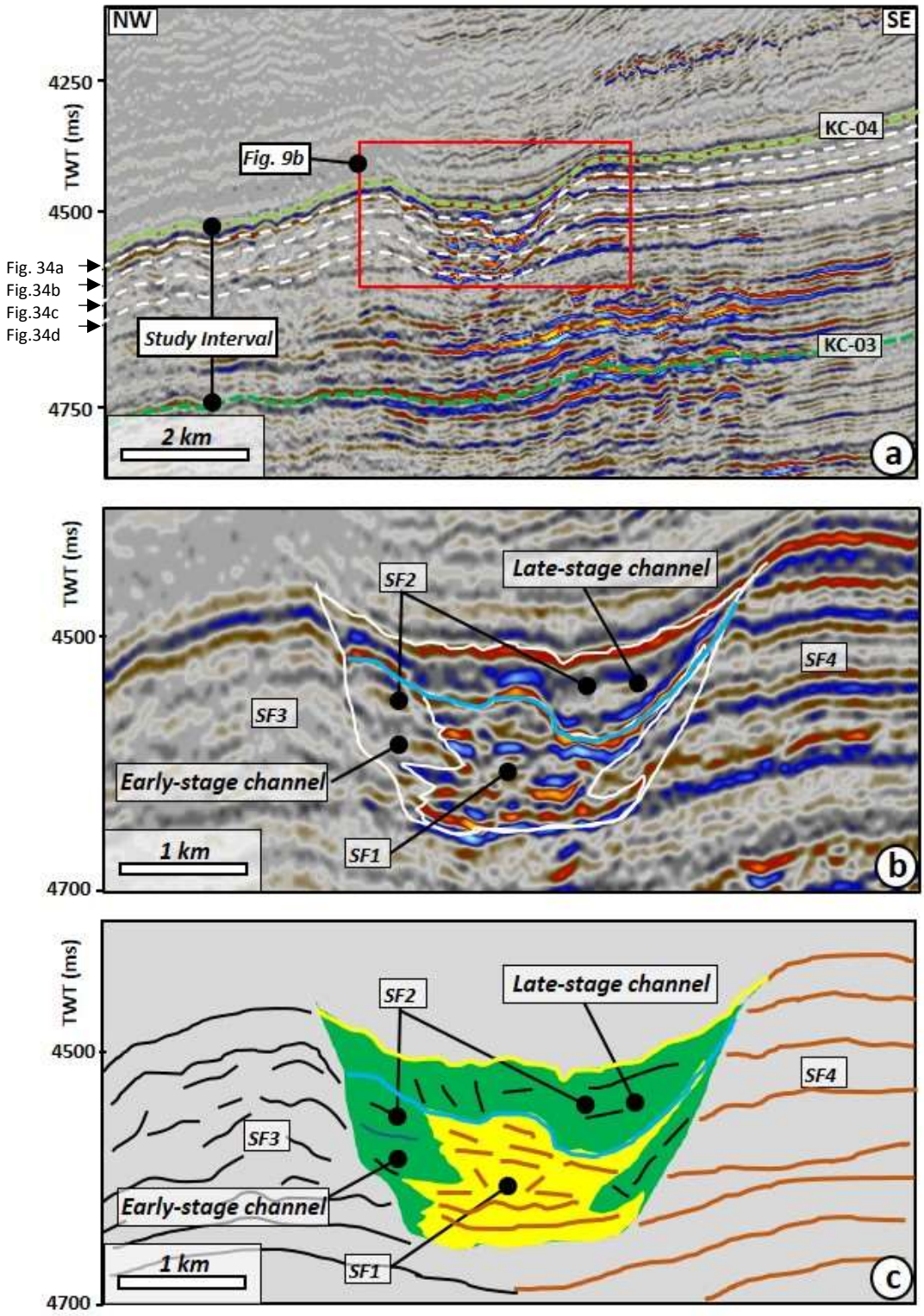

Figure 32. a) Seismic profile showing the channel geometry is U-shaped and iso-proportional slice used to unravel the internal architecture of the channel. b) and c) Channel system are composed of two stages: early-stage channel and late-stage channel. SF1 is coarse while SF2 is fine sediments. The submarine channel is 56 km long and 3–5 km wide with an incision depth of 89–197 m.

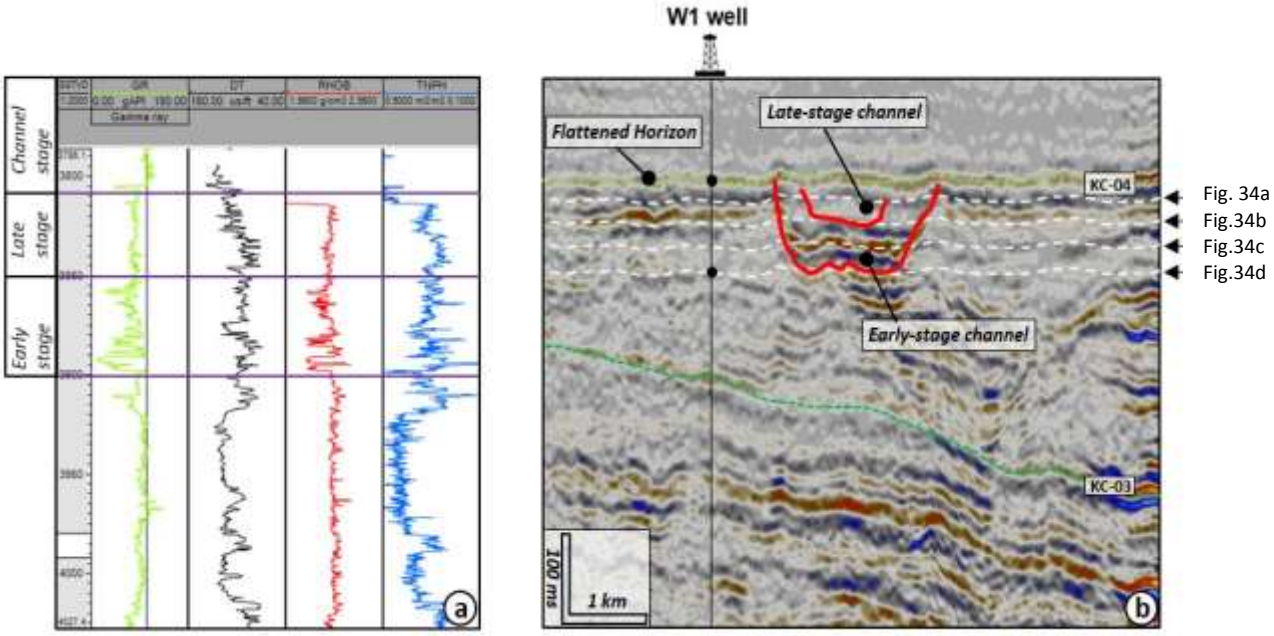

Figure 33. Characteristic of study unit from the well-seismic calibration, a) Wireline logs (GR, DT, RHOB, and TNPH) for well W1 through the submarine channel system. b) submarine channel time slices showing two incision stages and flattened horizon KC-04.

The depth profile of the early-stage channel thalweg also shows remarkable variation along the channel path (Fig. 36a), correlating with the variation in the depths of the early channel (Fig. 36c). A plot of channel thalweg versus along channel distance also revealed three intervals (Fig. 36a and c; Table 7). The first interval (0–12 km) begins with the lowest value of channel depth to the northeast of the seismic survey (Fig. 36c), followed by an increase to 170 m at 9 km in the early channel (Fig. 36c). The depth of the early-stage channel in this interval ranges from 89 m to 171 m. In interval 2, between 12 and 33 km, the channel depth begins with an increase from 109 m at 12 km to 179 m at 15 km (Fig. 36c). Then, the channel depth decreases to its minimum value of 87 m at 24 km, before fluctuating with a general increase from 153 m to 183 m for the rest of the interval (Fig. 36c). The third interval (33–44 km) has the highest value of early channel depth, 197 m at 35 km (Fig. 36c). In this interval, the depth of the early-stage channel begins with an increase followed by a decreasing trend after reaching its maximum depth. The depth fluctuates between 112 m and 197 m. The width/depth ratio of the early-stage channel varies from 18 to 54 (Fig. 36d; Table 7) in the three intervals along the channel.

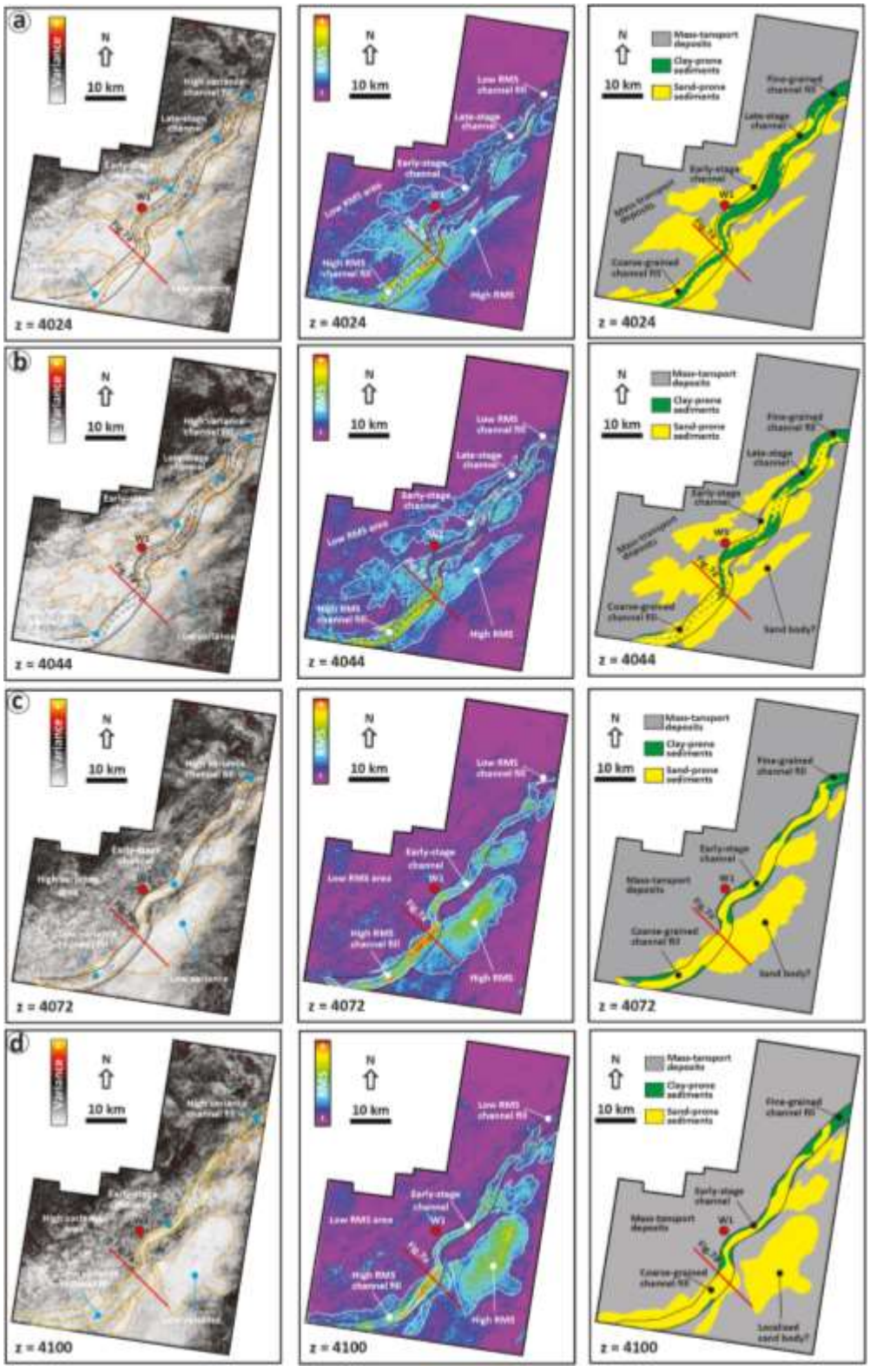

Figure 34. Variance and RMS seismic attributes and their interpretations, of the various slices within the early and late-stage channel (see Fig. 32a). The seismic attributes analysis shows the distribution of several types of sediments deposited during the evolution of the submarine channel system. The late-stage channel is narrower and is more sinuous.

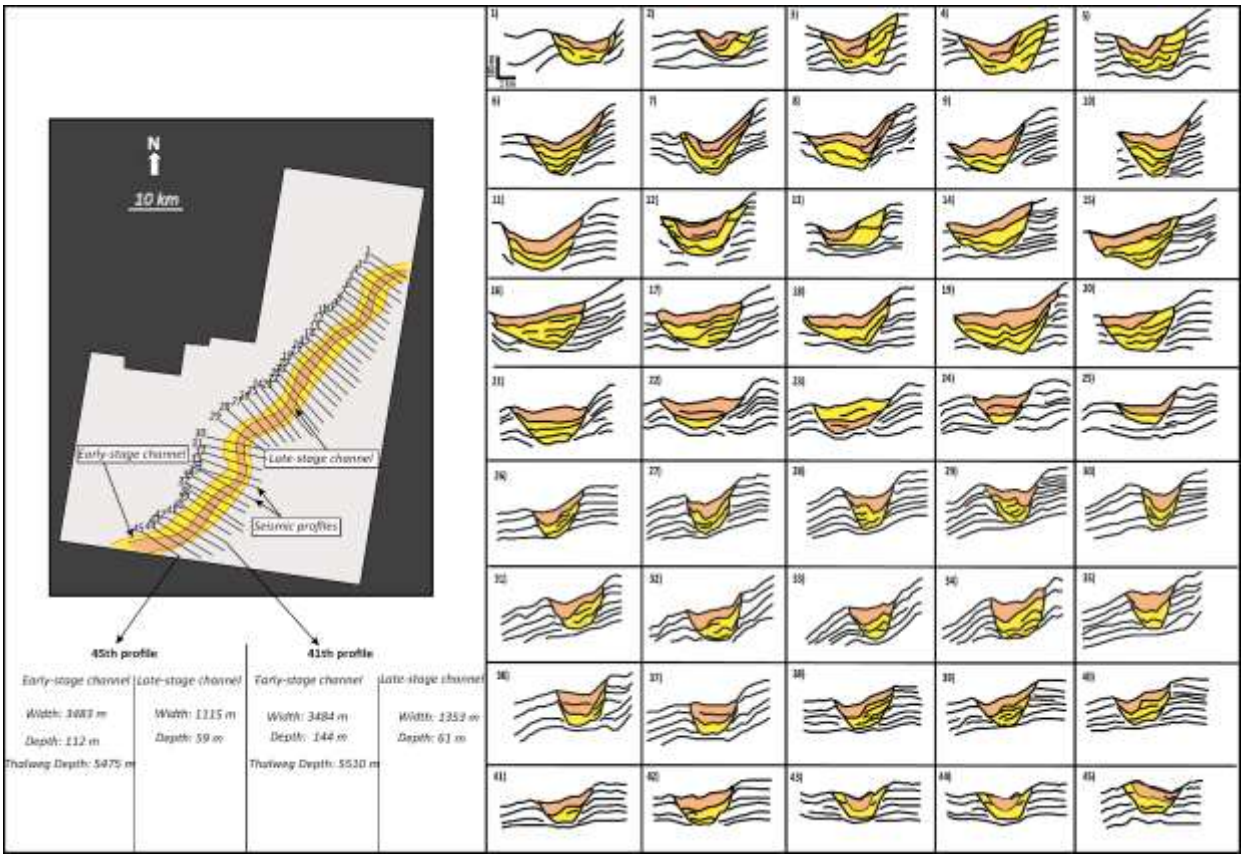

Figure 35. Series of line drawings of seismic profiles oriented perpendicular to the trend of the submarine channel system (every other profile shown, from 1 km spaced profiles). Notice the variation in the geometry and infill of the channel system along the slope.

The first interval begins with a decrease in the ratio and fluctuates along the rest of the interval between 27 and 42 for the early-stage channel (Fig. 36d). The ratio fluctuates within interval 2 (13 and 33 km), reaching its maximum value from 51 to 24 km before decreasing to its minimum value from 17 to 25 km in the early-stage channel. Between 33 and 44 km, the width/depth ratio in interval 3 shows an increasing trend to the northeast of the study area, where it reaches 43 (Fig. 36d). With respect to the late-stage channel, the channel depth in the first interval varies from 41 m to 79 m. In the second interval, the depth of the late-stage channel starts with a decrease, followed by an increasing trend from 47 m to 97 m at 23 km. The rest of the channel varies between 68 m and 98 m in depth. The depth in the third interval reaches a highest value of 103 m at 35 km (Fig. 36c). The depth profile of the late-stage channel starts with a decrease. The general trend of channel depths is downward in this interval and ranges from 103 m to 59 m. The latter value corresponds to the northeastern edge of the submarine channel in the seismic volume (Figs. 37 and 36c). The width/depth ratio of the late-stage channel varies from 17 to 51 (Fig. 36d; Table 7) in the three intervals along the channel. The

first interval begins with a decrease in the ratio, followed by fluctuations along the remaining segment of the channel between 21 and 42 for the late-stage channel. In interval 2 (13 and 33 km), the late-stage channel reaches a maximum value of 54 at 18 km and a minimum value of 25 at 33 km. Between 33 and 44 km, the ratio shows a decreasing trend towards the northeastern edge, where it reaches a minimum value of 18 (Fig. 36d).

Table 7. The result of morphological analysis along the submarine channel system.

	Downslope →		
Intervals / Measurements	1 (0-12 km)	2 (12-33 km)	3 (33-44 km)
Channel gradient (°)	2.64	2.02	0.40
Thalweg depth (m)	4188-4820	4820-5463	5417- 5522
Early/Late stage Channel width (m)	3224-4677/1094-2865	2879-5573/1452-3802	3483-4260/1115-3300
Early/Late stage Channel depth (m)	89-171/ 41-79	109-179/45-98	112-197/59-103
Aspect Ratio Early/Late Channel	25-42/21-42	26-51/25-54	18-34/18-42

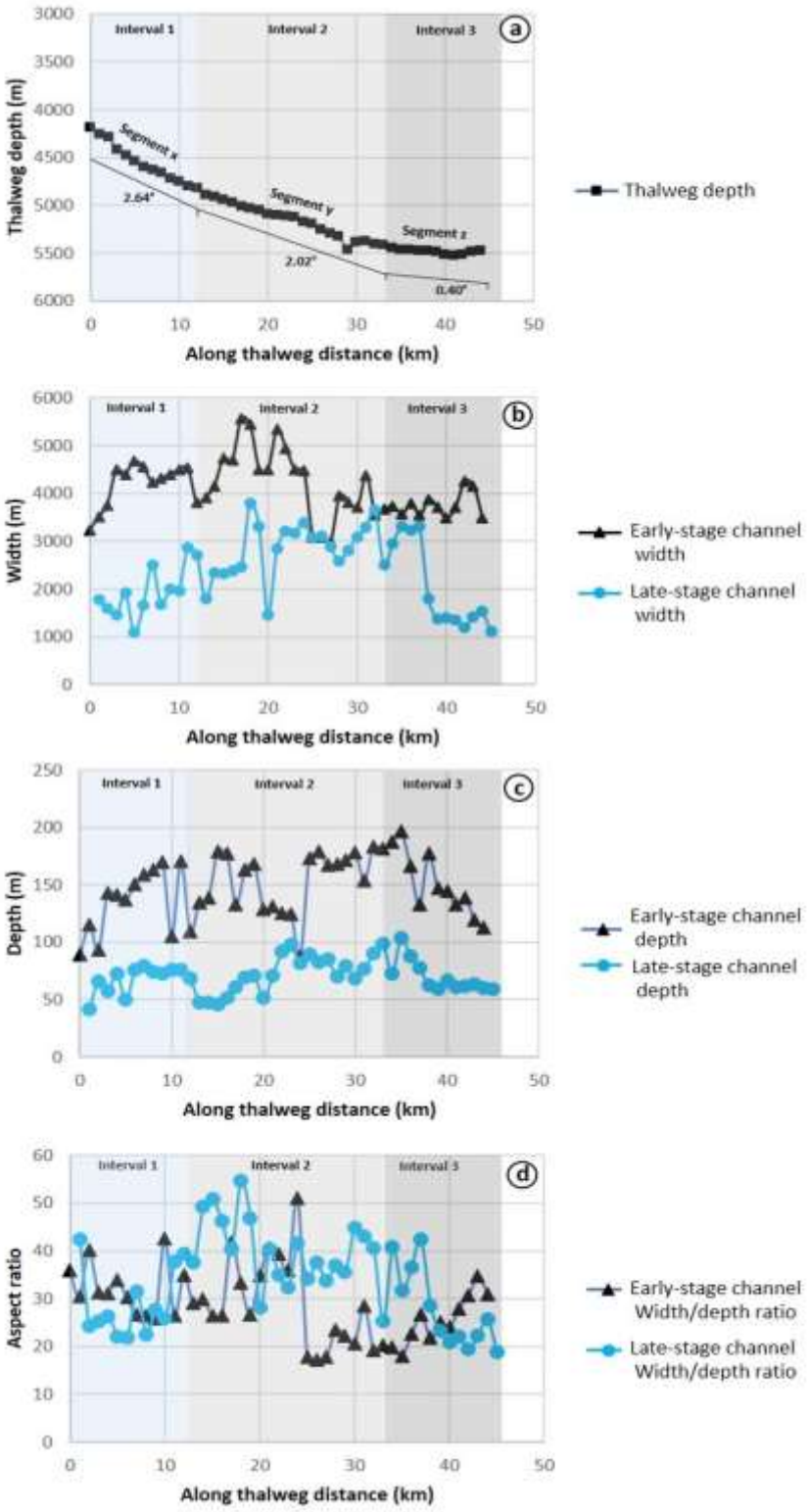

Figure 36. Quantitative analysis of the submarine channel system. a) Width of early-stage channel and late-stage channel. b) Early-stage channel and late-stage channel depth profile. c) Aspect ratio (width/depth) of the early-stage channel and late-stage channel. d) Depth profile of channel thalweg along the channel.

In conclusion, the integrated analysis of high-resolution 3D seismic reflection data and borehole information has enabled the identification and detailed characterization of a well-developed Late Cretaceous submarine channel system in the deep-water Kribi-Campo Sub-basin, offshore Cameroon. This channel system, trending NE–SW, exhibits a complex two-phase evolution with distinct morphological and architectural features, including segmentation into three parts based on geometry and internal fill characteristics. The study reveals that the development and depositional architecture of the system were primarily influenced by tectonic activity, sediment supply, relative sea-level fluctuations, and paleotopographic gradients. Notably, variations in slope gradient were found to control sediment grain size distribution along the channel. The results also underscore the role of the Sanaga and Nyong Rivers as major sediment sources. These insights not only enhance our understanding of deep-water depositional systems but also hold significant implications for predicting reservoir distribution and guiding hydrocarbon exploration in frontier deep-water settings.

Chapter 5: Submarine fans in the Kribi-Campo sub-basin, offshore Cameroon: geomorphology and stratigraphic evolution during the Late Cretaceous

This chapter aims to define the key seismic horizons and carrying out seismic facies analysis of the Late Cretaceous sequence, with particular emphasis on the identification and interpretation of deep-water depositional elements (i.e., channel/fan systems). It is also focuses on stratigraphy and morphology of submarine fans.

5.1. Seismic stratigraphic framework

The seismic stratigraphic framework for this study area has been divided it into nine seismic sequences, separated by ten horizons (KC-1 to KC-9 and the seafloor), based on the combination of internal seismic reflection configuration and on seismic well-tie (Fig. 37). The interval of interest in the study area is a Late Cretaceous stratigraphy, which is bounded by the KC-2 and KC-4 horizons at the base and top, respectively.

The Late Cretaceous stratigraphy of the Kribi-Campo sub-Basin was subdivided into two seismic sequences named S1 and S2, based on the observed changes in seismic geometries and depositional environments (Fig. 38). S1 is bounded below by KC-2 and above by the KC-3 horizon. KC-2 horizon is characterized by onlap above in the southeast area (Fig. 38). The surface extends across almost all the study area, but onlaps against the Kribi High in the east. KC-3 is top of sequence S1 and has a high-amplitude reflection with good continuity. The surface is also characterized by onlap above in the Kribi High area and defines the top of the stack of high to bright amplitude reflection laterally migrating westward which extends from the east to the southern half of the study area (Fig. 38). Sequence S1 is Santonian to Campanian in age, consists of sub-parallel, low amplitude discontinuous reflections, but also contains discrete high amplitude reflections observed to the east and to the base of horizon KC-3 (Fig. 38). The high to bright amplitude reflections observed is interpreted as the submarine fan. Immediately below of high amplitude, there are the features showing lateral offset stacking patterns which are interpreted to be the product of laterally shifting, vertical aggrading channels. They are interpreted to be sinuous channel complexes evolving through time, constrained by the Kribi High to the east. Sequence S2 forms the uppermost sequence in the Late Cretaceous, bounded by KC-3 at the base and the KC-4 surface at the top. S2 is Campanian to Maastrichtian in age and corresponds to low to high amplitude. There is also a large incision that occurs within this sequence.

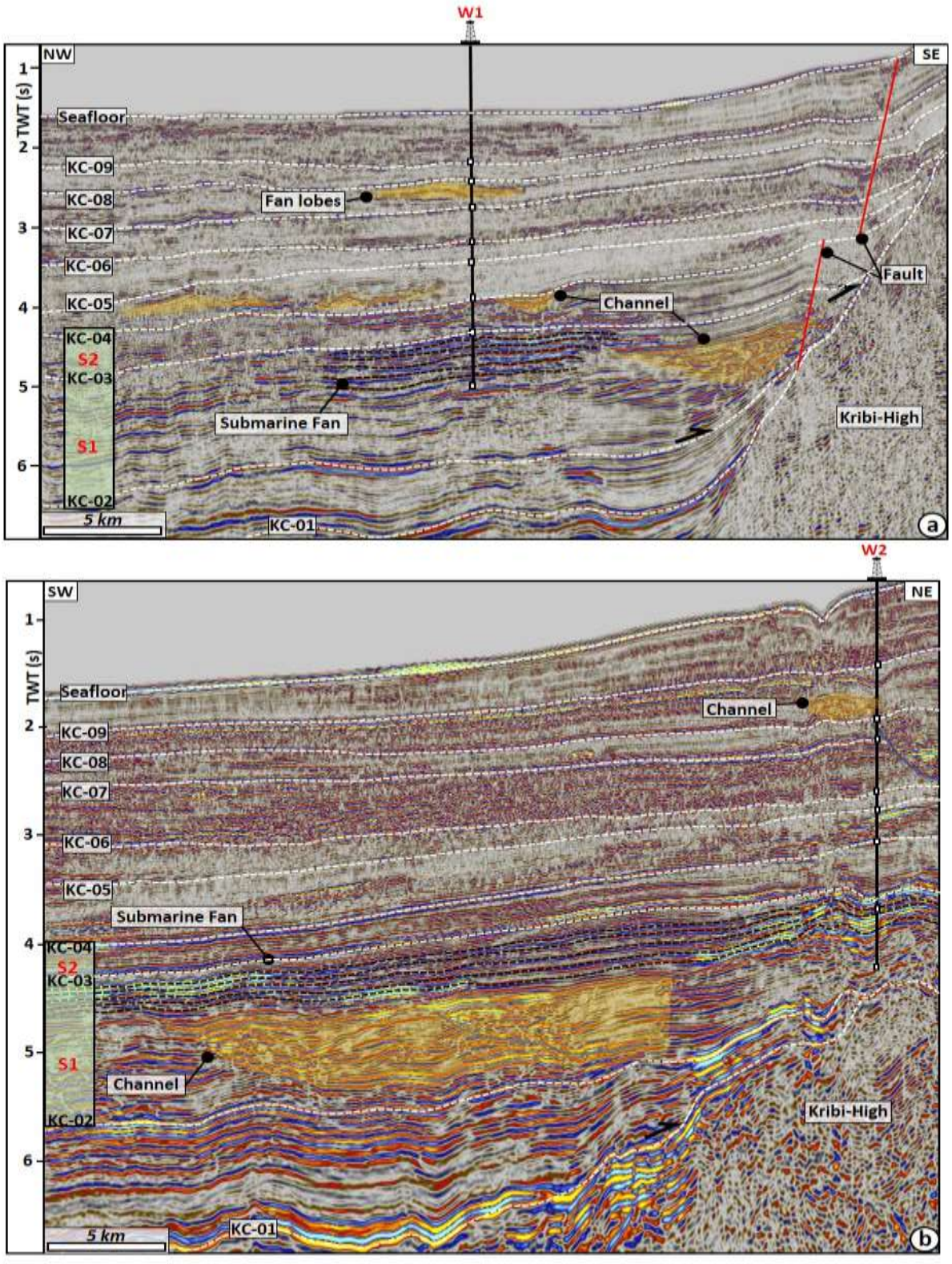

Figure 37. a) Seismic line through W1 well showing the entire basin successions and channel complex deposits identified within the dataset. Ten Horizon name (KC-1 to KC-9 and the seafloor) are identified in the study area. b) Seismic section through W2 well, taken perpendicular to regional dip, showing the channel complex deposits within the study interval.

5.2. Seismic facies and depositional elements

According to recognition criteria on the previous studies of submarine depositional elements (Posamentier and Kolla, 2003; Deptuck et al., 2007; Niyazi et al., 2018; Bouchakour et al., 2023), four major seismic facies were identified within the study interval (sequence S2 and S1). They are interpreted as: submarine channel system, levee deposits, submarine fans, and hemipelagic sediments (Table 8).

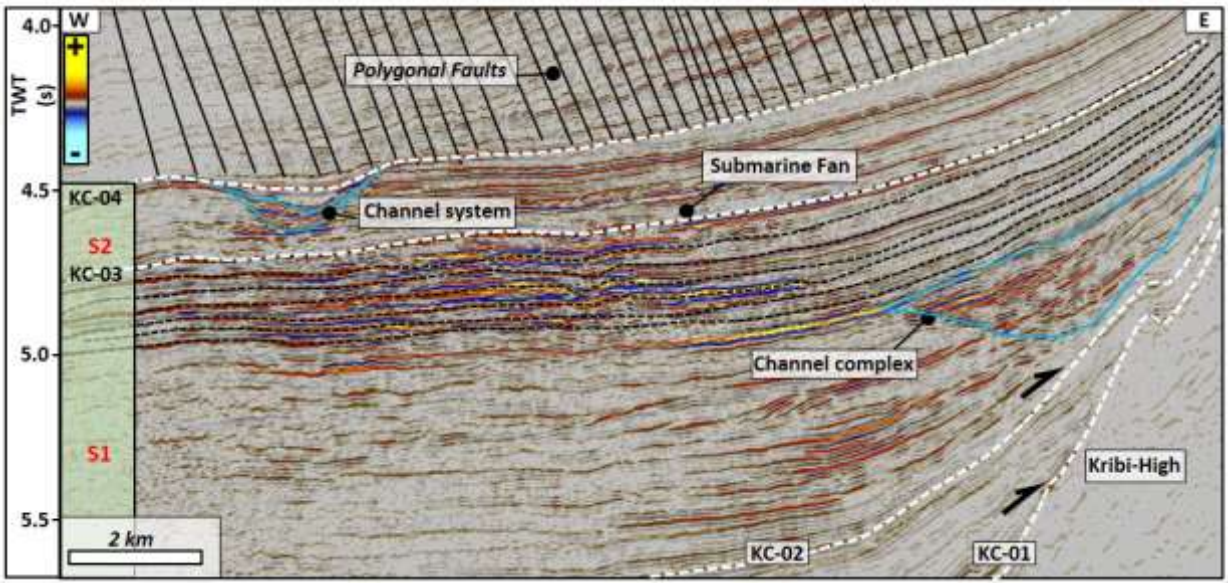

Figure 38. Interpreted seismic stratigraphy of the slope Late Cretaceous showing the submarine fan, channel complex located within (S1) and the submarine channel system is located within sequence (S2).

5.2.1. Submarine channel system

This seismic facies has U-shaped features of stacked, somewhat chaotic reflections, with medium to high amplitude at the base and low amplitude at the top (Table 8). This facies exhibits two stages of channel infilling with a maximum incision depth of 197 m. The high amplitude channel fills are interpreted to be sand rich, whereas the low amplitude channel fills are interpreted, to be mud rich, show flat overlying reflections (Posamentier and Kolla, 2003). Similar seismic facies and seismic geomorphology have been observed in many other studies of deep-water depositional systems (Deptuck et al., 2007; Niyazi et al, 2018) and as a result of this work, they are interpreted as submarine channel deposits.

5.2.2. Levee deposits

This facies was observed on either side of the submarine channel system, characterized by high to low amplitude convergent reflectors. Its seismic reflection amplitude varies laterally and, typically decreasing away from the channel axis before downlapping onto underlying deposits (Fig. 38). The geometry and reflection characteristics of this seismic facies has been recognised by other authors as external levees associated with channel system, formed when the height of turbidity currents exceeds the confinement of the channel form and spill sediment onto the areas surrounding the channel axis (Deptuck et al., 2007; Posamentier & Kolla, 2003). Often this overspill is fine-grained due to flow stripping, resulting in a mud-dominated deposit and the low-amplitude response commonly observed in seismic reflection data (Table 8).

5.2.3. Submarine fans

This seismic facies is composed of distinctive, sub-parallel continuous medium- to high-amplitude reflections displaying an aggradational pattern in cross-section and it has a maximum thickness of 500 m, typically thinning and downlapping towards the outer edges (Table 8). On seismic attribute maps, these deposits represent the fans with an internal distributary channel. These fans-shaped deposits have been observed along the slope through to basin-floor, in deep-water settings (Posamentier & Kolla, 2003), and they are variably referred to as channelised lobes, frontal splays, sheet sands and submarine fans.

5.2.4. Hemipelagic sediments

The seismic facies are semi-transparent, low-amplitude reflections, discontinuous to continuous seismic reflections, that are parallel and conformable to underlying deposits (Table 8). It occurs in the entire seismic volume on the map-view outside the submarine fans. These seismic characteristics have been observed in many areas, and even in the study area and correspond to pelagic and hemipelagic mud and silt during sediment starvation in low-energy environments (Bouchakour et al., 2023).

5.3. Submarine fans: stratigraphy and morphology

The stratigraphy of the interval of interest shows that the submarine fan in the study area is framed at the base and top by two distinct channels. The lower channel is wider, located within the older Santonian-Campanian sequence. In cross-section, it is U-shaped and these patterns are constrained between the Kribi High and a fault (Fig. 39b and c). Its mapping reveals a large amplitude sinuous pattern-oriented NE-SW (Fig. 40a). Above this lower channel, the development of Campanian submarine fan deposits is clearly observed (Fig. 39d). The internal

architecture and geometry of the submarine fan was analysed by observing the cross-sections and seismic attribute maps, but also based on the integration of the W1 well logs. The submarine fans are buried at 4550 m below the seafloor and its large amplitude seismic facies shows an aggradation pattern with parallel reflectors and good continuity.

Table 8. Description and the interpretation of the seismic facies observed within the Late Cretaceous sequence

Seismic facies interpretation	Seismic section	Description	Plan/map view
Submarine Channel System	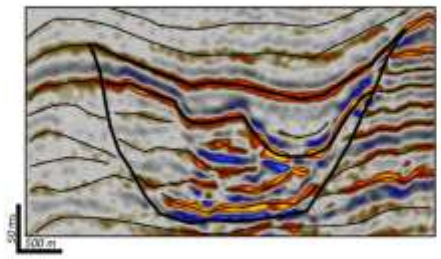	Chaotic, high amplitude, discontinuous reflections, basal lags usually confined within a V- or U- shaped external geometry	
Levees	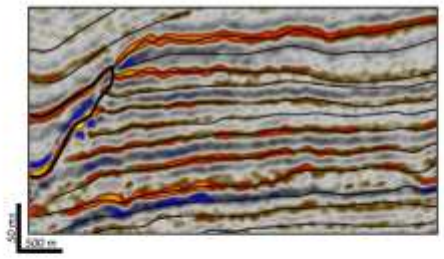	high- to low-amplitude, continuous, parallel to subparallel reflections	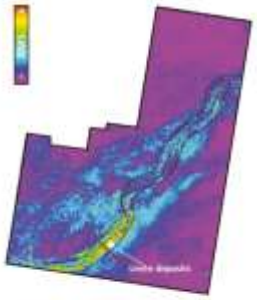
Submarine Fan	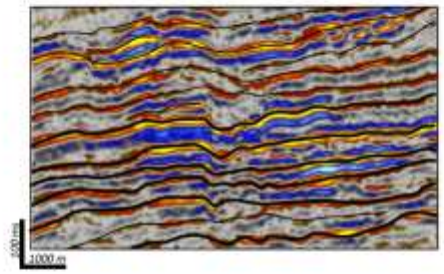	High amplitude seismic facies displaying an aggradational pattern with parallel and good continuity reflectors	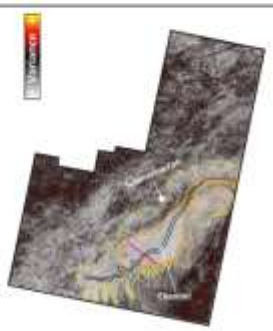
Hemipelagics sediments	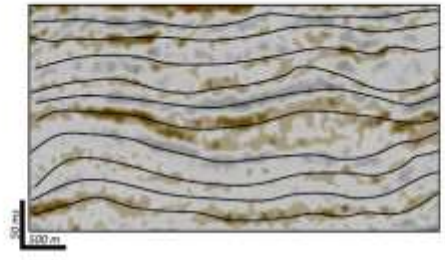	Semi transparent, low amplitude, semi-continuous to continuous reflections	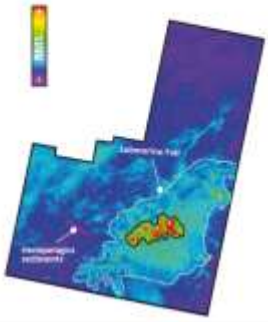

In cross sections, submarine fans reflectors onlap the slope face until the Kribi-Campo High, and the fan thins distally and laterally (Fig. 39). The stratal onlap is also observed against local slopes (Fig. 39c and d), near the Kribi-Campo high, suggesting that relief already existed during submarine fan deposition. The fan-shaped stacked features are up to 500 m thick and locally contain U-shaped features of varying dimensions ranging from (10 km long, 2 km wide and 70 m depth), relatively linear upslope, to (20 km long, 0.2 km wide and 10 m depth), highly sinuous downslope (Figs. 40, 41 and 42). Prominent levees are observed on the larger scale features and decrease high and amplitudes away the channels (Fig. 39a). Seven mapped stratal slices and labelled from fan A to fan G, highlight different evolutionary stages of the submarine fans. Along each of the stratal slices plotted on the seismic sections, variations in seismic reflection amplitudes are observed laterally. From left to right of the cross-sections, low amplitude reflectors (LARs) are observed. Then the trend increases towards moderate amplitude reflectors (MAR) and high amplitude reflectors (HARs) near the channel (Fig. 39a). As the amplitudes move away from the channel axis (Fig. 39a), there is a decreasing trend in seismic reflections from the MARs towards the LARs that strike the Kribi High to the east (Fig. 39c and d). On the amplitude maps, the LARs correspond to amplitudes of low RMS and high variance, conversely the HARs correspond to amplitudes of high RMS and low variance. (HAR) representing the filling of the fan with sandy-prone deposits, with a large area of low to medium reflection amplitude (LAR and MAR) which generally represent muddy-prone deposits with pasts of silty-prone deposits (Figs. 40, 41 and 42).

Furthermore, based on observation criteria such as fan shape, channel inclusion and difference in sand volume within the submarine fan, the submarine fan system was grouped into three distinct periods. These distinct periods of initiation, growth and retreat can be clearly identified (Figs. 40, 41 and 42), sufficient to map the geometry and internal architecture of the submarine fans in some detail. Amplitude attribute maps of the stratal slice (from fan A to fan G) of the submarine fan system cover an area of 600 km^2 and are oriented NE-SW, close to the Kribi High. Fans A and B are the lowest in the submarine fan system (Fig. 40b and c).

Fan A is a low-amplitude and not clearly defined by seismic attributes (Fig. 40b). It also lies close to the lower large channel and has a base seal risk due to proximity to the lower channel (Figs. 39 and 40a). The fan has an elongate lobate geometry and it is interpreted to be stratigraphically trapped through shale plugging of the feeder channel, expressed by an absence or a low presence of a sand-prone attribute response.

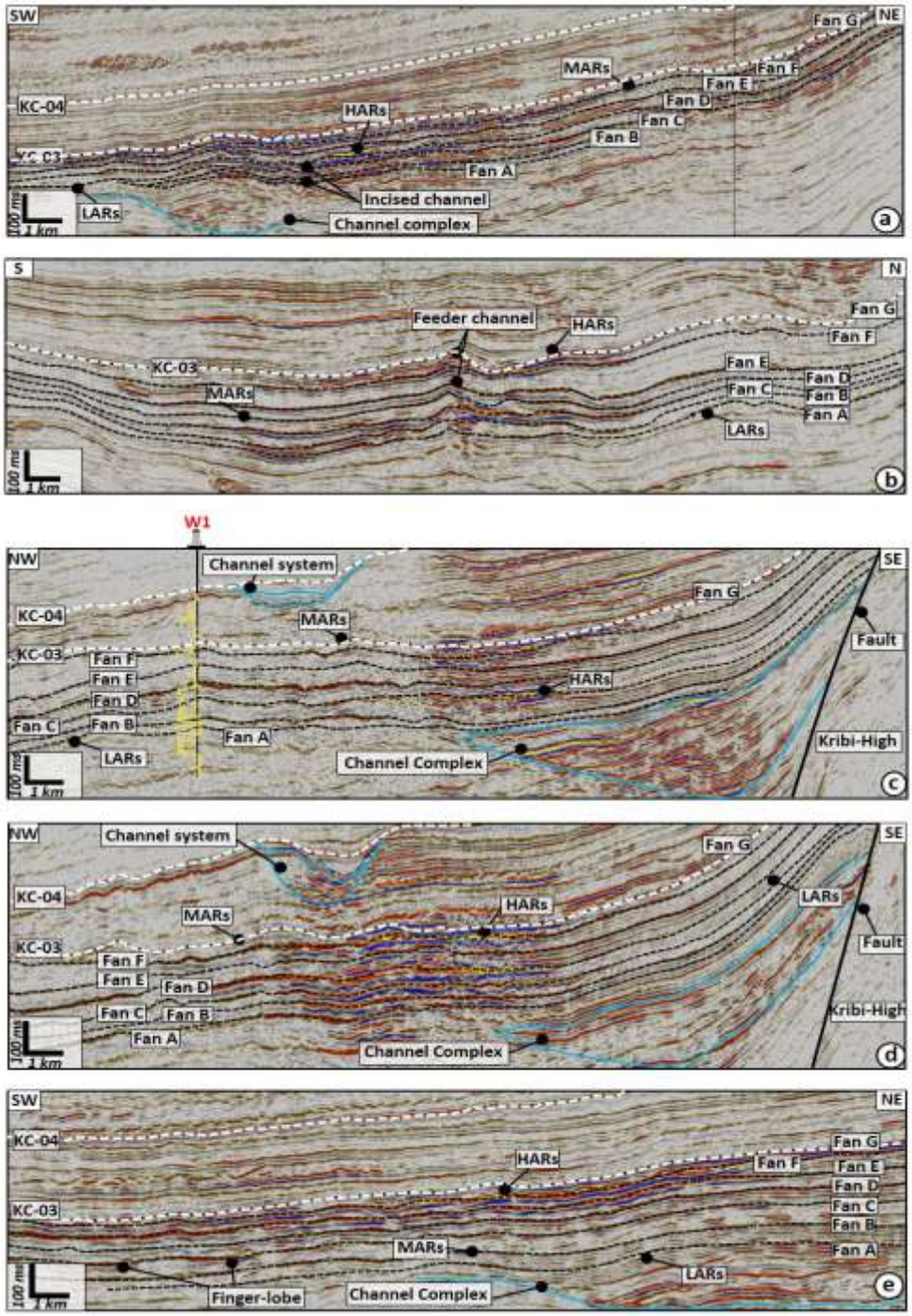

Figure 39. Submarine fan external morphology and stratigraphy in the cross-section with indication of seven stratal horizons (fan A to fan G). a) Dip-oriented seismic section showing incised channel within the submarine fan, b) strike-oriented seismic sections showing feeder channel within the submarine fan, c) and d) seismic sections showing submarine fan between channel complex and channel system, e) seismic section showing a finger-lobe in the submarine fan. MARS: Moderate amplitude seismic reflection, HARS and LARS indicate High and Low amplitude seismic reflection.

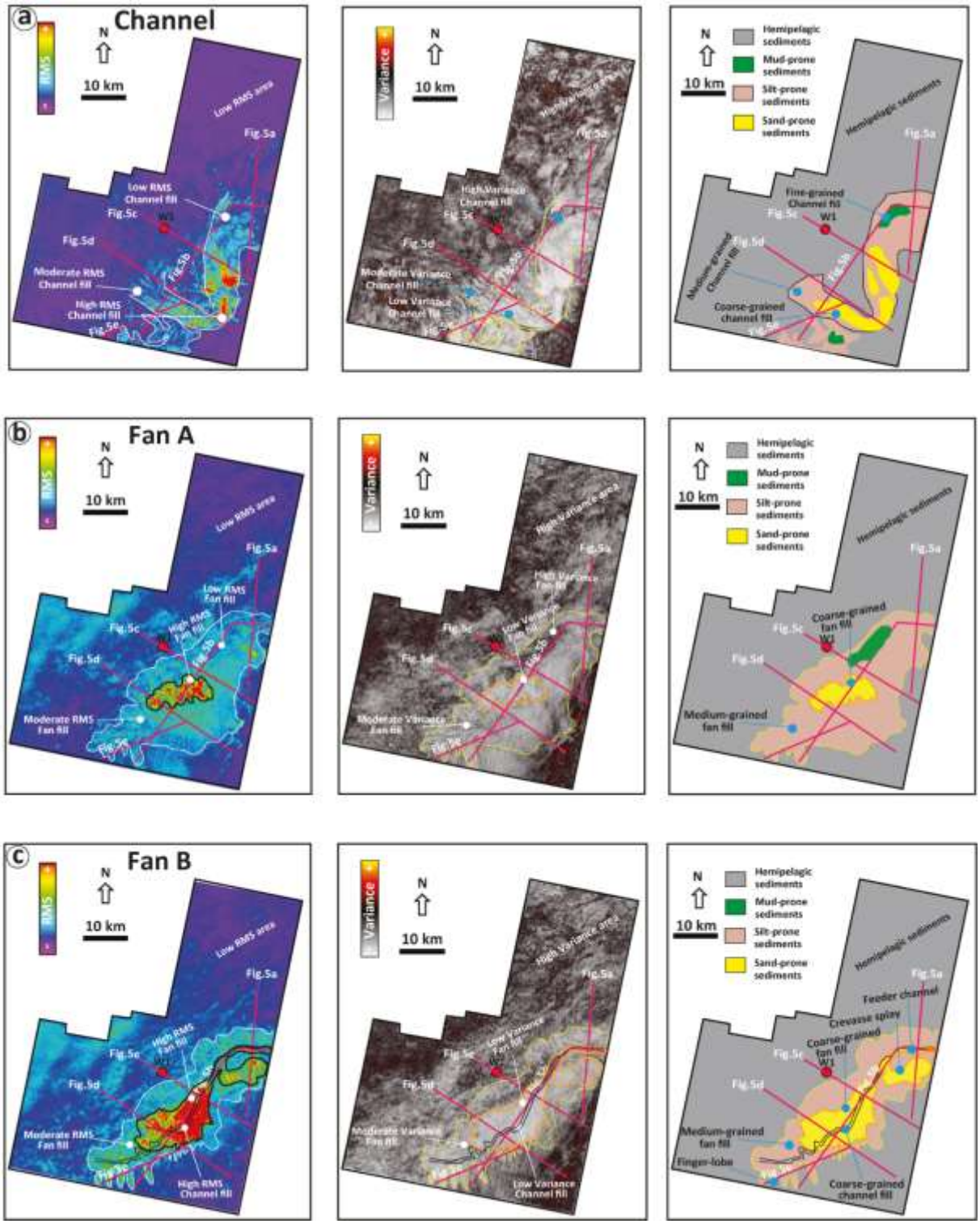

Figure 40. RMS, Variance seismic attributes, and their interpretations, of the various stratal slice within the bottom and base fan (see Fig. 39). a) The seismic attributes analysis shows the distribution of several types of sediments deposited of the channel complex. b) and c) The seismic attributes analysis shows the distribution of several types of sediments deposited during the initiation phase of the submarine fan (Fan A to B).

Fan B has similar morphological characteristics to fan A which lies above it, but fan B is large, with very high amplitude on the SE margin, and weak amplitude to the NW. The very high lithology amplitude values on the SE margin may indicate thin cemented sandstones. The fan B has a large lobate geometry and a sinuous distributary channel is present on the SE margin (Fig. 40c). This submarine fan shows an initial phase of submarine fan development that manifests itself as a prominent channel in the upslope area that slopes downwards in a NE-SW orientation, ending in a large-scale lobe in the southern area downslope (Fig. 41c). Thus, as it goes farther downslope, the channel is replaced by large-scale lobe, which may result from the varied seafloor topography.

The geometry of the fan shows that sediment entry occurred from the east of the canyon (Fig. 6b and 6c). At its downstream end, high amplitudes stack from the SW area and are interpreted as a sand-prone lobe (Fig. 40b and c).

Fans C, D, and E are in the middle of the submarine fan system (Fig. 41a, b and c). They are bright to high-amplitude reflectors with good continuity and are clearly defined in the cross-section (Fig. 39). The fan locally contains U-shaped features (Fig. 41a), and Theses U-shaped features are linear to sinuous in map view and interpreted as a channel; channel-levees are observed in the upper slope. These submarine fans are relatively large compared to other submarine fans and have a prominent lobate geometry comprising a sinuous distribution channel radiating from the east feeder channel to a south-west downslope end (Fig. 41). The channel sinuosity is low in the upslope area, and increases gradually downslope, the feeder channel appears to be relatively constant in size and location during the evolution of the fan (Fig. 41). Thus, the submarine fans (C-E) mark the growth phase. Fan C is a large well-defined fan with High amplitudes on its SE margin, and weaker amplitudes to the NW (Fig. 41a). The high lithology amplitudes are likely to indicate more cemented sandstones. The fan C geometry shows sediment entry was via the east canyon.

The fan C also has a large lobate geometry and a sinuous distributary channel is present to the SE. It overlies Fan B and Fan A, and is itself overlain by the silt prone Fan D. Fan D show an elongate lobe geometry and can be is interpreted as a silt prone interval (Fig. 41b). The variation of amplitudes within the feeder channel which suggest variable lithologies here (silt and sand prone sequences). Fan E is a large well-defined fan with bright amplitudes (Fig. 41c). The fan shows a high amplitude within the main fan channel and within an interpreted crevasse splay in the SE.

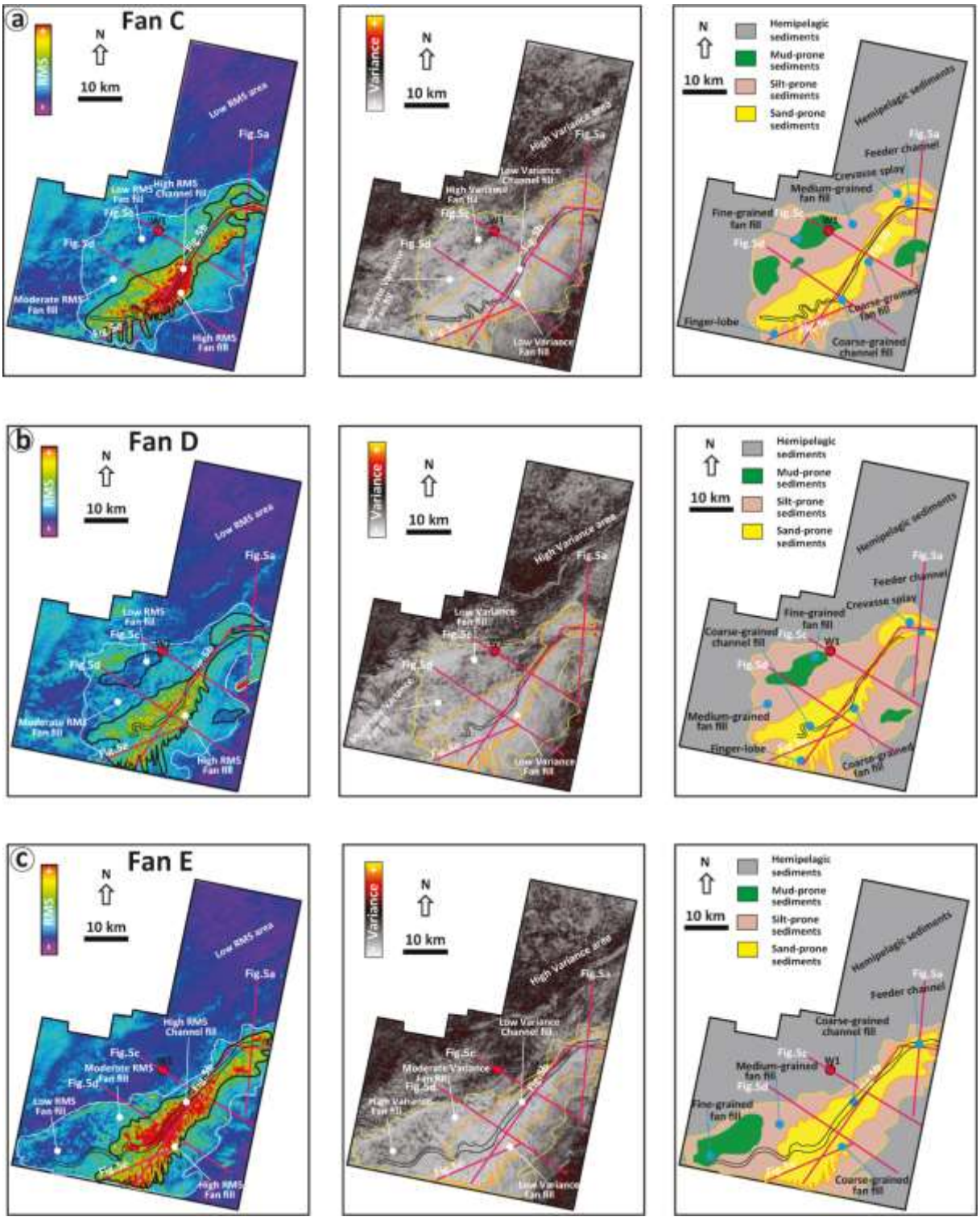

Figure 41. RMS, Variance seismic attributes, and their interpretations, of the various stratal slice within the bottom and base fan (see Fig. 39). a), b) and c) The seismic attributes analysis shows the distribution of several types of sediments deposited during the growth phase of the submarine fan (Fan C to E).

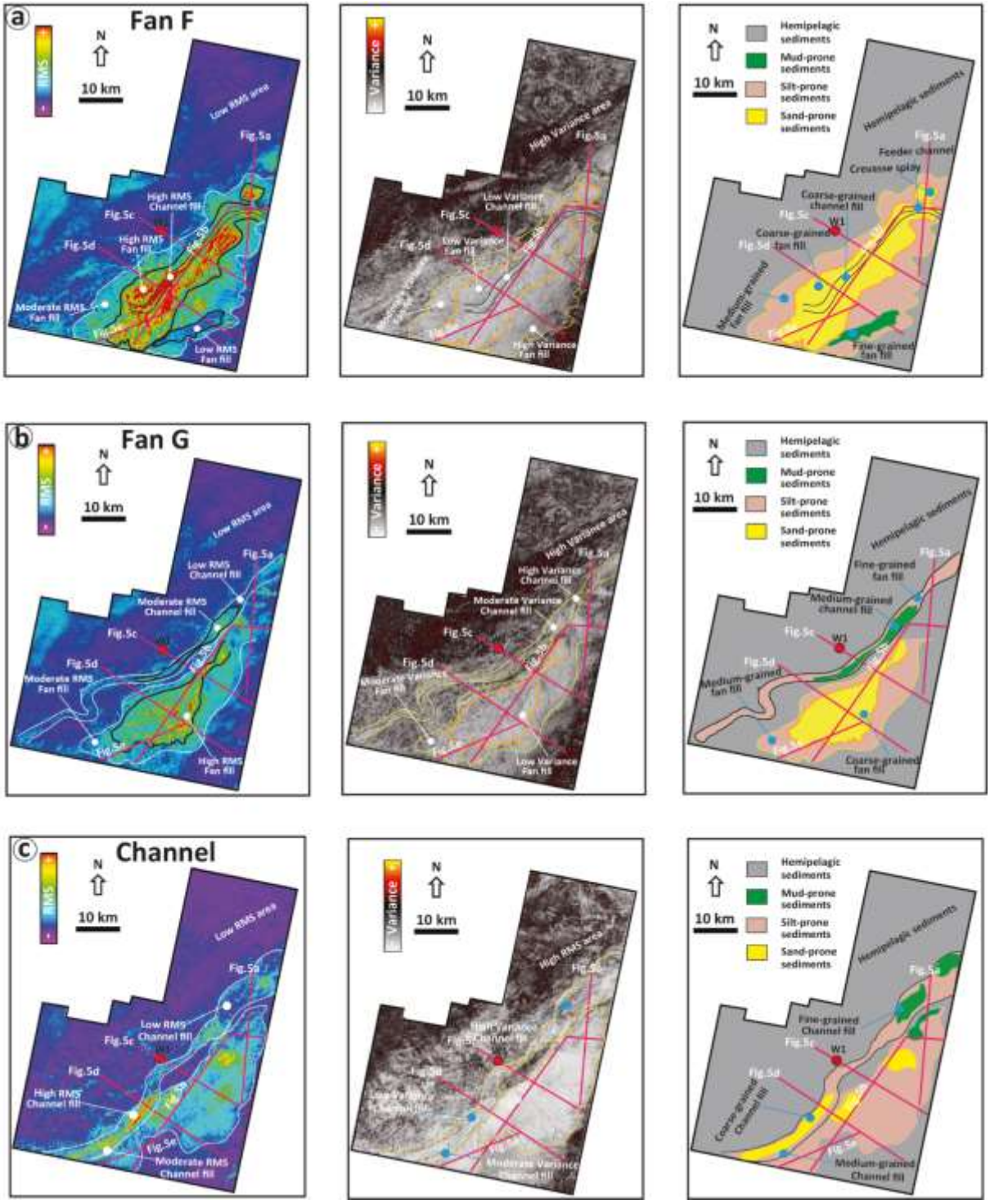

Figure 42. RMS, Variance seismic attributes, and their interpretations, of the various stratal slice within the bottom and base fan (see Fig. 39). a) and b) The seismic attributes analysis shows the distribution of several types of sediments deposited during the retreat phase of the submarine fan (Fan F to G). c) The seismic attributes analysis shows the distribution of several types of sediments deposited of the channel system.

The fan E has a large lobate geometry and a sinuous distributary channel on the SE side of the fan. The map for these fans shows separation of the fan amplitude from feeder channel and overbank amplitude updip. Furthermore, a most remarkable observation of the lobe morphology during this phase is the presence of a series of relatively parallel elongated features during the growth phase is the presence of series of relatively parallel high amplitude elongate features with finger-like terminations at the margin of the submarine fan, with the dimension of 0.5 to 5 km length and up to 2 km width (Figs. 39d and 41). They branch off at high angles downslope, with an angle of up to 90^{o} to the overall transport direction. This feature is clearly visible in fan C, it is characterised by high RMS amplitudes and low variance amplitudes and is interpreted as thick massive sands, formed as a result of sedimentary gravity flows that deviate from the main flow and erode into a pelagic clay substrate.

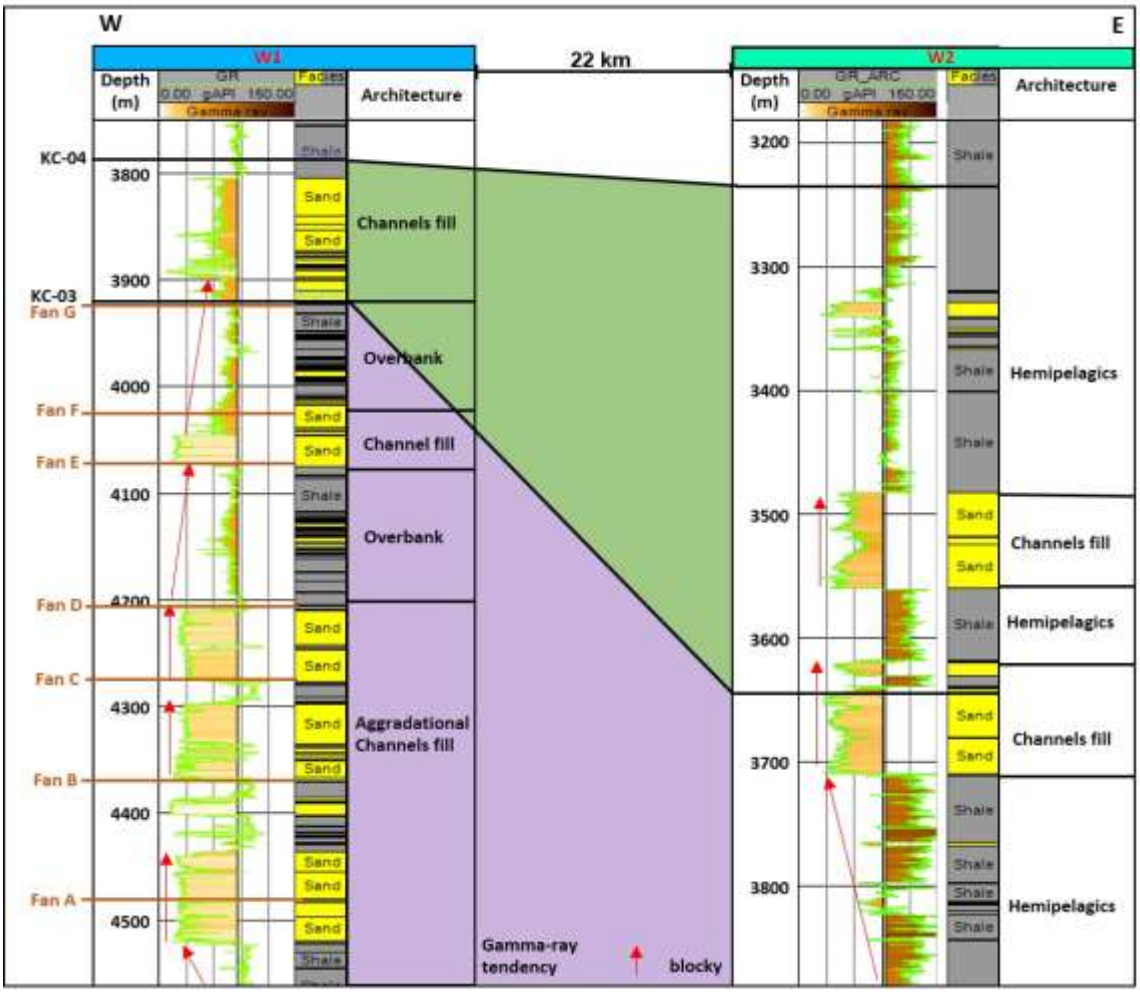

Figure 43. Well-log correlation and interpretation of the submarine fan architecture. Approximate location of stratal slices, which correspond to Fan A-G extracted from seismic data is indicated.

Fans F and G are the youngest within the submarine fan system (Fig. 42a and b). Fan F is a large well-defined elongate fan. The amplitude map shows a prominent channel feature running down the axis of the fan then turning west (Fig. 42a). These fans are relatively small compared to the other submarine fans and probably represent a retreat/terminal phase of submarine fan development (Fig. 42a and b). At the top, the fan G is capped by a major Maastrichtian channel that comprises two episodes of erosion and infilling as indicated by the recent work of Secke et al., 2022 (Fig. 42c). The blocky GR log signature of the entire interval of interest suggests the nature of thick-bedded amalgamated sands and interbedded mud sets, showing a cylindrical shape consistent with channel fills within a submarine fan system (Fig. 43).

In summary, seismic geomorphological analysis of 3D seismic and well data has revealed the internal architecture and evolution of a deeply buried Campanian basin-floor fan system in the Kribi-Campo Basin. The fan, oriented NE–SW, developed through distinct initiation, growth, and abandonment phases and was fed by sediment input from an eastern canyon linked to the paleo-Nyong fluvial system. It comprises stacked, coarse-grained turbidite sandstones with minor fine-grained interbeds. The fan's evolution was primarily driven by sea-level fluctuations and tectonic uplift along the Kribi-Campo High, which shaped the basin's unconfined topography and facilitated the accumulation of thick Late Cretaceous clastic deposits.

Chapter 6: Petrophysical analysis of the Late-Cretaceous Logbaba Formation in the Kribi/Campo sub-basin: implication on deep-water hydrocarbon exploration

The availability of a suite of conventional well logs from two deep-water boreholes (W1 and W2) targeting the Kribi-Campo sub-basin provide an excellent opportunity to further characterize potential reservoirs within the Late Cretaceous basin fill. Therefore, the objective of this part is oriented towards the detailed petrophysical analysis of the reservoir intervals of the Logbaba Formation from two wells W1 and W2 in the Kribi-Campo sub-basin. The ultimate goal is to evaluate the reservoir potential of the formation and thus ultimately provide additional information on the hydrocarbon potential of the sub-basin and aid future deep-water exploration for characterization of the carbone capture storage sites.

6.1 Lithological and mineralogical interpretation

The lithological and mineralogical components of Logbaba Formation reservoirs within selected wells were interpreted using different cross plots (Figs. 44-48), where different matrix types appear by integrating different well logs (Table 9).

6.1.1 Neutron (NPHI) versus density (RHOB), Neutron (NPHI) vs gamma ray (GR) and Neutron (NPHI) vs Sonic (DT) cross-plot

The neutron (NPHI) versus density (RHOB) cross-plot shows that the Logbaba Formation reservoirs within selected wells consist mainly of sandstone with carbonates (limestone and dolomite) (Fig. 44). This neutron-derived cross plot against density also helps to estimate the relationship between different types of lithology and porosity (Al-Qayim and Rashid, 2012; Hakimi et al., 2017; Chongwain et al., 2018; Qadri et al., 2019). The cross plot indicates the presence of both sandstone and carbonates, while also showing the presence of intergranular and secondary porosities in equal proportion.

The neutron vs. gamma ray cross plot shows the presence of scattering data points, indicating that the Logbaba Formation reservoirs have a varied lithology. Low gamma rays (10-40 API) and intermediate neutron values indicate clean sandstone (Fig. 44a) while medium gamma rays (40-75 API) and neutron values indicate shaly sandstone (Qadri et al., 2019). Intermediate gamma ray values but higher neutron values above 0.22 indicate the presence of carbonates (limestone and dolomite) (Fig. 45). Shale rich contents are identified by high gamma values (above 90 API) with neutron values above 0.22. This classification is based on the schemes of El-Din et al., (2013) and Hakimi et al., (2017). In comparison, the neutron/gamma ray cross-plot (Fig. 45) is consistent with the neutron/density cross plots (Fig. 44), suggesting that the main lithology of the Logbaba Formation reservoirs is composed of sandstones interbedded with carbonates and shales. The clusters indicating sandstone and carbonates are dense compared to the clusters of shale-rich data points.

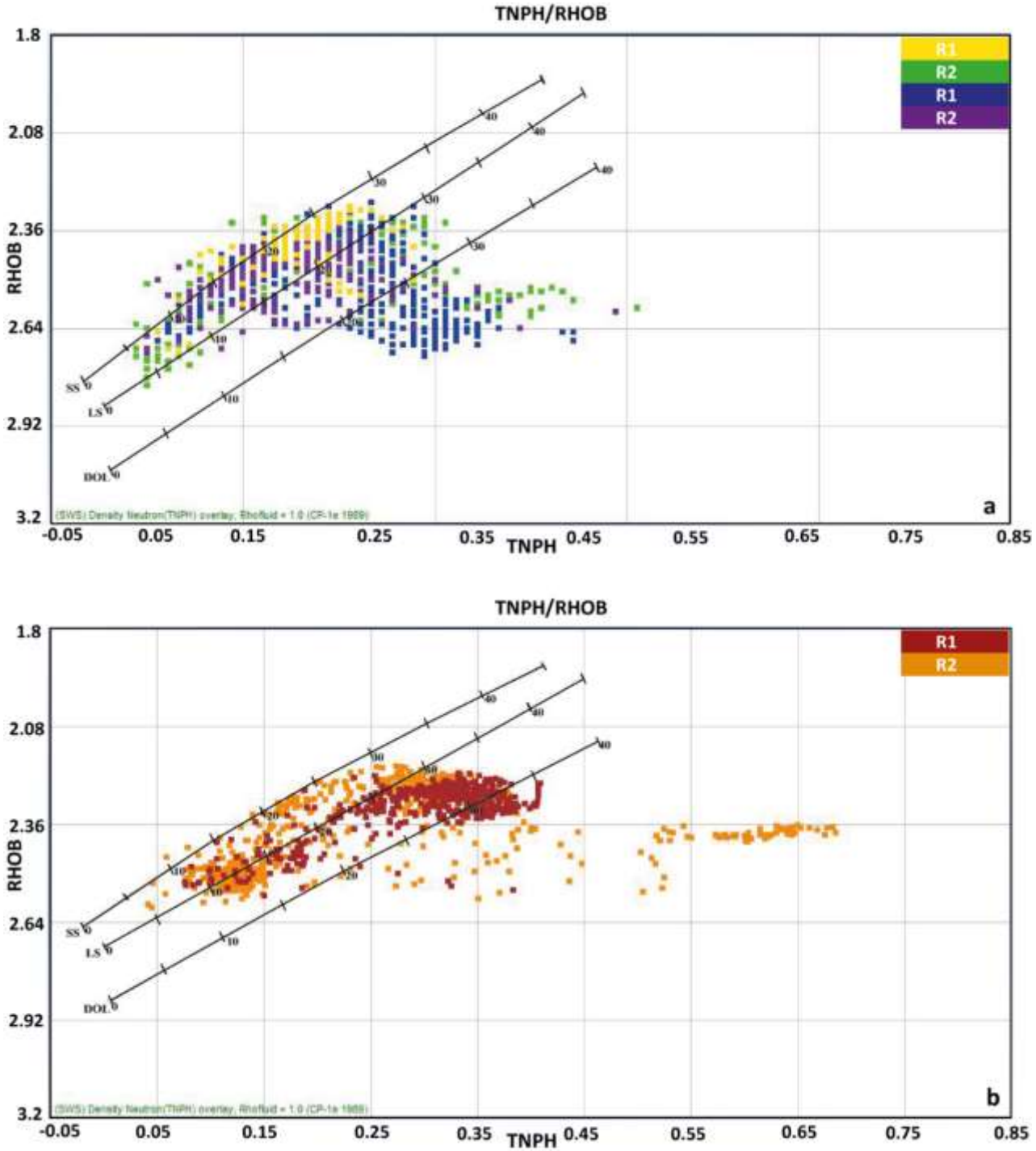

Figure 44. a) Density-neutron for Well W1 reservoirs depicting points scattered across the various lithological field indicating the heterogeneous character of the reservoirs. b) Density-neutron for Well W2 reservoirs depicting points scattered across the various lithological field indicating the heterogeneous character of the reservoirs.

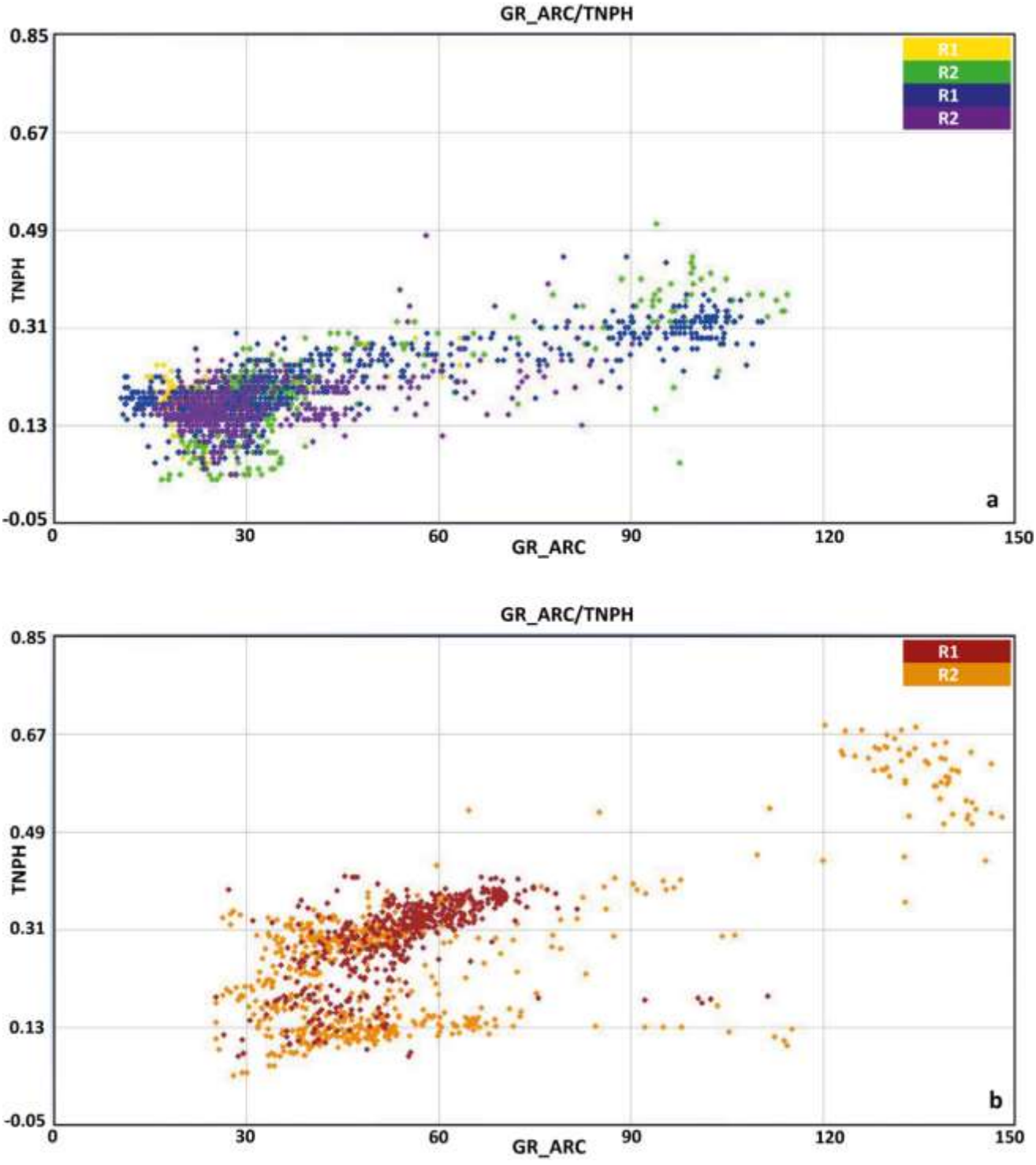

Figure 45. a) Neutron vs. gamma ray cross plot displaying the lithological composition of Logbaba Formation reservoirs within the studied well W1. b) Neutron vs. gamma ray cross plot displaying the lithological composition of Logbaba Formation reservoirs within the studied well W2.

The Logbaba Formation reservoirs are predominantly sandstone and carbonate, as shown by the neutron versus sonic porosity cross plot. The cross plot indicates that the limestone concentration is dominant among the carbonates while dolomite is a subordinate, in agreement with Qadri et al., (2019). The cross plot further reveals that the shale content appears to be high in the Formation's reservoirs (Fig. 46). The results deduced from Fig. 46 are consistent with those of Fig. 45, but differ somewhat from those of Fig. 44 in terms of shale content.

6.1.2 M-N and Potassium (HFK) vs Thorium (HTHO) cross-plot

Following Burke et al., (1969), the M–N cross-plot shown in Fig. 47 reveals that most of the data points appear to be sandstones and carbonates. Most of carbonate points are plotting in the calcite field. In addition to sandstones and carbonates few points show the downward movement and indicate the shale effect. The findings of the M–N cross plot are consistent with the those of the NPHI vs. RHOB and NPHI vs. DT cross plots.

The potassium vs thorium cross-plot allows to identify the clay mineralogy in the reservoir formation (Tiyan and Ayers, 2010). The reservoir formation in the studied well contains a variety of clay minerals (Fig. 48). In well W2, the data points appear to be located mainly within the chlorite field, where the dominant clay mineral is chlorite and montmorillonite, as well as a small group of data points in the mixed clay layer zone. The mixed layers of clay minerals formed as a result of the inter-layering of various clay minerals in a single structure (Srodo´n, 1999).

6.2 Lithological zonation of the reservoirs

Based on the GR log responses from the W1 and W2 boreholes, six reservoir units were identified at depths ranging between 3947 - 4736 m (W1) and 3215 - 4051 m (W2) in the study area (Figs. 49 and 50). In W1, four sand bodies were identified and named R1, R2, R3 and R4 with thicknesses of 27, 73.4, 105.7 and 87.3 m, respectively (Fig. 49a). In W2, on the other hand, only two sand bodies were delineated, R1 and R2, with thicknesses of 77.2 and 93.6 m (Fig. 49b). Analysis of the GR log from well W1 in reservoir R1 (4073 - 4100 m) reveals this interval is composed of sandstone, predominantly coarse grained, with intercalations of dolomite (Figs. 49 and 50a). Reservoirs R2 (4230 - 4303.4 m) and R3 (4323 - 4428 m) are separated by a 20 m thick unit comprising claystone with dolomite layers. R2 and R3 consists of medium grained sandstone, and rare dolomite (Figs. 49 and 50a). The interval R4 (4463 - 4550.3 m) consists medium to very coarse grained sandstones (Figs. 49 and 50a).

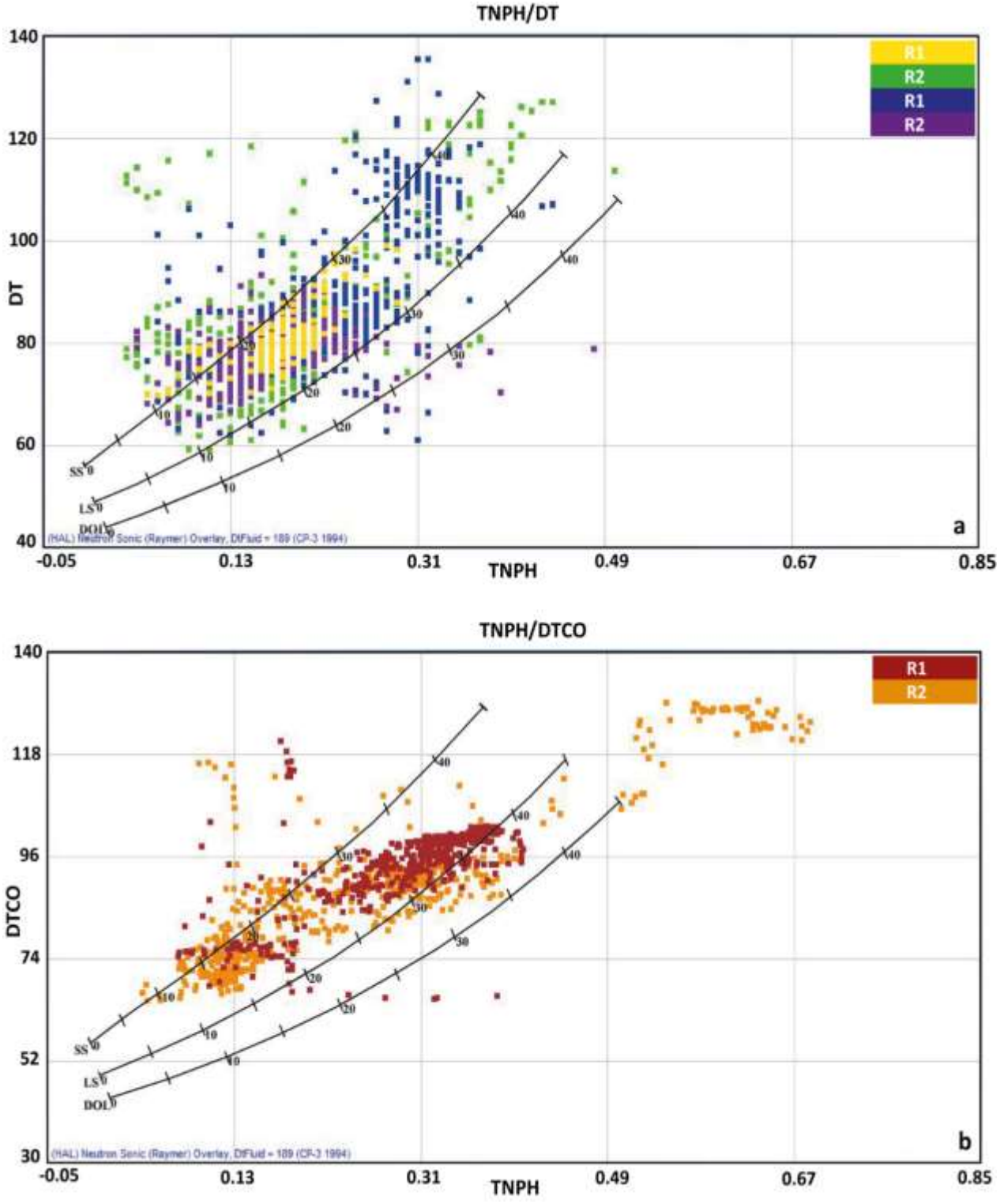

Figure 46. a) Neutron vs. sonic cross plot displaying the lithological composition of Logbaba Formation reservoirs within the studied well W1. b) Neutron vs. sonic cross plot displaying the lithological composition of Logbaba Formation reservoirs within the studied well W2.

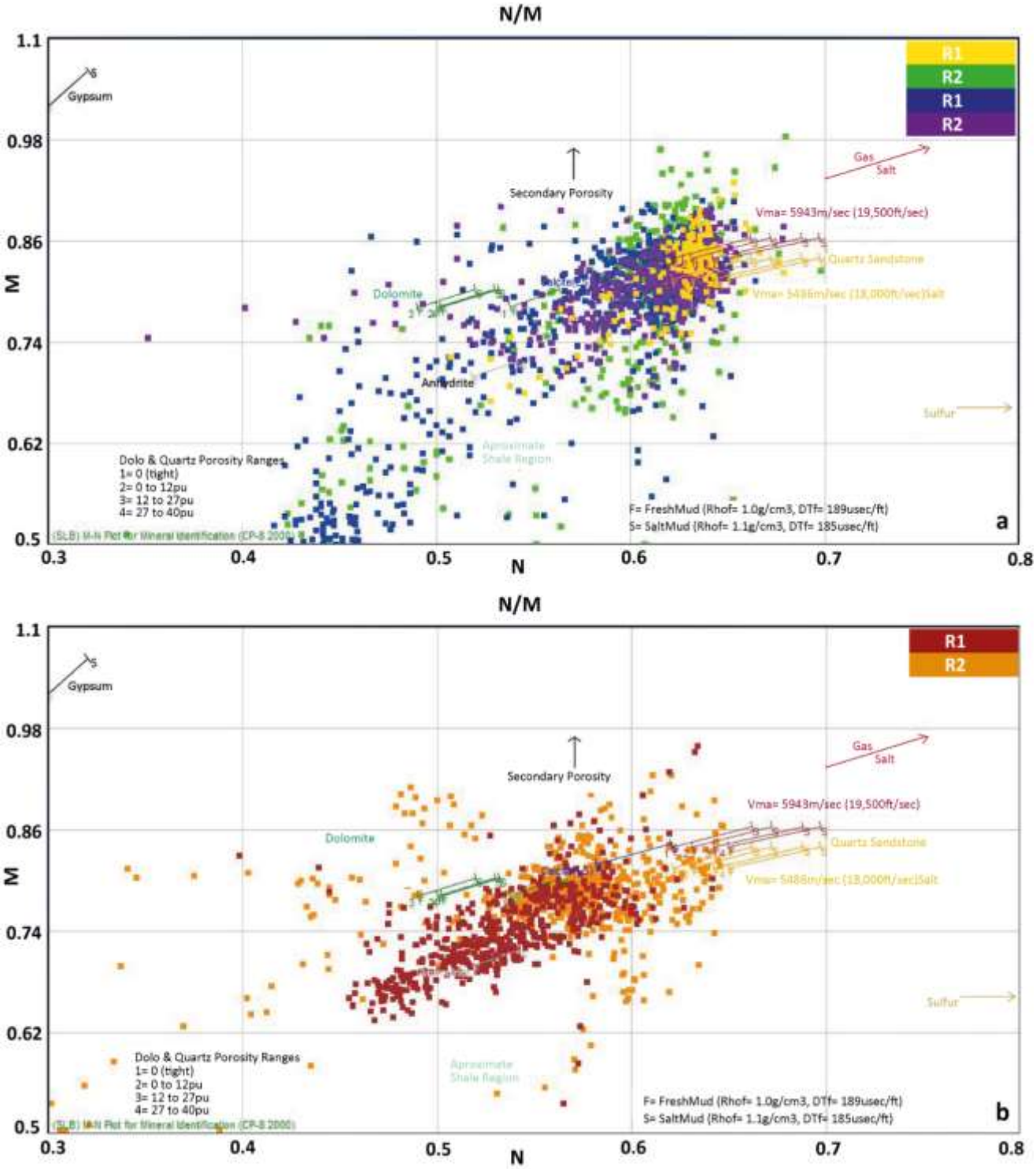

Figure 47. a) M-N cross plot of the Logbaba formation reservoirs within the studied well W1. b) M-N cross plot of the Logbaba formation reservoirs within the studied well W2.

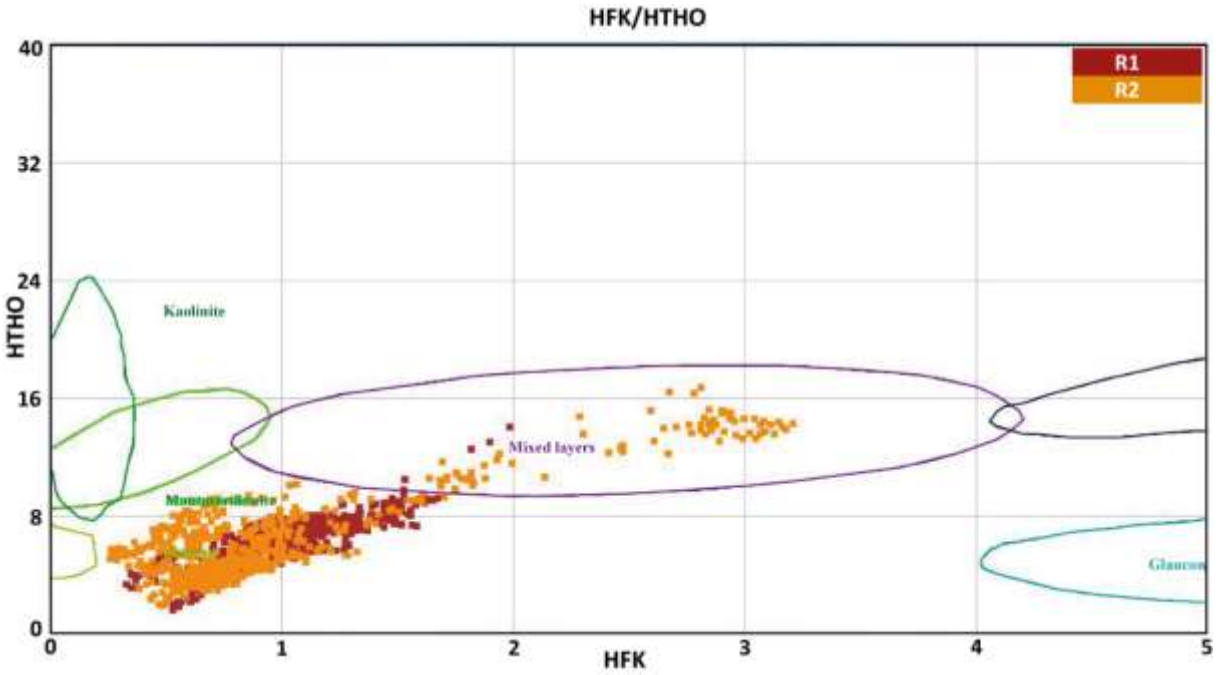

Figure 48. Thorium vs. Potassium cross plot indicating different clay minerals within the Logbaba Formation reservoirs of W2 well.

In well W2, analysis of the GR log of reservoir R1 (3510 - 3587.2 m) interval consists of alternating massive layers of very fine to fine-silt size silty sandstone with thin to meter scale of limestone and siltstone and minor stringers of claystone (Fig. 49). These sandstones are organised in several amalgamated packages mostly showing shaling upward trends. (Figs. 49 and 50b).

The R2 reservoir unit (3644.3 - 3737.9 m) is mostly composed of thick massive sandstone packages, and subordinate stratified, cross-stratified, and argillaceous sandstones separated by a thick interval of massive shale (3658 - 3667 m) (Figs. 49 and 50b).

6.3 Petrophysical evaluation

Petrophysical properties such as shale volume, total and effective porosity, permeability and fluid saturation (oil and water) were determined by well log analysis to understand the hydrocarbon potential of the Logbaba Formation reservoirs identified in W1 and W2 (Fig. 51).

The results show that the Logbaba Formation reservoirs have a low volume of shale (V_{sh}) in the reservoirs of the studied wells, ranging from 6.3 to 19.8%. The lowest shale volume is observed in well W1, while the highest shale volume is observed in well W2.

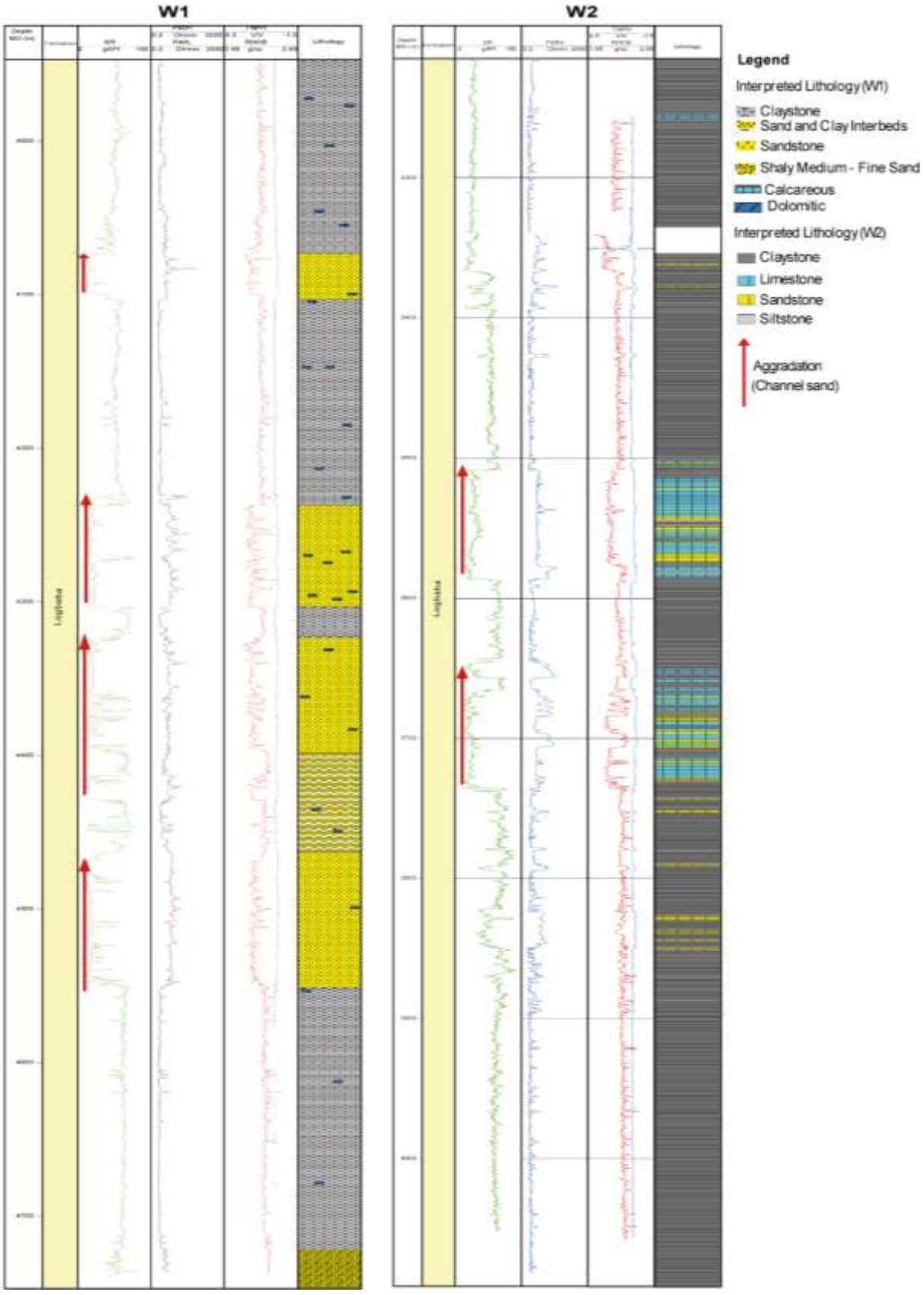

Figure 49. Lithological log and depositional environment of reservoir in the Logbaba Formation based on GR signature adopted from Emery and Myers (1996).

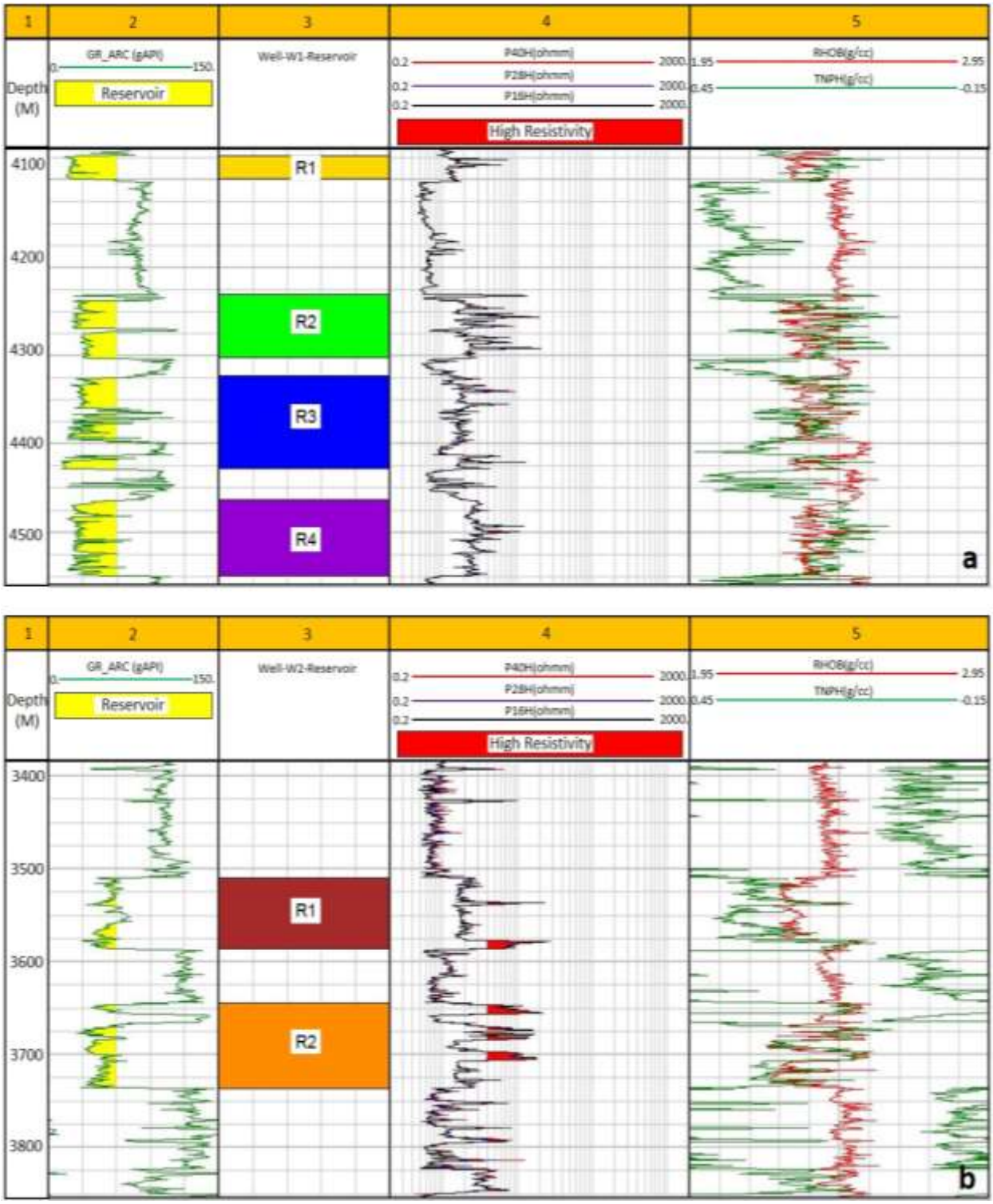

Figure 50. a) Well log signatures of studied interval in Well W1 and the identified reservoirs (R1, R2, R3 and R4). b) Well log signatures of studied interval in Well W2 and the identified reservoirs (R1 and R2).

The reservoirs of the Logbaba Formation in the studied wells are likewise identified as sandstone according to the shale volume classification established by Hilchie, (1978). Based on the porosity classification established by Rider, (1996), the Logbaba Formation reservoirs in the studied wells have relatively good porosity. The effective porosity in the two studied wells is between 15.5 and 21.3%, with a permeability range from 5.65 to 75.09 md (Table 9). The water saturation (S_w) ranged from 34.5 to 74.2% (Table 9). The lowest water saturation is observed in well W2 while the highest water saturation is observed in well W1. Although it is important to calculate the water saturation, the most essential part is to estimate the hydrocarbon saturation using equation (5). The results indicate that the Logbaba Formation reservoirs have moderate to high hydrocarbon saturation (S_h) ranging from 25.8 to 65.5% (Table 9).

The overall thickness of the net reservoir zones between 9 and 30.5 m is shown in Table 9. The analyzed W2 well included two pay zones that indicated hydrocarbon accumulation; these two pay zones were merged to obtain the overall net pay zone thickness for this well, which ranged from 0 to 8 m. Fig. 52 displays the sand zones (green) and net pay zones (red) in the formation reservoirs encountered by the W2 well.

According to Asquith and Gibson, (1982), the estimated bulk water volume values of the W2 reservoirs are scattered (Fig. 53), indicating an increase in the amount of formation water. This finding suggests that the reservoirs are heterogeneous and that there is more water in the formation than can be contained by the capillary pressure. Consequently, the reservoirs can not produce a water-free hydrocarbon during production since they are not saturated with irreducible water (Swirr).

6.4 Reservoir Fluids

Further analysis of the resistivity log data shows that the three resistivity logs in the reservoir interval overlap, indicating the presence of a water-bearing zone (Fig. 50). The higher deep resistivity readings (P40H) observed in the reservoirs W1 and W2 indicate the presence of hydrocarbons (Fig. 50). The cross-plot of neutron and reservoir density in the individual wells shows no “balloon effect”, suggesting the presence of oil as the hydrocarbon phase (Chongwain et al., 2018 and 2019). However, the reservoirs in W1 contain no producible hydrocarbons (i.e., no pay zone), but with low GR and high resistivity values based on Zhu et al., (2018), which is typical of calcareous interbeds, which have lower natural gamma (less than 80 API) and higher lateral resistivity values than any other sandstone.

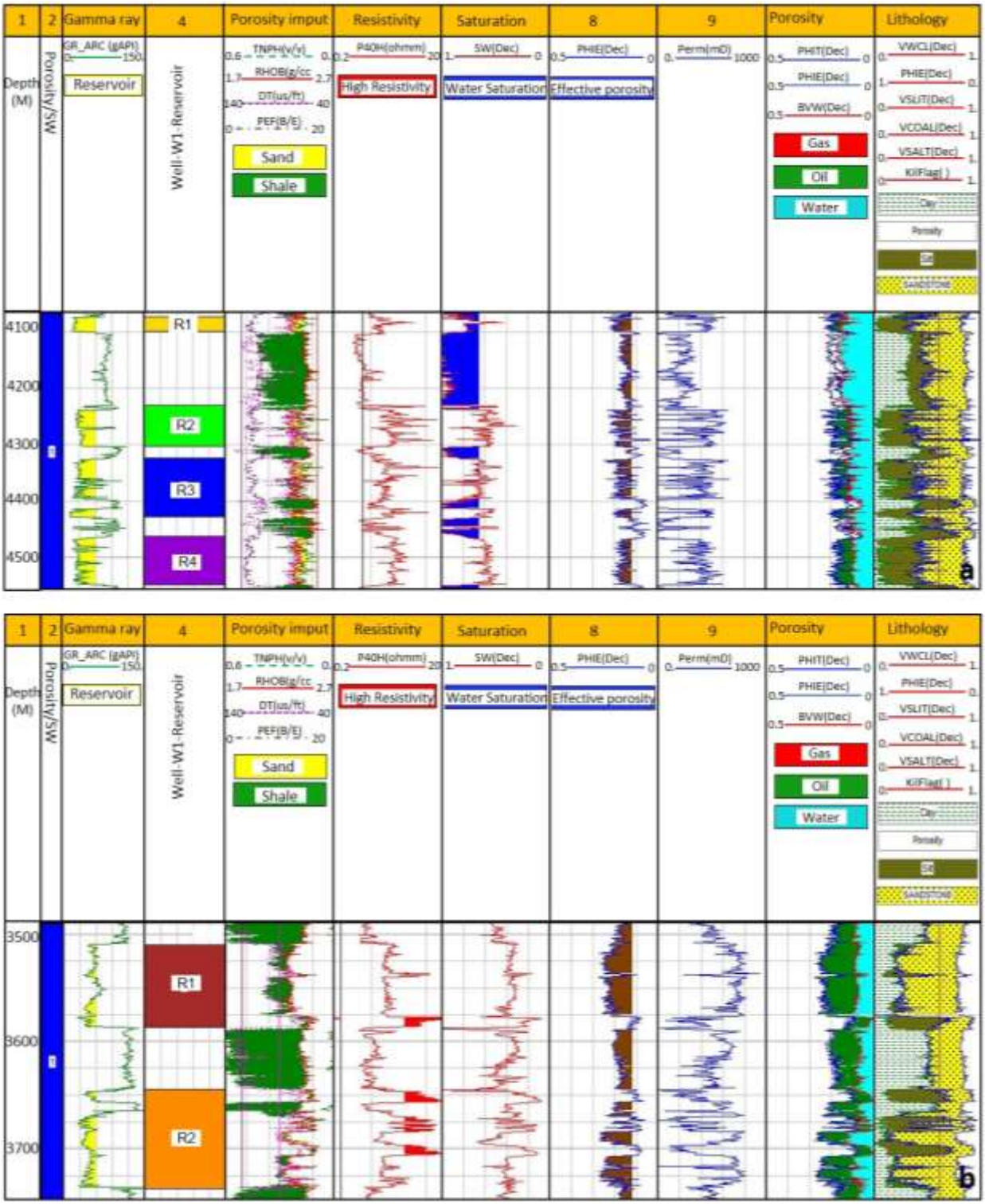

Figure 51. a) Litho-saturation cross-plots of the Logbaba Formation reservoirs showing porosity, permeability, shale volume, water saturation, and hydrocarbon saturation within W1 well. b) Litho-saturation cross-plots of the Logbaba Formation reservoirs showing porosity, shale volume, water saturation, and hydrocarbon saturation within W2 well.

Calcareous interbeds are classified into four types: 1) the bottom type, 2) the top type, 3) and 4) the central and the complete types (Qi et al., 2006; Zhang et al., 2007; Wang et al., 2009; Zhang et al., 2009; Sun et al., 2010). The reservoir intervals that W1 penetrated may be typical of the complete type of calcareous interlayer, where the thin isolated mudstone-draped sand layer and the sand as a whole has been fully cemented by carbonate to produce a tight reservoir (Chongwain et al. 2018) (Fig. 50a).

Table 9. Quantitative results of the petrophysical analysis of all identified sand zones within the Logbaba Formation through the studied W1 and W2 wells.

Reservoir	Top (m)	Bottom (m)	Gross (m)	Net (m)	Net/Gross	Net Pay (m)	Avg PhiE(%)	Avg Sw(%)	Avg Vsh(%)	Avg Sh(%)	Perm (mD)
Well W1											
R1	4073	4100	27	-	-	-	19.3	74.2	6.3	25.8	8.73
R2	4230	4303.4	73.4	-	-	-	16.5	60.6	13.6	39.4	8.87
R3	4323	4428.7	105.7	-	-	-	15.5	70.1	16.5	29.9	5.65
R4	4463	4550.3	87.3	-	-	-	16.1	59.4	10.6	40.6	5.70
Well W2											
R1	3510	3587.2	77.2	9.0	0.1	0.0	21.3	34.5	19.8	65.5	75.09
R2	3644.3	3737.9	93.6	30.5	0.3	8.0	17.5	36.5	19.3	63.5	35.22
Cutoffs											
Reservoir	-	-	-	-	-	-	≥12	≤65	≤40	-	-
Pay	-	-	-	-	-	-	≥12	≤65	≤40	-	-

Avg Phi E average effective porosity, Avg Sw average water saturation, Avg Vsh average volume of shale, Avg Sh average hydrocarbon saturation, Perm permeability

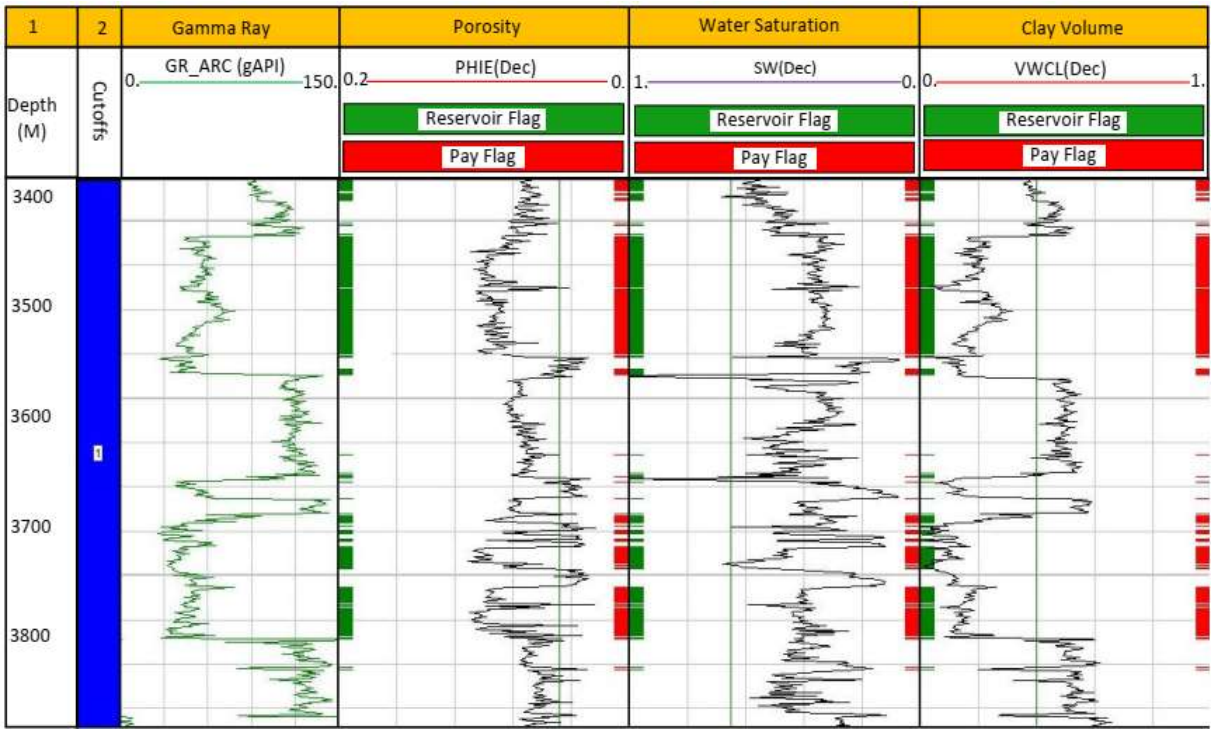

Figure 52. Petrophysical and Pay zone summary graphical representation of W2 well reservoirs.

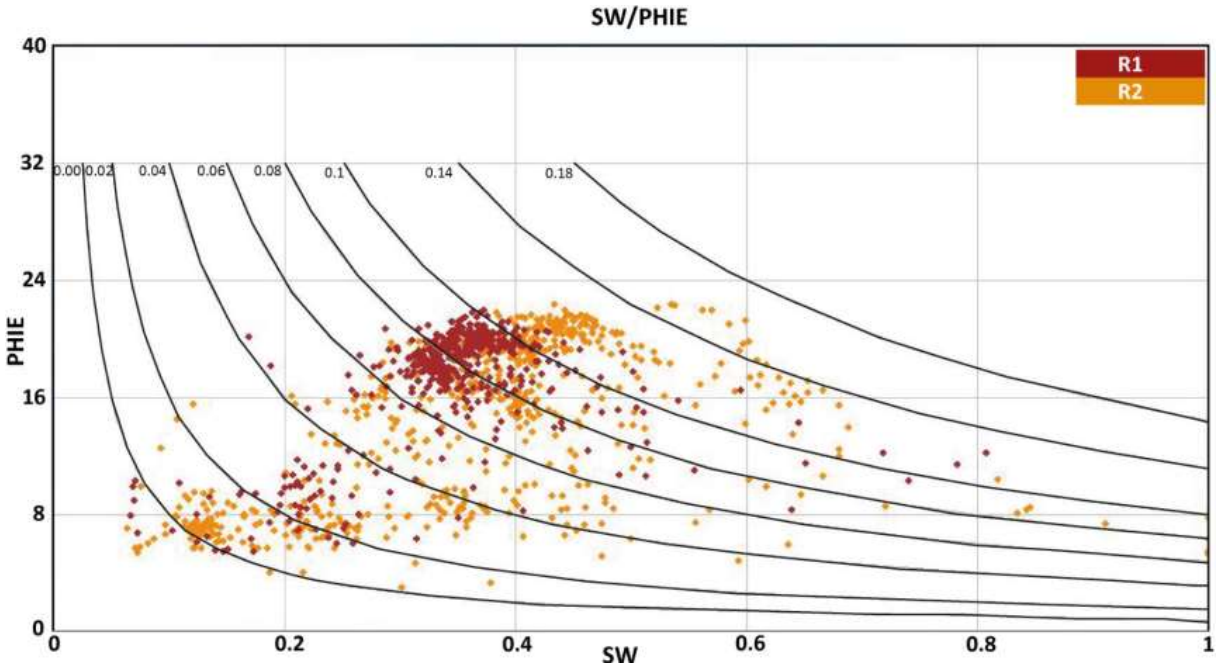

Figure 53. Buckle plot of water saturation against porosity for Logbaba Formation reservoirs within the well W2.

In conclusion, petrophysical analysis of the Upper Cretaceous Logbaba Formation in the Kribi-Campo sub-basin, based on data from wells W1 and W2, reveals that the reservoirs are primarily composed of turbiditic sandstones interbedded with carbonates and shales. The reservoirs exhibit good quality, with effective porosity ranging from 15.5% to 21.3%, moderate permeability, and low shale content. Although all intervals are water-bearing with no recoverable hydrocarbons, the presence of chlorite-dominated clay minerals appears to have minimal impact on reservoir quality. These findings provide valuable insights into the formation's depositional and diagenetic history.

Chapter 7 : Discussion

Having interpreted and described the geometry and morphology of the submarine channel and fans structures characterized from the high-resolution 3-D seismic dataset, we now discuss the factors controllings their formation. We also propose in this final chapter a conceptual model for the genesis of the channel and fans and highlight the implication of the turbidite systems on deep-water hydrocarbon exploration and production.

7.1. Controls on the evolution of the Cretaceous submarine channel system

Submarine channels can be influenced by sea-level change, sediment flux, tectonics, and climate, and have a significant impact on the sedimentary architecture of continental margins (Reading and Richards, 1994; Wu et al., 2018). Several factors can be suggested as the principal controls on the development of the Late Cretaceous submarine channel system within the SU2 in the study area. This encompasses tectonics, relative sea-level fluctuations, fluvial sediment supply, and slope gradient. Here, these factors are examined first in terms of whether and how they might have influenced the evolution of the submarine channel system.

7.1.1. Tectonics

One structural high (Kribi high) was mapped in the study area (Fig. 31). There are highs that are believed to have significant control on the sourcing and distribution of Cretaceous sediments from the onshore to the offshore depocentres. However, these highs have been active during the evolution of the submarine channel system in the Late Cretaceous. The Kribi high lies to the SE of the study area (Fig. 31) and it is a NE-SW trending feature, which has a similar trend to the submarine channel (Le, 2012; SPT, 1995). It comprises a thick Early Cretaceous syn-rift sequence, which is overlain by a Late Cretaceous post-rift sequence (Le, 2012; Loule et al., 2018). Late Cretaceous sediments filled the developing basin, which is bounded by the eroded paleotopographic high to the southeast (Kribi High). Furthermore, the reactivation of some of these structures (e.g., Kribi Campo High, Kribi and Campo Fracture Zones) during the Cretaceous and Tertiary times also affected and promoted the entry and deposition of gravity flow deposits of coarse clastics which represents the primary reservoir targets in the study area (Sterling, 2010; Le, 2012).

7.1.2. Relative sea-level fluctuations

It is widely accepted that relative sea-level oscillation can promote the occurrence of submarine channels in deep-water settings (Posamentier, 2001; Posamentier and Kolla, 2003). Seismic based investigations (Posamentier and Kolla, 2003; Niyazi et al., 2018), numerical modellings (Soutter et al., 2021), outcrop analogues (Sprague et al., 2002; Pr´elat, 2010) and

studies focusing on the Pliocene to modern submarine channel systems (Samuel et al., 2003; Chima et al., 2020) showed that lowering sea-level is one of the important mechanisms by which sediments could be transported beyond the shelf break more efficiently, and form turbidity channels even in the distal area of the deep-sea. Although, submarine turbidity channel development during high sea-level were documented in the Congo and Bengal fans, their presence was also linked to increased tectonic activity (Van Weering and Van Iperen, 1984; Weber et al., 1997). In fact, the sea-level fluctuations can act as a switch on the continental shelf, by capturing and storing most of the coarse-grained sediments within the shelf during the period of high sea-level, while by-passing them to the deep basin during sea-level fall and connecting the catchment area to the deep-sea (Posamentier and Kolla, 2003).

An apparent high sea-level can be observed during the late Campanian, which corresponds to the KC-3 horizons (Fig. 12). Interestingly, deep-water fans were documented in this period within SU1 and likely developed due to the rising sea-level (Fig. 30). When the sea-level stands high, the shelf will be submerged and coarse-grained sediments are primarily deposited on the shelf, and only fine-grained materials could be transported to deep waters, forming clay dominated submarine fans (Myers and Milton, 1996; Posamentier and Kolla, 2003; Samuel et al., 2003). As the sediments accumulated in the study area, and sea-level start to drop, coarser materials stored during the previous lowstand (around KC-3) could be transported to deep sea, and those deep-water fans could transit into turbidity channel system (Posamentier and Kolla, 2003; Cross et al., 2009). Due to lower hydraulic pressures and abundance in coarser grain size sediments, gravity flows during lower sea-level tend to be more erosive and finally could form submarine channels (Catuneanu, 2006). Coincidently, we observed channel incision within SU2 (Figs. 30 and 34), which can be correlated to the lowering sea-level curve of Haq et al. (1987). Since the submarine channels during lowstands are highly erosive and comprise a higher sand proportion (Figs. 33 and 34), it is plausible to suggest that the abundance of coarse-grained sediments available from the shelf and through the fluvial sediment supply during the early stage of sea-level fall, played important role in the formation of the submarine channels. Nevertheless, continuous sea-level drop also could demise the submarine channels, as the coarser materials available on the shelf were consumed by the early-stage channel (Posamentier and Kolla, 2003; Cross et al., 2009). The subsequent channel contains large number of fine-grained materials, and it is no longer as erosive as the early-stage counterpart, since the energy of the turbidity current is directly linked to the sand/mud ratio of the flow (Shanley and McCabe, 1994; Tripsanas et al., 2008). This interpretation also explains

the narrower morphology of the late-stage channel comparing to the early-stage channel (Fig. 36).

7.1.3. Fluvial sediment supply

Sediment supply is the material basis for the development of deepwater channel systems (Catuneanu, 2006; Gong et al., 2016). The types and abundance of sediments provided by source area may have had great influence on the formation and characteristics of the deep-water depositional systems in the study area. It is known that following the Santonian tectonic event, a large amount of terrigenous sediment was transported to deep-water basins, forming a widely developed deep-water gravity channel system in the Maastrichtian (SPT/Simon Petroleum and Technology, 1995). During this time, sediment supply from the Sanaga River also played a significant role in the type of infill and the nature of the sediment within the submarine channel systems. Coarse clastic sediments are therefore predicted to have been extensively deposited in the study area, particularly in the vicinity of the Sanaga River (SPT/Simon Petroleum and Technology, 1995). Tracing the conduits that fed the submarine channel system using root-mean-square amplitude slices indicates a transported from the shelf-edge delta systems formed by Sanaga and Nyong Rivers during the depositional stage of the Late Cretaceous (Fig. 34). The infilling of the submarine channel system in this study reflects a deltaic (Sanaga and Nyong) origin of the sediments deposited on the continental shelf margin in the northeast of the study area. The NE-SW trending channels mapped in this study indicate that sediments originate primarily to the northeast (Figs. 36 and 37). This corroborates the interpretation made by Meyers et al. (1996), Iboum Kissaaka et al. (2016), and Yugye et al. (2021).

7.1.4. Paleotopographic gradient

Paleotopographic gradient features appear to have played a key role in controlling the morphology, internal architecture and fills of the submarine channel in the Late Cretaceous (Zhao et al., 2018). The Intervals 1 and 2 were characterized by a strong gradient (2.64° and 2.02°) with a large channel width and shallow depth (Table 7. Fig. 36). However, Interval 3 is characterized by a gentle gradient (0.40°) with a small channel width and large depth. The possible reason for such a difference in morphology over such a short distance could be related to the different palaeotopographic gradients (Fig. 36a). Therefore, the degree of widening is commonly larger than that of deepening with increase in the channel scale. This means that a larger width/depth ratio commonly coincides with a larger-scale channel (Zhao et al., 2018).

The highest amplitudes observed in the map view characterize areas of lower channel gradient, while the lowest amplitude channel amplitude areas are in the upslope to the mid-slope of the channel and characterize the high gradient (Fig. 34). Thus, the amplitude change may reflect a change in lithology from fine to coarse-grained deposits (Sullivan et al., 2000; Morend et al., 2002). In the case of the slope segments x, the low amplitude lithofacies corresponds to fine-grained deposits. On the other hand, when the slope is low (segment z), high amplitude lithofacies indicate deposits of coarse-grained deposits (Figs. 34 and 37). This type of sedimentary submarine channel fill is similar to the indented sedimentary channel fill suggested by Li et al. (2020).

7.2. Evolutionary model for the Late Cretaceous channel system

The local tectonics, sea-level fluctuations, and fluvial sediment supply are likely controls on the occurrence and absence of the submarine channel system in the long term. The paleotopographic gradient is responsible for the morphological evolution of the channel system and the distribution of coarse-grained sediments. The overall formation and development of the studied submarine channel system could be explained by four steps conceptual model (Fig. 54). During the high sea level at the late Campanian (KC-3), most of the sediments accumulated on the continental shelf and deep-water fans developed at the distal part (Fig. 54a). Following the drop in sea-level, increase of fluvial sediment supply, previously accumulated sediments on the shelf and sourced from the fluvial system were delivered to the deep basin, and formed the Late Cretaceous channel system (Fig. 54b). The differences in the gradient for the topography, on which the channels developed, influenced the distribution of sand-prone sediments. As a result, coarser-grained materials mainly accumulated along the channel at the gentler lower stream (Fig. 54b). Following continuous sea-level fall and the discharge of coarser sediments on the shelf, more fine-grain materials were delivered to the system, decreasing the flow energy, by which only narrower (late-stage) channel could be developed (Fig. 54c). The late-stage channel is also characterized as more mud-prone and less erosive compared to the early-stage channel (Fig. 54c). In the final stage, from the Late Cretaceous to the Tertiary, the study area was submerged by the rapid sea level rise, and then the submarine channel system died out quickly due to the lack of sufficient sediment supply (Fig. 54d).

7.3. Implications for hydrocarbon exploration in deep-water Kribi-Campo sub-basin

Turbidite channel systems are one of the most common types of hydrocarbon reservoirs found along the West Africa margin and elsewhere (Weimer et al., 2000). Therefore, the

investigation of these late Cretaceous submarine channels system, have implications for hydrocarbon prospectivity in the deep-water Kribi-Campo sub-basin.

The early-stage channel consists of coarse grain sediments alternating with fine grain sediments rather than being isolated on a basal erosional surface, suggesting multiple barriers and possible thief zones at the base of the channel (Figs. 33 and 34; Mayall et al., 2006). In addition, the late-stage channel is predominantly fine-grained. However, the presence of coarse-grained sediments in the early-stage channel originating from erosive energetic flows may result into good reservoirs in the study area (Loule et al., 2018; Sterling, 2010; Jobe et al., 2011).

Sediment transport models indicate that grain size distribution, as well as slope gradients, are key variables dictating the presence of good reservoir development (McCaffrey and Kneller, 2001; Stevenson et al., 2015). The coarse-grained sediments of the early-stage channel in this study were deposited along the low slope gradients (segment z) and the fine-grained sediments were deposited in the high slope gradients (segment x) (Figs. 34d and 37). As a result, the channel system with gentle gradients and coarse-grained sediments offers the highest potential for hydrocarbon discoveries (McCaffrey and Kneller, 2001; Stevenson et al., 2015).

Another potential application of this study lies in the well-log motif of the submarine channel system where various stages of channel evolution have distinct logs responses (Fig. 33a). The basal coarse-grained lags of the early-stage channel in well W1 show a large kick in GR and display a serrate GR log motif with some blocky/bell-shaped intervals (Well W1 in Fig. 33a). The late-stage channel fills are mainly characterized by a serrate GR motif with some low-amplitude bell-shaped GR intervals (Fig. 33a). The log responses observed in this study is similar to those reported from other slope channel systems (e.g., Fig. 36 of Mayall et al., 2006, Fig. 35 of Li et al., 2021). This suggests that evolutionary stages and associated 2D or 3D reservoir elements of submarine channel systems may be recognized from 1D vertical log patterns or sections.

7.4. Evolution of the submarine fan system

The submarine fan system consists of a single broad lobe fed from the east by a shelf incised canyon (Fig. 40b and c). As the fan system evolves, it exhibits variable planforms, sand content, stacking patterns and lithologic characters (Figs. 40, 43 and 44). This difference reflects the architecture evolution of a single submarine fan system, during an aggradation phase with a particular interaction with the underlying topography marked by the presence of the Kribi-high. Based on observation criteria such as fan shape, channel inclusion and difference

in sand abundance within the submarine fan, we establish three-stage architecture evolution for submarine fan system (Zhang et al., 2018).

At the early stage of the fan evolution, deposition occurred as a minor submarine fan at the toe of slope fed by a single (narrow) feeder channel. Both Fan A and B developed in a stacking pattern with a lobed geometry and the presence of a channel within the submarine fan and can be interpreted as a channelized lobe (Fig. 40c). In the Well log W1, these fans are characterized by high-amplitude blocky GR log motifs and are interpreted as a sand-prone channel fill (Fig. 43). This stage represents the initiation of the submarine fan system (sensu Gardner et al., 2003, Hadler-Jacobsen et al., 2005).

In the second stage slope channel avulsion followed by submarine fan deposition at the toe of slope to proximal basin floor was initiated. Submarine fans C, D, and E are correspond to this stage and were formed associated with crevasse splay deposits and large volumes of sediments. Moreover, our results indicate the presence of a series of relatively parallel high amplitude elongate features with finger-like terminations at the margin of the submarine fan (Fig. 41). These finger-like terminations appear to be only developed on SE lobe margin. The morphology and scale of the finger-like features are comparable to similar features described on the Melas Chasma sub-lacustrine fan on Mars (Metz et al., 2009), on the Monterey Fan and in the distal areas of Permian submarine fans preserved in the Tanqua Karoo Basin, South Africa (Klaucke et al., 2004) and also on the distal edge of the Mississippi submarine fan. The distal Mississippi submarine fan also has a lobate morphology with finger-like dendritic terminations, elongated lobes, and splays that branch off of the main deposit at high angles up to 90° (Twichell et al., 2009). The distal Mississippi submarine fan also has low relief mildly sinuous channels and is very flat, with a surface slope of 0.08° (Gardner, 2007). It consists of mudstone facies with interbedded sand and silts, formed by abrupt deposition of channelized flows to form small lobes at their distal reaches (Nelson et al., 1992, Klaucke et al., 2004). Therefore, the high amplitude finger-like features in our study could be interpreted as a thick, massive sands formed by sediment-laden flows driven by gravity that diverge from the primary flow and erode into the hemipelagic sediments (Le, 2012). Well W1 (Fig. 43) shows that submarine fans C to E consists of sandstone and subordinate claystone with blocky to funnel-shaped GR log motifs. This phase is interpreted as fan growth stage (sensu Gardner et al., 2003, Hadler-Jacobsen et al., 2005).

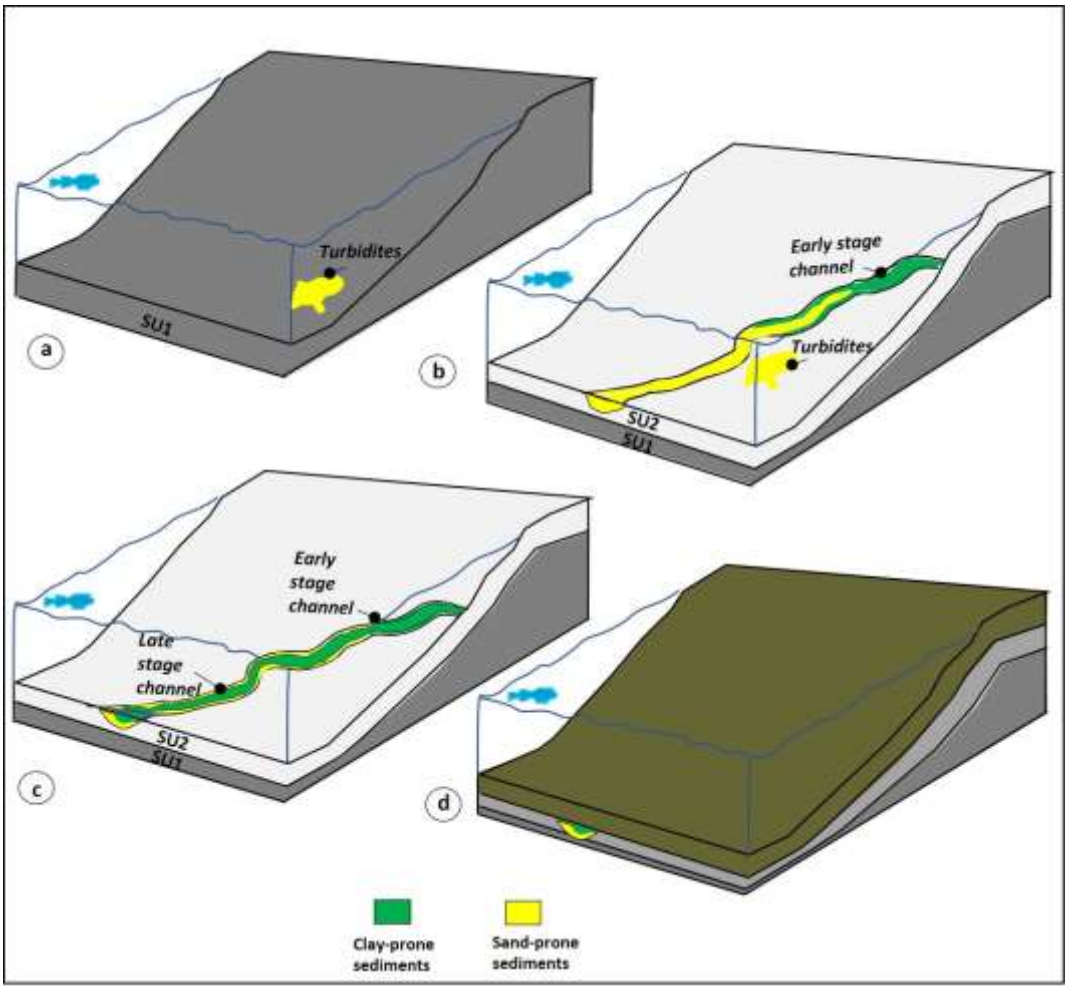

Figure 54. Diagram of the deposition facies in the study area showing the temporal and spatial evolution of the Late Cretaceous submarine channel. a) Turbidites fan came into being first before the formation of the early-stage of the channel. b) The early-stage channel is characterized by Sand-prone sediments and some Clay-prone sediments. c) The late-stage channel deposit is narrow and is more sinuous characterized by Clay-prone. d) In the final stage, from the Late Cretaceous to the Tertiary, the submarine channel system died out.

In the final stage, the submarine fan retreated and the feeder channel backfilling and significant slope overbank splay deposition as a function of reduced feeder-channel margin relief occurred. Although, the submarine fan F presents some similarities with fan E, it lacks finger-like features. Fan G is characterized by the absence of a feeding and distribution channel within this fan (Fig. 42b). Fan G is narrowing and tending to disappear to make way for a submarine channel system reported by Secke et al., 2022. Well W1 (Fig. 43) reveal that the

submarine fans F to G are characterized by low-amplitude bell-shaped GR log responses and are interpreted as overbank.

7.5. Allogenic and autogenic controls on submarine fan architecture

According to, Catuneanu and Zecchin, 2013, allogenic and autogenic processes that may interact with each other still control submarine fan deposits. Factors such as tectonics, sea level fluctuations, topography and channel incision, probably controlled the development of the submarine fan in the study area.

During the Santonian (KC-02), there was a tectonic readjustment along the Kribi-Campo High, which was uplifted relative to the deep basal zone to the west, resulting in significant erosion and leading to the deposition of thick Late Cretaceous clastics, characterized by slope and basin floor fans containing multiple channel complexes (Fig. 37; Sterling, 2010; Le, 2012). A series of eustatic depressions during the Campanian-Maastrichtian and Santonian uplift facilitated the episodic transport of major clastic sequences across the relatively narrow shelf into the deeper basin to the west (Secke et al., 2022). Following the drop in sea-level, increase of fluvial sediment supply, previously accumulated sediments on the shelf and sourced from the fluvial system were delivered to the deep basin, and formed the during the Santonian a complex channel (Fig. 39 and 42a). As sea level falls (Fig. 12), the shoreline migrates seaward for several kilometers, and may have caused a direct connection between shelf edge systems and canyon heads, which could facilitate the delivery of voluminous clastic material into the deep-water setting (Gong et al., 2016), and thus develop submarine fan sediments. The initiation of submarine fan A atop of the submarine channel system indicate the sea level rises, as the proximal (channel) part of the source to sink system was overlain by distal (fan) system. This was also evident by the Gamma ray that shows fining upward trend towards the fan A. Submarine fan B to C represents the continues development to the fans, and D has the largest area coverage, indicating the sea-level reached it is peak during this time. In general, during the development of Fan A to Fan D, the low GR signatures is separated by high amplitude values, indicating the level is fluctuating even though the general trend is a rising stage (Figs. 45, 55). Further subsidence along the West African margin occurred in the Late Cretaceous (Campanian-Maastrichtian) as continental drift continued (SPT/Simon Petroleum and Technology, 1995; Iboum et al., 2016). New coarse clastics were introduced into the Kribi-Campo horst and the study area. These coarse clastics were fed by paleo-fluvial deltaic systems (Ntem, Nyong and Sanaga) that organized into shallow marine sediments along the inner shelf area, only to be remobilized into the deeper basin areas as gravity flow deposits of high density

turbidites and debrites in fan channel geometries vis-à-vis submarine canyon feeder systems (Sterling, 2010; Secke et al., 2022). From Fan D to G, the areal coverage of the fans is decreasing, indicating a possible fall in sea level. However, the GR shows an increasing trend, suggesting the sediments intersected by the wells are mainly fine-grained material. The fall in sea level is also evident by the observation of a channel system that developed atop of the Fan G (Figs. 44c, 45, 55). Although allogenic effects dominate the control of submarine fan architecture in the study area in the Late Cretaceous, autogenic factors may still exert some influence. Seafloor topography is an important autogenous factor that could influence the morphology of the submarine fan (Adeogba et al., 2005; Gervais et al., 2006; Prélat et al., 2010). For example, laterally confined topography may facilitate the development of submarine channel systems, while relatively unconfined topography may accommodate large-scale submarine lobe sediments, such as those observed in this study with an elongated shape and size around 600 km^2, falling in the lower range of the range dimensions (Pickering et al. (1989)). According to Janocko et al. (2013), frequent channel incision is another common autogenous process in the deep-water environment that may explain the diversity of submarine fan architecture. When channel incision occurs largely at one of the evolutionary stages, downstream submarine fan systems may be abandoned and end up with incomplete successions, as illustrated in this study (Fig. 42b).

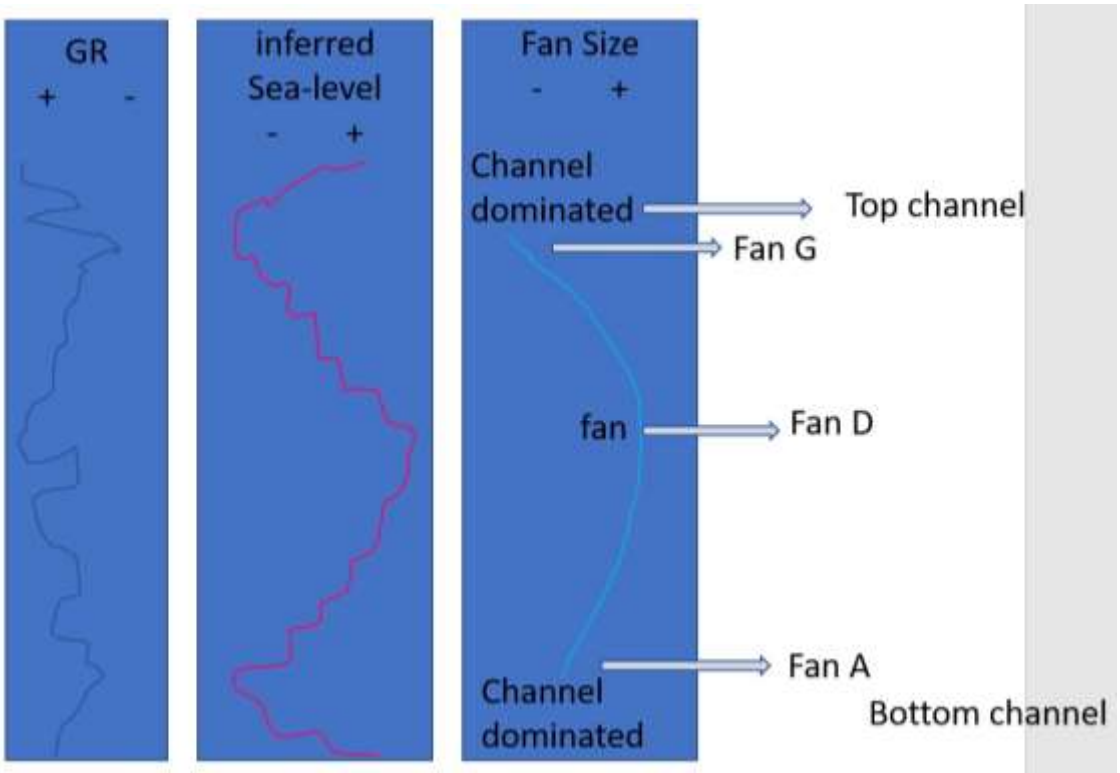

Figure 55. Relative sea-level of the submarine fan inferred from gamma ray log

7.6. Conceptual models of submarine fan

Campanian depositional form (primarily fans) was quite different from the large, well confined submarine channel of the Santonian. In Campanian times (KC-3), the dominant depositional form has been interpreted as large (Loule et al., 2018), relatively unconfined basin floor fans with well-defined internal structures such as channels, levee deposits, crevasse splay and breat-out fan lobes to the main basin floor fan (Sterling, 2010; Fig. 56). The stage of evolution of these submarine fans, shows characteristics very similar to the Type I depositional system of Mutti (1985), where a vertical succession of aggradational fan lobes and channels produce a complex sedimentological mix of facies types and this is what would be expected in the Campanian of the study area (Fig. 56). At the beginning of this period, the sea level coincides with a period of fall sea level which would have led to the development of the first stage of fan evolution (Fan A and B) marked by a single (narrow) feeder channel associated with a single sand-rich lobe (Gardner et al., 2003, Hadler-Jacobsen et al., 2005; Fig. 56a). During the growth phase (Fan D), the geometry of the fan increases with a more sinuous channel developing within the lobe (Fig. 56b). The slope channel avulsion was followed by the submarine fan deposition at the toe of slope. This suggests significant sediment supply to an expansive, unconfined basin floor area where is dominated by the fan channel and stacked lobes developed in a relatively lowest sea level period (Zhang et al., 2018). Immediately after this stage, as sea level rises, there is an upward trend in the GR log reading (Fig. 43) which is characterized by a decrease in the area coverage of the lobe, and decrease in the slope gradient in its upslope feeder system. This period also accompanied by the incision of main channel (Fan G). A retreat of the submarine fan combined with feeder channel backfilling and significant slope overbank splay deposition as a function of reduced feeder-channel margin relief occurred (Gardner et al., 2003, Hadler-Jacobsen et al., 2005; Fig. 56c). The submarine fan becomes increasingly rich in fine sediment and poor in sand (Fig. 56c).

Overall, these are stacked, low relief sheets or lobes located outboard from the main feeder channel system in the eastern sector of the study area. The high amplitude reflection packages (HAR) give strong support for a mix of clastic types and there are evidence of compaction draping over the more sand-rich areas of the fans (Mutti, 1985, Sterling, 2010). The presence of erosive channels with moderately developed levees indicate the effects of turbidity flow processes that associated with the debris flow units (debrites) interbedded with sands and other rock assemblages (Sterling, 2010). With the onset of the Maastrichtian (KC-04), the dominant deep-water deposition system changed from a submarine fan series in the Campanian to a more confined and incised channel system (Fig. 56c).

7.7 Depositional environment of reservoir

The sediments of Logbaba formation comprise a series of sandstone and shale successions that have been deposited during different relative sea level changes. This suggests two depositional conditions occurring during the Campanian-Maastrichtian (SPT, 1995). A transgressive episode, was distinguished by finer grained facies (deep-water sediments e.g. shale, siltstone) overlying coarser facies (shallow water sediments e.g. sandstone), indicating deposition during sea level rise. A regressive episode, where shallower marine and nearshore deposits, indicating deposition during falling sea level, overlie marine deposits. These sediments of Logbaba Formation have characteristic coarsening upward, fining upward, and blocky gamma ray log signatures. The cylindrical or blocky gamma ray log motifs recorded in this study are serrated with quite abrupt upper and lower limits. This characterized the reservoir sand bodies "R1, R2, R3, and R4" (well W1), and "R1 and R2" of well W2. This reservoir thickness ranges from 27 to 105.7 m (Table 4), and are usually associated with fine-grained sands of good reservoir quality due to low shale content as a result of high energy conditions leading to clean porous sands. However, according to Emery and Myers (1996) stated that cylindrical patterns with greater range of thickness, as those of reservoir sands of well W1 and W2 (Table 4), could be interpreted as turbidite sand depositional environment (i.e. deposited in an aggradation/still stand depositional sequence; Fig. 49). In addition, Secke et al. (2022) reported that the high amplitude seismic facies displaying an aggradational pattern with parallel and continuous reflections observed within the Logbaba Formation in the same study area corresponds to turbidite fan system, composed reservoir sands in the deep-water of the Kribi-Campo sub-basin.

7.8 Implication for reservoir quality

The results indicate that the Logbaba Formation reservoirs do not consist solely of clean sandstone, but rather include intercalations of carbonates and shales. The heterogeneous matrix of the reservoirs, consisting of sand, limestone and dolomite in this case, probably indicates that the detrital carbonate originated from fluvial sediment influx from the Sanaga and Nyong Rivers (Regnoult, 1986; ECL, 2001; SNH, 2005). Further diagenesis led to the dissolution of the biogenic carbonate-forming calcite matrix generating secondary intragranular porosity (Irwin et al., 1977; Curtis and Coleman, 1986; Chongwain et al., 2019). Reservoirs are generally organized into several amalgamated packages, mostly with blocky sands (Fig. 50). These are interpreted to represent a stacked set of overall upward sanding packets that may

represent a phase discharge deposited primarily by granular flows in a poorly confined channel in a proximal lobe (Sterling, 2010).

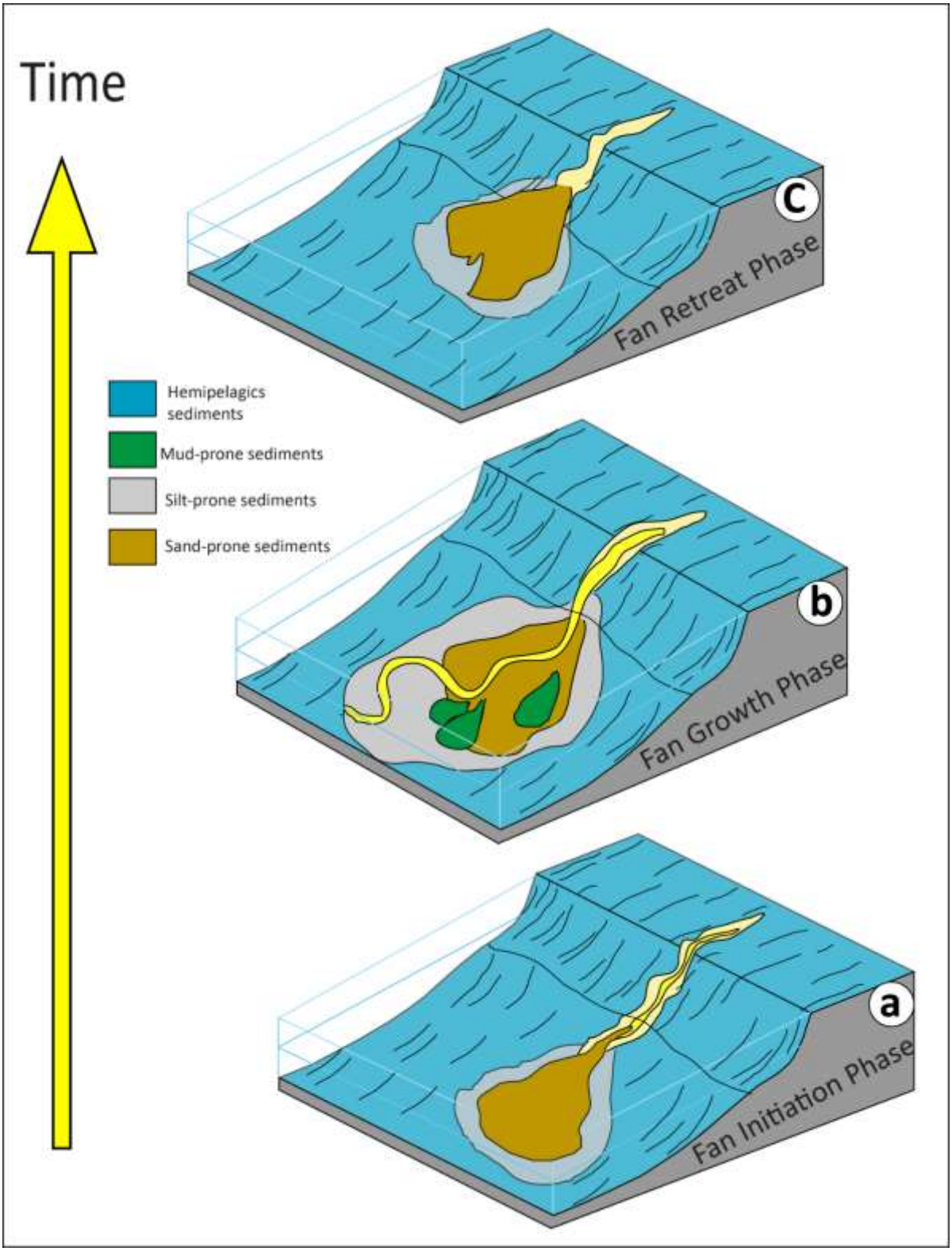

Figure 56. Depositional model of submarine fan in the studied area within Campanian time of the Kribi-campo sub-basin a) initiation phase, b) growth phase and c) retreat phase.

This result would be consistent with the work of SPT, (1995), Le, (2012), Loule et al., (2018), who suggested that the sediments observed in the Logbaba Formation are mud-rich deposits with local sandy deposits associated with channels and fans. This is evidence for the presence of medium- and locally coarse-grained sandstones with overlying net thicknesses greater than 80 m.

The inferred results of the study indicate the presence of chlorite and montmorillonite as dominant clay minerals and some small in the mixed clay layer zone (Fig. 48). The mixed layers of clay minerals formed as a result of the inter-layering of various clay minerals in a single structure (Srodo´n, 1999). Clay minerals are generally considered detrimental when assessing the quality of sandstone reservoirs (Jiang, 2012). Clay minerals reduce porosity and permeability as they can clog pore throats when they are in the form of films, plates and bridges on the grain surface (Jiang, 2012). Some clay minerals increase chemical compaction while accelerating the rate of porosity loss in a limestone deposit, lowering reservoir quality (Brown, 1997; Chongwain et al., 2019; Qadri et al., 2019). However, the presence of clay minerals does not necessarily indicate a deterioration in reservoir quality but can also contribute to improving reservoir quality (Heald and Larese, 1974; Bloch et al., 2002; Taylor et al., 2004). The present study shows an abundance of chlorite in the W2 well reservoirs, which can protect and maintain reservoir quality by coating the sand grains and prevent it from quartz cementation. The chlorite mineral may have formed early in the diagenesis of micas and feldspar on the seafloor, or it may have been the result of detrital chlorite influx from nearby river sediments during rapid deposition (Chongwain et al., 2018; Qadri et al., 2019). The good porosity values (21.3%) estimated for the first reservoir in well W2 indicate a minimal impact of clay minerals on reservoir quality. The W1 well encountered thick and porous sand reservoirs. However, there is no evidence that hydrocarbons migrated into any reservoirs, suggesting that the source rock and/or hydrocarbon migration pathways are the main risk factors and reason for the well failure (Loule et al., 2018). The W2 well encountered good quality reservoirs in the Logbaba Formation, but all were water bearing and did not contain commercial quantities of hydrocarbons.

In conclusion, the development and depositional architecture of both the submarine channel and fan systems in the Kribi-Campo sub-basin were primarily controlled by the dynamic interplay of tectonic activity, sediment supply, relative sea-level fluctuations, and paleotopographic gradients. In particular, tectonic uplift along the Kribi-Campo High and associated sea-level changes played a key role in shaping the unconfined basin topography, driving significant erosion and the accumulation of thick Late Cretaceous clastic deposits.

Conclusions and Future Research

Conclusions

This thesis presents results from the analysis of a suite of high-resolution subsurface geophysical dataset employed in unravelling the deep-water turbidite systems architecture in the Kribi-Campo sub-basin, Offshore Cameroon. The main conclusions from the thesis are provided below:

Integrated analysis of a high-resolution, 3D seismic reflection dataset and borehole data from the deep-water Kribi-Campo Sub-basin, offshore Cameroon has revealed a well-developed submarine channel system that developed during the Late Cretaceous.

- The submarine channel system recognized in the Late Cretaceous trends approximately NE–SW with a total length of about 56 km and a maximum width and height of 5 km and 197 m respectively within the study area. The submarine channel system is U-shaped and of two parts: (1) the early-stage channel with a linear morphology and: (2) the late-stage channel located within the early channel which is narrower with a sinuous morphology. According to width to depth ratio and variation of erosion bases of the channels, the channel system can be divided into three segments (x, y and z), each of which is characterized by unique internal structure and infilling processes.
- The development and depositional architecture of the submarine channel system are mainly controlled by the changing interplay of tectonic, sediment supply, relative sea level changes and paleotopographic gradient. The segmentation of the submarine channel system was constrained by the paleotopographic gradient of alternating uplifts and depressions. The findings from this study demonstrate that a decreasing slope gradient favours coarser-grained deposits primarily along the axis of the channel system, while a strong slope gradient leads to the deposition of fine-grained sediments. The abundant sediments feeding the submarine channel system were transported from the Sanaga and Nyong River source areas.
- Understanding the channel morphology is crucial for facies prediction and efficient development of deep-water channel reservoirs especially as hydrocarbon exploration moves into deeper waters in the study area and elsewhere.

Detailed seismic geomorphological analysis of 3D seismic reflection and well data for the Late Cretaceous sequences studied in the Kribi-Campo basin, offshore Cameroon has

enabled the internal architecture and geomorphological evolution of a deeply buried Campanian basin floor fan system to be described. The results of this work are as follows:

- The submarine fan exists in stacked form and its depositional history has been reconstructed using seven strata slices and seismic attributes grouped into initiation, growth and abandonment phases.

- The submarine fan is in the form of an elongated lobe-oriented NE-SW, the sediment of which entered via an east canyon probably originating from the Palaeo-Nyong fluvial system migrating through the area. This fan contains a sinuous distribution channel.

- The sediments in the fan were mainly gravity-flow deposits of coarse-grained turbidite sandstone with minor interbedded fine-grained hemipelagic sediments that were vertically stacked.

- The evolution of the fan architecture was mainly conditioned by changes in sea level, and tectonic readjustment along the Kribi-Campo High, which was uplifted relative to the deep basal zone to the west, resulting in significant erosion and leading to the deposition of thick Late Cretaceous clastics and the unconfined topography of the basin.

An assessment of the petrophysical properties of the Upper Cretaceous reservoirs of Logbaba Formation in the Kribi-Campo sub-basin, offshore Cameroon was investigated using well log data from two key wells W1 and W2. The results of this study provide important insights into the reservoir quality of the Logbaba formation, as follows:

- The lithofacies of the Logbaba Formation reservoirs consist mainly of sandstone interbedded with carbonates and shales. The shapes of the gamma-ray signatures are cylindrical; however, these reservoirs correspond to a turbidite sand depositional environment.

- The analyzed wells show good reservoir quality, with relatively moderate and good effective porosity (15.5% - 21.3%), with medium permeability (5.65 - 75.09 md) and low shale content (6.3% - 19.8%). Water saturation is high (34.5% - 74.2%). However, all reservoirs were water-bearing and the hydrocarbon residues were not recoverable and did not contain commercial quantities.

- Clay minerals such as chlorite, montmorillonite and mixed layers were found in the reservoirs. The dominant clay mineral is chlorite, and its development is related to primary deposition before rock formation or to secondary diagenetic events that occurred after

sedimentation. The good porosities, on the other hand, indicate that the clay mineral has little influence on reservoir quality.

The findings of this study can also guide exploration in similar basins awaiting further exploration and development but also aid future estimation of the potential geological storage capacity in this basin.

Limitations of the research

The limitation of the existing regional seismic dataset has undoubtedly been an obstacle in the detailed study of the stratigraphic architecture of the Upper Cretaceous targets. In addition, the legacy seismic data is not optimised for examining the finer details of fault systems nor for delineating the architecture of the target reservoirs. Therefore, better seismic imaging will be required especially wider coverage of 3D seismic reflection dataset.

Future Research

This thesis has opened opportunities for future research works, which could be undertaken to extend the understanding of the processes modulating the deep-water evolution of the Kribi-Campo sub-basin. Other detailed analysis of the channel has to be performed to further unravel the fluid-bearing (hydrocarbon vs pore-water) potential of the channels identified in this study. Seismic evaluation like amplitude versus offset (AVO) analysis would be important with fluid substitution to know the fluid composition of the sandy channel facies. Also, Prestack depth migration (PSDM) data or velocity modelling would be important to have accurate depth measurement of the channel dimensions.

A 3-D petroleum system modelling taking into consideration the manifestation of the turbidite systems as potential hydrocarbon reservoirs or transient reservoirs is necessary for unravelling the workings of the petroleum system in the Kribi-Campo Basin. This will also provide a quantitative estimate of hydrocarbon volume.

Having interpreted and described the geometry and morphology of the turbidite systems characterized from the high-resolution 3-D seismic dataset and the reservoir properties from boreholes. Concerning possible future carbon capture and storage (CCS) activities in the study area off the coast of Cameroon, it is an ideal natural laboratory for CCS based on the following:

- The formations are suitable because the reservoirs studied are located at a depth of more than 800 m (to allow storing CO_2 in the supercritical state), have a thick and extensive seal, have sufficient porosity for large volumes and can be sufficiently permeable to

allow injection at high flow rates without the need for excessive pressure. CO_2 sequestration at depths of more than 800 meters offers two advantages, both of which result from the high pressures encountered at these depths: the density of the CO_2 is high enough to allow efficient filling of the pores and to reduce the difference in buoyancy compared with in situ fluids.

- There are available wells that can be used to reinject CO_2 into the reservoir. Therefore, future studies can model the fate of CO_2 stored in the reservoir and likewise the volume of CO_2 that can be stored in the reservoir.

References

Abreu, V., Sullivan, M., Pirmez, C., Mohrig, D., 2003. Lateral accretion packages (LAPs): an important reservoir element in deep-water sinuous channels. Mar. Petrol. Geol. 20 (6–8), 631–648.

Ackerman, W.C., Boatwright, D.C., Burwood, B.M., Van Lerberche, D., Bondjo, E., Tamfu, S.F., Ovono, D., 1993. Geochemical analysis of selected hydrocarbon samples in the Douala Basin, Cameroon. Implications for an oil-prone source rock. AAPG Bull. 77 (9), 1604.

Adeogba, A.A., McHargue, T.R., Graham, S.A., 2005. Transient fan architecture and depositional controls from near-surface 3-D seismic data, Niger Delta continental slope. AAPG Bull. 89, 627–643.

Al-Qayim, B., Rashid, F., 2012. Reservoir characteristics of the Albian Upper Qamchuqa Formation Carbonates, Tqa oil-field, Kurdistan, Iraq. J. Pet. Geol. 35(4), 317–34.

Asquith, G., Gibson, C., 1982. Basic well log for geologists. American Association of Petroleum Geologist, Tulsa Methods in Exploration, Tulsa, 216p.

Asquith, G., Krygowski, D., 2004. Basic Well Log Analysis: AAPG Methods in Exploration Series, 16p.

Asquith, G.B., 1985. Handbook of Log Evaluation Techniques for Carbonate Reservoirs. Methods in Exploration Series N^{o}. 5. The American Association of Petroleum Geologists Tulsa, Oklahoma, USA, 1–47p.

Babonneau, N., Savoye, B., Cremer, M. and Bez, M., 2004. Multiple terraces within the deep incised Zaire Valley (ZaiAngo Project): are they confined levees? Geological Society, London, Special Publications, 222, 91–114. https://doi.org/10.1144/GSL.SP.2004.222.01.06.

Babonneau, N., Savoye, B., Cremer, M., Bez, M., 2010. Sedimentary architecture in meanders of a submarine channel: detailed study of the present congo turbidite channel (zaiango project). J. Sediment. Res. 80, 852–866.

Babonneau, N., Savoye, B., Cremer, M., Klein, B., 2002. Morphology and architecture of the present canyon and channel system of the Zaire deep-sea fan. Mar. Petrol. Geol. 19 (4), 445–467. https://doi.org/10.1016/S0264-8172(02)00009-0.

Bahorich, M., Farmer, S., 1995. 3-D seismic discontinuity for faults and stratigraphic features: The coherence cube. Lead. Edge 14, 1053–1058.

Balaky, M.S., Al-Dabagh, M.M., Asaad, Sh. I., Tamar-Agha, M., Ali, S.M., Radwan, E.A., 2023. Sedimentological and petrophysical heterogeneities controls on reservoir characterization of the Upper Triassic shallow marine carbonate Kurra Chine

Formation, Northern Iraq: Integration of outcrop and subsurface data. Marine and Petroleum Geology 149: 106085. https://doi.org/10.1016/j.marpetgeo.2022.106085.

Bardon and Pied, 1969. Formation water saturation in shaly sands: 10th annual logging symposium SPWLA, 1-19.

Beglinger, S.E., Doust, H., Cloetingh, S., 2012. Relating petroleum system and play development to basin evolution: West African South Atlantic basins. Marine and Petroleum Geology 30, 1-25. doi:10.1016/j.marpetgeo.2011.08.008.

Benkhelil, J., Giresse, P., Poumot, C., Ngueutchoua, G., 2002. Lithostratigraphic, geophysical, and morpho-tectonic studies of the South Cameroon shelf. In: Marine and Petroleum Geology 19: 499–517. https://doi.org/10.1016/ S0264 8172(02)00002-8.

Binks, R.M., Fairhead, J.D., 1992. A plate tectonic setting for Mesozoic rifts of West and Central Africa. Tectonophysics 213, 141–151.

Bloch, S., Lander, R.H., Bonnell, L.M., 2002. Anomalously high porosity and permeability in deeply buried sandstone reservoirs: origin and predictability. AAPG Bull. 86, 301–328.

Boggs, S., 2006. Principles of sedimentology and stratigraphy. Pearson Prentice Hall. 662p.

Booth, J.R., Dean, M.C., DuVernay, A.E. and Styzen, M.J., 2003. Paleo-bathymetric controls on the stratigraphic architecture and reservoir development of confined fans in the Auger Basin: central Gulf of Mexico slope. Marine and Petroleum Geology 20, 563-586. https://doi.org/10.1016/j.marpetgeo.2003.03.008.

Bouchakour, M., Zhao, X., Miclăus, C., Yang, B., 2023. Lateral migration and channel bend morphology around growing folds (Niger Delta continental slope). Basin Research 35(9). 10.1111/bre.12750.

Boulesteix, K., Poyatos-Moré, M., Flint, S.S., Taylor, K.G., Hodgson, D.M. and Hasiotis, S.T., 2019a. Transport and deposition of mud in deep-water environments: Processes and stratigraphic implications. Sedimentology 66, 2894-2925. https://doi.org/10.1111/sed.12614.

BrBuckles, R.S., 1965. Correlating and averaging connate water saturation data. J Can Petrol Technol 9 (1), 42–52.

Briggs, S.E., Cartwright, J., Davies, R. J., 2009. Crustal structure of the deepwater west Niger Delta passive margin from the interpretation of seismic reflection data. Marine and Petroleum Geology 26 (6)**,** 936-950.

Brown, A., 1997. Porosity variation in carbonates as a function of depth. Mississippian Madison Group, Williston Basin, 29–46p.

Brown, A.R., 2004. Interpretation of Three-dimensional Seismic Data. American Association of Petroleum Geologists and the Society of Exploration Geophysicists. 540p.

Brown, A.R., 2011. Interpretation of Three-Dimensional Seismic Data, Seventh. ed. Society of Exploration Geophysicists and American Association of Petroleum Geologists. 665p. https://doi.org/10.1190/1.9781560802884.

Brownfield, M.E., Charpentier, R.R., 2006. Geology and Total Petroleum Systems of the West-Central Coastal Province (7203), West Africa: U.S. Geological Survey Bulletin 2207-B, 52p.

Burke, A.W., Campbell Jr, J.A., 1969. The litho-porosity cross plot A method of determining rock characteristics for computation of log data. SPWLA tenth annual logging symposium, 29p. https://doi.org/10.2118/2771-MS.

Catterall, V., Redfern, J., Gawthorpe, R., Hansen, D., Thomas, M., 2010. Architectural style and quantification of a submarine channel-levee system located in a structurally complex area: offshore Nile Delta: Journal of Sedimentary Research 80, 991-1017.

Catuneanu, O., 2006. Principles of Sequence Stratigraphy. Elsevier, Amsterdam. 375p.

CGG Robertson 2015. Petroleum Geological Evaluation: Niger Delta to the Congo Fan. CGG Robertson Multiclient. Report No. AM086. 16p.

Chen, H., Lin, C., Zhang, Z., Zhang, D., Li, M., Wu, G., Zhu, Y., Xu, H., Lu, W., Chen, J., 2021. Evolution and controlling factors of the gravity flow deposits in the Miocene sequence stratigraphic framework, the Lower Congo-Congo Fan Basin, West Africa. Petroleum Exploration and Development, 48(1), 146–158.

Chiang, C.S., Hsiung, K.H., Yu H.S., Chen, S.C., 2020. Three types of modern submarine canyons on the tectonically active continental margin ofshore southwestern Taiwan. Marine Geophysical Research 41, 4.

Chima, K.I., Do Couto, D., Leroux, E., Gardin, S., Hoggmasacall, N., Rabineau, M., Granjean, D., and Gorini, C., 2019. Seismic stratigraphy and depositional architecture of Neogene intraslope basins, offshore western Niger Delta. Marine and Petroleum Geology 109, 449-468. doi: 10.1016/j.marpetgeo.2019.06.030.

Chima, K.I., Gorini, C., Rabineau, M., Granjeon, D., Do Couto, D., Leroux, E., Hoggmascall, N., 2020. Pliocene and Pleistocene stratigraphic evolution of the western Niger Delta intraslope basins: a record of glacio-eustatic sea-level and basin tectonic forcings. Global Planet. Change 195 (103355), 1–23. https://doi.org/ 10.1016/j.gloplacha.2020.103355.

Chongwain, G.M., Osinowo, O.O., Ntamak-Nida, M.J., Biouele, S.E.A., Nkoa, N.E., 2018. Petrophysical characterisation of reservoir intervals in well-X and well-Y, M-Field, offshore Douala Sub-Basin, Cameroon. J Pet Explor Prod Technol 9, 911–925. https://doi.org/10.1007/s13202-018-0562-0

Chongwain, G.C., Osinowo, O.O., Ntamak-Nida, M.J., Nkwanyang, T.L., 2019. Lithological typing, depositional environment, and reservoir quality characterization of the "M-Field," offshore Douala Basin, Cameroon. J Pet Explor Prod Technol 9, 1705–1721. https://doi.org/10.1007/s13202-019-0648-3

Chough, S. and Hesse, R., 1976. Submarine meandering thalweg and turbidity currents flowing for 4000 km in the Northwest Atlantic Mid-Ocean Channel, Labrador Sea. Geology 4, 529–534.

Clifford, A., 1986. African oil-Past, present, and future. In Halbouty, M.T., (Ed. Future petroleum provinces of the world. AAPG memoir 40, 339-372.

Collins, J., Kenyon-Roberts, S., Cullen, B., White, J., Bordas-Le Floch, N. and Downey, J., 2015. Arran Field: a complex heterolithic reservoir on the margins of the Forties Fan System, In McKie, T., Rose, P.T.S., Hartley, A.J., Jones, D.W. and Armstrong, T.L. (Eds.), Tertiary Deep-Marine Reservoirs of the North Sea Reservoirs of the North Sea Region, The Geological Society London Special Publication 403, 185-217p. https://doi.org/10.1144/SP403.10.

Covault, J.A., Kostic, S., Paull, C.K., Ryan, H.F., Fildani, A., 2014. Submarine channel initiation, filling and maintenance from seafloor geomorphology and morphodynamic modelling of cyclic steps. Sedimentology 61, 1031–1054.

Covault, J.A., Sylvester, Z., Hudec, M.R., Ceyhan, C., Dunlap, D., 2019. Submarine channels 'swept' downstream after bend cutoff in salt basins. The Depositional Record 6, 259–272.

Coward, M.P., Purdy, E.G., Ries, A.C., Smith, D.G., 1999. The distribution of petroleum reserves in basins of the South Atlantic margins. In: The Oil and Gas Habitats of the South Atlantic Geological Society of London Special Publications 153:101-131.

Cross, N.E., Cunningham, A., Cook, R.J., Taha, A., 2009. Three-dimensional seismic geomorphology of a deep-water slope-channel system: The Sequoia field, offshore west Nile Delta, Egypt. AAPG Convention, 20078.

Curray, J.R., Emmel, F.J., Moore, D.G., 2002. The Bengal Fan: morphology, geometry, stratigraphy, history and processes. Mar. Petrol. Geol. 19 (10), 1191–1223. https:// doi.org/10.1016/S0264-8172(03)00035-7.

Curtis, C.D., Coleman, M.L., 1986. Controls on the precipitation of early diagenetic calcite, dolomite and siderite concretions in complex depositional sequences. In: Gautier DL (ed) Roles of organic matter in sedimentary diagenesis, 23–35p. (Special Publication N^{o}. 38. Society of Economic Paleontologists and Mineralogists, Tulsa.)

Dailly, P., 2000. Tectonics and stratigraphic development of Rio Muni basin. Equatorial Guinea: the role of transform zone in Atlantic basin evolution. Atlantic Rifts and Continental Margins. Geophysical Monograph Series 115, 105-128.

Dailly, P., Lowry P., Goh., and Gene. M., 2002. Exploration and development of Ceiba field, Rio Muni basin, Southern Equatorial Guinea, The leading edge, November, 1140-1146.

Davies, R.J., Posamentier, H.W., Wood, L.J., Cartwright, J.A., 2006. Seismic Geomorphology: Applications to Hydrocarbon Exploration and Production. GSL Special Publication 277, 274p.

Davison, I., 1997. Wide and narrow margins of the Brazilian South Atlantic. Journal of the Geological Society of London, 154, 471-476.

De Matos, R.M.D., 1992. The northeast Brazilian rift system. Tectonics 11 (4)**,** 766-791.

Deptuck, M.E., Steffens, G.S., Barton, M., Pirmez, C., 2003. Architecture and evolution of upper fan channel-belts on the Niger Delta slope and in the Arabian Sea. Mar. Pet. Geol. 20, 649–676.

Deptuck, M.E., Sylvester, Z., Pirmez, C., O'Byrne, C., 2007. Migration–aggradation history and 3-D seismic geomorphology of submarine channels in the Pleistocene Benin major Canyon, western Niger Delta slope. Mar. Pet. Geol. 24, 406–433.

Deptuck, M.E., Piper, D.J.W., Savoye, B. and Gervais, A., 2008. Dimensions and architecture of late Pleistocene submarine lobes off the northern margin of East Corsica. Sedimentology 55, 869-898. https://doi.org/10.1111/j.1365-3091.2007.00926.x.

Dewan, J.T., 1983. Essentials of Modern Open-Hole Log Interpretation. PennWell Books, PennWell Publishing Company, Tulsa, Oklahoma, 361p.

Di Celma, C., Cantalamessa, G., Didaskalou, P., Lori, P., 2010. Sedimentology, architecture, and sequence stratigraphy of coarse-grained, submarine canyon fills from the Pleistocene (Gelasian-Calabrian) of the Peri-Adriatic basin, central Italy. Mar. Pet. Geol. 27, 1340–1365.

Dong, S.P., Shalaby, M.R., Islam, A., 2018. Integrated reservoir characterization study of the McKee formation, onshore Taranaki basin, New Zealand. Geosciences 8(4), 105.

Doughty-Jones, G., Mayall, M., Lonergan, L., 2017. Stratigraphy, facies, and evolution of deep-water lobe complexes within a salt controlled intraslope mini basin. AAPG Bull. 101 (11), 1879–1904. https://doi.org/10.1306/ 01111716046.

El-Din, E.S., Mesbah, M.A., Kassab, M.A., Mohammed, I.F., Cheadle, B.A., 2013. Assessment of petrophysical parameters of clastics using well logs: the Upper Miocene in El-Wastani gas field, onshore nile Delta, Egypt. Pet Explot Dev 40(4), 488–494.

Elmahdy, M., Radwan, A.A., Nabawy, B.S., Abdelmaksoud, A., Nastavkin, A.V., 2023. Integrated geophysical, petrophysical and petrographical characterization of the carbonate and clastic reservoirs of the Waihapa Field, Taranaki Basin, New Zealand. Marine and Petroleum Geology 151: 106173. https://doi.org/10.1016/j.marpetgeo.2023.106173

Emery and Myers, 1996. Sequence stratigraphy. Blackwell Science, Oxford, 297.

Eruteya, O.E., Safadi, M., Waldmann, N., Makovsky, Y., Ben-Avraham, Z., 2016. Seismic Geomorphology of the Israel Slump Complex in the Levant Basin (SE Mediterranean), in: Lamarche, G., Mountjoy, J., Bull, S., Hubble, T., Krastel, S., Lane, E., Micallef, A., Moscardelli, L., Mueller, C., Pecher, I., Woelz, S. (Eds.), Submarine Mass Movements and their Consequences: 7th International Symposium. Springer International Publishing, Cham, 39-47p.

Estrada, F., Ercilla, G., Alonso, B., 2005. Quantitative study of a Magdalena submarine channel (Caribbean Sea): implications for sedimentary dynamics. Marine and Petroleum Geology, 22(5), 623-635.

Etienne, S., Mulder, T., Bez, M., Desaubliaux, G., Kwasniewski, A., Parize, O., 2012. Multiple scale characterization of sand-rich distal lobe deposit variability: examples from the Annot Sandstones Formation, Eocene–Oligocene, SE France. Sedimentary Geology, 273-274, 1-18. https://doi.org/10.1016/j.sedgeo.2012.05.003.

Exploration Consultants Limited (ECL), 2001. An Integrated Study Development, Source Rock Maturity and Hydrocarbon Generation in the Douala/Kribi-Campo Basin, Republic of Cameroon: Henley-On-Thames. Cameroon National Hydrocarbons Corporation, Oxfordshire, United Kingdom, 183p.

Ferry, J.-N., Mulder, T., Parize, O. and Raillard, S., 2005. Concept of equilibrium profile in deep-water turbidite system: effects of local physiographic changes on the nature of sedimentary process and the geometries of deposits. Geological Society, London, Special Publications, 244, 181–193. https://doi.org/10.1144/GSL.SP.2005.244.01.11.

Fertl, W.H., Vercellino, W.C., 1978. Practicla log analysis. 4. Predict water cut from well logs. Oil Gas J. 76(25), 111–116.

Fonnesu, M., Felletti, F., Haughton, P.D.W., Patacci, M., McCaffrey, W.D. and Mangiagalli, V., 2018. Hybrid event bed character and distribution linked to turbidite system sub-environments: The North Apennine Gottero Sandstone (north-west Italy). Sedimentology, 65, 151–190. https://doi.org/10.1111/sed.12376.

Friedmann, S.J., Beaubouef, R.T., Pirmez, C., Jennette, D.C., 2000. The effects of gradient changes on deep-water depositional systems: an integrated approach: American Association of Petroleum Geologists, 2000 Annual Meeting, Extended Abstracts, New Orleans, U.S., 51p.

Fusion Oil & Gas NL., 2002. Cameroon, Ntem Exploration Permit, Technical Evaluation Report. Proprietary Report, Fusion Oil & Gas NL.

Gamberi, F., Rovere, M., Marani, M., 2011. Mass-transport complex evolution in a tectonically active margin (Gioia Basin, Southeastern Tyrrhenian Sea). Mar. Geol. 279, 98–110.

Gamboa, D., Alves, T.M., 2015. Spatial and dimensional relationships of submarine slope architectural elements: a seismic-scale analysis from the Espírito Santo Basin (SE Brazil). Mar. Pet. Geol. 64, 43–57.

Gamboa, D., Alves, T.M., Cartwright, J., 2012. A submarine channel confluence classification for topographically confined slopes. Mar. Pet. Geol. 35, 176–189.

Gardner, M. H., Borer, J. M., Melick, J. J., Mavilla, N., Dechesne, M. & Wagerle, R. M. 2003. Stratigraphic process-response model for submarine channels and related features from studies of Permian Brushy Canyon outcrops, West Texas. Marine and Petroleum Geology, 20, 757–787.

Gee, M.J.R., Uy, H.S., Warren, J., Morley, C.K., Lambiase, J.J., 2007. The Brunei slide: a giant submarine landslide on the Northwest Borneo Margin revealed by 3D seismic data. Mar. Geol. 246, 9–23.

Gee, M.J.R. and Gawthorpe, R.L., 2006. Submarine channels controlled by salt tectonics: Examples from 3D seismic data offshore Angola. Marine and Petroleum Geology 23, 443-458. https://doi.org/10.1016/j.marpetgeo.2006.01.002.

Gee, M.J.R., Gawthorpe, R.L., Bakke, K. and Friedmann, S.J., 2007. Seismic geomorphology and evolution of submarine channels from the Angolan continental margin. Journal of Sedimentary Research 77, 433–446. https://doi.org/10.2110/jsr.2007.042.

Georgiopoulou, A. and Cartwright, J.A., 2013. A critical test of the concept of submarine equilibrium profile. Marine and Petroleum Geology 41, 35–47. https://doi.org/10.1016/j.marpetgeo.2012.03.003.

Gervais, A., Savoye, B., Mulder, T., Gonthier, E., 2006. Sandy modern turbidite lobes: a new insight from high resolution seismic data. Mar. Petrol. Geol. 23, 485–502.

Gibbs, P., Brush, E., Fiduk, 2003. The evolution of the syn rift and transition phase of the central/southern Brazilian and W. African conjugate margins: the implications for source rock distribution in time and space, and their recognition on seismic data: Presented at the Eighth International Congress of the Brazillian Geophysical Society,, Rio de Janeiro, 1–7p.

Gong, C.L., Steel, R.J., Wang, Y.M., et al., 2016. Shelf-margin architecture variability and its role in sediment-budget partitioning into deep-water areas. Earth Sci. Rev. 154, 2–101.

Hadler-Jacobsen, F., Johannessen, E. P., Ashton, N., Henriksen, S., Johnson, S. D. & Kristensen, J. B., 2005. Submarine fan morphology and lithology distribution. In: DORE´ , A. G. & VINING, B. A. (eds). Petroleum Geology: North-West Europe and Global Perspectives—Proceedings of the 6th Petroleum Geology Conference, 1121–1145. Petroleum Geology Conferences Ltd. Published by the Geological Society, London.

Hakimi, M.H., Al-Qadasi, B.A., Al-Sharrabi, Y., Al-Sorore, O.T., Al-Samet, N.G., 2017. Petrophysical properties of Cretaceous clastic rocks (Qishn Formation) in the Sharyoof oilfield, onshore Masila Basin, Yemen. Egypt J. Pet. 26(2), 439–455.

Hansen, L.A.S., Callow, R.H.T., Kane, I.A., Gamberi, F., Rovere, M., Cronin, B.T. and Kneller, B.C., 2015. Genesis and character of thin-bedded turbidites associated with submarine channels. Marine and Petroleum Geology 67, 852–879. https://doi.org/10.1016/j.marpetgeo.2015.06.007.

Hansen, L.A.S., Hodgson, D.M., Pontén, A., Bell, D. and Flint, S., 2019. Quantification of basin-floor fan pinchouts: Examples from the Karoo Basin, South Africa. Frontiers in Earth Science 7, 12. https://doi.org/10.3389/feart.2019.00012.

Hansen, L., Janocko, M., Kane, I., Kneller, B., 2017. Submarine channel evolution, terrace development, and preservation of intra-channel thin-bedded turbidites: Mahin and Avon channels, offshore Nigeria. Mar. Geol. 383, 146–167.

Haq, B.U., Hardenbol, J., Vail, P.R., 1987. Chronology of fluctuating sea levels since the triassic. Science 235, 1156–1167.

Harishidayat, D., Omosanya, K.O., Johansen, S.E., Eruteya, O.E., Niyazi, Y., 2018. Morphometric analysis of sediment conduits on a bathymetric high: implications for palaeoenvironment and hydrocarbon prospectivity. Basin Research 30, 1015–1041. https://doi.org/10.1111/bre.12291

Haughton, P., Davis, C., McCaffrey, W. and Barker, S., 2009. Hybrid sediment gravity flow deposits - Classification, origin and significance. Marine and Petroleum Geology 26, 1900–1918. https://doi.org/10.1016/j.marpetgeo.2009.02.012.

Heald, M.T., Larese, R.E., 1974. Influence of coatings on quartz cementation. J Sediment Petrol 44:1269–1274

Helm, C., 2009. Quantification des flux sédimentaires anciens à l'échelle d'un continent: le cas de l'Afrique au Méso-cénozoïque, vol. 1. Thesis. Univ. Rennes, p. 299.

Hilchie, D.W., 1978. Applied openhole log interpretation. DW Hilchie. Inc., Golden. 161p.

Hodgson, D.M. and Haughton, P.D., 2004. Impact of syndepositional faulting on gravity current behaviour and deep-water stratigraphy: Tabernas-Sorbas Basin, SE Spain. Geological Society, London, Special Publications, 222, 135-158. https://doi.org/10.1144/GSL.SP.2004.222.01.08.

Hodgson, D.M., Kane, I.A., Flint, S.S., Brunt, R.L. and Ortiz-Karpf, A., 2016. Time-transgressive confinement on the slope and the progradation of basin-floor fans: implications for the sequence stratigraphy of deep-water deposits. Journal of Sedimentary Research, 86, 73-86. https://doi.org/10.2110/jsr.2016.3.

Howlett, D.M., Gawthorpe, R.L., Ge, Z., Rotevatn, A., Jackson, C., 2020. Turbidites, topography and tectonics: Evolution of submarine. Basin Research 33(2), 1076-1110. https://doi.org/10.1111/bre.12506.

Hu, K., Chen, Z., Yang, C., Jiang, C., Liu, X., 2020. Integrated petrophysical evaluation of the Lower Middle Bakken Member in the Viewfield Pool, southeastern Saskatchewan, Canada. Marine and Petroleum Geology 122: 104601. https://doi.org/10.1016/j.marpetgeo.2020.104601.

Huang, Y., 2018. Sedimentary characteristics of turbidite fan and its implication for hydrocarbon exploration in Lower Congo Basin. Petroleum Research 3, 189-196.

Hühnerbach, V., Masson, D.G., Partners, C.., 2004. Landslides in the North Atlantic and its adjacent seas: an analysis of their morphology, setting and behaviour. Mar. Geol. 213, 343–362.

Iboum Kissaaka, J.B., Ntamak-Nida, M.J., Mvondo, F., Fowe Kwetche P.G., Djomeni Nitcheu, A,L,, Abolo, G.M.; 2016. Postrift depositional evolution and sequence stratigraphy from offshore subsurface data of the Kribi-Campo sub basin (Cameroon, West African margin), Society of Exploration Geophysicists and American Association Petroleum Geologists 13: 79–101 https://doi.org/10.1190/INT-2015-0073.1.

Irwin, H., Curtis, C., Coleman, M., 1977. Isotopie evidence for source of diagenetic carbonates formed during burial of organic-rich sediments. Nature 269:20.

Iverson, R.M., 1997. The physics of debris flows. Review of Geophysics, 35, 245–296. https://doi.org/10.1029/97RG00426.

Janocko, M., Nemec, W., Henriksen, S., Warchoł, M., 2013. The diversity of deep-water sinuous channel belts and slope valley-fill complexes. Mar. Pet. Geol. 41, 7–34.

Jiang, S., 2012. Clay minerals from the perspective of oil and gas exploration. In: Valašcova M, Martynkova GS (eds) Clay minerals in nature-their characterization, modification and application, 21–38p. https://doi.org/10.5772/47790

Jobe, Z.R., Lowe, D.R. & Uchytil, S.J., 2011. Two fundamentally different types of submarine canyons along the continental margin of Equatorial Guinea. Marine and Petroleum Geology, 28(3): 843-860.

Jobe, Z.R., Sylvester, Z., Parker, A.O., Howes, N., Slowey, N., and Pirmez, C., 2015. Rapid adjustment of submarine channel architecture to changes in sediment supply: Journal of Sedimentary Research 85, 729–753, doi:10.2110/jsr.2015.30.

Jolly, B.A., Lonergan, L., Whittaker, A.C., 2015. Growth history of fault-related folds and interaction with seabed channels in the toe-thrust region of the deep-water Niger Delta. Marine and Petroleum Geology 70, 58–76.

Jumat, N., Shalaby, M.R., Islam, M.A., 2018. Integrated reservoir characterization of the Paleocene Farewell Formation, Taranaki Basin, New Zealand, using petrophysical and petrographical analyses. J Pet Explor Prod Technol 8, 685–701.

Kane, I.A., Pontén, A.S.M., Vangdal, B., Eggenhuisen, J.T., Hodgson, D.M. and Spychala, Y.T. 2017. The stratigraphic record and processes of turbidity current transformation across deep-marine lobes. Sedimentology, 64, 1236-1273. https://doi.org/10.1111/sed.12346.

Kane, I.A. and Hodgson, D.M., 2011. Sedimentological criteria to differentiate submarine channel levee subenvironments: Exhumed examples from the Rosario Fm. (Upper Cretaceous) of Baja California, Mexico, and the Fort Brown Fm. (Permian), Karoo Basin, S. Africa. Marine and Petroleum Geology, 28, 807-823. https://doi.org/10.1016/j.marpetgeo.2010.05.009.

Kane, I.A., Kneller, B.C., Dykstra, M., Kassem, A. and McCaffrey, W.D., 2007. Anatomy of a submarine channel-lee: An example from Upper Cretaceous slope sediments, Rosario Formation, Baja California, Mexico. Marine and Petroleum Geology, 24, 540-563. https://doi.org/10.1016/j.marpetgeo.2007.01.003.

Kane, I.A., Mc Caffrey, W.D., Peakall, J., 2008. Controls on sinuosity evolution within submarine channels. Geology 36 (4), 287–290.

Kearey, P., Brooks, M., Hill, I., 2002. An introduction to geophysical exploration. Wiley-Blackwell. 288p.

Klauche, I., Masson, D.G., Kenyon, N.H. & Gardner, J.V. 2004. Sedimentary processes of the lower Monterey Fan channel and channel-mouth lobe. Marine Geology, 206 (1-4), 181-198.

Kneller, B. and Buckee, C., 2000. The structure and fluid mechanics of turbidity currents: a review of some recent studies and their geological implications. Sedimentology, 47 (suppl. 1), 62–94. https://doi.org/10.1046/j.1365-3091.2000.047s1062.x.

Kneller, B., Dykstra, M., Fairweather, L. and Milana, J.P., 2016. Mass-transport and slope accommodation: Implications for turbidite sandstone reservoirs. AAPG Bulletin 100, 213–235. https://doi.org/10.1306/09011514210.

Kneller, B., 1995. Beyond the turbidite paradigm: physical models for deposition of turbidites and their implications for reservoir prediction. Geological Society, London, Special Publications, 94, 31–49. https://doi.org/10.1144/GSL.SP.1995.094.01.04.

Kneller, B., 2003. The influence of flow parameters on turbidite slope channel architecture. Marine and Petroleum Geology 20, 901-910.

Kolla, V., Posamentier, H.W., Wood, L.J., 2007. Deep-water and fluvial sinuous channels characteristics, similarities and dissimilarities, and modes of formation. Mar. Pet. Geol. 24, 388–405.

Labourdette, R., Bez, M., 2010. Element migration in turbidite systems: random or systematic depositional processes? AAPG Bull. 94 (3), 345–368.

Larionov, V.V., 1969. Radiometry of boreholes. NEDRA, Moscow (in Russian). 127p.

Lawrence, R.S., Beach, A., Owain, J., Jackson, A., 2016. Deformation of oceanic crust in the eastern Gulf of Guinea: role in the evolution of the Cameroon Volcanic Line and influence on the petroleum endowment of the Douala-Rio Muni Basin, Geological Society of London, 438**.**

Lawrence, R.S., Munday, S., Bray, R., 2002. Regional Geology and Geophysics of the Eastern Gulf of Guinea (Niger Delta). The leading Edge, 1112–1117p.

Le, A.N., 2012. Stratigraphic Evolution and Plumbing System in the Cameroon Margin, West Africa. Thesis for the Degree of Doctor of Philosophy, Faculty of Engineering and Physical Science, University of Manchester, 258p.

Le, A.N., 2021. Striations at the Base of the Paleo-Fan and Channel revealed by 3D Seismic Data, Offshore Cameroon, Indonesian Journal on Geoscience 8, 101-107.

Le, A.N., Huuse, M., Redfern, J., Gawthorpe, R.L., Irving, D., 2014. Seismic characterization of a Bottom Simulating Reflection (BSR) and plumbing system of the Cameroon margin, offshore West Africa, Marine and Petroleum Geology 68, 629-647.

Li, P., Kneller, B., Hansen, L., 2021. Anatomy of a gas-bearing submarine channel-lobe system on a topographically complex slope (offshore Nile Delta, Egypt). Mar. Geol. 437, 106496 https://doi.org/10.1016/j.margeo.2021.106496.

Li, Q., Wu, W., Liang, J., Kang, H., Liu, W., Wang, G., Cai, L., 2020. Deep-water channels in the lower Congo basin: Evolution of the geomorphology and depositional environment during the Miocene, Marine and Petroleum Geology 115, 104260 doi.org/10.1016/j.marpetgeo.2020.104260.

Li, S., Gong, C., 2016. Flow dynamics and sedimentation of lateral accretion packages in sinuous deep-water channels: a 3D seismic case study from the northwestern South China Sea margin. J. Asian Earth Sci. 124, 233–246.

Lin, H.M., Shi, H.S., 2014. Hydrocarbon accumulation conditions and exploration direction of Baiyun–Liwan deepwater areas in the Pearl River Mouth Basin. Nat. Gas. Ind. B1, 150–158.

Loule, J.P., Jifon, F., Angoua Biouele, S.E., Nguema, P., Spofforth, D., Carruthers, D., Watkins, C., Johnston, J., 2018. An opportunity to re-evaluate the petroleum potential of the Douala/Kribi-Campo Basin, Cameroon. Special topic: Petroleum Geology. First break 36: 61-70.

Magoba, M., Opuwari, M., 2019. Petrophysical interpretation and fluid substitution modelling of the upper shallow marine sandstone reservoirs in the Bredasdorp Basin, offshore South Africa. J Pet Explor Prod Technol 10, 783–803.

Marini, M., Milli, S., Ravnås, R. and Moscatelli, M., 2015. A comparative study of confined vs. semiconfined turbidite lobes from the Lower Messinian Laga Basin (Central Apennines, Italy): Implications for assessment of reservoir architecture. Marine and Petroleum Geology, 63, 142–165. https://doi.org/10.1016/j.marpetgeo.2015.02.015.

Marsden, D., 1989. Layer cake depth conversion. Geophys Lead Edge 8: 10–14.

Marsset, T., Droz, L., Dennielou, B., Pichon, E., 2009. Cycles in the architecture of the Quaternary Zaïre turbidite system: a possible link with climate. In: Kneller, B., Martinsen, O.J., McCaffrey, B. (Eds.), Extern. Controls Deep-Water Depositional Systems, vol. 92. SEPM, Special Publication, 89–106p.

Mayall, M., Jones, E., Casey, M., 2006. Turbidite reservoirs-key elements in facies prediction and effective development. Marine and Petroleum Geology 23, 821-841.

Mbina Mounguengui, M., and Guiraud, M., 2009. Neocomian to early Aptian syn-rift evolution of the normal to oblique-rifted North Gabon Margin (Interior and N'Komi Basins). Marine and Petroleum Geology 26 (6)**,** 1000-1017.

McArthur, A.D. and McCaffrey, W.D., 2019. Sedimentary architecture of detached deep-marine canyons: Examples from the East Coast Basin of New Zealand. Sedimentology, 66, 1067-1101. https://doi.org/10.1111/sed.12536.

McCaffrey, W.D., Gupta, S. and Brunt, R., 2002. Repeated cycles of submarine channel incision, infill and transition to sheet sandstone development in the Alpine Foreland Basin, SE France. Sedimentology, 49, 623–635. https://doi.org/10.1046/j.1365-3091.2002.00477.x.

McCaffrey, W. & Kneller, B. 2001. Process controls on the development of stratigraphic trap potential on the margins of confined turbidite systems and aids to reservoir evaluation. AAPG bulletin, 85(6): 971-988.

McHargue, T., Pyrcz, M.J., Sullivan, M.D., Clark, J.D., Fildani, A., Romans, B.W., Covault, J.A., Levy, M., Posamentier, H.W., Drinkwater, N.J., 2011. Architecture of turbidite channel systems on the continental slope: patterns and predictions. Mar. Petrol. Geol. 28 (3), 728–743.

Metz, J.M., Grotzinger, J.P., Mohrig, D., Milliken, R., Prather, B., Pirmez, C., Mcewen, A.S. & Weitz, C.M. 2009. Sublacustrine depositional fans in southwest Melas Chasma. J. Geophys. Res, 114, 17p.

Meyers, J.B., Rosendhal, B.R., Groschel-Becker, H., Austin, J.J.A., Rona, P.A., 1996. Deep penetrating MCS imaging of the rift-to-drift transition, offshore Douala and North Gabon Basins, West Africa. Marine and Petroleum Geology 13, 791-835. https://doi:10.1016/0264-8172 (96)00030-X.

Miall, A.D., 1989. Architectural elements and bounding surfaces in channelized clastic deposits: Notes on comparisons between fluvial and turbidite systems. Sedimentary facies in the active plate margin: Tokyo, Terra Scientific Publishing Company: 3-15.

Mienlam Essi, M.F., Yene Atangana, J.Q., Abate Essi, J.M., Mbida Yem, Angoua Biouele S.E., Nguema, P., Tsimi Ntsengue, C., 2021. Stratigraphical nature of the Top Albian surface, from seismic and wells data analyses, in the south Sanaga area (Cameroon Atlantic margin): palaeogeographical significance and petroleum implications. Mar. Petrol. Geol. 129: 105073. https://doi.org/10.1016/j. marpetgeo.2021.105073.

Mitchell, W.H., Whittaker, A.C., Mayall, M., Lonergan, L., 2021. New models for submarine channel deposits on structurally complex slopes: Examples from the Niger delta system. Marine and Petroleum Geology 129, 105040. doi.org/10.1016/j.marpetgeo.2021.105040.

Mitchum, Jr., Vail, P.R., Sangree, J.B., 1977. Seismic stratigraphy and global changes of sea level: part 6. In: Stratigraphic Interpretation of Seismic Reflection Patterns in Depositional Sequences: Section 2. Application of Seismic Reflection Configuration to Stratigraphic Interpretation.

Morend, D., Pugin, A., and Gorin, G.E., 2002. High-resolution seismic imaging of outcrop-scale channels and an incised-valley system within the fluvial-dominated Lower Freshwater Molasse (Aquitanian, western Swiss Molasse Basin): Sedimentary Geology 149: 245–264.

Morgan, J., Camerlenghi, A., Silver, E., Dugan, B., Kirby, S., Shipp, C., Suyehiro, K., 2009. Addressing geologic Hazrds through Ocean drilling. Sci. Drill. 7, 15–30.

Morris, E.A., Hodgson, D.M., Flint, S.S., Brunt, R.L., Butterworth, P.J. and Verhaeghe, J., 2014. Sedimentology, stratigraphic architecture, and depositional context of submarine frontal-lobe complexes. Journal of Sedimentary Research, 84, 763-780. https://doi.org/10.2110/jsr.2014.61.

Morris, R.L., Biggs, W.P., 1967. Using log-derived values of water saturation and porosity. In: PWLA 8th annual logging symposium. 26p.

Mulder, T. and Alexander, J., 2001. The physical character of subaqueous sedimentary density flow and their deposits. Sedimentology, 48, 269–299. https://doi.org/10.1046/j.1365-3091.2001.00360.x.

Mutti, E. and Normark, W.R., 1991. An integrated approach to the study of turbidite systems. In Osborne, R. H. (Ed.), Seismic facies and sedimentary processes of submarine fans and turbidite systems, New York, Springer, 75–106. https://doi.org/10.1007/978-1-4684-8276-8_4.

Mutti, E., Normark, W.R., 1987. Comparing examples of modern and ancient turbidite systems: problems and concepts. In: Legett, J.K., Zuffa, G.G. (Eds.),

Marine Clastic Sedimentology: Concepts and Case Studies. Graham and Trotman, London, 1-38p.

Mvondo, O.F., 2010. Surrection cénozoïque l'Ouest de l'Afrique à partir de deux exemples : le plateau sud-namibien et la marge nord camerounaise. Thèse de Doctorat, Université de Rennes, 324p.

Myers, K.J., Milton, N.J., 1996. Concepts and Principles of Sequence Stratigraphy, in: Sequence Stratigraphy. Blackwell Publishing Ltd., 9–41p. https://doi.org/10.1002/9781444313710.ch2.

Navarre, J.-C., Claude, D., Librelle, F., Safa, P., Villon, G. and Keskes, N., 2002. Deepwater turbidite system analysis, West Africa: sedimentary model and implications for reservoir model construction. The Leading Edge, 21, 1132–1139. https://doi.org/10.1190/1.1523754.

Ndonwie Mahbou, E., 2007. Petrophysical characterization of petroleum reservoirs and source beds of the Batanga sub-block, Kribi-Campo sub-basin, Cameroon. AAPG Annual Convention, Abstract, 1p.

Nelson, C.H., Twichell, D.C., Schwab, W.C., Lee, H.J., Kenyon, N.H., 1992. Upper Pleistocene turbidite sand beds and chaotic silt beds in the channelized, distal, outer-fan lobes of the Mississippi fan. Geology, 20 (8)**,** 693-696.

Ngo, E.N.J., Ntamak-Nida, M.J., Bisso, D., Mvondo Owono, F., Ngos III, S., Bilong, P., Njandjock Nouck, P., 2018. Depocenters Repartition and Sequence Stratigraphy of the Northern Part of the Kribi-Campo sub-basin (Cameroon). European Journal of Scientific Research 149, 258-278.

Nguene, F.R., Tamfu, S., Loule, J., Ngassa, C., 1992. Palaeoenvironments of the Douala and Kribi/Campo sub-basins, in Cameroon, west Africa, in Curnelle,R.,ed., Géologie Africaine, 1er Colloque de Stratigraphie et de Paléogéographie des Bassins Sédimentaires Ouest-Africains, 2e Colloque Africain de Micropaléontologie, Libreville, Gabon, 1991, Recueil des Communications: Boussens, Elf Aquitaine, 129–139p.

Ngueutchoua, G., Giresse, P., 2010. Sand bodies and incised valleys within the Late Quaternary Sanaga-Nyong delta complex on the middle continental shelf of Cameroon: Marine and Petroleum Geology 27(10), 2173– 2188. doi:10.1016/j.marpetgeo.2010.06.011.

Nichols, G., 2009. Sedimentology and Stratigraphy. 2nd ed. s.l.: Wiley-Blackwell. 432p.

Niyazi, Y., Eruteya, O.E., Omosanya, K.O., Harishidayat, D., Johansen, S.E., Waldmann, N., 2018. Seismic geomorphology of submarine channel-belt complexes in the Pliocene of the Levant basin. Offshore Central Israel. Mar. Geol. 403, 123–128.

Niyazi, Y., Eruteya, O.E., Warne, M., Lerodiaconou, D., 2021. Discovery of large-scale buried volcanoes within the Cenozoic succession of the Prawn Platform, offshore Otway Basin, southeastern Australia. Marine and Petroleum Geology 123:104747. doi:10.1016/j.marpetgeo.2020. 104747.

Normark, W.R., Piper, D.J.W. and Hess, G.R., 1979. Distributary channels, sand lobes, and mesotopography of Navy Submarine Fan, California Borderland, with applications to ancient fan sediments. Sedimentology, 26, 749–774. https://doi.org/10.1111/j.1365-3091.1979.tb00971.x.

Normark, W.R., & Carlson, P.R., 2003. Giant submarine canyons: Is size any clue to their importance in the rock record? Geological Society of America Special Papers, 370: 175-190.

Normark, W.R., Piper, D.J.W., 1991. Initiation processes and flow evolution of turbidity currents: Implications for the depositional record. SEPM Special Publication 46, 207–230. https://doi.org/10.2110/pec.91.09.0207.

Ntamak-Nida, M.J, Bourquin, S., Makong, J.C., Baudin, F., Mpesse, J.E., Ngouem, C.I., Komguem, P.B., Abolo, G.M., 2010. Sedimentology and sequence stratigraphy from outcrops of the Kribi-Campo sub-basin: lower Mundeck Formation (Lower Cretaceous, Southern Cameroon). J Afr Earth Sci. 58, 1–18. https://doi.org/10.1016/j.jafrearsci.2010.01.004.

Ntamak-Nida, M.J., Baudin, F., Schnyder, J., Makong, J.C., Komguem, P.B., Abolo, G.M., 2008. Depositional environments and characterisation of the organic matter of thelower mundeck formation (Barremian?-Aptian) of the kribi-campo sub-basin (south Cameroon): implications for petroleum exploration. J. Afr. Earth Sci. 51, 207–219. https://doi.org/10.1016/j.jafrearsci.2008.01.006.

Oluboyo, A.P., Gawthorpe, R.L., Bakke, K., Hadler-Jacobsen, F., 2014. Salt tectonic controls on deep-water turbidite depositional systems: Miocene, southwestern Lower Congo Basin, offshore Angola. Basin Research 26, 597-620.

Omosanya, K.O., Alves, T.M., 2013. A 3-dimensional seismic method to assess the provenance of Mass-Transport Deposits (MTDs) on salt-rich continental slopes (Espírito Santo Basin, SE Brazil). Mar. Pet. Geol. 44, 223–239. http://dx.doi.org/10.1016/j. marpetgeo.2013.02.006.

Opuwari, M., Afolayan, B., Mohammed, S., Amaechi, P.O., Bareja, Y., Chatterjee, T., 2022. Petrophysical core-based zonation of OW oilfield in the Bredasdorp Basin South Africa. Scientific Reports 12, 510. https://doi.org/10.1038/s41598-021-04447-6.

Ortiz-Karpf, A., Hodgson, D.M. and McCaffrey, W.D., 2015. The role of mass-transport complexes in controlling channel avulsion and the subsequent sediment dispersal patterns on an active margin: the Magdalena Fan, offshore Colombia. Marine and Petroleum Geology 64, 58-75. https://doi.org/10.1016/j.marpetgeo.2015.01.005.

Pauken, R.J., 1992. Sanaga Sud field, offshore Cameroon, West Africa, in M. T. Halbouty, ed., Giant oil and gas fields of the decade 1978–1988: AAPG Bull. 54, 217–230.

Pauken, R.J., Thompson, J.M., Schuman, J.R., Cooke, J.C., 1991. Geology of the Douala Basin, offshore Cameroon. AAPG Bull. 75 (3), 651–652.

Pauken, R. J. 1992. Sanaga Sud Field, offshore Cameroon, West Africa. In: Halbouty, M.T. (ed.) Giant Oil and Gas Fields of the Decade 1978-1988. Memoir. American Association of Petroleum Geologists 54, 217-230.

Peakall, J., MCCaffrey, B. and Kneller, B., 2000. A Process Model for the Evolution, Morphology, and Architecture of Sinuous Submarine Channels. Journal of Sedimentary Research 70, 434–448. https://doi.org/10.1306/2DC4091C-0E47-11D7-8643000102C1865D.

Peakall, J., Sumner, E.J., 2015. Submarine channel flow processes and deposits: a process-product perspective. Geomorphology 244, 95–120. https://doi.org/10.1016/j.geomorph.2015.03.005.

Pickering, K.T., Corregidor, J. and Clark, J.D., 2015. Architecture and stacking patterns of lower-slope and proximal basin-floor channelised submarine fans, Middle Eocene Ainsa System, Spanish Pyrenees: An integrated outcrop-subsurface study. Earth-Science Reviews 144, 47–81. https://doi.org/10.1016/j.earscirev.2014.11.017.

Pickering, K. T., Hiscott, R. N. & Hein, F. J. 1989. Deep marine environments, clastic sedimentation and tectonics. Kluwer Academic Publishers Group.

Picot, M., Droz, L., Marsset, T., Dennielou, B., Bez, M., 2016. Controls on turbidite sedimentation: insights from a quantitative approach of submarine channel and lobe architecture (Late Quaternary Congo Fan). Mar. Petrol. Geol. 72, 423–446.

Picot, M., Droz, L., Marsset, T., Dennielou, B., Bez, M., 2016. Controls on turbidite sedimentation: insights from a quantitative approach of submarine channel and lobe architecture (Late Quaternary Congo Fan). Mar. Petrol. Geol. 72, 423–446.

Piper D.J.W., and Normark W.R., 1983. Turbidite depositional patterns and flow characteristics, Navy Submarine Fan, California Borderland. Sedimentology, 30, 681-694.

Piper, D.J.W., Shor, A.N. and Hughes Clarke, J.E., 1988. The 1929 'Grand Banks' earthquake, slump, and turbidity current. GSA Special Papers 229, 77–92. https://doi.org/10.1130/SPE229-p77.

Pirmez, C., Beaubouef, R.T., Friedmann, S.J. and Mohrig, D.C., 2000. Equilibrium profile and baselevel in submarine channels: examples from Late Pleistocene systems and implications for the architecture of deepwater reservoirs. In Weimer, P. (Ed.), Deep-Water Reservoirs of the World, Gulf Coast Section, 20th Annual Research Conference, Proceedings, Houston, SEPM, 782–805. https://doi.org/10.5724/gcs.00.15.0782.

Posamentier, H.W., Davies, R.J., Cartwright, J.A., Wood, L., 2007. Seismic geomorphology - an overview. Geological Society, London, Special Publications 277, 1-14.

Posamentier, H. & Walker, R.G., 2006. Deep-water turbidites and submarine fans. Facies models revisited, 84, SEPM Special Publication, 397-520.

Posamentier, H.W. Kolla, V., 2003. Seismic geomorphology and stratigraphy of depositional elements in deep-water settings. J. Sediment. Res. 73, 367–388. https://doi.org/10.1306/111302730367.

Posamentier, H.W., 2001. Lowstand alluvial bypass systems: incised vs. unincised. AAPG Bull. 85, 1771–1793.

Prélat, A., Hodgson, D.M., Flint, S.S., 2009. Evolution, architecture and hierarchy of distributary deep-water deposits: a high-resolution outcrop investigation from the Permian Karoo Basin, South Africa. Sedimentology 56, 2132–2154.

Prélat, A. and Hodgson, D.M., 2013. The full range of turbidite bed thickness patterns in submarine lobes: controls and implications. Journal of the Geological Society 170, 209-214. https://doi.org/10.1144/jgs2012-056.

Qadri, S.M.T., Shalaby, M.R., Islam, M.A., 2019. Application of well log analysis to estimate the petrophysical parameters and evaluate the reservoir quality of the Lower Goru Formation, Lower Indus Basin, Pakistan. Geomech Geophys Geoenergy Georesour. 5, 271–288. https ://doi.org/10.1007/s40948-019-00112-5.

Qadri, S.M.T., Islam, M.A., Shalaby, M.R., El-Aal, A.K.A., 2020. Reservoir quality evaluation of the Farewell sandstone by integrating sedimentological and well log analysis in the Kupe South Field, Taranaki Basin-New Zealand. Journal of Petroleum Exploration and Production 11, 11–31.

Qi, B.W., Lin, C.M., Qiu, G.Q., Li, Y.L., Liu, H.M., Gao, Y.J., 2006. Formation mechanism of calcareous incrustation in lenticular sandbody of the shahejie formation of paleogene and its influence on hydrocarbon accumulation in Dongying Sag. J. Palaeogeogr. 8, 519–530.

Qin, Y., Alves, T.M., Constantine, J. & Gamboa, D. 2016. Quantitative seismic geomorphology of a submarine channel system in SE Brazil (Espírito Santo Basin): Scale comparison with other submarine channel systems. Marine and Petroleum Geology 78, 455-473.

Rabinowitz, P., and LaBrecque J., 1979. The Mesozoic South Atlantic Ocean and evolution of its continental margins, J. Geophys. Res. 84(B11), 5973-6002.

Radwan, A.A., Nabawy, B.S., Abdelmaksoud, A., Lashin, A., 2021. Integrated sedimentological and petrophysical characterization for clastic reservoirs: A case study from New Zealand. Journal of Natural Gas Science and Engineering 88, 103797. https://doi.org/10.1016/j.jngse.2021.103797.

Reading, H.G., Richards, M., 1994. Turbidite systems in deep-water basin margins classifed by grain size and feeder system. American Association of Petroleum Geologists Bulletin 78, 792–822.

Regnoult, 1986. Synthèse géologique du Cameroun. DMG, Yaoundé, Cameroun, 118 p.

Rider, M. and Kennedy, M., 2011. The Geological Interpretation of Well Logs. Sutherland: Rider-French Consulting Limited, 432p.

Rider, M.H. 1996. Geological interpretation of well logs. 2nd Edition, Rider-French Consulting Ltd., Sucherland.

Rosendahl, B.R., Groschel-Becker, H., 1999**.** Deep seismic structure of the continental margin in the Gulf of Guinea: a summary report. In: Cameron, N.R., Bate, R.H. and Clure, V.S. (eds). The oil and Gas habitats of the South Atlantic. Geological Society, London, Special Publications, 153, 75-83.

Samuel, A., Kneller, B., Raslan, S., Sharp, A., Parsons, C., 2003. Prolific deep-marine slope channels of the Nile Delta, Egypt. AAPG Bull. 87, 541–560.

Schlumberger, 1989. Log Interpretation Principles/Applications. Schlumberger, USA. 241p.

Secke Bekonga Gouott, B., Mbida Yem, Yene Atangana, J.Q., Nkoa Nkoa, P.E., Angoua Biouele, S.E, Niyazi, Y., Eruteya, O.E., 2022. Seismic geomorphology of a Late Cretaceous submarine channel system in the Kribi/Campo sub-basin, offshore Cameroon. Marine and Petroleum Geology 145, 105865. https://doi.org/10.1016/j.marpetgeo.2022.105865.

Seiglie, G.A., Baker, M.B., 1984. Relative sea-level changes during the Middle and Late Cretaceous from Zaire to Cameroon (Central West Africa). AAPG Spec. A166, 81–88.

Seranne, M., Seguret, M., Fauchier, M., 1992. Seismic super-units and post-rift evolution of the continental passive margin of sourthern Gabon. Bulletin Societe Geologique de France, 163, 135-146.

Shanley, K.W., McCabe, P.J., 1994. Perspectives on the sequence stratigraphy of continental strata. AAPG Bull. 78, 544–568.

Shanmugam, G., 2006. Deep-water processes and facies models: Implications for sandstone petroleum reservoirs: Amsterdam, Elsevier, Handbook of petroleum exploration and production 5, 476p.

Shepard, F.P., 1981. Submarine canyons: multiple causes and long-time persistence. AAPG Bulletin 65(6), 1062-1077.

Sheriff, R., Geldart, L., 1995. Exploration Seismology, Second Edition. Cambridge University Press, 628 pages.

Shier, D.E., 2004. Well log normalization: Methods and guidelines. Petrophysics, 45(3), 268-280.

Shumaker, L., Jobe, Z., Johnstone, S., Pettinga, L., Cai, D., Moody, J., 2018. Controls on submarine channel-modifying processes identifed through morphometric scaling relationships. Geosphere 14 (5), 2171–2187.

Simon Petroleum Technology (SPT), 1995. Petroleum geology and hydrocarbon potential of the Douala Basin, Cameroon Unpubl. non-exclusive report.

SNH/UD, 2005. Stratigraphie séquentielle et tectonique des dépôts mésozoïques syn-rifts du Bassin de Kribi/Campo, Auteurs. In: Ntamak-Nida, M.J., Mpesse, J.E., Ketchemen-Tandia, B., Ndong Ondo, S., Courville, P., Baudin, F. (Eds.), Rapport Interne, 11 Planches, 02 Rapports Annexes D'analyses, 134p.

Soutter, E.L., Kane, I.A., Fuhrmann, A., Cumberpatch, Z.A. and Huuse, M., 2019. The stratigraphic evolution of onlap in siliciclastic deep-water systems: Autogenic modulation of allogenic signals. Journal of Sedimentary Research 89, 890-917. https://doi.org/10.2110/jsr.2019.49.

Soutter, E., Kane, I., Hodgson, D.M., Flint, S.S., 2021. Controls on submarine canyon connection to the shoreline: a numerical modelling approach. EarthArXiv, https://doi.org/10.31223/X5P33S.

Sprague, A.R., Sullivan, M.D., Campion, K.M., Jensen, G.N., Goulding, F.J., Garfield, T.R., Sickafoose, D.K., Rossen, C., Jennette, D.C., Beaubouef, R.T., Others, 2002. The

physical stratigraphy of deep-water strata: A hierarchical approach to the analysis of genetically-related stratigraphic elements for improved reservoir prediction. AAPG Annual Meeting, A167-A168.

Srodo´n, J., 1999. Use of clay minerals in constructing geological processes: recent advances and some perspectives. Clay Miner 34, 27–37.

Sterling, 2010. Prospectivity review of the Ntem Block (PH-78) in the Douala/Kribi-Campo basin. Unpublished report.

Stevenson, C.J., Jackson, C.A.-L., Hodgson, D.M., Hubbard, S.M. & Eggenhuisen, J.T., 2015. Deep-water sediment bypass. Journal of Sedimentary Research 85(9): 1058-1081.

Stone, D., 1994. Designing Seismic Surveys in Two and Three Dimensions. Society of Exploration Geophysicists, 244p.

Oklahoma. Stow, D.A.V. & Mayall, M., 2000. Deep-water sedimentary systems: New models for the21st century. Marine and Petroleum Geology, 17(2), 125-135.

Su, M., Hsiung, K.H., Zhang, C.M., Xie, X.N., Yu, H.S., Wang, Z.F., 2015. The linkage between longitudinal sediment routing systems and basin types in the northern South China Sea in perspective of source-to-sink. J. Asian Earth Sci. 111, 1–13.

Sullivan, M.D., Jensen, G.N., Goulding, F.J., Jennette, D.C., Foreman, J.L., Stern, D., 2000. Architectural analysis of deep-water outcrops: Implications for exploration and production of the Diana Sub-basin, western Gulf of Mexico. In: Weimer, P., Slatt, R.M., Coleman, J., Rosen, N.C., Nelson, H., Bouma, A.H., Styzen, M.J., Lawrence, D.T. (Eds.), Deep-Water Reservoirs of The World. Gulf Coast Section SEPM 20th Bob F. Perkins Research Conference, 1010-1032p.

Sun, Z.X., Sun, Z.L., Lu, H.J., Yin, X.J., 2010. Characteristics of carbonate cements in sandstone reservoirs: a case from yanchang formation, middle and Southern Ordos Basin, China. Petrol Explor Dev 37, 543–551. https://doi.org/10.1016/S1876-3804(10)60054-7.

Sylvester, Z., Pirmez, C. and Cantelli, A., 2011. A model of submarine channel-levee evolution based on channel trajectories: Implications for stratigraphic architecture. Marine and Petroleum Geology 28, 716-727. https://doi.org/10.1016/j.marpetgeo.2010.05.012.

Sylvester, Z., Covault, J.A., 2016. Development of cutoff-related knickpoints during early evolution of submarine channels. Geology 44, 835–838.

Sylvester, Z., Pirmez, C., Cantelli, A., 2011. A model of submarine channel-levee evolution based on channel trajectories: implications for stratigraphic architecture. Mar. Pet. Geol. 28, 716–727.

Talling, P.J., Masson, D.G., Sumner, E.J. and Malgesini, G., 2012. Subaqueous sediment density flows: depositional processes and deposit types. Sedimentology 59, 1937–2003. https://doi.org/10.1111/j.1365-3091.2012.01353.x.

Tamfu, S.F., Batupe, M., Pauken, R.J., Boatwright, D.C., 1995. Geological setting, stratigraphy and hydrocarbon habitat of the Douala Basin, Cameroon. Am Assoc Petrol Geol Bull. 79, 13–95.

Taner, M.T., 2001. Seismic attributes. In: CSEG Recorder 26, 48–56.

Taylor, T.R., Stancliffe, R., Macaulay, C.I., Hathon, L.A., 2004. High temperature quartz cementation and the timing of hydrocarbon accumulation in the Jurassic Norphlet sandstone, offshore Gulf of Mexico, U.S.A. In: Cubit JM, England WA, Larter S (eds) Understanding petroleum reservoirs: towards an integrated reservoir engineering and geochemical approach, Geological Society (London) Special Publication 237, 257–278.

Tek, D.E., Mcarthur, A.D., Poyatos-Moré, M., Colombera, L., Patacci, M., craven, B., Mccaffrey, W.D., 2021. Relating seafloor geomorphology to subsurface architecture: How mass transport deposits and knickpoint-zones build the stratigraphy of the deep-water Hikurangi Channel. Sedimentology, 12890. doi:10.1111/SED.12890.

Terlaky, V., Rocheleau, J. and Arnott, R.W.C. (2016). Stratal composition and stratigraphic organization of stratal elements in an ancient deep-marine basin-floor succession, Neoproterozoic Windermere Supergroup, British Columbia. Sedimentary Geology 63, 136–175. https://doi.org/10.1111/sed.12222.

Tiyan, Y., Ayers, W.B., 2010. Barnett Shale (Mississippian), Fort Worth Basin, Texas: regional variations in gas and oil production and reservoir properties CSUG/SPE 137766. In: Canadian unconventional resources and international petroleum conference Calgary, Alberta, Canada, 19–21 October. https://doi.org/https://doi. org/10.2118/137766-MS.

Tripsanas, E.K., Piper, D.J.W., Campbell, D.C., 2008. Evolution and depositional structure of earthquake-induced mass movements and gravity flows: Southwest Orphan Basin, Labrador Sea. Mar. Pet. Geol. 25, 645–662. https://doi.org/10.1016/j.marpetgeo.2007.08.002.

Turner, J.P., 1995. Gravity-driven structures and rift basin evolution: Rio Muni Basin, offshore West Africa. Am. Assoc. Petr. Geol. Bull. 79 (8), 1138–1158.

Turner, J.P., 1999. Detachment faulting and petroleum prospectivity in the Rio Muni Basin, Equatorial Guinea, West Africa. *In:* Cameron, N. R., Bate, R. H. & Clure, V. S. (eds) The Oil and Gas Habitats of the South Atlantic. Geological Society, London, Special Publication 153, 303-320.

Twichell, D., Nelson, C.H., Kenyon, N. & Schwab, W., 2009. The influence of external processes on the Holocene evolution of the Mississippi Fan. External controls on deepwater depositional systems. Society for Sedimentary Geology Special Publication, 92, 145–157.

Vail, P.R., Mitchum, R.M., Thompson, S., 1977. Seismic stratigraphy and global changes of sea level, Part 4, Global cycles of relative changes of sea level. In: Payton, C.E. (Ed.), Seismic Stratigraphy—Applications to Hydrocarbon Exploration. AAPG Memoir. 26, 83–97.

Van Weering, T.C.E., Van Iperen, J., 1984. Fine-grained sediments of the Zaire deepsea fan, southern Atlantic Ocean. Geol. Soc. Lond. Spec. Publ. 15, 95-113. http://dx.doi.org/10.1144/GSL.SP.1984.015.01.06.

Vermeer, G.J., 2000. 3-D Seismic Survey Design. Society of Exploration Geophysicists, 18p.

Walker, R.G., 1992. Turbidites and submarine fans. In: Walker, R.G., James, N.P. (Eds.), Facies Models - Response to Sea Level Change. Geological Association of Canada, 239–264p.

Wang, F.R., He, S., He, Z.L., 2009. Carbonate cements features and its genetic significance of sandstones in Yongjin Area of Junggar Basin. Acta Petrol et Mineralogica 28, 169–178.

Weaver, P.P.E., Wynn, R.B., Kenyon, N.H., Evans, J., 2000. Continental margin sedimentation, with special reference to the north-east Atlantic margin. Sedimentology 47, 239–256.

Weber, M.E., Wiedicke, M.H., Kudrass, H.R., Hübscher, C., Erlenkeuser, H., 1997. Active growth of the Bengal Fan during sea-level rise and highstand. Geology 25, 315–318.

Weimer, P., Slatt, R.M., Coleman, J., Rosen, N.C., Nelson, H., Bouma, A.H., Styzen, M.J., Lawrence, D.T. (Eds.), 2000. Deep-water Reservoirs of the World. Gulf Coast Section SEPM 20th Bob F. Perkins Research Conference, 473–477.

Weimer, P., Davis, T., 1996. Applications of 3-D Seismic Data to Exploration and Production. Society of Exploration Geophysicists, 270p.

Wilson, P.G., Turner, J.P., Westbrook, G.K., 2003. Structural architecture of the ocean-continent boundary at a transform margin through deep-imaging seismic interpretation and gravity modelling: Equatorial Guinea, West Africa. Tectonophysics 374, 19-40.

Wonham, J.P., Jayr, S., Mougamba, R., Chuilon, P., 2000. 3D sedimentary evolution of a canyon fill (Lower Miocene-age) from the Mandorove Formation, offshore Gabon. Marine and Petroleum Geology 17, 175–197.

Wornardt, W.W.Jr., Jory, P., Batupe, M., 1999. Seismic Sequence Stratigraphic analysis of The Douala Basin, Cameroon. Offshore Technology Conference, 10p.

Wu, W., Li, Q., Yu, J., et al., 2018. The Central Canyon depositional patterns and filling process in east of Lingshui Depression, Qiongdongnan Basin, northern South China Sea. Geol. J. 53, 3064–3081.

Wynn, R.B., Cronin, B.T., Peakall, J., 2007. Sinuous deep-water channels: genesis, geometry and architecture. Mar. Petrol. Geol. 24 (6–9), 341–387. doi.org/10.1016/j.marpetgeo.2007.06.001.

Yamassaki, H. S., Vesely, F. F., 2022. Timelapse of the geomorphologic and stratigraphic evolution of a Late Cretaceous deep-sea fan, northern Santos basin, Brazil. Marine and Petroleum Geology 136, 105475.

Yilmaz, O., 2001. Seismic data analysis: processing, inversion, and interpretation of seismic data. Society of Exploration Geophysicists, 1028 p. https://doi.org/10.1190/1.9781560801580.

Yugye, J.A., Chavom, B.M., Chima, K.I., N'nanga, A., Angoua Biouele, S.E., Nkoa Nkoa, P.E., Ngos III, S., 2022. Seismic-stratigraphic analysis and depositional architecture of the Cenozoic Kribi-Campo sub-basin offshore deposits (Cameroon): Seismic attributes approach and implication for the hydrocarbon prospectivity. Journal of African Earth Sciences 194, 104621. https://doi.org/10.1016/j.jafrearsci.2022.104621.

Yugye, J.A., Ngos III, S., Angoua Biouele, S.E., Nkoa Nkoa, P.E., 2021. Seismic stratigraphic interpretation and modeling of offshore synrift and postrift Cretaceous sequences in the Kribi-Campo sub-basin, southern Cameroon. AAPG (Am. Assoc. Pet. Geol.) Bull. 105 (11), 1–20. https://doi.org/10.1306/06092118040.

Zeng, H.L., Ambrose, W.A., 2001. Seismic sedimentology and regional depositional systems in Miocene Norte, lake Maracibo, Venezuela. Lead. Edge 20 (11), 1260–1269.

Zeng, H.L., Backus, M.M., Barrow, K.T., Tyler, N., 1998a. Stratal slicing, part I: realistic 3-D seismic model. Geophysics 63 (2), 502–513.

Zhang, J., Wu, S., Hu, G., Fan, T.-e., Yu, B., Lin, P., Jiang, S., 2018. Sea-level control on the submarine fan architecture in a deep-water sequence of the Niger Delta Basin. Marine and Petroleum Geology. doi: 10.1016/j.marpetgeo.2018.04.002.

Zhang, J., Wu, S., Wang, X., Lin, Y., Fan, H., Jiang, L., Wan, Q., Yin, H., Lu, Y., 2015. Reservoir quality variations within a sinuous deep-water channel system in the Niger delta basin, offshore West Africa. Mar. Petrol. Geol. 63, 166–188.

Zhang, Y.W., Zeng, J.H., Gao, X., Zhou, S.Y., 2009. Distribution characteristics and main controlling factors of carbonate cements in the paleogene reservoirs in dongying depression. J Jilin Univ (Earth Sci Ed) 39, 16–22.

Zhang, M.Q., Huang, S.J., Wu, Z.X., Hu, Z.W., 2007. Carbonate cements and their formation mechanism in palaeogene sandstones of Lishui Sag, East China Sea Basin. J Chengdu Univ Technol (Sci Technol Ed), 34, 259–266.

Zhao, X.M., Qi, K., Liu, L., Xie, T., Li, M.H., Hu, G.Y., 2018. Quantitative characterization and controlling factor analysis of the morphology of bukuma-minor channel on southern Niger Delta slope. Interpretation 6, 57–69. doi.org/10.1190/INT-2017-0147.1.

Zhu, P.Y., You, L., Yuan, Q.T., Zhong, J., Liu, A.Q., 2018. Mechanism and distribution of calcareous interbeds in songtao uplift and its periphery of Qiongdongnan Basin. Open J Marine Sci 8, 370–385.

Published papers

Marine and Petroleum Geology 170 (2024) 107051

Contents lists available at ScienceDirect

Marine and Petroleum Geology

journal homepage: www.elsevier.com/locate/marpetgeo

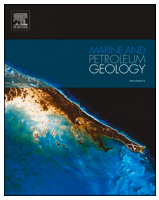

Petrophysical characterization of the Late-Cretaceous Logbaba Formation in the Kribi/Campo sub-basin, Cameroon: Implication on deep-water hydrocarbon exploration

Boris G. B. Secke [a,b,c,*], Ovie Emmanuel Eruteya [a], Yakufu Niyazi [d], Mbida Yem [b], Joseph Quentin Yene Atangana [b], Pierre Eric Nkoa Nkoa [e], Elias Samankassou [a]

[a] Department of Earth Sciences, University of Geneva, Geneva, 1205, Switzerland
[b] Department of Earth Sciences, University of Yaoundé I, Faculty of Science, P.O. Box: 812, Yaoundé, Cameroon
[c] Centre for Geological and Mining Research, P.O. Box: 333, Garoua, Cameroon
[d] Minderoo-UWA Deep-Sea Research Centre, School of Biological Sciences and UWA Oceans Institute, The University of Western Australia, Perth, 6009, Australia
[e] National Hydrocarbon Corporation (NHC), P.O. Box: 955, Yaoundé, Cameroon

ARTICLE INFO

Keywords:
Petrophysical analysis
Borehole data
Reservoir quality
Petrophysical parameters
Kribi-Campo sub-basin
Logbaba Formation

ABSTRACT

Deep-water hydrocarbon exploration in the Kribi/Campo sub-basin offshore Cameroon is targeting the promising Campanian-Maastrichtian turbidite reservoirs. However, a detailed understanding of the petrophysical properties of these Upper Cretaceous reservoirs is not well documented. In this study, well logs from two boreholes W1 and W2 located in the southern part of the sub-basin provide a unique opportunity to assess the reservoir quality of the Upper Cretaceous Logbaba Formation. Four potential reservoir intervals with thickness ranging between 27 and 105.7 m were delineated in W1, compared with two intervals in W2 with thickness ranging between 72.2 and 93.6 m. Lithological analysis of these reservoir intervals indicates a heterogeneous reservoir matrix consisting of sand, limestone, and dolomite. These reservoir intervals are interpreted as turbidite sand deposits with a clay content ranging from 6.3 to 19.8%, porosity ranging from 15.5 to 21.3%, permeability ranging between 5.65 and 75.09 mD and a water saturation of 34.5–74.2%. Fluid free index, reservoir quality index, and flow zone indicator are insignificant and suggest reservoirs with poor transmissibility. These analyses reflects good petrophysical characteristics for the sandstones of Logbaba Formation. However, both wells were water-bearing with non-mobile hydrocarbon residuals and did not contain commercial quantities of hydrocarbons. There is no evidence of hydrocarbon migration in either reservoir, suggesting that the source rock and the hydrocarbon migration pathways are the main risk factors and reason for the failure of the wells. The findings from this study extend the understanding of the reservoir characteristics of the Upper Cretaceous Logbaba Formation, which will further enhance hydrocarbon prospectivity offshore Cameroon. Since these reservoirs are water-laden, they may serve as potential offshore saline aquifers for geological storage of CO_2 offshore Cameroon.

1. Introduction

The Kribi-Campo sub-basin is located along the West African continental margin that extends from the Walvis Ridge near the Angola-Namibia border to the edge of the Niger Delta in Cameroon (Rabinowitz and Labrecque, 1979; Benkhelil et al., 2002; Le, 2012; Iboum Kissaaka et al., 2016). Most of the basins in this region contain significant hydrocarbon discoveries, making this part of the world one of the richest provinces in terms of oil and gas accumulation (Huang, 2018). While most of the basins along the West African margin are well characterized by both borehole drillings and seismic reflection surveys, the development and quality of reservoirs in the Kribi-Campo sub-basin remains poorly resolved (Ntamak-Nida et al., 2010; Le, 2012; Loule et al., 2018).

Previous works in the Kribi-Campo sub-basin, such as Le et al. (2014), 2021; Loule et al. (2018); Mienlam Essi et al., 2021; Yugye et al. (2021), 2022; Secke Bekonga Gouott et al., 2022 and others have focused on unravelling the tectonostratigraphic evolution of the Kribi-Campo sub-basin. The emphasis has been on submarine channel/fan development and distribution, with a limited assessment of its

* Corresponding author. Department of Earth Sciences, University of Geneva, Geneva, 1205, Switzerland.
E-mail addresses: boris.secke@etu.unige.ch, bsecke@yahoo.fr (B. G. B. Secke).

https://doi.org/10.1016/j.marpetgeo.2024.107051
Received 30 December 2023; Received in revised form 23 July 2024; Accepted 9 August 2024
Available online 23 August 2024

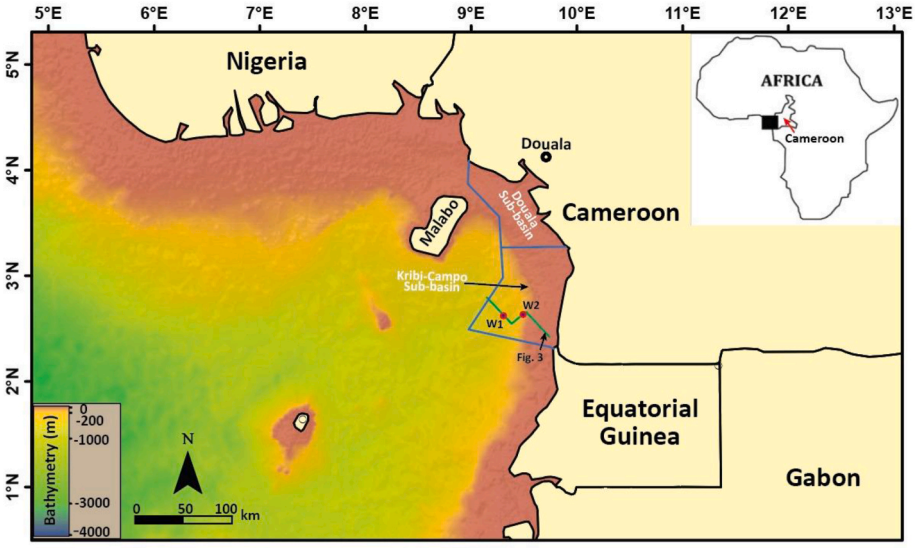

Fig. 1. Superimposed relief and bathymetric map of Cameroon, showing the location of the study area. Insert map on the right-hand corner of the map shows the location of Cameroon in the Gulf of Guinea. The regional 2D seismic profile, which we studied is outlined in the green box, while the red circles with black outlines labelled W1 and W2, represent well locations (Loule et al., 2018; Secke Bekonga Gouott et al., 2022).

hydrocarbon potential. Only very few works have analysed reservoir characterization to better understand the reservoirs of the formations in the Kribi-Campo sub-basin (Simon Petroleum and Technology, 1995; ECL, 2001; Ndonwie Mahbou, 2007). As a result, the petrophysical properties of deep-water reservoirs, especially those of the upper Cretaceous unit, remain unresolved in this part of the sub-basin. This is probably because there were few borehole data in this area and access to them was difficult before the present study.

A suite of conventional well logs, now available from two deep-water boreholes (W1 and W2) targeting the Kribi-Campo sub-basin, provides an excellent opportunity to further characterize potential reservoirs within the Late Cretaceous basin fill. Many authors have successfully employed well-log data together with the resultant petrophysical parameters to identify and characterize the formations' reservoirs of many petroleum-bearing basins worldwide. Prominent among these are the works of Kim et al. (2016) in the Horn River Basin, Canada, Qadri et al. (2020) in the Taranaki Basin, New Zealand, Sarhan et al. (2021) in the Rabeh East oil field, Southern Gulf of Suez Basin, Egypt, Opuwari et al. (2022) in the Bredasdorp Basin South Africa (Magoba and Opuwari, 2020). Similar studies along the Cameroonian margin using a qualitative and quantitative interpretation of well logs successfully evaluated the reservoirs of the N'kapa Formation in the Douala sub-basin (Chongwain et al., 2018, 2019).

This study focuses on the Campanian-Maastrichtian Logbaba Formation of interest in deep-water exploration for the Kribi-Campo sub-basin (Simon Petroleum and Technology, 1995; Secke Bekonga Gouott et al., 2022). The Logbaba Formation consists of fossiliferous sandstones and mudstones with a thickness that can exceed 2000 m (Nguene et al., 1992; Tamfu et al., 1995; Simon Petroleum and Technology, 1995; ECL, 2001; SNH/UD et al., 2005). The objective of this study is to use well log data of Wells W1 and W2 to determine the petrophysical properties of the identified reservoirs. The goal is to evaluate the reservoir potential of the formation, ultimately promoting hydrocarbon exploration in the deep-water Kribi-Campo sub-basin, an area with limited drilling and low success rates. Additionally, the study seeks to provide novel insights into the petrophysical characteristics of the deep-water region in the Kribi-Campo sub-basin offshore Cameroon, using wireline logs.

2. Geological setting

The Douala/Kribi-Campo Basin, located offshore Cameroon, is situated in the northernmost portion of a set-echelon chain of West African Basins that developed from the Walvis Ridge in the south and the volcanic line of Cameroon to the north (Brownfield and Charpentier, 2006; Ntamak-Nida et al., 2010). West African Basins formed as a result of right lateral shear conditions (Coward et al., 1999) during the opening of the South Atlantic (about 115 Ma) in the Early Cretaceous (Wilson et al., 2003). From south to north, the main basins are named Mocamedes, Kwansa, Bas-Congo, Gabon, Rio-Muni and Douala/Kribi-Campo (Rabinowitz and Labrecque, 1979; Benkhelil et al., 2002). Most of these basins contain significant accumulations of oil and gas. The Kribi-Campo sub-basin encompasses an area of 6600 km^2 and is the southernmost depocentre of Douala/Kribi-Campo Basin and is itself bordered to the south by the Rio Muni Basin through the bounding oceanic transfer 'Bata Fracture Zone' (Sterling Cameroon Limited, 2010). The study area is located entirely offshore in the Kribi-Campo sub-basin, around 40 km off the coast of Cameroon in water depths ranging from 600 to 2000 m (Fig. 1).

Characterised by a deep-water post-rift sequence, the Kribi-Campo sub-basin contains a Mesozoic-Cenozoic sedimentary sequence almost 7500 m thick (Lawrence et al., 2002; Ntamak-Nida et al., 2010; Sterling Cameroon Limited, 2010). The infilling sequence consists of nine Formations, namely the Lower Mundeck (Barremian-Aptian), Upper Mundeck (Albian-Turonian), Logbadjeck (Turonian-Campanian), Logbaba (Campanian-Maastrichtian), N'Kapa (Palaeocene-Eocene), Souellaba (Oligocene to Lower Miocene), Kribi (Upper Miocene), Matanda and Wouri (Pliocene to recent) (Fig. 2). The Logbaba Formation, which is the interval of interest in this study, is dominated by argillites and its top is characterised by the Upper Cretaceous unconformity (ECL, 2001; SNH/UD et al., 2005). This sequence composing the Formation was deposited during a high sea level (Iboum Kissaaka et al., 2016). The sediments of the Logbaba Formation are marine, were deposited in deep water and were then rapidly buried, which is peculiar to the development of West African Basins where deep-water claystones were deposited. This formation is made up of fossiliferous sandstones and claystone (Regnoult, 1986; ECL, 2001; SNH/UD et al., 2005). The Logbaba Formation is recorded in most of the basin except in the highest part of the Kribi-Campo High (Pauken, 1992). Overall the Logbaba Formation has a westward thickening pattern. At its thickest, this formation is probably over 2000 m (Nguene et al., 1992; Simon Petroleum and Technology, 1995). The reservoirs developed in the turbiditic sandstones sourced via palaeo-Wouri, Sanaga and Nyong rivers (Simon Petroleum and

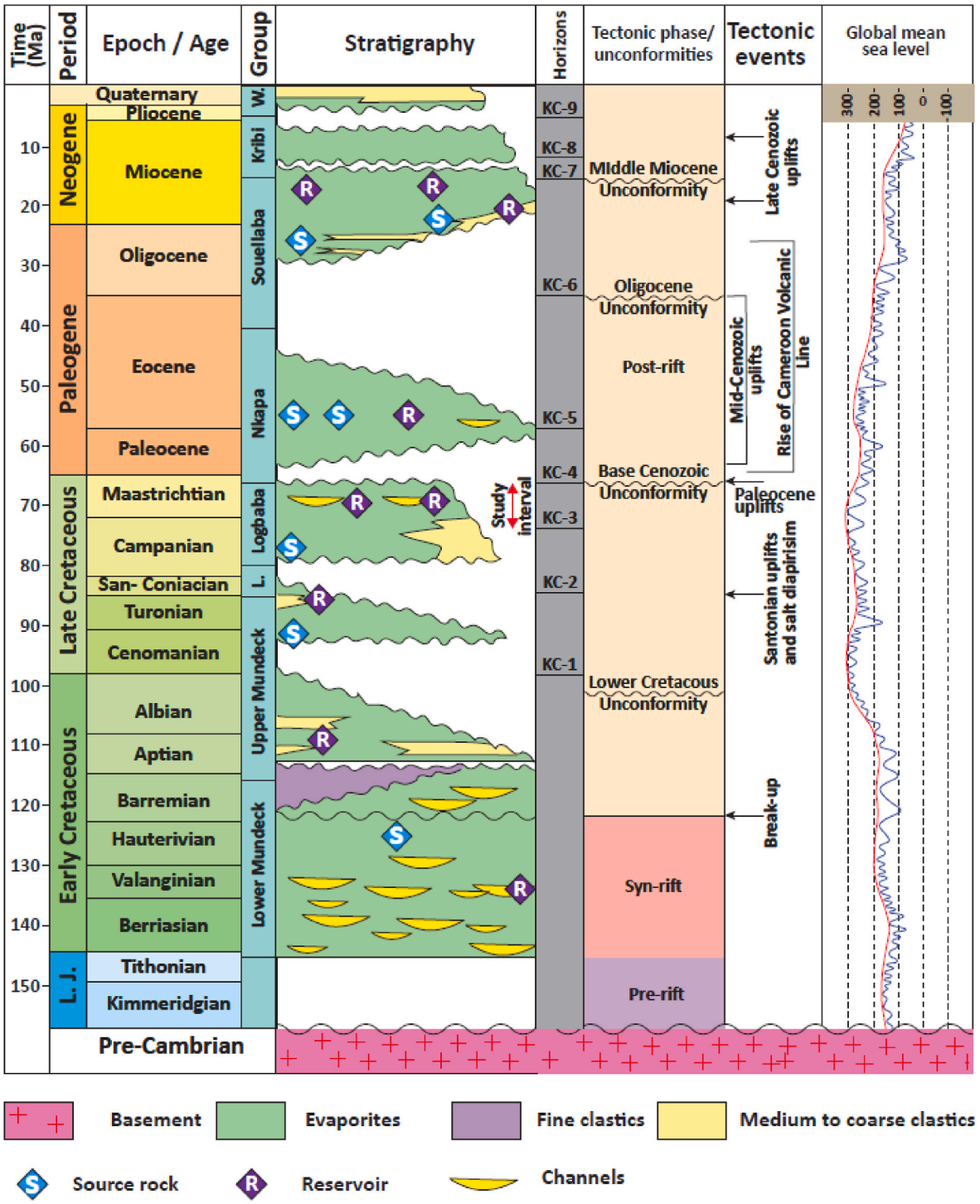

Fig. 2. Stratigraphic column of the Kribi-Campo Sub-basin showing the tectonic-sedimentary phases and global mean sea level (Secke Bekonga Gouott et al., 2022).

Technology, 1995). The formation is characterized mostly by stratigraphic trap (syn-sedimentary) such as channel/fan lobe in the Upper Cretaceous unit (Fig. 3) (Loule et al., 2018; Secke Bekonga Gouott et al., 2022). According to Simon Petroleum and Technology (1995), poro-perm data for the Logbaba Formation are restricted, with some log analysis data in the Kribi-Campo sub-basin. Porosities range from about 6 to 23%, with maximum permeabilities of 50 mD.

3. Data and methods

3.1. Data

Two wells W1 and W2 from the southern part of the Kribi/Campo sub-basin were analysed to assess the reservoir quality and hydrocarbon potential of the clastic reservoir rocks of the Logbaba Formation (Figs. 1 and 3). The well data was made available by the National Hydrocarbon Corporation (NHC), Republic of Cameroon. The available well logs from W1 and W2 consist of conventional well log data including Gamma ray (GR), shallow, medium and deep resistivity logs (P16H, P28H and P40H

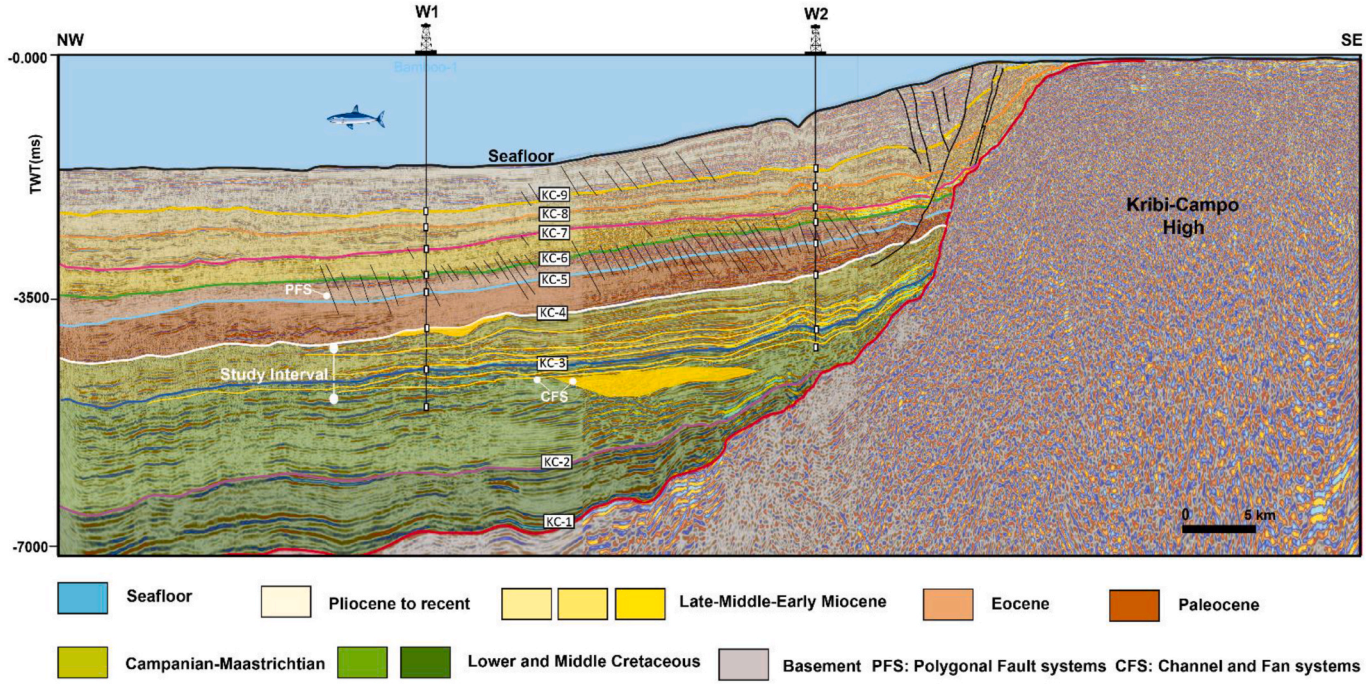

Fig. 3. Regional 2D seismic profile showing the tectonostratigraphic framework of the study area.

Table 1
List of available well log data of the Logbaba Formation in the studied wells from the Kribi-Campo sub-Basin.

Well name	Top (m)	Bottom (m)	thickness (m)	Available well logs
Well-W1	3947	4736	789	GR-DCAV-P16H-P28H-P40H-DT-RHOB-TNPH-DRHO
Well-W2	3215	4051	836	GR-ARC-DCAV-P16H-P28H-P40H-DTCO-RHOB-TNPH-DRHO-HFK-HTHO

respectively), density (RHOB), neutron (NPHI) and sonic (DT) (Table 1). The two wells were drilled between 2013 and 2014 with a total depth of 4090 m and 4747 m respectively for W2 and W1 wells. The distance between the two wells is 22 km and these wells were selected because they penetrated the Late Cretaceous reservoir of the Logbaba Formation.

3.2. Petrophysical analysis

The well log data were interpreted qualitatively and quantitatively to derive the petrophysical properties of the reservoir intervals. The interpretation of the well log data has primarily used the Senergy LR company Interactive Petrophysics (IP) software. This software comprises distinct modules to ensure the dependable interpretation of all Petrophysical data and lithological features, including environmental corrections and statistical analyses using several equations, empirical relationships and charts (Schlumberger, 1989; Hakimi et al., 2017; Chongwain et al., 2018, 2019; Hu et al., 2020; Radwan et al., 2021; Elmahdy et al., 2023).

3.2.1. Lithological and reservoir identification

The lithological and mineralogical components of the clastic rocks of the Logbaba Formation were identified using Schlumberger charts such as neutron-density, neutron-gamma, neutron-sonic and M-N cross plots (Schlumberger, 1989). The potassium vs thorium cross-plot allows us to identify the clay mineralogy in the reservoir formation (Tiyan and Ayers, 2010). The impact of these identified clay minerals on the reservoir quality was also analysed.

The well log analysis was used to delineate reservoir sands characterized by cylindrical or blocky gamma-ray shapes, which are utilized to understand the depositional environment of reservoir sands in this study. Following the methodology adopted by Shier (2004), the gamma-ray logs of the two wells were standardized. Subsequently, the gamma-ray logs were used to identify the reservoir units and establish a clay (shale) cut-off value of 60 API for W1 and W2. Also, this was used to establish the sand baseline and the reservoir units which were discriminated based on the lower gamma ray readings (Chongwain et al., 2018, 2019). Also, reservoirs were identified using gamma ray and resistivity log signatures. Intervals with high resistivity are hydrocarbon while low resistivity areas are aquifer intervals. In this study, zones with resistivity values greater than 4 Ω m are identified as hydrocarbons (Chongwain et al., 2018, 2019). The resistivity (P40H), neutron (TNPH) and bulk density (RHOB) logs were used together to discriminate the types of hydrocarbons (oil or gas) present in the reservoirs.

In addition, the well logs were analysed to determine the reservoir thickness, net-to-gross (NTG), volume of shale (V_{sh}), effective porosity ($Ø_{eff}$) and hydrocarbon saturation (1- S_w). These parameters were also used to assess the hydrocarbon potential of the study area.

3.2.2. Fraction shale volume

The shale content (V_{Sh}) in the reservoirs was calculated from the gamma ray logs. The first step is to determine the gamma index using (Eq. (1)).

$$I_{GR} = \frac{GRlog - GRmin}{GRmax - GRmin} \quad (1)$$

where I_{GR} = gamma-ray index, GR_{log} = gamma ray reading of formation, GR_{min} = minimum gamma ray (clean carbonate), GR_{max} = maximum gamma ray (shale). After obtaining the gamma index, the volume of shale was then calculated according to formula (2). Given that the Logbaba Formation is of Cretaceous age (Nguene et al., 1992; Simon Petroleum and Technology, 1995; Lawrence et al., 2002; Brownfield and Charpentier, 2006), the estimation of shale volume utilized Eqs. (1) and (2) from Larionov's (1969) Cretaceous model (Asquith and Krygowski, 2004).

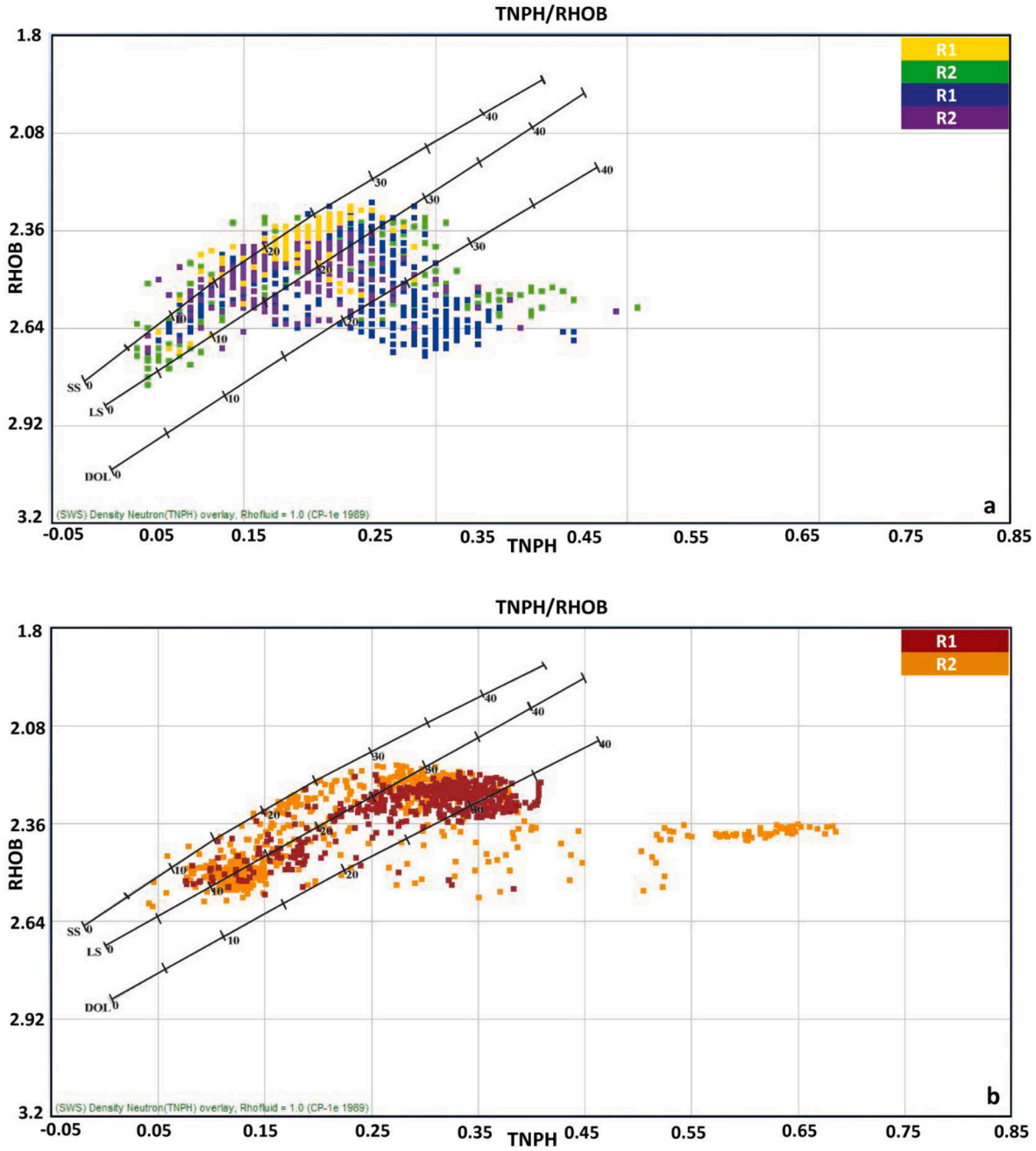

Fig. 4. a) Density-neutron for Well W1 reservoirs depicting points scattered across the various lithological field indicating the heterogeneous character of the reservoirs. b) Density-neutron for Well W2 reservoirs depicting points scattered across the various lithological field indicating the heterogeneous character of the reservoirs.

$$V_{sh} = 0.33\left(2^{2\times I_{GR}} - 1\right) \quad (2)$$

Determining the shale volume (Vsh) holds significance within petrophysical assessment due to its impact on reservoir porosity and permeability (Balaky et al., 2023).

3.2.3. Porosity estimation

The porosity estimation is determined by a combination of density and neutron logs using (Eq. (3)) below (Chongwain et al., 2018).

$$\varnothing = \frac{(\rho_{ma} - \rho_b - V_{cl} \times (\rho_{ma} - \rho_{cl}))}{\rho_{ma} - \rho_f \times S_{xo} - \rho_{HyAp} \times (1 - S_{xo})} \quad (3)$$

where ρ_{ma} is the matrix density, ρ_b is the bulk density, ρ_{cl} is the density of wet clay, ρ_f is the mud filtrate density, ρ_{HyAp} is the apparent hydrocarbon density, V_{cl} is the volume of wet clay, and S_{xo} is the water saturation of the flushed zone.

3.2.4. Water saturation and hydrocarbon saturation estimation

The modified Simandoux equation was used to estimate the water saturation (Sw) values, using (Eq. (4)) below (Bardon and Pied, 1969):

$$\frac{1}{R_t} = \frac{\varnothing^m \times S_w^n}{a \times R_w \times (1 - V_{sh})} + \frac{V_{sh} \times S_w}{R_{sh}} \quad (4)$$

where S_w is the effective water saturation, R_w is the water resistivity, R_t is the true formation resistivity, a is the tortuosity factor, m is the cementation factor, $\varnothing$ is the formation porosity, V_{sh} is the volume of wet clay, and R_{sh} is the clay resistivity. The hydrocarbon saturation for the

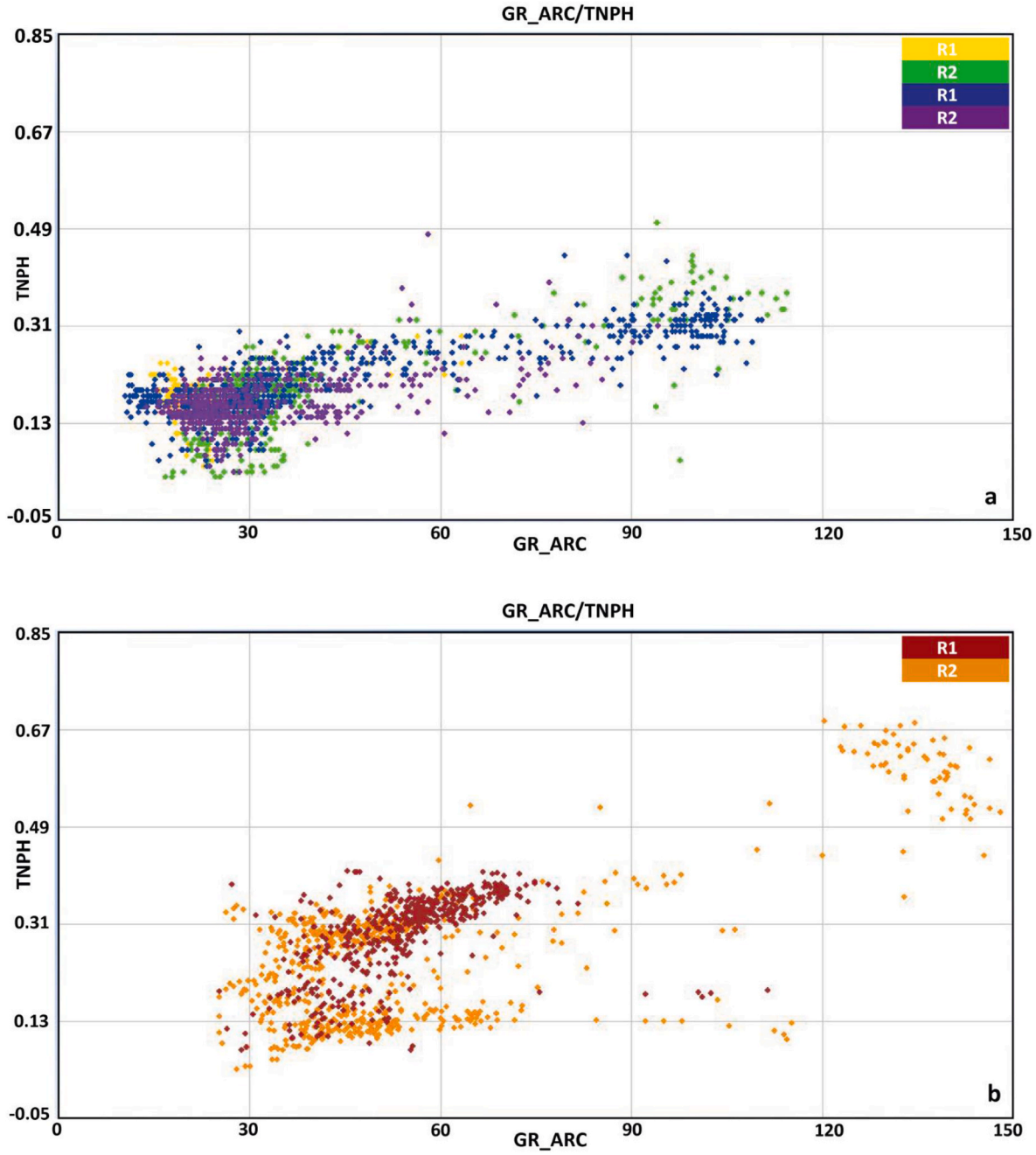

Fig. 5. a) Neutron vs. gamma-ray cross plot displaying the lithological composition of Logbaba Formation reservoirs within the studied well W1. b) Neutron vs. gamma-ray cross plot displaying the lithological composition of Logbaba Formation reservoirs within the studied well W2.

reservoir zone was then calculated using Eq. (5) below. The hydrocarbon saturation (Sh) was obtained by subtracting the value obtained for the 100% water saturation (Rider, 1996):

$$S_h = 1 - S_w \text{ or } S_h = 100 - S_w(\%) \quad (5)$$

where S_h = Hydrocarbon Saturation; S_w = Water Saturation.

The reservoir net-pay values were evaluated using 40% shale volume (V_{sh}), 12% effective porosity ($\varnothing_{eff}$), and 65% water saturation (S_w) cutoff values (Sterling Cameroon Limited, 2010; Chongwain et al., 2018). These values are generally chosen based on published literature, detailed petrophysical analysis, and parameters used for similar reservoirs in the same area with comparable petrophysical properties (Jumat et al., 2018; Radwan et al., 2021).

Finally, using the comparison table provided by Fertl and Vercellino (1978), the bulk water volume (BVW), which is a product of porosity (∅) and water saturation (S_w) (Eq. (6)), was utilized to estimate the grain size of the reservoir formation. The bulk volume of water (BVW) is further used for differentiating between reservoir/non-reservoir intervals to estimate the net pay thickness (Buckles, 1965; Dewan, 1983; Asquith, 1985).

$$BVW = S_w \times \varnothing \quad (6)$$

3.2.5. *Permeability estimation*

Since core data was not available in this study, the permeability equation of Morris and Biggs (1967) was used to calculate the permeability from well log data. This equation is as follows:

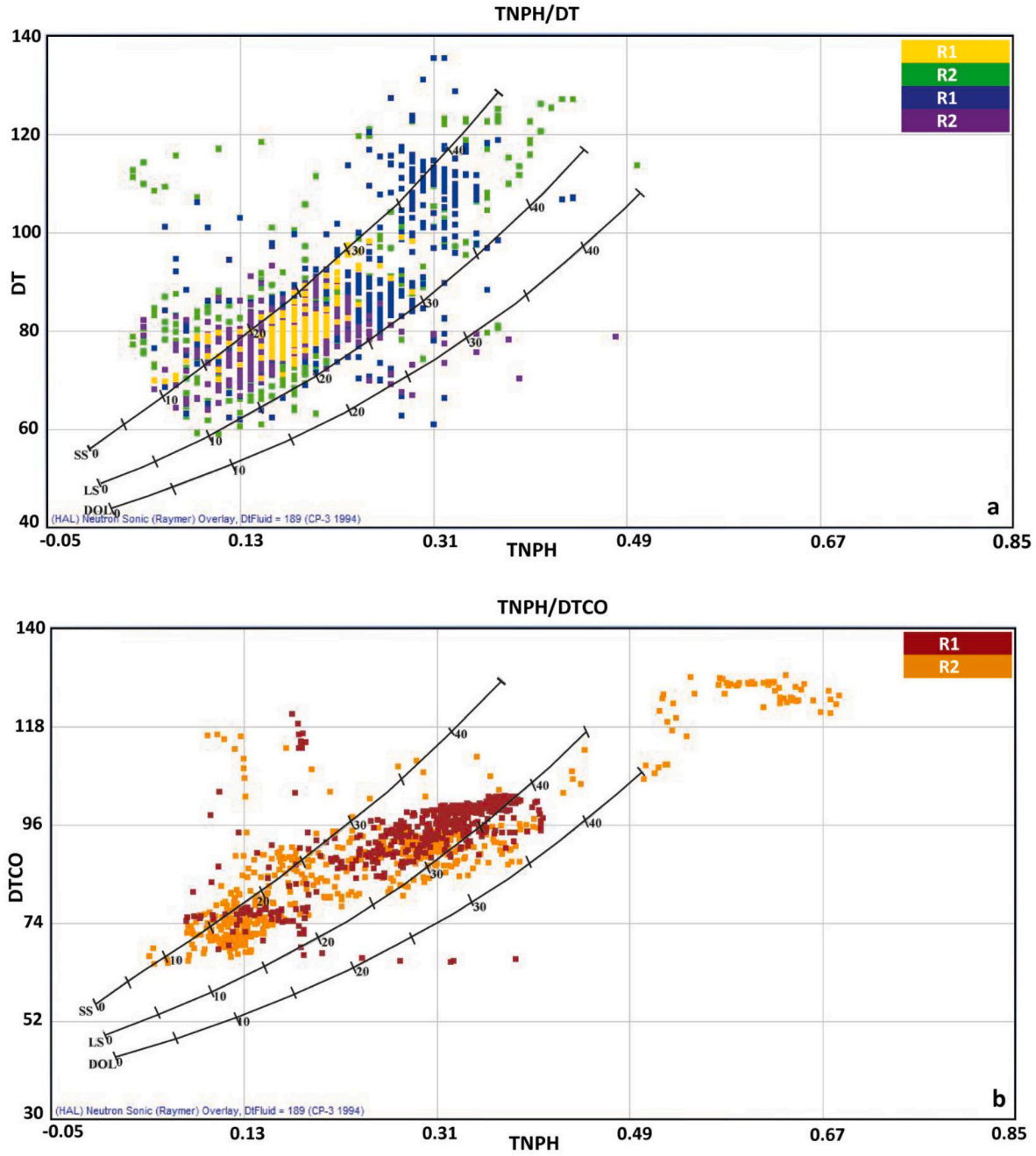

Fig. 6. a) Neutron vs. sonic cross plot displaying the lithological composition of Logbaba Formation reservoirs within the studied well W1. b) Neutron vs. sonic cross plot displaying the lithological composition of Logbaba Formation reservoirs within the studied well W2.

$$K = a\frac{Phi^b}{Swi^c} \tag{7}$$

where: K = permeability (mD); Phi = effective porosity; Swi = irreducible water saturation; a = 62,500; b = 6; and c = 2.

3.2.6. Evaluation of flow hydraulic units

Poro-perm estimation of two well logs were applied for flow unit determination using the flow zone indicator (FZI) method. FZI evaluates texture, shale content, grain size, and tortuosity (Tiab and Donaldson, 2012). It is also influenced by the reservoir quality index (RQI) which is a parameter that assesses pore integrity and grain distribution (Amaefule et al., 1993). Flow units are defined according to the expressions of Tiab and Donaldson (2012) [Eqs. (8)–(10)].

$$RQI = 0.0314\sqrt{K/\varnothing} \tag{8}$$

$$FZI = \frac{RQI}{PMR} \tag{9}$$

$$PMR = \frac{\varnothing}{1-\varnothing} \tag{10}$$

where the reservoir quality index is in micrometer (μm), K is permeability in milli Darcy (mD), and the porosity ($\varnothing$) is fractional. PMR is Porosity to Matrix Ratio.

According to Tiab and Donaldson (2012), fluid free index (FFI) defines the movable fluid in the reservoir unit. In this study, the FFI equation was modified for reservoir sands using equation (11) from

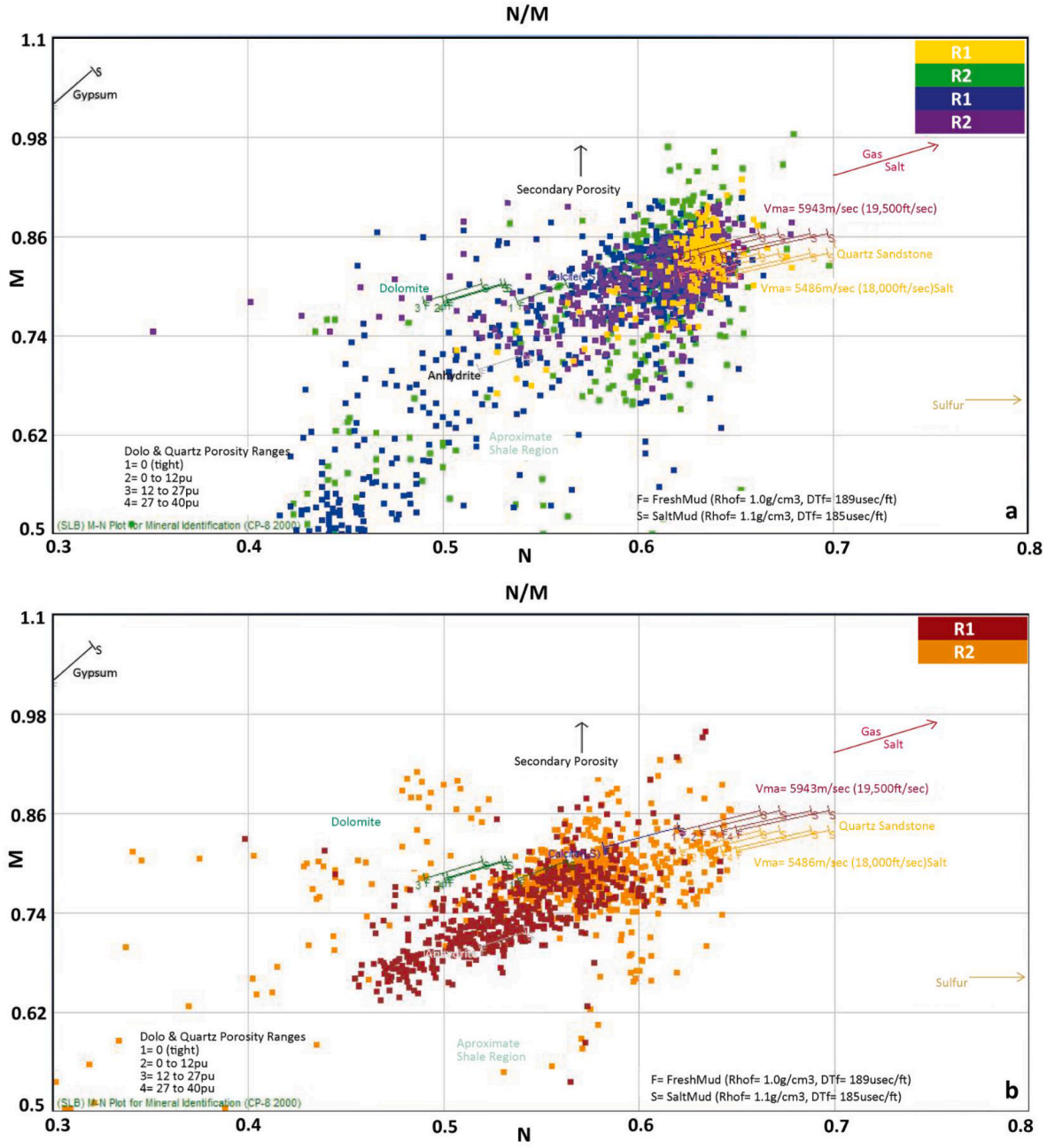

Fig. 7. a) M-N cross plot of the Logbaba Formation reservoirs within the studied well W1. b) M-N cross plot of the Logbaba Formation reservoirs within the studied well W2.

Abraham-A and Taioli (2019).

$$FFI = \varnothing - \frac{a^{0.5}}{44.72} \tag{11}$$

where FFI is Fluid Free Index, a = 0.8 is tortuosity factor and (∅) is porosity.

These three parameters were computed at 7 m intervals each reservoir in the two well logs.

4. Results and interpretation

4.1. Mineralogical and lithological identification

4.1.1. Neutron (NPHI) versus density (RHOB), neutron (NPHI) vs gamma ray (GR) and neutron (NPHI) vs sonic (DT) cross-plot

The neutron (NPHI) versus density (RHOB) cross-plot shows that the Logbaba Formation reservoirs within selected wells consist mainly of sandstone with some carbonates (limestone and dolomite) (Fig. 4). Furthermore, it also indicates the presence of intergranular and secondary porosities in equal proportion (Fig. 4).

The neutron vs. gamma-ray cross-plot shows the presence of scattering data points, indicating that the Logbaba Formation reservoirs have a varied lithology. Low gamma rays (10–40 API) and intermediate neutron values indicate clean sandstone (Fig. 5a) while medium gamma

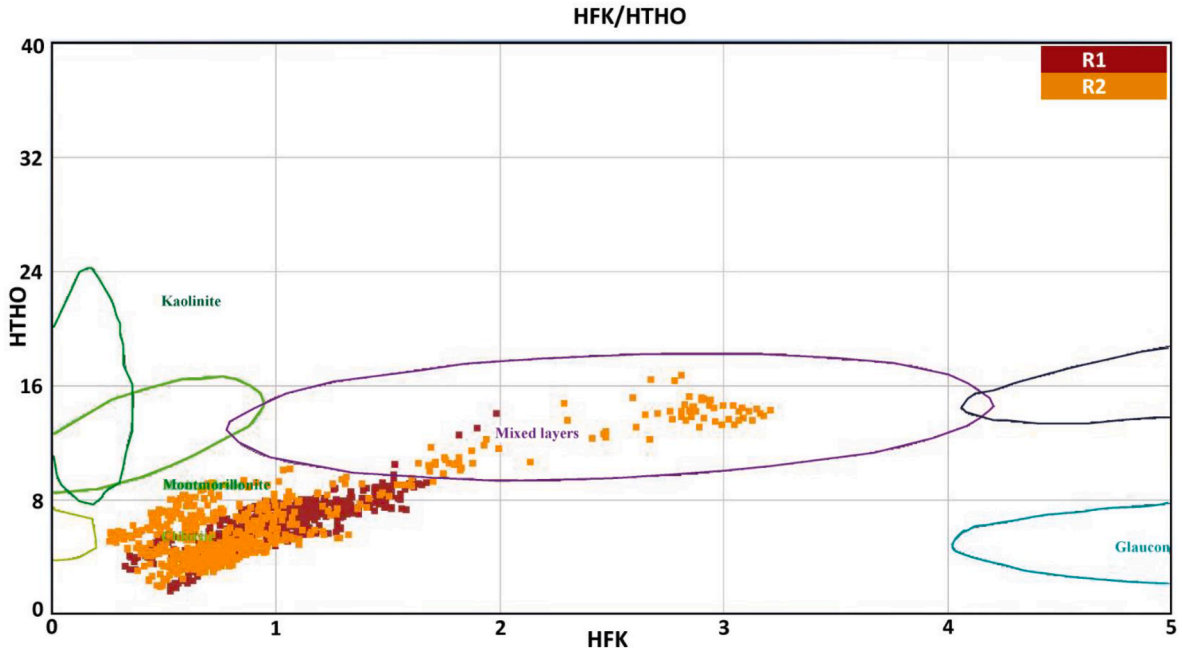

Fig. 8. Thorium vs. Potassium cross plot indicating different clay minerals within the Logbaba Formation reservoirs of the W2 well.

rays (40–75 API) and neutron values indicate shaly sandstone (Qadri et al., 2019). Intermediate gamma ray values but higher neutron values above 0.22 indicate the presence of carbonates (limestone and dolomite) (Fig. 5). Shale-rich contents are identified by high gamma values (above 90 API) with neutron values above 0.22. This classification is based on the schemes of El-Din et al. (2013) and Hakimi et al. (2017). In comparison, the neutron/gamma-ray cross-plot (Fig. 5) is consistent with the neutron/density cross-plots (Fig. 4), suggesting that the main lithology of the Logbaba Formation reservoirs is composed of sandstones interbedded with carbonates and shales. The clusters indicating sandstone and carbonates are dense compared to the clusters of shale-rich data points (Fig. 5).

The sonic porosity cross plot also supports that the Logbaba Formation reservoirs are predominantly sandstones and carbonates (Fig. 6). The cross plot indicates that the limestone concentration is dominant among the carbonates while dolomite is a subordinate, in agreement with Qadri et al. (2019). The cross-plot further reveals that the shale content appears to be high in the Formation's reservoirs (Fig. 6). The results deduced from Fig. 6 are consistent with those of Fig. 5 but differ somewhat from those of Fig. 4 in terms of shale content.

4.1.2. *M-N and potassium (HFK) vs thorium (HTHO) cross-plot*

Following Burke and Campbell Jr (1969), the M–N cross-plot shown in Fig. 7 reveals that most of the data points appear to be sandstones and carbonates (Fig. 7). Most of the carbonate points are plotted in the calcite field. In addition to sandstones and carbonates few points show the downward movement and indicate the shale effect (Fig. 7). The findings of the M–N cross plot are consistent with those of the NPHI vs. RHOB and NPHI vs. DT cross plots (Fig.7; Figs. 4 and 6).

The reservoir formation in the studied well contains a variety of clay minerals (Fig. 8). In well W2, the data points appear to be located mainly within the chlorite field, where the dominant clay minerals are chlorite and montmorillonite, as well as a small group of data points in the mixed clay layer zone.

4.2. *Lithological zonation of the reservoirs*

Based on the GR log responses from the W1 and W2 boreholes, six reservoir units were identified at depths ranging between 3947 and 4736 m (W1) and 3215–4051 m (W2) (Figs. 9 and 10). In W1, four sand bodies were identified and named R1, R2, R3 and R4 with thicknesses of 27, 73.4, 105.7 and 87.3 m, respectively (Fig. 9a). In W2, on the other hand, only two sand bodies were delineated, R1 and R2, with thicknesses of 77.2 and 93.6 m (Fig. 9b).

Analysis of the GR log from well W1 in reservoir R1 (4073–4100 m) reveals this interval is composed of sandstone, predominantly coarse-grained, with intercalations of dolomite (Figs. 9 and 10a). Reservoirs R2 (4230–4303.4 m) and R3 (4323–4428 m) are separated by a 20 m thick unit comprising claystone with dolomite layers. R2 and R3 consist of medium-grained sandstone, and rare dolomite (Figs. 9 and 10a). The interval R4 (4463–4550.3 m) consists of medium to very coarse-grained sandstones (Figs. 9 and 10a).

In well W2, analysis of the GR log of reservoir R1 (3510–3587.2 m) reveals alternating massive layers of very fine to fine-silt size silty sandstone with thin to metre scale of limestone and siltstone and minor stringers of claystone (Fig. 9). These sandstones are organised in several amalgamated packages mostly showing shaling upward trends. (Figs. 9 and 10b). The R2 reservoir unit (3644.3–3737.9 m) is mostly composed of thick massive sandstone packages, and subordinate stratified, cross-stratified, and argillaceous sandstones separated by a thick interval of massive shale (3658–3667 m) (Figs. 9 and 10b).

4.3. *Petrophysical evaluation*

Petrophysical properties such as shale volume, total and effective porosity, permeability, and fluid saturation (oil and water) were determined by well log analysis to understand the hydrocarbon potential of the Logbaba Formation reservoirs identified in W1 and W2 (Fig. 11). The results show that the Logbaba Formation reservoirs have a low volume of shale (V_{sh}) in the reservoirs of the studied wells, ranging from 6.3 to 19.8%. The lowest shale volume is observed in well W1, while the highest shale volume is observed in well W2. The reservoirs of the Logbaba Formation in the studied wells are likewise identified as sandstone according to the shale volume classification established by Hilchie (1978). Based on the porosity classification established by Rider (1996), the Logbaba Formation reservoirs in the studied wells have relatively good porosity. The effective porosity in the two studied wells is between 15.5 and 21.3%, with a permeability range from 5.65 to

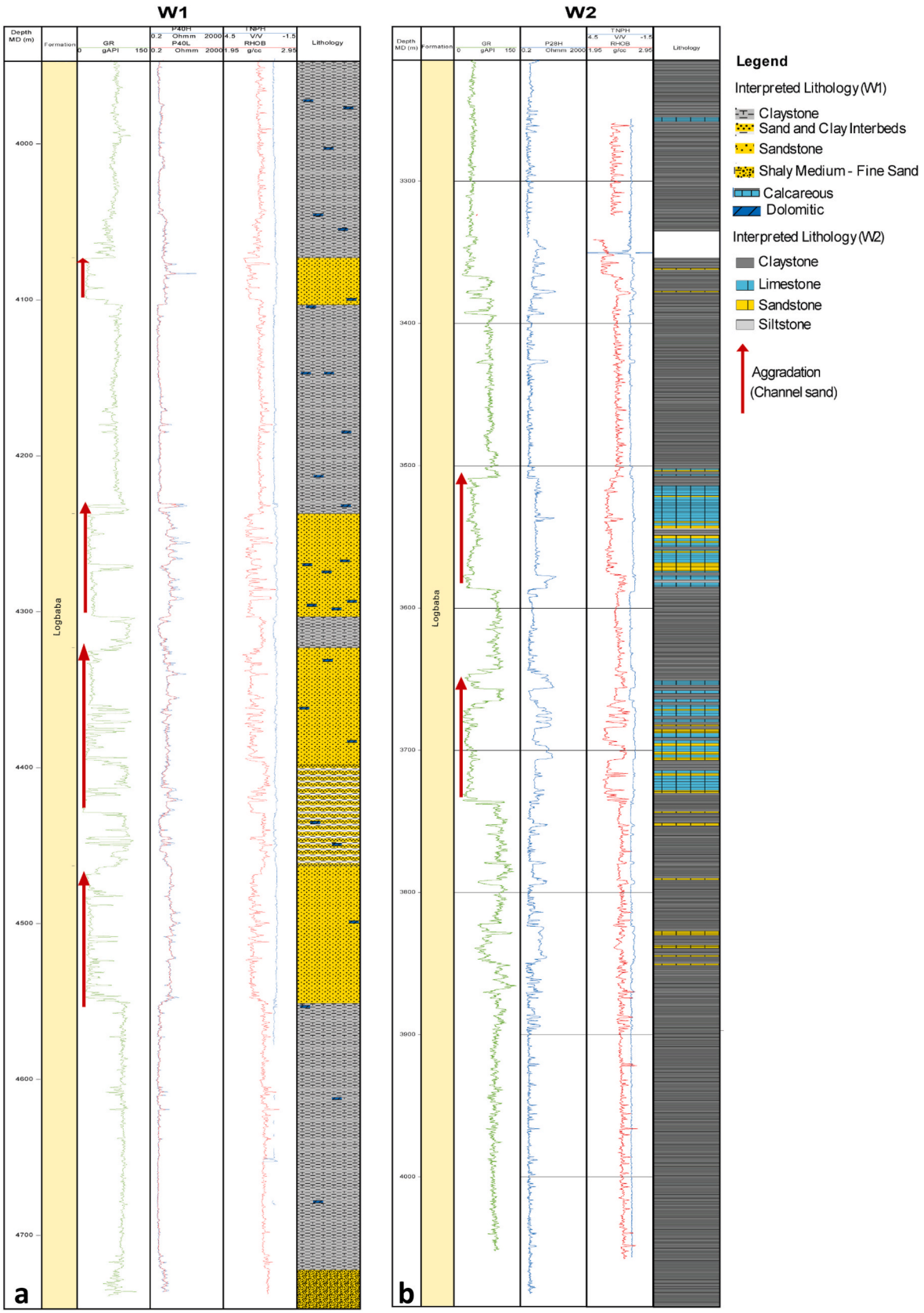

Fig. 9. lithological log and depositional environment of the reservoir in the Logbaba Formation based on GR signature adopted from Emery and Myers (1996).

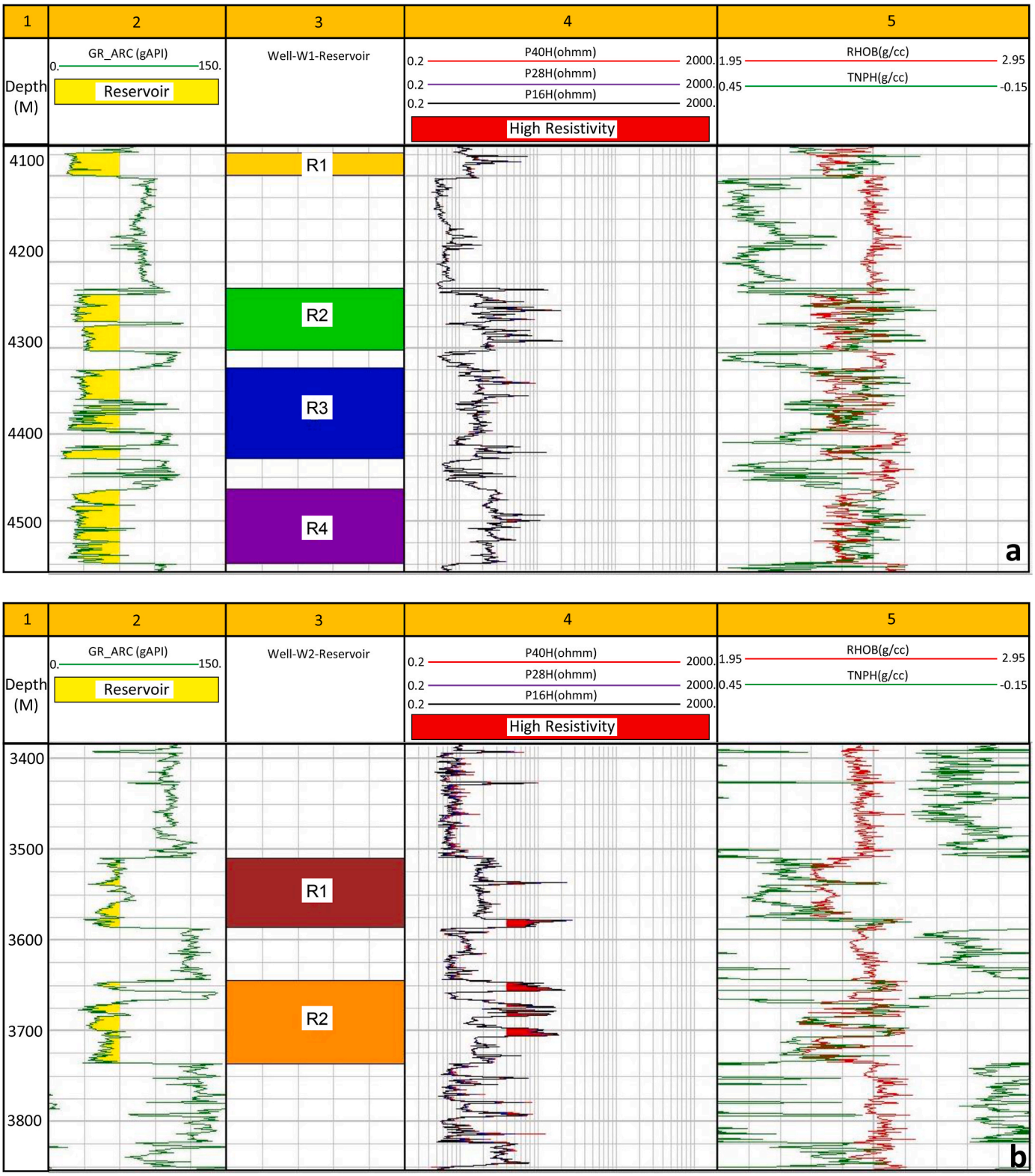

Fig. 10. a) Well log signatures of the studied interval in Well W1 and the identified reservoirs (*R*1, R2, R3 and R4). b) Well log signatures of the studied interval in Well W2 and the identified reservoirs (*R*1 and *R*2).

75.09 mD (Table 2). The water saturation (S_w) ranged from 34.5 to 74.2% (Table 2). The lowest water saturation is observed in well W2 while the highest water saturation is observed in well W1. Although it is important to calculate the water saturation, the most essential part is to estimate the hydrocarbon saturation using equation (5). The results indicate that the Logbaba Formation reservoirs have moderate to high hydrocarbon saturation (S_h) ranging from 25.8 to 65.5% (Table 2). The overall thickness of the net reservoir zones between 9 and 30.5 m is shown in Table 2. The analysed W2 well included two pay zones that indicated hydrocarbon accumulation; these two pay zones were merged

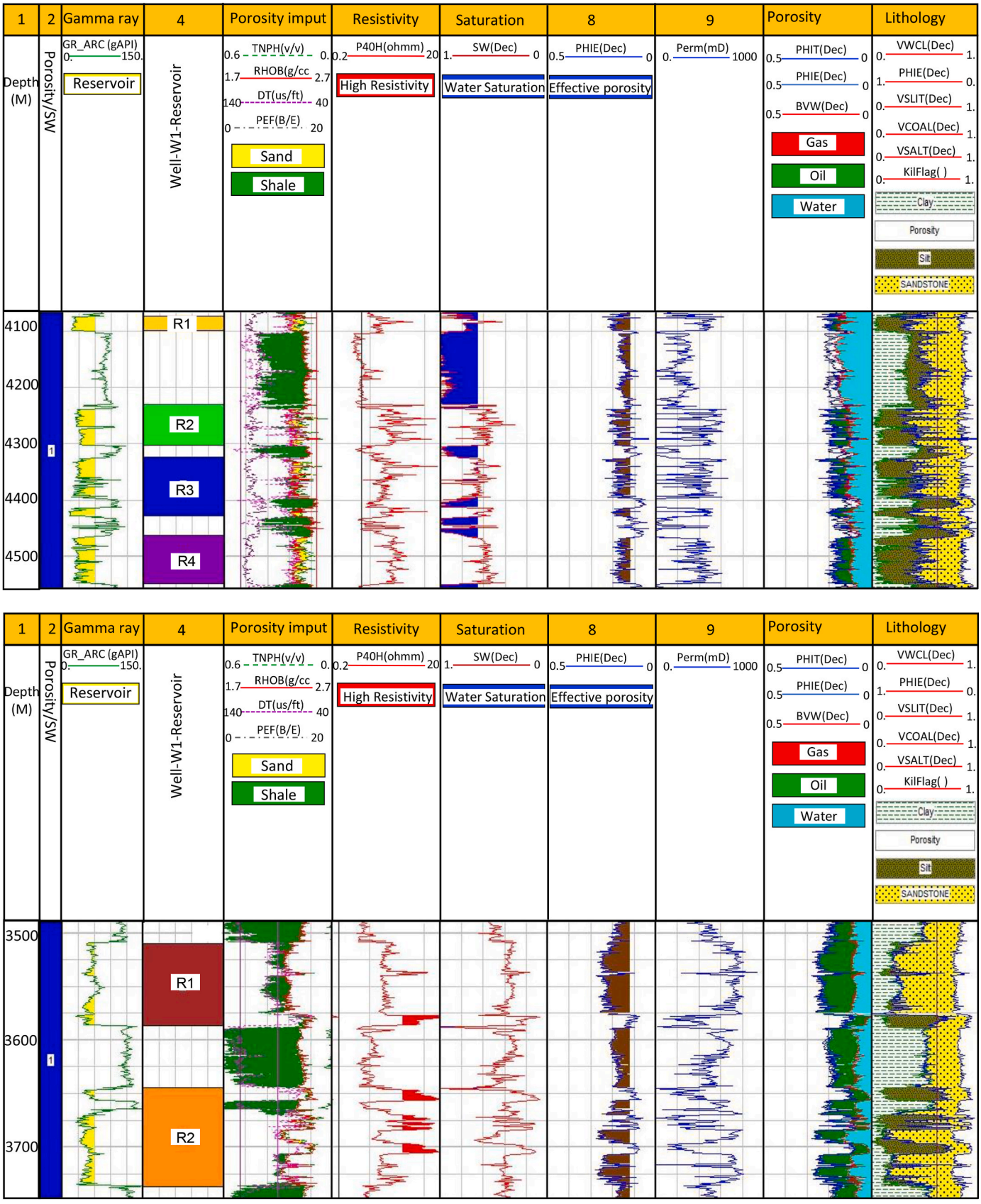

Fig. 11. a) Litho-saturation cross-plots of the Logbaba Formation reservoirs showing porosity, permeability, shale volume, water saturation, and hydrocarbon saturation within W1 well. b) Litho-saturation cross-plots of the Logbaba Formation reservoirs showing porosity, shale volume, water saturation, and hydrocarbon saturation within W2 well.

Table 2
Quantitative results of the petrophysical analysis of all identified sand zones within the Logbaba Formation through the studied W1 and W2 wells.

Reservoir	Top (m)	Bottom (m)	Gross (m)	Net (m)	Net/Gross	Net Pay (m)	Avg PhiE(%)	Avg Sw(%)	Avg Vsh(%)	Avg Sh(%)	Perm (mD)
Well W1											
R1	4073	4100	27	–	–	–	19.3	74.2	6.3	25.8	8.73
R2	4230	4303.4	73.4	–	–	–	16.5	60.6	13.6	39.4	8.87
R3	4323	4428.7	105.7	–	–	–	15.5	70.1	16.5	29.9	5.65
R4	4463	4550.3	87.3	–	–	–	16.1	59.4	10.6	40.6	5.70
Well W2											
R1	3510	3587.2	77.2	9.0	0.1	0.0	21.3	34.5	19.8	65.5	75.09
R2	3644.3	3737.9	93.6	30.5	0.3	8.0	17.5	36.5	19.3	63.5	35.22
Cutoffs											
Reservoir	–	–	–	–	–	–	≥12	≤65	≤40	–	–
Pay	–	–	–	–	–	–	≥12	≤65	≤40	–	–

Avg Phi E average effective porosity, Avg Sw average water saturation, Avg Vsh average volume of shale, Avg Sh averagehydrocarbon saturation, Perm permeability.

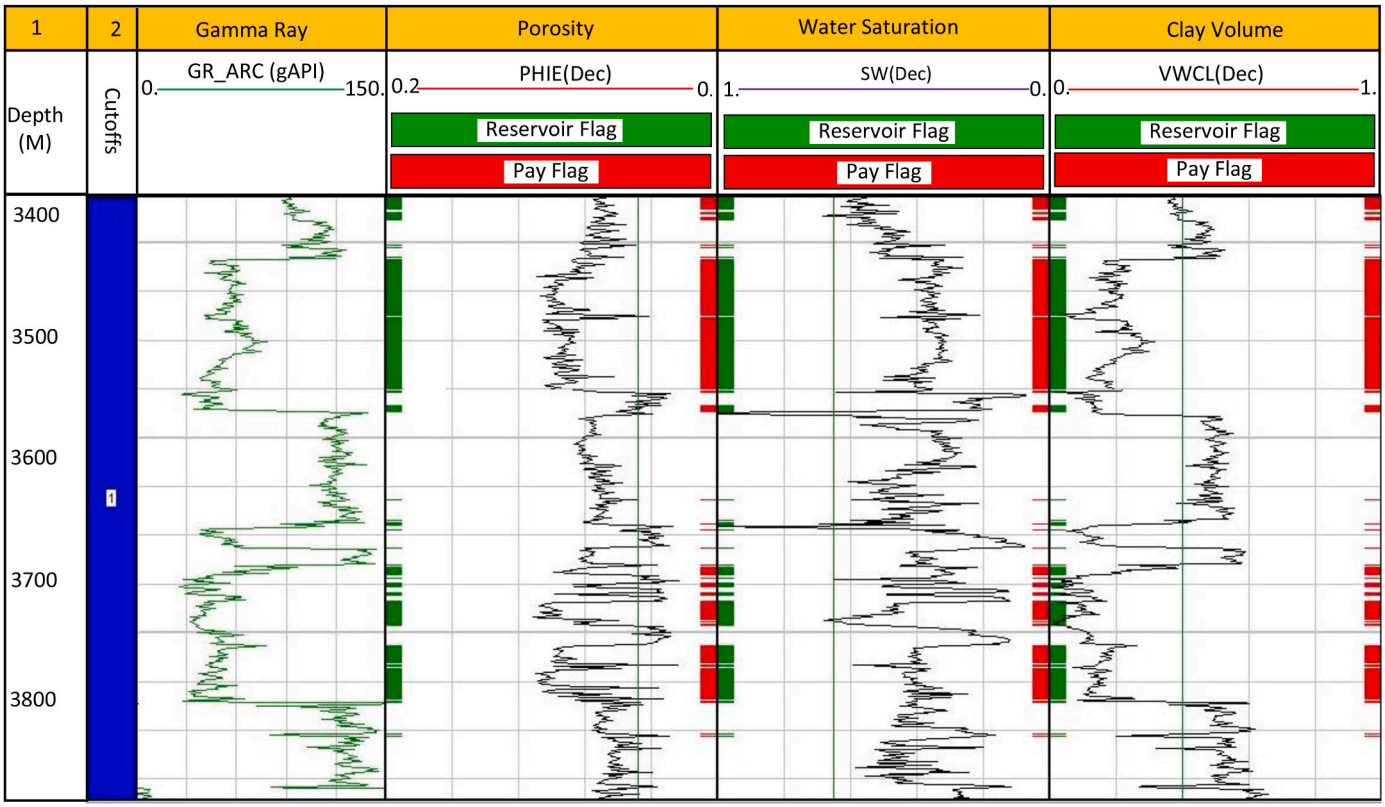

Fig. 12. Petrophysical and Pay zone summary graphical representation of W2 well reservoirs.

to obtain the overall net pay zone thickness for this well, which ranged from 0 to 8 m. Fig. 12 displays the sand zones (green) and net pay zones (red) in the formation reservoirs encountered by the W2 well. According to Asquith and Gibson (1982), the estimated bulk water volume values of the W2 reservoirs are scattered (Fig. 13), indicating an increase in the amount of formation water. This finding suggests that the reservoirs are heterogeneous and that there is more water in the formation than can be contained by the capillary pressure. Consequently, the reservoirs cannot produce a water-free hydrocarbon during production since they are not saturated with irreducible water (Swirr).

The average values of FFI, RQI and FZI within the reservoirs in well W1 are 0.13, 0.16 μm and 0.69 for reservoir R1; respectively compared to 0.13, 0.17 μm and 0.78 respectively for reservoir R2 (Tables 3 and 4). In the case of reservoir R3, the average values of FFI, RQI and FZI are 0.12, 0.12 μm and 0.62 respectively; 0.13, 0.17 μm and 0.82 respectively for reservoir R4 (Tables 3 and 4). In well W2, the average values of FFI, RQI and FZI within the reservoirs are 0.18, 0.48 μm, and 1.65 respectively for R1 and 0.15, 0.33 μm, and 1.29 respectively for R2 (Tables 3 and 4).

4.4. Reservoir fluids

Further analysis of the resistivity log data shows that the three resistivity logs in the reservoir interval overlap, indicating the presence of a water-bearing zone (Fig. 10). The higher deep resistivity readings (P40H) observed in the reservoirs W1 and W2 indicate the presence of hydrocarbons (Fig. 10). The cross-plot of neutron and reservoir density in the individual wells shows no "balloon effect", suggesting the presence of oil as the hydrocarbon phase (Chongwain et al., 2018, 2019). However, the reservoirs in W1 contain no producible hydrocarbons (i.e., no pay zone), but with low GR and high resistivity values based on Zhu et al. (2018), which is typical of calcareous interbeds. These calcareous are often identified by their natural gamma below 80 API and higher lateral resistivity values than any other sandstone. Calcareous interbeds

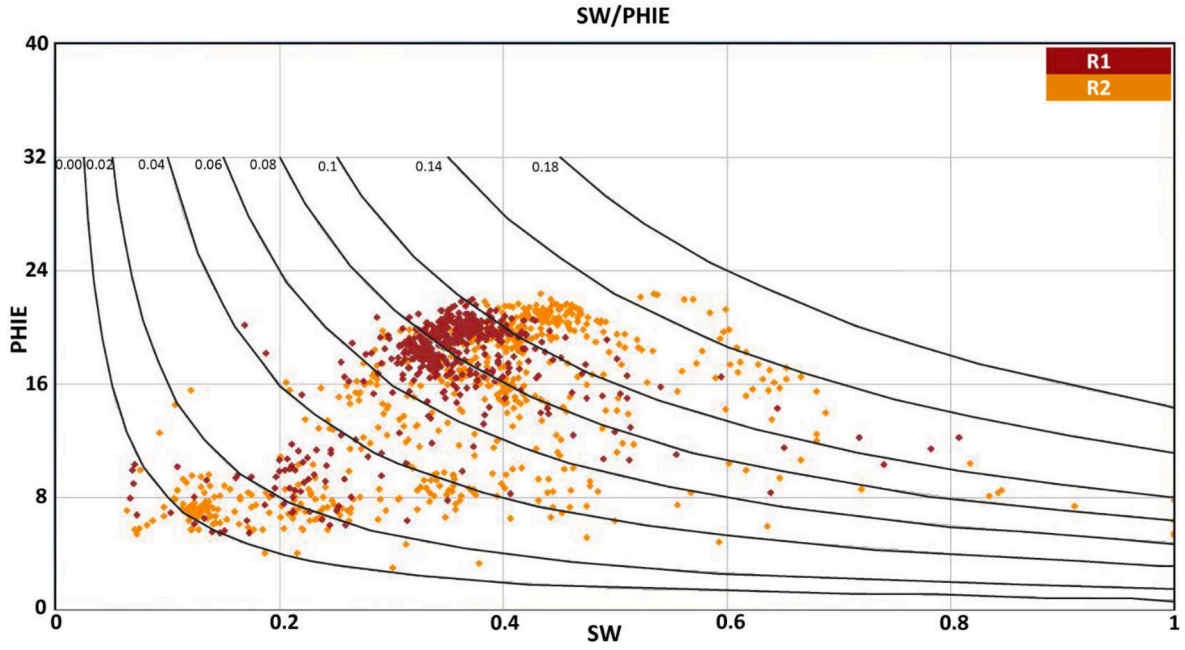

Fig. 13. Buckle plot of water saturation against porosity for Logbaba Formation reservoirs within the well W2.

are classified into four types: 1) the bottom type, 2) the top type, 3) the central and 4) the complete types (Qi et al., 2006; Zhang et al., 2007, 2009; Wang et al., 2009; Sun et al., 2010). The reservoir intervals that W1 penetrated may be typical of the complete type of calcareous interlayer, where the thin isolated mudstone-draped sand layer and the sand as a whole has been fully cemented by carbonate to produce a tight reservoir (Chongwain et al., 2018) (Fig. 10a).

5. Discussion

5.1. Depositional environment of reservoir

The sediments of Logbaba Formation comprise a series of sandstone and shale successions that have been deposited during two phases of relative sea level changes. This suggests two depositional conditions occurring during the Campanian-Maastrichtian (Simon Petroleum and Technology, 1995; Secke Bekonga Gouott et al., 2022). A transgressive episode was distinguished by finer-grained facies (deep-water sediments e.g., shale, siltstone) overlying coarse facies (shallow-water sediments e.g., sandstone), indicating deposition during sea level rise. A regressive episode, where shallower marine and nearshore deposits, indicating deposition during falling sea level, overlie marine deposits. These sediments of the Logbaba Formation have characteristic coarsening upward, fining upward, and blocky gamma ray log signatures. The cylindrical or blocky gamma ray log motifs recorded in this study are serrated with quite abrupt upper and lower limits. This characterized the reservoirs and bodies "R1, R2, R3, and R4" (well W1), and "R1 and R2" of well W2. This reservoir thickness ranges from 27 to 105.7 m (Table 2) and is often linked with fine-grained sands of excellent reservoir quality because of their low shale content, a consequence of high energy conditions that foster clean porous sands. However, Emery and Myers (1996) stated that cylindrical patterns with greater range of thickness, as those of reservoir sands of well W1 and W2 (Table 2), could be interpreted as turbidite sand depositional environment (i.e., deposited in an aggradation/still stand depositional sequence; Fig. 9). In addition, Secke Bekonga Gouott et al. (2022) reported that the locally high amplitude seismic facies displaying an aggradational pattern observed from seismic data within the Late Cretaceous succession in the studied area corresponds to submarine fans, composed of reservoir sands in the Kribi-Campo deep water sub-basin.

5.2. Implication for reservoir quality

The sandstones of the Logbaba Formation are considered the main reservoir target for the wells drilled beyond the shelf of the Kribi-Campo sub-basin (Sterling Cameroon Limited, 2010; Loule et al., 2018). However, the results of this study indicate that the Logbaba Formation reservoirs do not consist solely of clean sandstone, but rather include intercalations of carbonates and shales. The heterogeneous matrix of the reservoirs, consisting of sand, limestone, and dolomite in this case, probably indicates that the detrital carbonate originated from fluvial sediment influx from the Sanaga and Nyong Rivers (Regnoult, 1986; ECL, 2001; SNH/UD et al., 2005). Further diagenesis led to the dissolution of the biogenic carbonate-forming calcite matrix generating secondary intragranular porosity (Irwin et al., 1977; Curtis and Coleman, 1986; Chongwain et al., 2019).

Reservoirs are generally organized into several amalgamated packages, mostly with blocky sands (Fig. 10). These are interpreted to represent a stacked set of overall upward sanding packets that may represent a phased discharge deposited primarily by granular flows in a poorly confined channel in a proximal lobe (Sterling Cameroon Limited, 2010). This result would be consistent with the work of Simon Petroleum and Technology (1995), Le (2012), Loule et al. (2018) and Secke Bekonga Gouott et al. (2022), who suggested that the sediments observed in the Logbaba Formation are mud-rich deposits with local sandy deposits associated with channels and fans. This is evidence for the presence of medium- and locally coarse-grained sandstones with overlying net thicknesses greater than 80 m.

The inferred results of the study indicate the presence of chlorite and montmorillonite as the dominant clay minerals and a few smaller ones in the mixed clay layer zone (Fig. 8). The mixed layers of clay minerals formed because of the inter-layering of various clay minerals in a single structure (Srodo'n, 1999). Clay minerals are generally considered detrimental when assessing the quality of sandstone reservoirs (Jiang, 2012). Clay minerals reduce porosity and permeability as they can clog pore throats in the form of films, plates, and bridges on the grain surface (Jiang, 2012). Some clay minerals increase chemical compaction while accelerating the rate of porosity loss in a limestone deposit, lowering

Table 3
Estimated parameters for the reservoirs in well W1.

Parameters	Depth	Φ	K	FFI	RQI	FZI
R1	4073	0.18	3.14	0.15	0.13	0.59
	4080	0.18	6.38	0.15	0.18	0.77
	4087	0.21	9.33	0.18	0.2	0.76
	4095	0.19	5.24	0.16	0.16	0.66
R2	4230	0.14	0.6	0.13	0.06	0.37
	4237	0.11	0.18	0.08	0.03	0.29
	4244	0.2	21.74	0.17	0.32	1.3
	4251	0.19	9.37	0.16	0.21	0.87
	4258	0.17	5.08	0.14	0.16	0.78
	4265	0.2	31.92	0.17	0.39	1.57
	4272	0.1	0.07	0.07	0.02	0.24
	4279	0.12	0.87	0.09	0.08	0.55
	4286	0.15	1.86	0.12	0.11	0.61
	4293	0.19	10.07	0.16	0.22	0.94
	4300	0.2	16.01	0.17	0.27	1.07
R3	4323	0.1	0.09	0.07	0.03	0.26
	4330	0.21	18.53	0.18	0.29	1.06
	4337	0.18	5.07	0.15	0.16	0.74
	4344	0.18	5	0.15	0.16	0.73
	4351	0.2	11.83	0.17	0.23	0.91
	4358	0.16	2.71	0.13	0.12	0.64
	4365	0.1	0.08	0.07	0.02	0.25
	4372	0.2	13.24	0.17	0.25	0.96
	4379	0.17	3.71	0.14	0.14	0.68
	4386	0.17	6.17	0.14	0.18	0.88
	4393	0.15	1.81	0.12	0.1	0.55
	4400	0.09	0.07	0.06	0.02	0.27
	4407	0.09	0.05	0.06	0.02	0.21
	4414	0.11	0.42	0.08	0.06	0.49
	4421	0.13	0.81	0.1	0.07	0.49
	4428	0.19	9.8	0.16	0.21	0.88
R4	4463	0.07	0.01	0.04	0.01	0.17
	4470	0.17	4.12	0.14	0.15	0.74
	4477	0.18	6.64	0.15	0.18	0.84
	4484	0.18	10.52	0.15	0.23	1.02
	4491	0.18	8.98	0.15	0.21	0.97
	4498	0.13	0.56	0.1	0.06	0.43
	4505	0.18	8	0.15	0.2	0.92
	4512	0.17	3.73	0.14	0.14	0.7
	4519	0.16	3.56	0.13	0.14	0.73
	4526	0.17	5.9	0.14	0.18	0.85
	4533	0.19	11.93	0.16	0.24	1.04
	4540	0.17	4.78	0.14	0.16	0.8
	4547	0.2	29.85	0.17	0.38	1.51

Table 4
Estimated parameters for the reservoirs in well W2.

Parameters	Depth	Φ	K	FFI	RQI	FZI
R1	3510	0.23	85.84	0.2	0.6	2.02
	3517	0.25	131.17	0.22	0.7	2.04
	3524	0.24	83.82	0.21	0.57	1.77
	3531	0.22	62.1	0.19	0.51	1.77
	3538	0.17	8.84	0.14	0.22	1.05
	3545	0.23	68.12	0.2	0.53	1.75
	3552	0.23	95.94	0.2	0.63	2.12
	3559	0.26	176.37	0.23	0.81	2.26
	3566	0.22	52.85	0.19	0.48	1.67
	3573	0.26	115.61	0.23	0.65	1.85
	3580	0.09	1.61	0.06	0.12	1.13
	3587	0.12	0.44	0.09	0.05	0.4
R2	3644	0.16	8.24	0.13	0.22	1.13
	3651	0.1	1.31	0.07	0.11	0.99
	3658	0.2	40.98	0.17	0.44	1.7
	3666	0.16	9.19	0.13	0.23	1.19
	3673	0.09	0.6	0.06	0.07	0.75
	3680	0.23	41.44	0.2	0.41	1.33
	3687	0.25	69.55	0.22	0.52	1.56
	3694	0.16	2.74	0.13	0.12	0.65
	3701	0.09	1.09	0.06	0.1	0.95
	3708	0.24	73.65	0.21	0.54	1.72
	3715	0.24	77.85	0.24	0.56	1.74
	3722	0.25	88.36	0.22	0.58	1.72
	3729	0.25	102.33	0.23	0.63	1.89
	3736	0.13	2.49	0.1	0.13	0.84

reservoir quality (Brown, 1997; Chongwain et al., 2019; Qadri et al., 2019). However, the presence of clay minerals does not necessarily indicate a deterioration in reservoir quality but can also contribute to improving it (Taylor et al., 2004; Chongwain et al., 2019). The present study shows an abundance of chlorite in the W2 well reservoirs, which can protect and maintain reservoir quality by coating the sand grains and preventing them from quartz cementation. The chlorite mineral may have formed early in the diagenesis of micas and feldspar on the sea-floor, or it may have been the result of detrital chlorite influx from nearby river sediments during rapid deposition (Chongwain et al., 2018; Qadri et al., 2019). The porosities of Logbaba formation range from 6% to 23% and the permeabilities average 50 mD (Simon Petroleum and Technology, 1995). The good porosity values (21.3%) estimated for the first reservoir in well W2 indicate a minimal impact of clay minerals on reservoir quality.

Kana et al. (2022) recently studied the Logbaba formation in the deep-water of the Kribi-Campo sub-basin and indicated the presence of reservoir oil potential. They indicate that the nature of the fluids present in the reservoirs is oil, gas and water with a porosity of 17.37–27.85%, a volume of shale is 3.81–29.47% and water saturation values between 47.74 and 56.02%. Based on the classification of Simon Petroleum and Technology (1995), Loule et al. (2018), Kana et al. (2022) and by taking the porosity and permeability values into consideration, the Logbaba formation is considered to have good reservoir quality. Supporting this from another margin is work of Alao and Oludare (2015) in the Niger Delta Basin where porosity values of 20–30% are considered very good, 10–20% as good quality reservoirs and moderate permeability (10–50 mD) is an indication of good sand quality. Therefore, the porosity and permeability values obtained in this study suggest well-sorted sands, which is an indication of good reservoir quality (Odundun and Nton, 2009).

Low RQI and FZI values observed in this study collectively suggest reservoirs with poor flow units, likely to exhibit limited hydrocarbon transmissibility and lower recovery rates. On the contrary, a high RQI values would have indicated that reservoir is characterized by well-sorted grain distribution and favorable pore-throat sizes, which are critical for assessing reservoir quality and fluid transmission (Tiab and Donaldson, 2012; Abraham-A and Taioli, 2019). Similarly, significant FZI values suggest the presence of less shale and more interconnected, coarse-grained, well-sorted sands, further highlighting the reservoir's potential (Tiab and Donaldson, 2012; Abraham-A and Taioli, 2019).

The W1 well displays thick and porous sand reservoirs. However, there is no evidence that hydrocarbons migrated into any reservoirs, suggesting that the source rock and hydrocarbon migration pathways are the main risk factors and reason for the well failure (Loule et al., 2018). The W2 well has good-quality reservoirs in the Logbaba Formation, but all were water-bearing and did not contain commercial quantities of hydrocarbons.

6. Conclusion

An assessment of the petrophysical properties of the Upper Cretaceous reservoirs of Logbaba Formation in the Kribi-Campo sub-basin, offshore Cameroon, was carried out using well log data from two key wells, W1 and W2. The results of this study provide important insights into the reservoir quality of the Logbaba Formation, as follows.

1) The lithofacies of the Logbaba Formation reservoirs consist mainly of sandstone interbedded with carbonates and shales. These reservoirs correspond to turbidite sand deposits.
2) The analysed wells show good reservoir quality, with relatively moderate and good effective porosity (15.5%–21.3%), with medium permeability (5.65–75.09 md) and low shale content (6.3%–19.8%).

Water saturation is high (34.5%–74.2%). FFI, RQI, and FZI are insignificant and suggest reservoirs with poor transmissibility. However, all reservoirs were water-bearing and did not contain commercial quantities of hydrocarbons.

3) Clay minerals such as chlorite, montmorillonite and mixed layers were found in the reservoirs. The dominant clay mineral is chlorite, forming during the primary deposition before burial or secondary during diagenetic events after sedimentation. The good porosities, on the other hand, indicate that the clay minerals have little influence on reservoir quality.

However, the lack of core samples is a limitation of the current study. Yet, this study has implications on hydrocarbon exploration in the deep-water Kribi-Campo sub-basin where only a few wells have been drilled with low success. The findings of this study can also guide exploration in similar basins awaiting further exploration and development.

CRediT authorship contribution statement

Boris G. B. Secke: Writing – original draft, Methodology, Investigation, Formal analysis, Conceptualization. **Ovie Emmanuel Eruteya:** Writing – review & editing, Investigation, Conceptualization, Supervision. **Yakufu Niyazi:** Writing – review & editing, Investigation, Data curation, Conceptualization. **Mbida Yem:** Writing – review & editing, Methodology, Investigation. **Joseph Quentin Yene Atangana:** Writing – review & editing, Supervision. **Pierre Eric Nkoa Nkoa:** Writing – review & editing, Resources, Methodology, Data curation. **Elias Samankassou:** Writing – review & editing, Supervision, Funding acquisition.

Declaration of competing interest

The authors declare that they have no known competing financial interests or personal relationships that could have appeared to influence the work reported in this paper.

Data availability

The authors do not have permission to share data.

Acknowledgements

The authors would like to thank the National Hydrocarbon Corporation (NHC), Yaoundé, Cameroon, for providing the data used in the study. BSBG thanks the Swiss Government Excellence Scholarship for awarding him a scholarship (ESKAS No. 2022.0697). We also appreciate the associate editor Dr. Lin Ma and two anonymous reviewers for their insightful reviews and constructive suggestions to make the paper a better contribution.

References

Abraham-A, M.R., Taioli, F., 2019. Hydrocarbon viability prediction of some selected reservoirs in Osland Oil and gas field, Offshore Niger Delta, Nigeria. Mar. Petrol. Geol. 100, 195–203.

Alao, O.A., Oludare, T.E., 2015. Classification of reservoir sand-facies distribution using multiattribute probabilistic neural network transform in "Bigola" Field, Niger Delta, Nigeria. IFE J. Sci. 17 (3), 579–589.

Amaefule, J.O., Altunbay, M.H., Tiab, D., Kersey, D.G., Keelan, D.K., 1993. Enhanced reservoir description using core and log data to identify hydraulic (flow) units and predict permeability in uncored intervals/well Soc. Petrol. Eng. SPE- 26436, 205–220.

Asquith, G., Gibson, C., 1982. Basic well log for geologists. American Association of Petroleum Geologist, Tulsa Methods in Exploration, Tulsa 216.

Asquith, G., Krygowski, D., 2004. Basic Well Log Analysis: AAPG Methods in Exploration Series, p. 16.

Asquith, G.B., 1985. Handbook of log evaluation techniques for carbonate reservoirs. In: Methods in Exploration Series N°. 5. The American Association of Petroleum Geologists, Tulsa, Oklahoma, USA, pp. 1–47.

Balaky, M.S., Al-Dabagh, M.M., Asaad, Sh I., Tamar-Agha, M., Ali, S.M., Radwan, E.A., 2023. Sedimentological and petrophysical heterogeneities controls on reservoir characterization of the Upper Triassic shallow marine carbonate Kurra Chine Formation, Northern Iraq: integration of outcrop and subsurface data. Mar. Petrol. Geol. 149, 106085 https://doi.org/10.1016/j.marpetgeo.2022.106085.

Bardon and Pied, 1969. Formation water saturation in shaly sands. In: SPWLA 10th Annual Logging Symposium.

Benkhelil, J., Giresse, P., Poumot, C., Ngueutchoua, G., 2002. Lithostratigraphic, geophysical, and morpho-tectonic studies of the South Cameroon shelf. Mar. Petrol. Geol. 19, 499–517.

Brown, A., 1997. Porosity Variation in Carbonates as a Function of Depth. Mississippian Madison Group, Williston Basin, pp. 29–46.

Brownfield, M.E., Charpentier, R.R., 2006. Geology and Total Petroleum Systems of the West-Central Coastal Province (7203), West Africa: U, 2207-B. Geological Survey Bulletin, p. 52.

Buckles, R.S., 1965. Correlating and averaging connate water saturation data. J. Can. Petrol. Technol. 9 (1), 42–52.

Burke, A.W., Campbell Jr, J.A., 1969. Schmidt AW the litho-porosity cross plot A method of determining rock characteristics for computation of log data. Society of Petroleum engineers. In: SPE Illinois Basin Regional Meeting.

Chongwain, G.M., Osinowo, O.O., Ntamak-Nida, M.J., Biouele, S.E.A., Nkoa, N.E., 2018. Petrophysical characterisation of reservoir intervals in well-X and well-Y, M-Field, offshore Douala Sub-Basin, Cameroon. J. Pet. Explor. Prod. Technol. 9, 911–925. https://doi.org/10.1007/s13202-018-0562-0.

Chongwain, G.C., Osinowo, O.O., Ntamak-Nida, M.J., Nkwanyang, T.L., 2019. Lithological typing, depositional environment, and reservoir quality characterization of the "M-Field," offshore Douala Basin, Cameroon. J. Pet. Explor. Prod. Technol. 9, 1705–1721. https://doi.org/10.1007/s13202-019-0648-3.

Coward, M.P., Purdy, E.G., Ries, A.C., Smith, D.G., 1999. The distribution of petroleum reserves in basins of the South Atlantic margins. The Oil and Gas Habitats of the South Atlantic Geological Society of London Special Publications 153, 101–131.

Curtis, C.D., Coleman, M.L., 1986. Controls on the precipitation of early diagenetic calcite, dolomite and siderite concretions in complex depositional sequences. In: Gautier, D.L. (Ed.), Roles of Organic Matter in Sedimentary Diagenesis. Special Publication N°. 38. Society of Economic Paleontologists and Mineralogists, Tulsa, pp. 23–35.

Dewan, J.T., 1983. Essentials of Modern Open-Hole Log Interpretation. PennWell Books, PennWell Publishing Company, Tulsa, Oklahoma, p. 361.

El-Din, E.S., Mesbah, M.A., Kassab, M.A., Mohammed, I.F., Cheadle, B.A., 2013. Assessment of petrophysical parameters of clastics using well logs: the Upper Miocene in El-Wastani gas field, onshore nile Delta, Egypt. Pet Explot Dev 40 (4), 488–494.

Elmahdy, M., Radwan, A.A., Nabawy, B.S., Abdelmaksoud, A., Nastavkin, A.V., 2023. Integrated geophysical, petrophysical and petrographical characterization of the carbonate and clastic reservoirs of the Waihapa Field, Taranaki Basin, New Zealand. Mar. Petrol. Geol. 151, 106173 https://doi.org/10.1016/j.marpetgeo.2023.106173.

Emery and Myers, 1996. Sequence Stratigraphy. Black Ltd, Oxford.

Exploration Consultants Limited (ECL), 2001. An Integrated Study Development, Source Rock Maturity and Hydrocarbon Generation in the Douala/Kribi-Campo Basin, Republic of Cameroon: Henley-On-Thames. Cameroon National Hydrocarbons Corporation, Oxfordshire, United Kingdom, p. 183.

Fertl, W.H., Vercellino, W.C., 1978. Practicla log analysis. 4. Predict water cut from well logs. Oil Gas J. 76 (25), 111–116.

Hakimi, M.H., Al-Qadasi, B.A., Al-Sharrabi, Y., Al-Sorore, O.T., Al-Samet, N.G., 2017. Petrophysical properties of cretaceous clastic rocks (qishn formation) in the sharyoof oilfield, onshore masila basin, Yemen. Egypt J Pet 26 (2), 439–455.

Hilchie, D.W., 1978. Applied Openhole Log Interpretation. DW Hilchie. Inc., Golden.

Hu, K., Chen, Z., Yang, C., Jiang, C., Liu, X., 2020. Integrated petrophysical evaluation of the lower middle bakken member in the viewfield pool, southeastern saskatchewan, Canada. Mar. Petrol. Geol. 122, 104601 https://doi.org/10.1016/j.marpetgeo.2020.104601.

Huang, Y., 2018. Sedimentary characteristics of turbidite fan and its implication for hydrocarbon exploration in Lower Congo Basin. Petrol Res 3, 189–196.

Iboum Kissaaka, J.B., Ntamak-Nida, M.J., Mvondo, F., Fowe, Kwetche, P.G., Djomeni Nitcheu, A.L., Abolo, G.M., 2016. Post-rift depositional evolution and sequence stratigraphy from offshore subsurface data of the Kribi-Campo sub-basin (Cameroon, West African margin). Soc Explor Geophys Am Assoc Petrol Geol 13 (1), 79–101. https://doi.org/10.1190/INT-2015-0073.

Irwin, H., Curtis, C., Coleman, M., 1977. Isotopie evidence for source of diagenetic carbonates formed during burial of organic-rich sediments. Nature 269, 20.

Jiang, S., 2012. Clay minerals from the perspective of oil and gas exploration. In: Valašcova, M., Martynkova, G.S. (Eds.), Clay Minerals in Nature-Their Characterization, Modification and Application, pp. 21–38. https://doi.org/10.5772/47790.

Jumat, N., Shalaby, M.R., Islam, M.A., 2018. Integrated reservoir characterization of the Paleocene Farewell Formation, Taranaki Basin, New Zealand, using petrophysical and petrographical analyses. J. Pet. Explor. Prod. Technol. 8, 685–701.

Kana, J.D., Tanembe, J.A., Diab, D.A., Ghomsi, F.E.K., Zakari, A., Mbida, S., Ahmadou, O. B., Nouck, P.N., 2022. Geophysical investigation of hydrocarbon in the southern part of Douala Kribi Campo basin, Cameroon. J. Afr. Earth Sci. 193, 104578 https://doi.org/10.1016/j.jafrearsci.2022.104578.

Kim, T., Hwang, S., JANG, S., 2016. Petrophysical approach for estimating porosity, clay volume, and water saturation in gas-bearing shale: a case study from the Horn River Basin, Canada. Austrian Journal of Earth Sciences Vienna 109 (2), 289–298.

Larionov, V.V., 1969. Radiometry of Boreholes. NEDRA, Moscow (in Russian).

Lawrence, R.S., Munday, S., Bray, R., 2002. Regional geology and geophysics of the eastern Gulf of Guinea (Niger Delta). Lead. Edge 1112–1117.

Le, A.N., 2012. Stratigraphic evolution and plumbing system in the Cameroon margin, West Africa. In: Thesis for the Degree of Doctor of Philosophy. Faculty of Engineering and Physical Science. University of Manchester.
Le, A.N., 2021. Striations at the base of the paleo-fan and channel revealed by 3D seismic data, offshore Cameroon. Indones. J Geosci 8, 101–107.
Le, A.N., Huuse, M., Redfern, J., Gawthorpe, R.L., Irving, D., 2014. Seismic characterization of a bottom simulating reflection (BSR) and plumbing system of the Cameroon margin, offshore west africa. Mar. Petrol. Geol. 68, 629–647.
Loule, J.P., Jifon, F., Angoua Biouele, S.E., Nguema, P., Spofforth, D., Carruthers, D., Watkins, C., Johnston, J., 2018. An opportunity to re-evaluate the petroleum potential of the Douala/Kribi-Campo Basin, Cameroon. Spec Top: Petrol. Geol. 36, 61–70 (First break).
Magoba, M., Opuwari, M., 2020. Petrophysical interpretation and fluid substitution modelling of the upper shallow marine sandstone reservoirs in the Bredasdorp Basin, offshore South Africa. J. Pet. Explor. Prod. Technol. 10 (2), 783–803.
Mienlam Essi, M.F., Yene Atangana, J.Q., Abate Essi, J.M., Mbida, Yem, Angoua, Biouele S.E., Nguema, P., Tsimi Ntsengue, C., 2021. Stratigraphical nature of the Top Albian surface, from seismic and wells data analyses, in the south Sanaga area (Cameroon Atlantic margin): palaeogeographical significance and petroleum implications. Mar. Petrol. Geol. 129, 105073 https://doi.org/10.1016/j.marpetgeo.2021.105073.
Morris, R.L., Biggs, W.P., 1967. Using log-derived values of water saturation and porosity. In: PWLA 8th Annual Logging Symposium, pp. 12–14. Denver.
Ndonwie Mahbou, E., 2007. Petrophysical Characterization of Petroleum Reservoirs and Source Beds of the Batanga Sub-block, Kribi-Campo Sub-basin, Cameroon. AAPG Annual Convention, p. 1. Abstract.
Nguene, F.R., Tamfu, S., Loule, J., Ngassa, C., 1992. Palaeoenvironments of the Douala and kribi/campo sub-basins, in Cameroon, west africa. In: Curnelle, R. (Ed.), Géologie Africaine, 1er Colloque de Stratigraphie et de Paléogéographie des Bassins Sédimentaires Ouest-Africains, 2e Colloque Africain de Micropaléontologie, Libreville, Gabon, 1991. Recueil des Communications, Boussens, pp. 129–139 (Elf Aquitaine).
Ntamak-Nida, M.J., Bourquin, S., Makong, J.C., Baudin, F., Mpesse, J.E., Ngouem, C.I., Komguem, P.B., Abolo, G.M., 2010. Sedimentology and sequence stratigraphy from outcrops of the kribi-campo sub-basin: lower Mundeck formation (lower cretaceous, southern Cameroon). J. Afr. Earth Sci. 58, 1–18.
Odundun, O., Nton, M., 2009. Facies interpretation from well logs: applied to SMEKS field. Offshore Western Niger Delta 25.
Opuwari, M., Afolayan, B., Mohammed, S., Amaechi, P.O., Bareja, Y., Chatterjee, T., 2022. Petrophysical core-based zonation of OW oilfield in the Bredasdorp Basin South Africa. Sci. Rep. 12, 510. https://doi.org/10.1038/s41598-021-04447-6.
Pauken, R.J., 1992. Sanaga sud field, offshore Cameroon, west africa. In: Halbouty, M.T. (Ed.), Giant Oil and Gas Fields of the Decade 1978–1988, vol. 54. AAPG Bull, pp. 217–230.
Qadri, S.M.T., Shalaby, M.R., Islam, M.A., 2019. Application of well log analysis to estimate the petrophysical parameters and evaluate the reservoir quality of the Lower Goru Formation, Lower Indus Basin, Pakistan. Geomech Geophys Geoenergy Georesour. https://doi.org/10.1007/s40948-019-00112-5.
Qadri, S.M.T., Islam, M.A., Shalaby, M.R., El-Aal, A.K.A., 2020. Reservoir quality evaluation of the Farewell sandstone by integrating sedimentological and well log analysis in the Kupe South Field, Taranaki Basin-New Zealand. Journal of Petroleum Exploration and Production 11, 11–31.
Qi, B.W., Lin, C.M., Qiu, G.Q., Li, Y.L., Liu, H.M., Gao, Y.J., 2006. Formation mechanism of calcareous incrustation in lenticular sandbody of the shahejie formation of paleogene and its influence on hydrocarbon accumulation in Dongying Sag. J. Palaeogeogr. 8, 519–530.
Rabinowitz, P., LaBrecque, J., 1979. The mesozoic South Atlantic ocean and evolution of its continental margins. J. Geophys. Res. 84 (B11), 5973–6002.
Radwan, A.A., Nabawy, B.S., Abdelmaksoud, A., Lashin, A., 2021. Integrated sedimentological and petrophysical characterization for clastic reservoirs: a case study from New Zealand. J. Nat. Gas Sci. Eng. 88, 103797 https://doi.org/10.1016/j.jngse.2021.103797.
Regnoult, 1986. Synthèse géologique du Cameroun. DMG, Yaoundé, Cameroun 118.
Rider, M.H., 1996. Geological Interpretation of Well Logs. French Consultant Ltd., Scotland.
Sarhan, M.A., 2021. Geophysical and hydrocarbon prospect evaluation of nukhul formation at Rabeh East oil field, southern Gulf of Suez Basin, Egypt. J. Pet. Explor. Prod. Technol. 11 (7), 2877–2890.
Schlumberger, 1989. Log Interpretation Principles/Applications. Schlumberger, USA.
Secke Bekonga Gouott, B., Mbida, Yem, Yene Atangana, J.Q., Nkoa Nkoa, P.E., Angoua Biouele, S.E., Niyazi, Y., Eruteya, O.E., 2022. Seismic geomorphology of a Late Cretaceous submarine channel system in the Kribi/Campo sub-basin, offshore Cameroon. Mar. Petrol. Geol. 145, 105865 https://doi.org/10.1016/j.marpetgeo.2022.105865.
Shier, D.E., 2004. Petrophysics 45 (2004), 268–280. ; 12 figures. Petrophysics, 45, 268.
Simon Petroleum and Technology, 1995. Petroleum Geology and Hydrocarbon Potential of the Douala Basin, Cameroon Unpubl. Non-exclusive Report.
SNH/UD, 2005. Stratigraphie séquentielle et tectonique des dépôts mésozoïques syn-rifts du Bassin de Kribi/Campo, Auteurs. In: Ntamak-Nida, M.J., Mpesse, J.E., Ketchemen-Tandia, B., Ndong Ondo, S., Courville, P., Baudin, F. (Eds.), Rapport Interne, 11 Planches. 02 Rapports Annexes D'analyses, p. 134.
Srodo'n, J., 1999. Use of clay minerals in constructing geological processes: recent advances and some perspectives. Clay Miner. 34, 27–37.
Sterling Cameroon Limited, 2010. Prospectivity Review of the Ntem Block (PH-78) in the Douala/Kribi-Campo Basin. Unpubl. Non-exclusive Report.
Sun, Z.X., Sun, Z.L., Lu, H.J., Yin, X.J., 2010. Characteristics of carbonate cements in sandstone reservoirs: a case from yanchang formation, middle and Southern Ordos Basin, China. Petrol. Explor. Dev. 37, 543–551. https://doi.org/10.1016/S1876-3804(10)60054-7.
Tamfu, S.F., Batupe, M., Pauken, R.J., Boatwright, D.C., 1995. Geological setting, stratigraphy and hydrocarbon habitat of the Douala Basin, Cameroon. Am. Assoc. Petrol. Geol. Bull. 79, 13–95.
Taylor, T.R., Stancliffe, R., Macaulay, C.I., Hathon, L.A., 2004. High temperature quartz cementation and the timing of hydrocarbon accumulation in the Jurassic Norphlet sandstone, offshore Gulf of Mexico, U.S.A. In: Cubit, J.M., England, W.A., Larter, S. (Eds.), Understanding Petroleum Reservoirs: towards an Integrated Reservoir Engineering and Geochemical Approach, vol. 237. Special Publication, London, pp. 257–278. Geological Society.
Tiab, D., Donaldson, E.C., 2012. Petrophysics: Theory and Practice of Measuring Reservoir Rock and Fluid Transport Properties. Gulf Professional Publishing, Houston, Texas, p. 950.
Tiyan, Y., Ayers, W.B., 2010. Barnett Shale (Mississippian), Fort Worth Basin, Texas: regional variations in gas and oil production and reservoir properties CSUG/SPE 137766. In: Canadian Unconventional Resources and International Petroleum Conference Calgary, Alberta. Canada. https://doi.org/10.2118/137766-MS, 19–21 October.
Wang, F.R., He, S., He, Z.L., 2009. Carbonate cements features and its genetic significance of sandstones in Yongjin Area of Junggar Basin. Acta Petrol et Mineralogica 28, 169–178.
Wilson, P.G., Turner, J.P., Westbrook, G.K., 2003. Structural architecture of the ocean-continent boundary at a transform margin through deep-imaging seismic interpretation and gravity modelling: Equatorial Guinea, West Africa. Tectonophysics 374, 19–40.
Yugye, J.A., Chavom, B.M., Chima, K.I., N'nanga, A., Angoua Biouele, S.E., Nkoa Nkoa, P.E., Ngos III, S., 2022. Seismic-stratigraphic analysis and depositional architecture of the Cenozoic Kribi-Campo sub-basin offshore deposits (Cameroon): Seismic attributes approach and implication for the hydrocarbon prospectivity. J. Afr. Earth Sci. 194, 104621 https://doi.org/10.1016/j.jafrearsci.2022.104621.
Yugye, J.A., Ngos III, S., Angoua Biouele, S.E., Nkoa Nkoa, P.E., 2021. Seismic stratigraphic interpretation and modeling of offshore synrift and postrift Cretaceous sequences in the Kribi-Campo sub-basin, southern Cameroon. Am Assoc Pet Geol Bull 105 (11), 1–20. https://doi.org/10.1306/06092118040.
Zhang, M.Q., Huang, S.J., Wu, Z.X., Hu, Z.W., 2007. Carbonate cements and their formation mechanism in palaeogene sandstones of Lishui Sag, East China Sea Basin. J. Chengdu Univ. Technol. (Sci. Technol. Ed.) 34, 259–266.
Zhang, Y.W., Zeng, J.H., Gao, X., Zhou, S.Y., 2009. Distribution characteristics and main controlling factors of carbonate cements in the paleogene reservoirs in dongying depression. J. Jilin Univ. (Earth Sci. Ed.) 39, 16–22.
Zhu, P.Y., You, L., Yuan, Q.T., Zhong, J., Liu, A.Q., 2018. Mechanism and distribution of calcareous interbeds in songtao uplift and its periphery of Qiongdongnan Basin. Open J Marine Sci 8, 370–385.

Marine and Petroleum Geology 145 (2022) 105865

Contents lists available at ScienceDirect

Marine and Petroleum Geology

journal homepage: www.elsevier.com/locate/marpetgeo

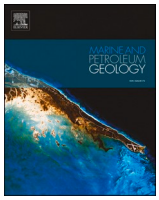

Seismic geomorphology of a Late Cretaceous submarine channel system in the Kribi/Campo sub-basin, offshore Cameroon

Boris Secke Bekonga Gouott [a,b,*], Mbida Yem [a], Joseph Quentin Yene Atangana [a], Pierre Eric Nkoa Nkoa [c], Serge Edouard Angoua Biouele [c], Yakufu Niyazi [d], Ovie Emmanuel Eruteya [e]

[a] University of Yaoundé I, Faculty of Science, Department of Earth Sciences, P.O. Box: 812, Yaoundé, Cameroon
[b] Centre for Geological and Mining Research, PO. Box: 333, Garoua, Cameroon
[c] National Hydrocarbon Corporation (NHC), P.O. Box: 955, Yaoundé, Cameroon
[d] School of Life and Environmental Sciences, Deakin University, Warrnambool, Victoria, 3280, Australia
[e] Department of Earth Sciences, University of Geneva, Geneva, 1205, Switzerland

ARTICLE INFO

Keywords:
3D seismic
Seismic geomorphology
Submarine channel
Kribi-Campo sub-basin
Offshore Cameroon

ABSTRACT

In this study, a 3D seismic reflection dataset and well-log data were integrated to investigate the geometry and internal configuration of a submarine channel system within the Late Cretaceous interval of the deep-water Kribi-Campo sub-basin, offshore Cameroon. This interval is characterized by a well-developed submarine channel system consisting of an early and a late-stage channel. Morphologically, the submarine channel system has a northeast-southwest trend and is U-shaped in cross-section with a length of 56 km within the study area. The early-stage channel has a relatively straight morphology and varies in width and depth from 3 to 5 km and 89–197 m, respectively. However, the late stage of the channel is characterized by a narrower (1–3 km) and shallower (41–103 m) incision, with sinuous morphology carved into the early channel infill. The changing interaction of differential local tectonic, relative sea level, source sediment supply and change in slope gradient are the major control on the geometry and internal characteristics of the submarine channel system. At local scale, basin tectonics is associated with the development of a structural high, controlling submarine channel morphology and depositional patterns in these filled ponded basins. The filling of the channel system coincided with the long-term Maastrichtian relative sea level rise, punctuated by higher order falls in relative sea level. Sand appears to have been fed to the channel system by the palaeo-Sanaga and palaeo-Nyong Rivers, with sand rich aprons developed were these rivers crossed into the study area. The early-stage of the submarine channel is dominated by coarse-grained sediments in the southwest and fine-grained sediments in the northeast, while the late-stage channel is mainly filled with fine-grained sediments. The presence of coarse-grained sediments occurring within the submarine channel axis downstream represents a potential for hydrocarbon reservoirs. The 3D seismic geomorphological analysis of this ancient submarine channel system along the western African margin, as presented in this study, has broad implications in the understanding of the distribution of deep-water sediments with potential for hydrocarbon exploration in the region.

1. Introduction

Deep-water turbidite channel systems are important submarine features formed by the erosion, diversion, and deposition of turbidity currents and other sediment loads and flows (Shepard, 1981; Peakall and Sumner, 2015; Chiang et al., 2020; Tek et al., 2021). Submarine channels are a vital component of ancient and modern deep-water settings and play an essential role in transporting sediments into the deep-sea (Stow and Mayall, 2000; Normark and Carlson, 2003; Posamentier and Kolla, 2003; Mayall et al., 2006; Posamentier and Walker, 2006; Shanmugam, 2006; Gamboa et al., 2012; Chima et al., 2019). Deep-water sediments within these channels record paleoclimatic and oceanographic information and are crucial in understanding the geological evolution of sedimentary basins (Marsset et al., 2009; Jobe

* Corresponding author. University of Yaoundé I, Faculty of Science, Department of Earth Sciences, P.O. Box: 812, Yaoundé, Cameroon.
E-mail address: bsecke@yahoo.fr (B. Secke Bekonga Gouott).

https://doi.org/10.1016/j.marpetgeo.2022.105865
Received 2 September 2021; Received in revised form 30 June 2022; Accepted 4 August 2022
Available online 18 August 2022

et al., 2015; Picot et al., 2016; Hansen et al., 2017; Niyazi et al., 2018; Chima et al., 2020). Deep-water sediments transported by submarine channels are a potential host for significant hydrocarbon accumulations (Mayall et al., 2006; Wynn et al., 2007; Weimer et al., 2007; Di Celma et al., 2010; Jobe et al., 2015).

Previous studies have focused on the origin, depositional processes and factors controlling the emplacement, composition, and morphological evolution of submarine channels (Kane et al., 2008; Babonneau et al., 2010; Covault et al., 2014; Li and Gong, 2016; Sylvester and Covault, 2016; Li et al., 2020). Also, the increased availability of marine geophysical data has significantly improved the understanding of the architecture, morphometry and processes leading to submarine channel development (Abreu et al., 2003; Deptuck et al., 2003, 2007, 2012; Kolla et al., 2007; Sylvester et al., 2011; Mitchell et al., 2021). High-resolution 3D seismic reflection data has been used in many studies to investigate the geomorphologic character of deep-water systems, and their implication for hydrocarbon exploration in the offshore settings (Deptuck et al., 2007; McHargue et al., 2011; Jobe et al., 2011; Qin et al., 2016; Covault et al., 2019; Mitchell et al., 2021).

Submarine channels in the deep offshore West Africa (e.g., Niger Delta, Congo, and Gabon) are well studied using high-quality seismic reflection and borehole datasets provided by hydrocarbon exploration companies operating in these regions (Abreu et al., 2003; Le et al., 2014; Jolly et al., 2015; Huang, 2018; Chima et al., 2019, 2020; Chen et al., 2021). These channel systems include channel levee systems, terraces, intraslope fans and lobes, and are important for hydrocarbon exploration. Submarine channel systems form major repositories for coarse-grained sediment (reservoirs) deposited along channel axes, and for fine-grained sands and silts deposited on levees (seals/traps). These are the primary targets of interest during hydrocarbon exploration (Mayall et al., 2006). In addition, hydrocarbon reservoirs (e.g., Okume, Oveng, Ebano and Ceiba oil fields) in similar geological settings within the offshore West African Basins, have been found in the Santonian-Maastrichtian turbidite sediments in the offshore of Equatorial Guinea (Dailly et al., 2002; Sterling, 2010). Along the Cameroonian margin, various Miocene channels, and fan system across the Douala/Kribi-Campo Basin are also proven to be hydrocarbon-rich (SPT/Simon Petroleum and Technology, 1995; Loule et al., 2018).

Many submarine channels occur in the Late Cretaceous and Tertiary in the Kribi-Campo sub-basin (Le, 2012, 2021; Loule et al., 2018). During the Late Cretaceous in the study area, there are relatively low sinuosity channel systems and several distinctive large, compound channel systems (Loule et al., 2018). These compound geobodies formed from the superposition of separate channel-fill phases having individual channels which have similar widths to the low sinuosity channels (1000–1500 m). These two types of channels are controlled by the local tectonics (Loule et al., 2018). Also, in the Early Pliocene, deep-water channels occurring in the study area are characterized by high amplitude reflections with bi-directional downlap on the base of the Pliocene (Le, 2021). These Pliocene channels flowed from east to west in the High Gradient Slope (HGS). The occurrence of striated unconformity at the base of the Pliocene sequence, overlain by the channels suggests a period of slope failure and high sedimentation rate which is possibly the result of a major tectonic uplift event or significant climatic changes (Le, 2021).

The Kribi/Campo sub-basin hosts the South Sanaga and Kribi oil fields in deep-water turbidite sediments (Pauken et al., 1991; Pauken, 1992; Nguene et al., 1992; Ackerman et al., 1993; Tamfu et al., 1995; Brownfield and Charpentier, 2006; Ndonwie Mahbou, 2007). In contrast to the well-studied submarine channels and their implications for hydrocarbon exploration in the West African basins (e.g., Niger Delta, Congo, and Gabon), those in the Kribi/Campo sub-basin are poorly understood in terms of their architectural elements, morphological variations and factors controlling the distribution of turbidity sands (see Iboum Kissaaka et al., 2016; Loule et al., 2018; Yugye et al., 2021).

Therefore, this study aims to investigate and analyze the geometry and internal configuration of a newly mapped well-developed Late Cretaceous submarine channel system in the Kribi-Campo sub-basin. This was achieved through the analysis of a 3D seismic reflection data and borehole data. The findings from this study extend the understanding of the architectural and morphological evolution of deep-water channel systems in the Kribi-Campo sub-basin and elsewhere with similar settings and its implication deep-water hydrocarbon prospectivity.

2. Geological setting

The study area is located along the continental slope of the Kribi-Campo sub-basin approximately 40 km off the coast of Cameroon (Fig. 1). It is situated in water depths ranging from 600 to 2000 m (Fig. 1). The Douala/Kribi-Campo Basin is one of a series of continental shelf basins extending in West Africa from the edge of the Niger delta in Cameroon to the Walvis ridge near the Angola–Namibia border (Brownfield and Charpentier, 2006; Brownfield, 2016; Ntamak-Nida et al., 2008). The basin is divided into two sub-basins, namely the Douala sub-basin in the northern part and the Kribi-Campo sub-basin in the south (Fig. 1). The Kribi-Campo sub-basin extends over 6150 km^2 offshore and 45 km^2 in a triangular onshore area (Ntamak-Nida et al., 2010). This sub-basin is limited to the south by the Campo high, which formed as a rift basin that deepened to the northeast (Meyers et al., 1996), and it separates the Kribi-Campo sub-basin and Equatorial Guinea Rio Muni Basins. Its northern limit corresponds to the Kribi Fracture Zone, which stops the extension of the Douala sub-basin. At the east, the Precambrian basement outcrops occur close to the shoreline (Nguene et al., 1992; Ntamak-Nida et al., 2010). The offshore part of the basin, which was investigated in this study, covers an area of approximately 1500 km^2, between 2°20′ and 3°00′N, and 9°00 and 9°50′E (Fig. 1).

The evolution of the Kribi-Campo sub-basin is closely related to the opening of the South Atlantic Ocean following the rifting of South America and Africa (Rabinowitz and LaBrecque, 1979; Beglinger et al., 2012). This continental rifting propagated from the South to the North, commencing in the Late Jurassic and lasting until the onset of seafloor spreading in Albian-Cenomanian time. Rifting started in the Kribi-Campo sub-basin from Barremian to Aptian time corresponding to deposition of the lower Mundeck formation (Ntamak Nida et al., 2010; Le et al., 2014).

During the later passive margin phase, the basin experienced several additional regional tectonic events resulting in inversion and folding in the Santonian, and gravity sliding during Early/Mid/Late Tertiary time (Brownfield and Charpentier, 2006; Le, 2012, 2021). These events are marked by major unconformities including the Albian-Aptian break up unconformity (115 Ma), Middle Cretaceous (Santonian - ~ 85 Ma), Late Cretaceous (K/T boundary - ~ 70 Ma), and Mid-Oligocene (~30 Ma), Mid-Miocene (~15 Ma), and Late Tertiary event (~5.3 Ma) (Lawrence et al., 2002; Iboum Kissaaka et al., 2016; Le, 2021; Mienlam Essi et al., 2021; Yugye et al., 2021) (Fig. 2). Eight litho-stratigraphic units which comprises the Mundeck, Logbadjeck, Logbaba, N'Kapa, Souellaba, Kribi, Matanda and Wouri formations have been identified (Fig. 2). Previous studies have demonstrated the presence of submarine channels in the Logbaba Formation, which is the formation of interest in this study area and adjoining areas (Sterling, 2010; Le, 2012 and Loule et al., 2018).

Following the end Santonian uplift event, the basin returned to rapid thermal sag subsidence (SPT/Simon Petroleum and Technology, 1995). As a result, a thick succession of Campanian-Maastrichtian sediments (Logbaba Formation) drapes the underlying structures and lie slightly unconformably over the Santonian (Logbadjeck Formation). The rapid subsidence caused a significant phase of halokinesis along the margin of the Kribi-Campo High (Nguene et al., 1992; SPT/Simon Petroleum and Technology, 1995). This Santonian tectonic event with its associated uplift led to the deposition of thick late Cretaceous clastics characterized by slope and basin floor fans containing multiple channel complexes

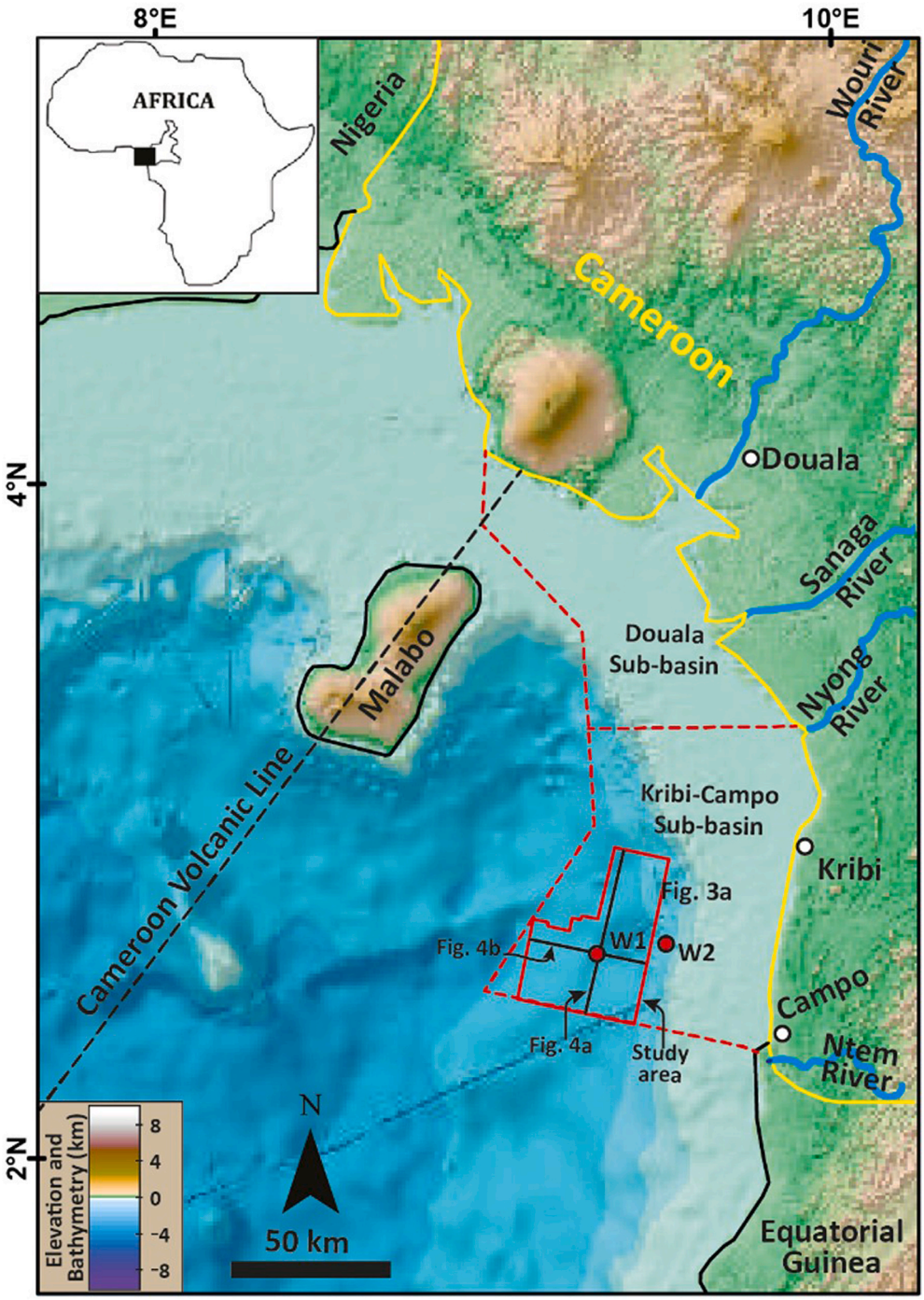

Fig. 1. Superimposed relief and bathymetric map of Cameroon, showing the location of the study area. Insert map on the left-hand corner of the map shows the location of Cameroon in the Gulf of Guinea. The 3D block, which we studied is outlined in red box, while the red circles with black outlines labelled W1 and W2, represent well locations (Modified from Le et al., 2014; Loule et al., 2018; Le, 2021). (For interpretation of the references to colour in this figure legend, the reader is referred to the Web version of this article.)

(Sterling, 2010; Le, 2012, 2021). A series of eustatic lowstands during the Campanian-Maastrichtian and the Santonian uplift facilitated the episodic transport of major clastic sequences across the relatively narrow shelf into the deeper basin to the west (i.e., in the study area) (Fig. 2). Sterling (2010) estimated that an excess of 1500–2000 m of Senonian deep-water clastic sediments were deposited in the study area during this phase of post-rift sedimentation.

Sag subsidence during the Campanian led to basin deepening and the widespread development of basinal sediments. Continued halokinesis in the south of the basin may have led to complex turbidite sand distribution. Eustatic sea-level fall during the Maastrichtian (Nguene et al., 1992; Seiglie and Baker, 1984) resulted in the progressive westward progradation of the shelf. Sand appears to have been fed to the basin by the palaeo-Ntem, palaeo-Sanaga and palaeo-Nyong Rivers, with sand rich aprons developed were these rivers debouched into the basin (SPT/Simon Petroleum and Technology, 1995). During the Early Tertiary, relative sea-level fall resulted in slumping and collapse of shelf-slope sediments and deposition of mounds on the Kribi-Campo basin floor (Iboum Kissaaka et al., 2016 and Le, 2021). An intra-Miocene unconformity marks an incision surface, with the development of canyons cutting down into underlying sediments. In the more proximal settings (i.e., east of Kribi-Campo High), there are multiple submarine incisions several kilometres wide and some amalgamated cut-and-fill submarine channel complexes downslope and parallel to present-day shelf-break in most of the Paleocene section (Wornardt et al., 1999; Le, 2012; Iboum Kissaaka et al., 2016). The late

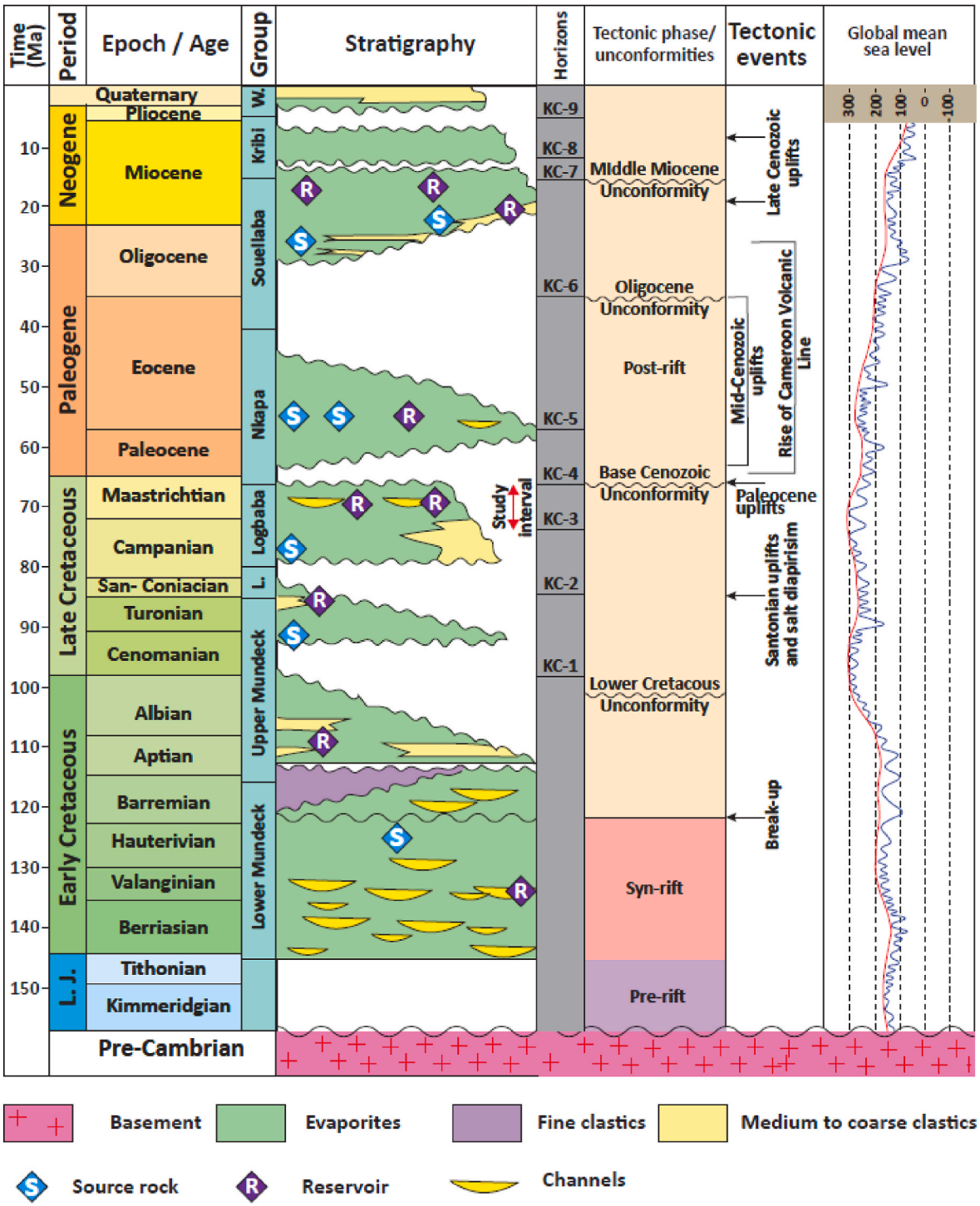

Fig. 2. Stratigraphic column of the Kribi-Campo Sub-basin showing the tectono-sedimentary phases and global mean sea level (Modified from Pauken, 1992; Lawrence et al., 2002; CGG Robertson, 2015; Iboum Kissaaka et al., 2016).

Eocene-early Oligocene tectonic event facilitated a relative sea-level fall, responsible for the widespread erosion and non-deposition in the deep-water of the basin (Wornardt et al., 1999; Helm, 2009; Mvondo, 2010; Iboum Kissaaka et al., 2016; Ngo et al., 2018; Le, 2021) (Fig. 2). Following this period of non-deposition, a thick Miocene-Pliocene clastic wedge originating from a combination of multiple continental paleo-river drainage systems (e.g., Proto-Sanaga, proto-Nyong and proto-Ntem River systems), prograded across the narrow shelf area (Sterling, 2010; Le, 2012). Sediments prograded down the steeply dipping fault margin into the offshore Kribi-Campo sub-basin and deposited a thick sequence of sand-rich turbiditic channels (Sterling, 2010; Le, 2012).

3. Dataset and methods

3.1. Dataset

The datasets analyzed in this study consist of a high-resolution 3D seismic reflection survey and borehole data from the Kribi-Campo Sub-basin offshore Cameroon (Fig. 1).

3.1.1. Seismic data

The 3D seismic survey is a pre-stack time migrated (PSTM) dataset that covers an area of about 1500 km^2 in water depths ranging between 600 m and 2000 m (Fig. 1). It was acquired using 10 streamers, with a 12.5 m group interval. The separation between the streamers was 100 m, with a spatial resolution of 25 × 25 m. It includes 1581 in-lines and 2051 crosslines with lines spacing of 25 m and a seismic recording sampling interval of 2 ms two-way travel time (TWT). The seismic survey was processed as a zero-phase at the seabed and displayed using the Society of Exploration Geophysicists (SEG) normal polarity (Brown, 2004). Hence, a positive event represents a downward increase in acoustic impedance (red, yellow, or orange reflection on seismic sections), and a negative event represents a downward decrease in acoustic impedance (blue reflection on seismic profiles) (Fig. 3). The seismic dataset reaches 6.6 s TWT. The dominant frequency of the data is 17 Hz for the Late Cretaceous and 45 Hz in the Cenozoic resulting in a vertical resolution ($\lambda/4$) of ~28 m and ~10 m, respectively (Le, 2012, 2021), with an average velocity of 2400 m/s derived from the check-shot data in the interval of interest (4000–5000 ms).

3.1.2. Well data

The study integrates well log data (gamma rays, resistivity, density, neutron, and sonic logging) from two offshore wells, W1 and W2 (Fig. 1). W1 reached a total depth of 4747 m and W2 a total depth of 4090 m below the seafloor corresponding to a stratigraphic interval ranging between Albian to Recent. The wells cover the Late Cretaceous interval and biostratigraphic data were available. Formations tops of the two wells and the checkshots data for the well W1 were used to correlate the seismic and borehole data. Well data from the W1 wellbore were used to constrain the lithology and ages of the different horizons and sedimentary intervals interpreted.

3.2. Methods

3.2.1. Seismic stratigraphy

The approach used here consists of the seismic interpretation of ten horizons (KC-1 to KC-9, and the seafloor) (Fig. 2). These seismic horizons were tied to the well W1 using the checkshot data. The interval of interest was divided into two main seismic units based on the characteristics (amplitude, frequency, and continuity) of the seismic reflections and the recognition of reflection termination patterns such as onlap, erosional truncations, seismic facies/configuration, and vertical stacking patterns (Mitchum et al., 1977). In the present study, submarine channel systems and submarine fans were identified based on seismic criteria and 3D geomorphology in both cross sections and plan-view maps (e.g., Posamentier and Kolla, 2003; Loule et al., 2018).

3.2.2. 3D seismic geomorphology

Identification and mapping of the submarine channels were achieved using a 3D seismic geomorphological approach (Zeng et al., 1998; Zeng and Ambrose, 2001; Posamentier and Kolla, 2003; Brown, 2004; Kolla et al., 2007; Niyazi et al., 2018; Chima et al., 2020). Seismic attributes such as RMS (Root Mean Square) amplitude and variance, were extracted along the horizons to illuminate and visualize the channels as well as to characterize geological anomalies that are isolated from background features by means of an amplitude response (Taner, 2001). The RMS amplitude maps are mathematically computed by squaring individual traces over a defined time window (Brown, 2004; Omosanya and Alves, 2013). They boost high amplitudes in an interpreted interval, allowing the amplitude reflections related to sands or other high-density

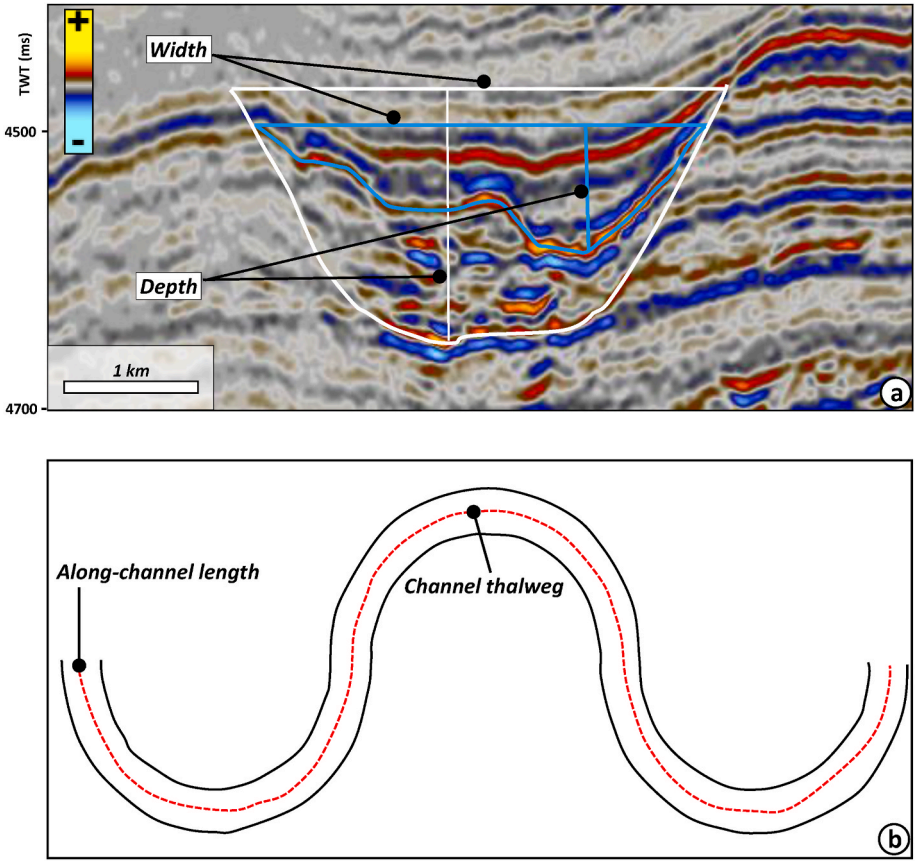

Fig. 3. a) A seismic cross section showing the definition of width and depth as used in this paper. The distances between two intersection points on the top surface and the left/right boundary are defined as the width, the vertical distance between the thalweg and the top surface as the depth. b) Schematic diagram showing the definition of the along channel length and channel thalweg.

materials within channels to be discriminated from their associated low amplitude chaotic facies (Brown, 2004; Omosanya and Alves, 2013; Chima et al., 2019). Variance is the direct measurement of the dissimilarity of seismic traces. Variance maps convert a volume of continuity into a volume of discontinuity, highlighting structural and stratigraphic boundaries (Brown, 2004; Niyazi et al., 2020, 2021). Features identified in the variance time slices were also used as additional verification for the seismic sections. For example, the channels are characterized as truncating the underlying seismic reflections and onlapping on their margins and by contrasting amplitudes between their fill and adjacent overbank deposits (Gamboa et al., 2012; Harishidayat et al., 2018; Omosanya and Alves, 2013). In this study, we generated a series of RMS and variance time slices to analyze the evolution of the submarine channel system during different periods.

3.2.3. Quantitative analysis of submarine channel

In addition to classical seismic stratigraphic methods, the quantitative analysis of the seismic geomorphology of submarine channels was performed following the methodologies proposed by Deptuck et al. (2007), Gamboa and Alves (2015), Qin et al. (2016), Hansen et al. (2017), Harishidayat et al. (2018) and Zhao et al. (2018). Morphometric parameters such as width (defined as the distance between the banks of the channel system), depth (defined as the depth of the channel from their overspill points to their bases), and depth of the channel thalweg (defined as a middle point of the channel walls and the lowest point of the erosional surface), were measured in cross-sectional seismic profiles (Fig. 3). These seismic profiles are perpendicular to the channel axis and are located at an interval of 1 km (average). The zero point was defined as the northernmost limit of the channel. The thalweg depth (in s TWT) was converted to depth (in m) using the time-depth relationship

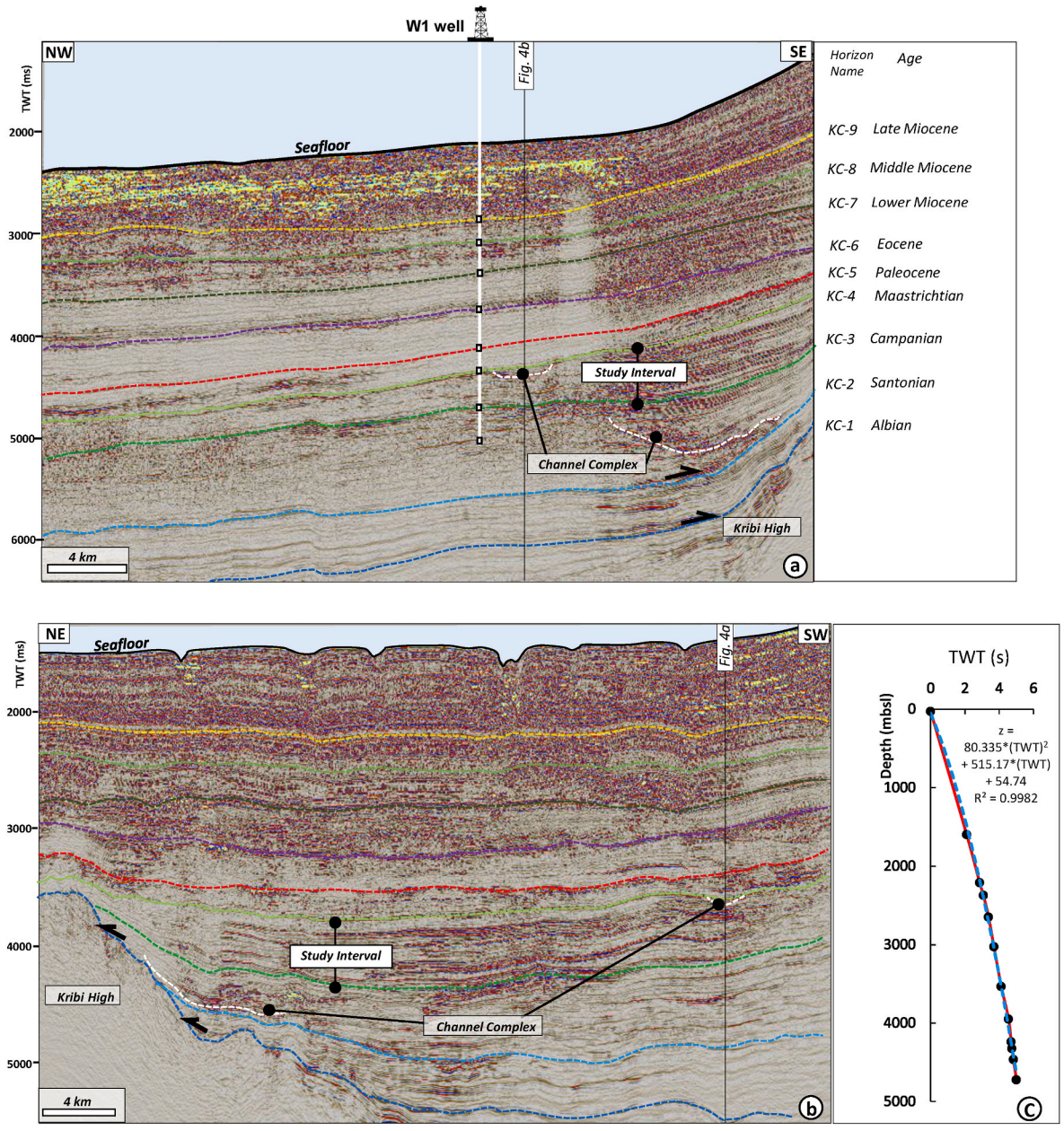

Fig. 4. a) Seismic line through W1 well showing the entire basin successions and channel complex deposits identified within the dataset. Ten Horizon name (KC-1 to KC-9 and the seafloor) are identified in the study area based on Le (2012); Iboum Kissaaka et al. (2016) and Loule et al. (2018). b) Seismic section, taken perpendicular to regional dip, showing the channel complex deposits within the study interval. The location of the seismic section is shown in Fig. 1 **c)** Depth conversion scheme.

produced from checkshot data available of Well W1 (Fig. 4c). Furthermore, the channel gradient was calculated based on changes in thalweg depth along the axis of the channel. For this purpose, the thalweg depth was measured on each profile along the channel. Subsequently, the paleo-topography on which the channel developed was divided into windows with different average gradient segments depending on the magnitude of the thalweg depth variations on the profiles. Vertical and horizontal distances (the vertical distance must be converted into depth profiles) between the starting and ending points of these windows were measured. Then final gradients were measured based on the arc tangent function (Deptuck et al., 2007; Gamboa and Alves, 2015; Qin et al., 2016; Harishidayat et al., 2018; Zhao et al., 2018).

4. Results and interpretation

4.1. Seismic stratigraphy of the study area

The interpreted ten horizons (KC-1 to KC-9 and the seafloor) were used to describe the seismic stratigraphic framework of the study area (Fig. 4). KC-1 to KC-9 horizons correspond to the Top Albian, Santonian, Campanian, Maastrichtian, Paleocene, Eocene, lower Miocene, middle Miocene, late Miocene, respectively (Le, 2012; Iboum Kissaaka et al., 2016). The interval of interest in the study area is bounded by the KC-3 and KC-4 horizons at the base and top, respectively. This interval is characterized by distinctive seismic facies of the Campanian-Maastrichtian Logbaba Formation (Fig. 4).

The KC-3 is located at approximately 4900 ms TWT and is characterized by a high-amplitude positive reflection with good continuity (Fig. 4). This horizon is characterized by onlap above the Kribi High area and defines the base of the stack of high to bright amplitude reflection laterally migrating westward. This probably corresponds to a turbidite fan system which extends from the east to the southern half of the study area (Fig. 5). Based on its seismic characteristics and according to Le (2012); the surface KC-3 corresponds to an unconformity in the study area which progressively shows greater truncation of underlying sequences toward the upper slope (Fig. 4). The isochore map shows values ranging from −3700 ms upstream to −5100 ms downstream (Fig. 6a). These two extreme values correspond respectively to a high and low topographic area on either side of the study area (Fig. 6a). It is separated by a steep slope on the east that decreases towards the seabed. The horizon KC-4 is located at approximately 4600 ms TWT and is also a positive reflection with high amplitude. The horizon is characterized by downlaps onto an erosional surface and separates the overlying high to moderate frequency, low to moderate amplitude reflection packages from the underlying low to moderate frequency, and high to moderate amplitude reflection packages (Fig. 5). The isochore map shows values ranging from −3200 ms to −4800 ms, respectively, at two downstream and upstream ends of the sub-basin (Fig. 6b). The contours lines of this

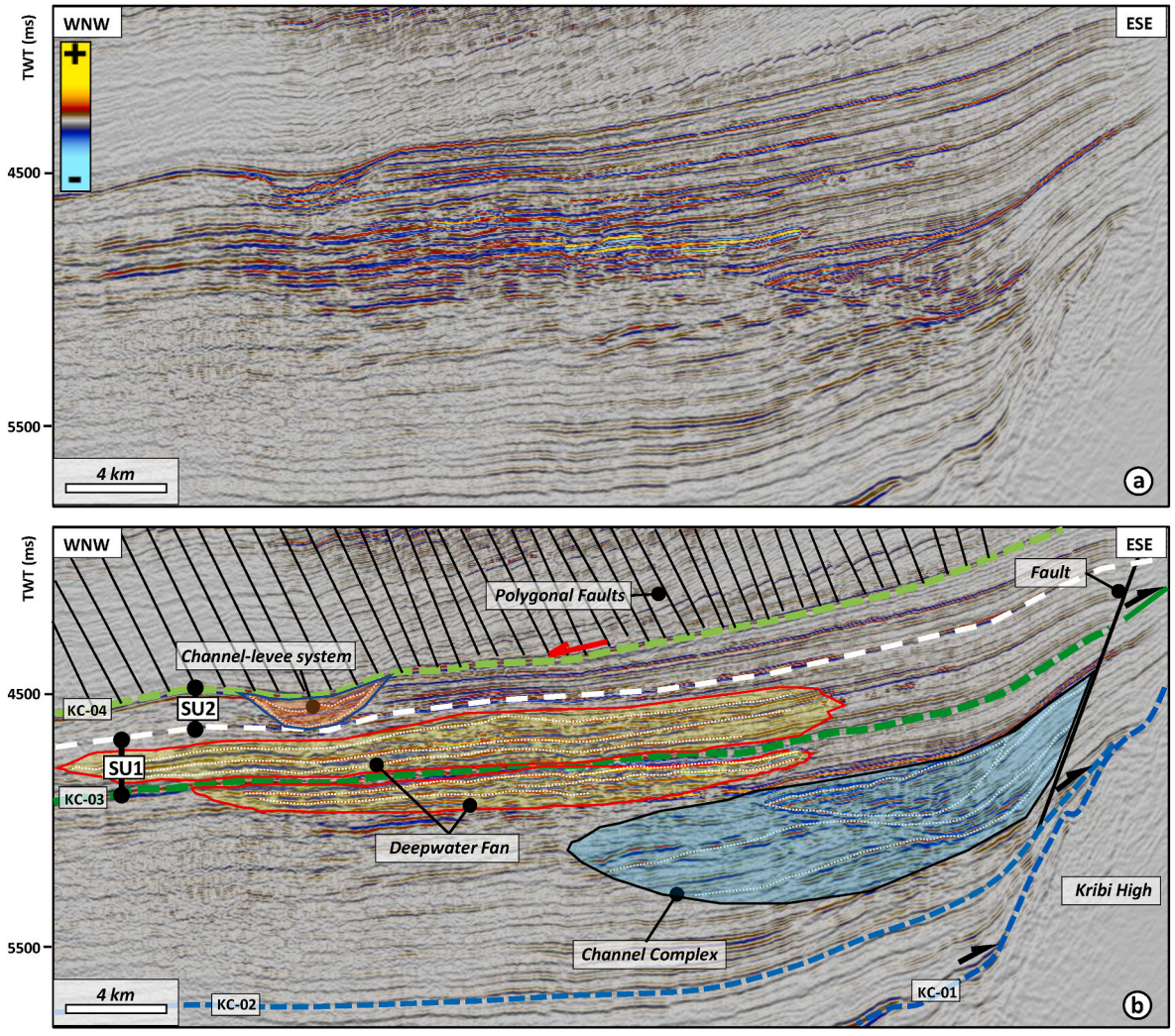

Fig. 5. Along the slope seismic profile showing. a) Uninterpreted and (b) The interpreted seismic stratigraphy of the slope. The submarine channel system is located within unit (SU2) and deep-water fan is located within (SU1) in the study interval.

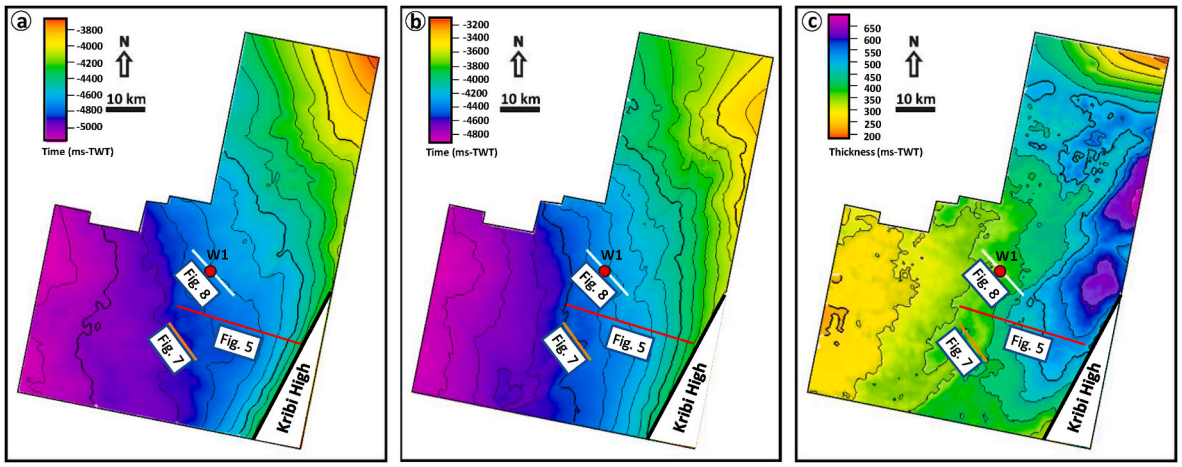

Fig. 6. a) Isochronal map of the KC 03 horizon. b) Isochronal map of the KC 04 horizon. c) Isopach map of Late Cretaceous between KC 03 and KC 04.

map have a preferred NE-SW direction (Fig. 6b).

The surface KC-4 is incised by a NE-SW trending channel and covers the Kribi High in the east (Fig. 4a and b). On the basin floor at the more distal end of the large incision (i.e., around W1), the surface marks the base of the relatively low-amplitude Tertiary package (Fig. 4a). This contrasts with the underlying Cretaceous sequences which in cross-section are more channelized and display higher amplitudes (Fig. 5). The thickest area reaches 1560 m (Vp = 2400 m/s) in the east, and the average thickness of the unit is 1080 m (Fig. 6c).

The interval of interest in this study (Campanian-Maastrichtian succession) has been divided into two seismic sub-units: seismic sub-unit 1 (SU1) and seismic sub-unit (SU2) based on the differences in the internal seismic reflection configurations (Fig. 5). SU1 consists of sub parallel and aggradational reflections (Fig. 5). SU1 is generally characterized by low amplitudes reflections with limited occurrence of high amplitude reflections and displays maximum thickness in the east (Fig. 5). The high amplitude seismic facies display an aggradational pattern with parallel and continuous reflections having a fan-shaped geometry (Table 1, Fig. 5). SU2 forms the uppermost sub-unit in the Late Cretaceous, and consists of low to high amplitude, sub-parallel and continuous reflectors. A large incision occurs within this unit, which is interpreted as a submarine channel, characterized by high-amplitude reflections at its base (Table 1, Fig. 5).

4.2. *Late Cretaceous submarine channel*

4.2.1. *Channel infill: distribution of seismic facies and interpretation*

Five seismic facies (SF1 to SF5) were identified in the study interval

Table 1
Description and the interpretation of the seismic facies observed in the submarine channel system within the study interval.

Seismic facies	Seismic profile	Schematic	Description	Plan/Map view	Interpretation
SF1	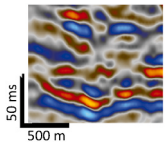	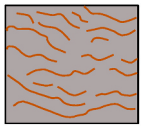	Chaotic, high amplitude, discontinuous reflections, basal lags usually confined within a U- shaped erosional surface	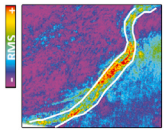	Coarse-grained channel fill
SF2	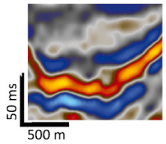	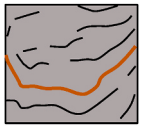	Low to high amplitude, discontinuous to chaotic reflections, with a U- shaped external geometry	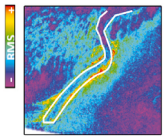	Fine-grained Channel fill
SF3	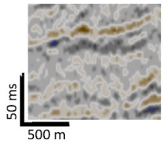	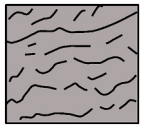	Semi transparent, low amplitude, semi-continuous to continuous reflections	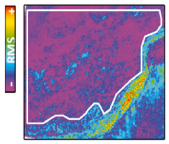	Hemipelagic sediments
SF4	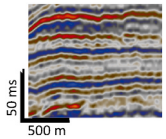	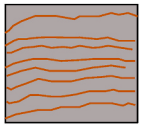	high- to low-amplitude, continuous, parallel to subparallel reflections	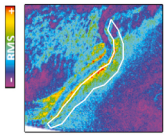	Levee deposits
SF5	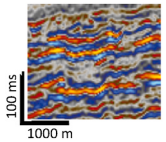	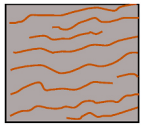	High amplitude seismic facies displaying an aggradational pattern with parallel and good continuity reflectors	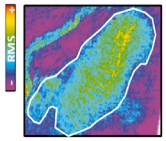	Turbidites fan system

and can be interpreted to represent five specific depositional settings in the area of interest (Table 1).

SF1 consists of high amplitude, chaotic reflections confined within a U-shaped erosional surface in cross section (Fig. 7b and c). In plan-view, SF1 is expressed as a more linear morphology compared to SF2 (Fig. 9). It occurs at the basal lags of the early-stage channel. This facies is interpreted as coarse-grained sediments deposited in the submarine channel axis (Mayall et al., 2006; Gee et al., 2007) (Fig. 9).

SF2 consists of low-amplitude, discontinuous to chaotic reflections, with a U- shaped external geometry (41–103 m depth, 1–3 km wide) in cross section (Fig. 7). SF2 is narrow and has a sinuous morphology in map-view (Fig. 9). This facies is interpreted as clay-prone channel fills that may record earlier channel bypassing (of coarse-grained sediments) and later abandonment (deposition of fine-grained sediments).

SF3 is composed of low-amplitude, discontinuous to continuous seismic reflections and occurs in the background unit that encompasses the submarine channel (Fig. 7b and c; Table 1). It occurs in the entire seismic volume on the map-view outside the submarine channel system (Fig. 9). SF3 can be interpreted as hemipelagic sediments (Fig. 9); SF3 is similar to those ofhemipelagic sediments as observed in other studies (e.g., Su et al., 2015; Gong et al., 2016).

SF4 is comprised of high-to low-amplitude, convergent reflections that show a broadly wedge-shaped geometry in cross section (Fig. 7b and c). This facies is widely recognized elsewhere and interpreted to represent levees deposits (Table 1) formed of fine-grained sediments from the overbanking of turbidity currents (e.g., Posamentier and Kolla, 2003; Deptuck et al., 2003; Catterall et al., 2010; Janocko et al., 2013).

SF5 is characterized by high-amplitude reflection displaying an aggradational pattern in cross-section (Table 1) and it is located below the submarine channel system in sub-unit SU1 (Fig. 5b). In map view, it

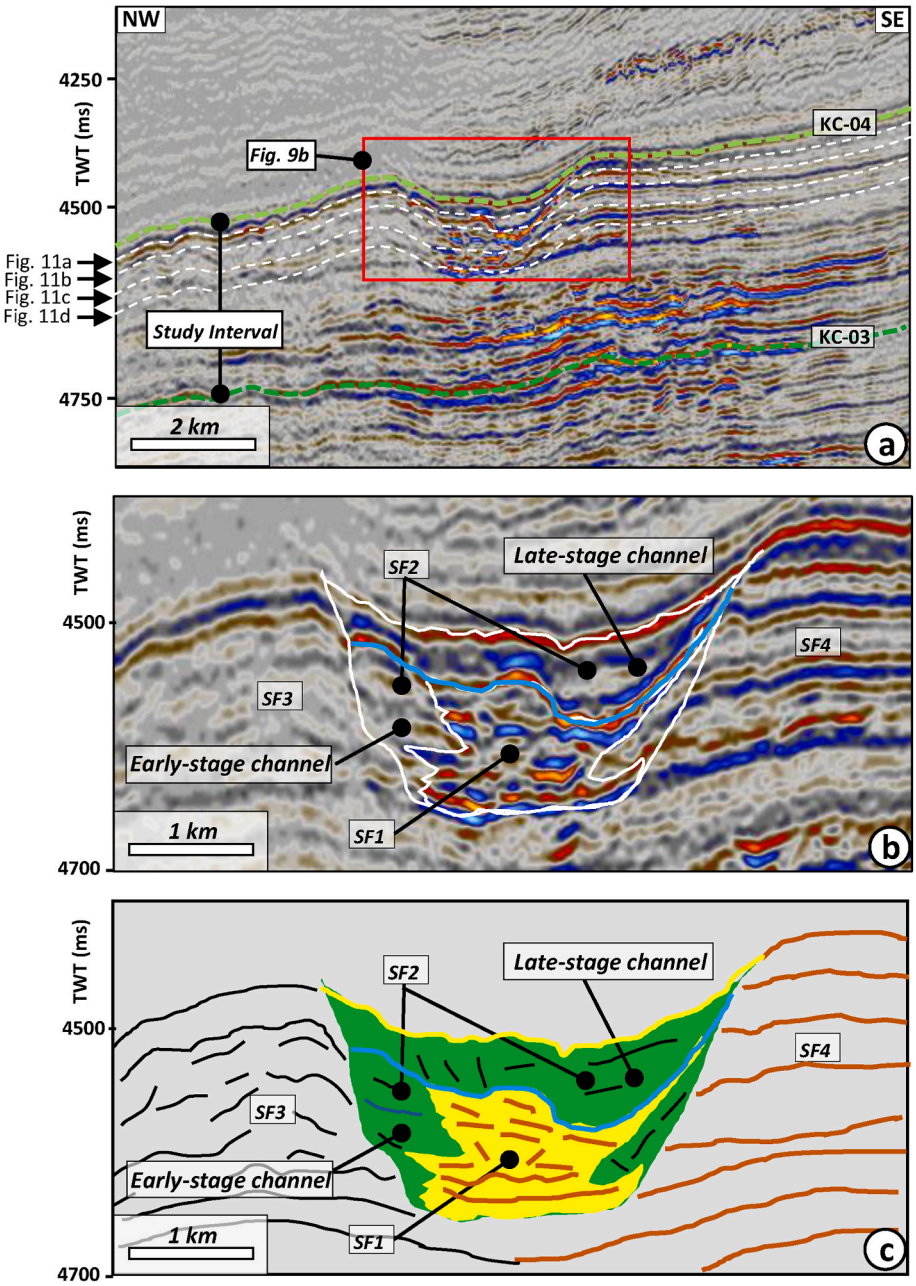

Fig. 7. a) Seismic profile showing the channel geometry is U-shaped and iso-proportional slice used to unravel the internal architecture of the channel. b) and c) Channel system is composed of two stages: early-stage channel and late-stage channel. SF1 is coarse while SF2 is fine sediments. The submarine channel is 56 km long and 3–5 km wide with an incision depth of 89–197 m.

occurs in the SE part of the study area (Fig. 9c and d). This facies correspond to the sand body which can be interpreted to fan deposits, and it is like those observed and described by Twichell et al. (2009).

4.2.2. Internal architecture and geometry of the submarine channel

The submarine channel observed in unit SU2 is U-shaped in cross-section (Fig. 7). It has two vertically stacked channels that developed at different stages. The late-stage channel lies completely within the early-stage channel, and both exhibit distinct seismic reflection characteristics (Fig. 7b and c). The early-stage of the channel is characterized by seismic facies SF1 and SF2. Seismic facies SF1 is mainly located along the thalweg of the early-stage of the channel. It occurs at the base of submarine channel analyzed in this study (Fig. 7b and c). Seismic reflection characteristics of this facies is like those of the channel axial deposits described by Deptuck et al. (2003), Mayall et al. (2006) and Catterall et al. (2010). SF2 is usually confined at the flanks of the channel (Fig. 7b and c). Specifically, the late-stage channel is embedded in this facies (Fig. 7b and c). The late-stage of the channel is dominated by the SF2. In addition, SF1 and SF2 are within the channel system, while SF3 and SF4 are located outside the system (Fig. 7b and c). SF3, mainly occurs in SU2, and it confined to the left side of the submarine channel (Fig. 7b and c). SF4 is seen outside of the early channel belt and occurs only locally (Fig. 7; Table 1). These reflections typically dip away from the channel axis and decrease in amplitude away from the channel axis (Fig. 7b).

To analyze the evolutionary history and infilling of the submarine channel system, SU2 was divided into four intervals (Figs. 7a and 8). The well-log in the vicinity of the submarine channel system indicates that the thickness between the top and base of the channel is approximately 90 m (Fig. 8a). The gamma-ray is characterized by sharp-based (between 3900 m and 3850 m), finning upward pattern (between 3850 m and 3810 m). The basal coarse-grained lags of the early-stage channel in well W1 show a large kick in GR and display a serrate GR log motif with some blocky/bell-shaped intervals (Well W1 in Fig. 8a). The late-stage channel fills are mainly characterized by a serrate GR motif with some low-amplitude bell-shaped GR intervals (Fig. 8a). The well-log patterns of this submarine channel consist of clay interbedded with thin layers of sands (Fig. 8a). The early-stage channel is visible on all the maps and is characterized by relatively linear morphology (Fig. 9). The channel is 56 km long and 3–5 km wide (Fig. 9), with an incision depth of 89–197 m (Fig. 10). In contrast, at the late-stage, the channel could only be imaged in the upper two slices, showing that it incises the infillings of the early-stage channel (Fig. 9a and b). The RMS and variance values also characterize the channel fills in the horizon slices. The high RMS amplitudes and low variance occur within the submarine channel axis. The channel also locally incises areas of high RMS amplitudes and low variances, characterized by lobate geometry outside the channel axis (Fig. 9). The low RMS values and high variances are observed in the northeast part of the channel while the high RMS values and low variances are observed in the southwest part of the channel (Fig. 9d). This high amplitude RMS channel fill observed in the horizon slice corresponds in cross section to seismic facies SF1 and the low amplitude RMS fill corresponds to seismic facies SF2. The late-stage channel is narrower and has a sinuous morphology, embedded in the early-stage channel (Fig. 9). The dimension of the late-stage channel is 1–3 km wide, 56 km long (Fig. 9), and vary in depth from 41 to 103 m (Fig. 10).

4.2.3. Morphometric analysis of the submarine channel

There is a significant morphological variation along the submarine channel system (Figs. 9 and 10). In the northeastern portion, near the sediment source area, the channel morphology varies considerably with smaller width and depth when compared to the southwestern portion where the channel is characterized by significantly greater width and depth (Fig. 10).

The depth profile of the early channel thalweg shows an exponential trend and can be divided into three intervals (1, 2 and 3) that correspond to three segments (x, y, and z) based on the channel gradient variations (Fig. 11a; Table 2). The gradient for the early-stage channel is 2.64° in the first segment, and decreases to 2.02° in the mid segment y, which spans between 12 km and 33 km along channel axis (Fig. 11a). In the rest of the channel, segment z, the channel slope decreases dramatically, and reaches its lowest value of 0.40° (Fig. 11a).

The channel width also displays three intervals. It varies between 3224 m and 4677 m for the early-stage channel to 1094 m and 2865 m for the late-stage channel in the first 12 km interval (Fig. 11b; Table 2). In interval 2, channel width increased to a maximum value of 5573 m at 17 km for the early channel to 3802 m at 18 km for the late-stage channel. This increasing trend is followed by a decrease in the width of the late channel to its lowest value of 2993 m at 27 km. In the interval 2, between 27 and 32 km the channel shows an increase in width with slight variation. In interval 3, between 33 and 44 km, the width of the early-stage channel varies from 3830 m to 4260 m. The width of this late-stage channel has a decreasing trend and varies between 3300 m and 1115 m (Fig. 11b).

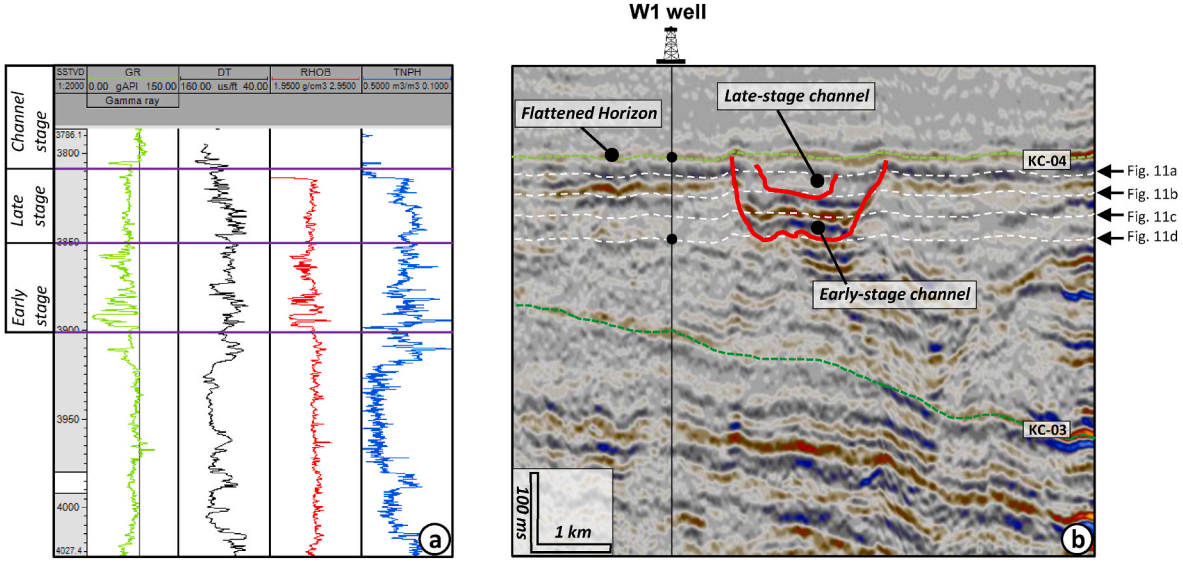

Fig. 8. Characteristic of study unit from the well-seismic calibration, a) Wireline logs (gamma ray (GR), neutron, density, and resistivity) for well W1 through the submarine channel system. b) submarine channel time slices showing two incision stages and flattened horizon KC-04.

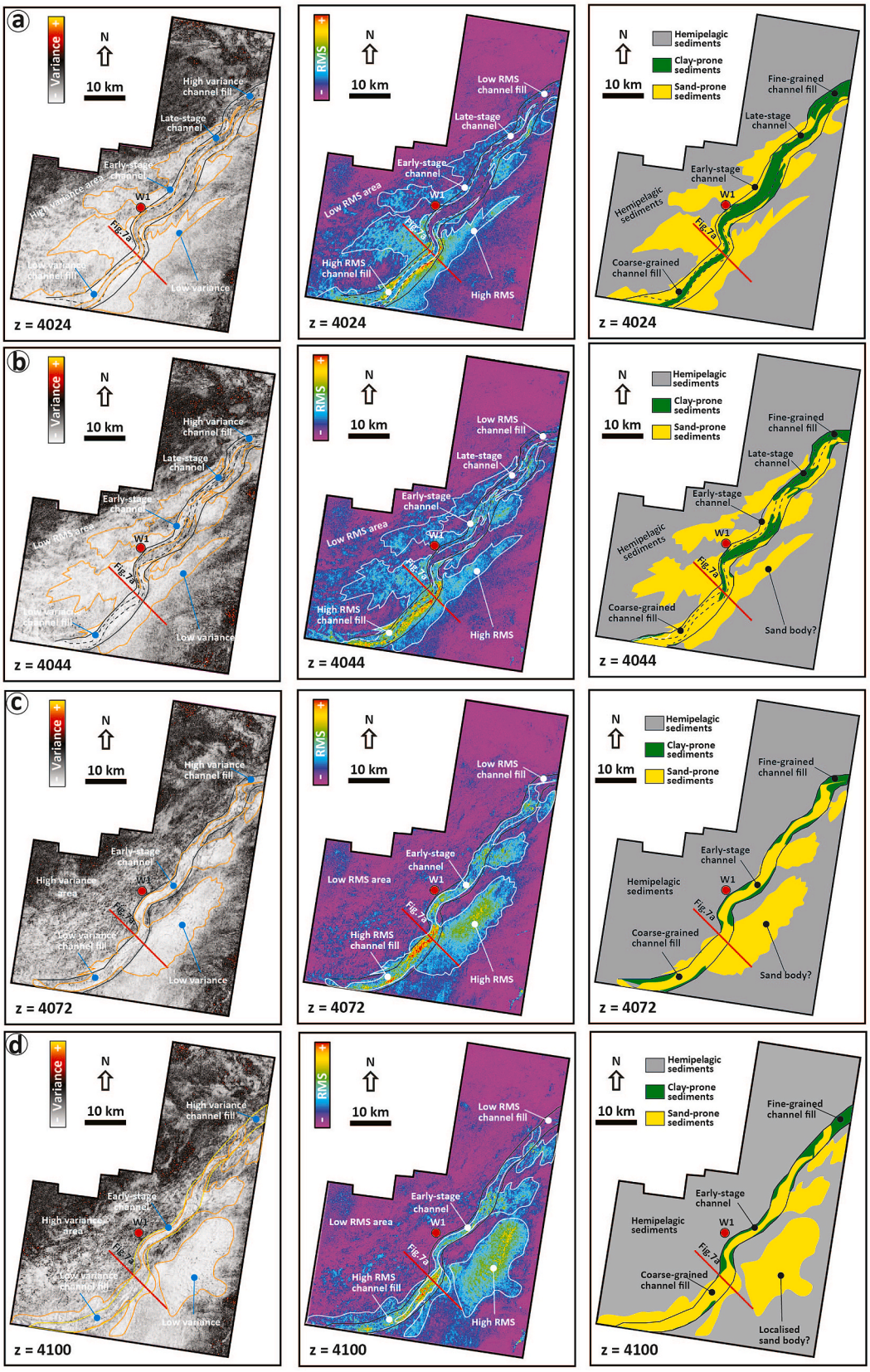

Fig. 9. Variance and RMS seismic attributes and their interpretations, of the various slices within the early and late-stage channel (see Fig. 7a). The seismic attributes analysis shows the distribution of several types of sediments deposited during the evolution of the submarine channel system. The late-stage channel is narrower and is more sinuous.

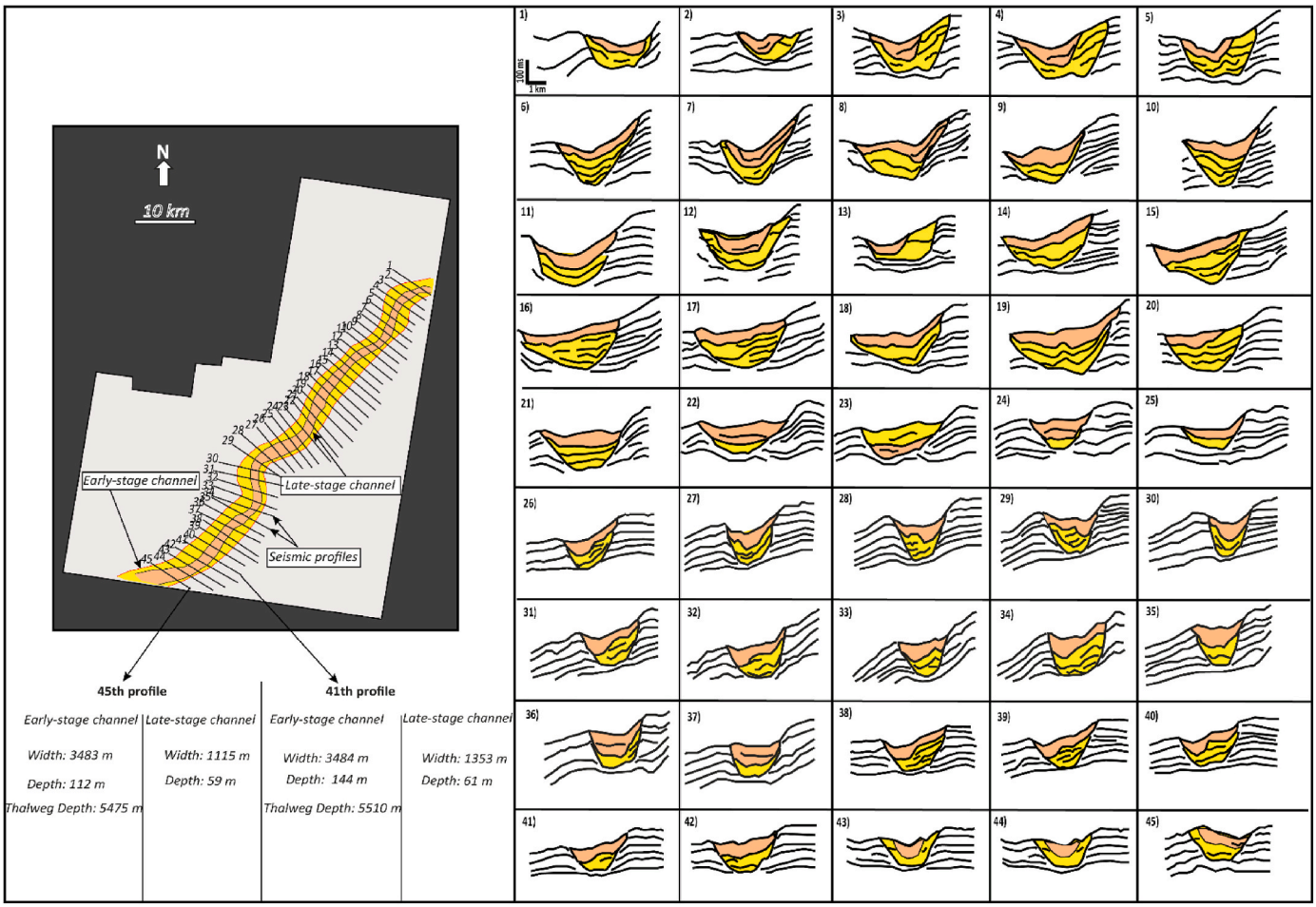

Fig. 10. Series of line drawings of seismic profiles oriented perpendicular to the trend of the submarine channel system (every other profile shown, from 1 km spaced profiles). Notice the variation in the geometry and infill of the channel system along the slope.

The depth profile of the early-stage channel thalweg also shows remarkable variation along the channel path (Fig. 11a), correlating with the variation in the depths of the early channel (Fig. 11c). A plot of channel thalweg versus along channel distance also revealed three intervals (Fig. 11a and c; Table 2). The first interval (0–12 km) begins with the lowest value of channel depth to the northeast of the seismic survey (Fig. 11c), followed by an increase to 170 m at 9 km in the early channel (Fig. 11c). The depth of the early-stage channel in this interval ranges from 89 m to 171 m. In interval 2, between 12 and 33 km, the channel depth begins with an increase from 109 m at 12 km to 179 m at 15 km (Fig. 11c). Then, the channel depth decreases to its minimum value of 87 m at 24 km, before fluctuating with a general increase from 153 m to 183 m for the rest of the interval (Fig. 11c). The third interval (33–44 km) has the highest value of early channel depth, 197 m at 35 km (Fig. 11c). In this interval, the depth of the early-stage channel begins with an increase followed by a decreasing trend after reaching its maximum depth. The depth fluctuates between 112 m and 197 m.

The width/depth ratio of the early-stage channel varies from 18 to 54 (Fig. 11d; Table 2) in the three intervals along the channel. The first interval begins with a decrease in the ratio and fluctuates along the rest of the interval between 27 and 42 for the early-stage channel (Fig. 11d). The ratio fluctuates within interval 2 (13 and 33 km), reaching its maximum value from 51 to 24 km before decreasing to its minimum value from 17 to 25 km in the early-stage channel. Between 33 and 44 km, the width/depth ratio in interval 3 shows an increasing trend to the northeast of the study area, where it reaches 43 (Fig. 11d).

With respect to the late-stage channel, the channel depth in the first interval varies from 41 m to 79 m. In the second interval, the depth of the late-stage channel starts with a decrease, followed by an increasing trend from 47 m to 97 m at 23 km. The rest of the channel varies between 68 m and 98 m in depth. The depth in the third interval reaches a highest value of 103 m at 35 km (Fig. 11c). The depth profile of the late-stage channel starts with a decrease. The general trend of channel depths is downward in this interval and ranges from 103 m to 59 m. The latter value corresponds to the northeastern edge of the submarine channel in the seismic volume (Figs. 10 and 11c).

The width/depth ratio of the late-stage channel varies from 17 to 51 (Fig. 11d; Table 2) in the three intervals along the channel. The first interval begins with a decrease in the ratio, followed by fluctuations along the remaining segment of the channel between 21 and 42 for the late-stage channel. In interval 2 (13 and 33 km), the late-stage channel reaches a maximum value of 54 at 18 km and a minimum value of 25 at 33 km. Between 33 and 44 km, the ratio shows a decreasing trend towards the northeastern edge, where it reaches a minimum value of 18 (Fig. 11d).

5. Discussion

5.1. Controls on the evolution of the Cretaceous submarine channel system

Submarine channels can be influenced by sea-level change, sediment flux, tectonics, and climate, and have a significant impact on the sedimentary architecture of continental margins (Reading and Richards, 1994; Wu et al., 2018). Several factors can be suggested as the principal controls on the development of the Late Cretaceous submarine channel

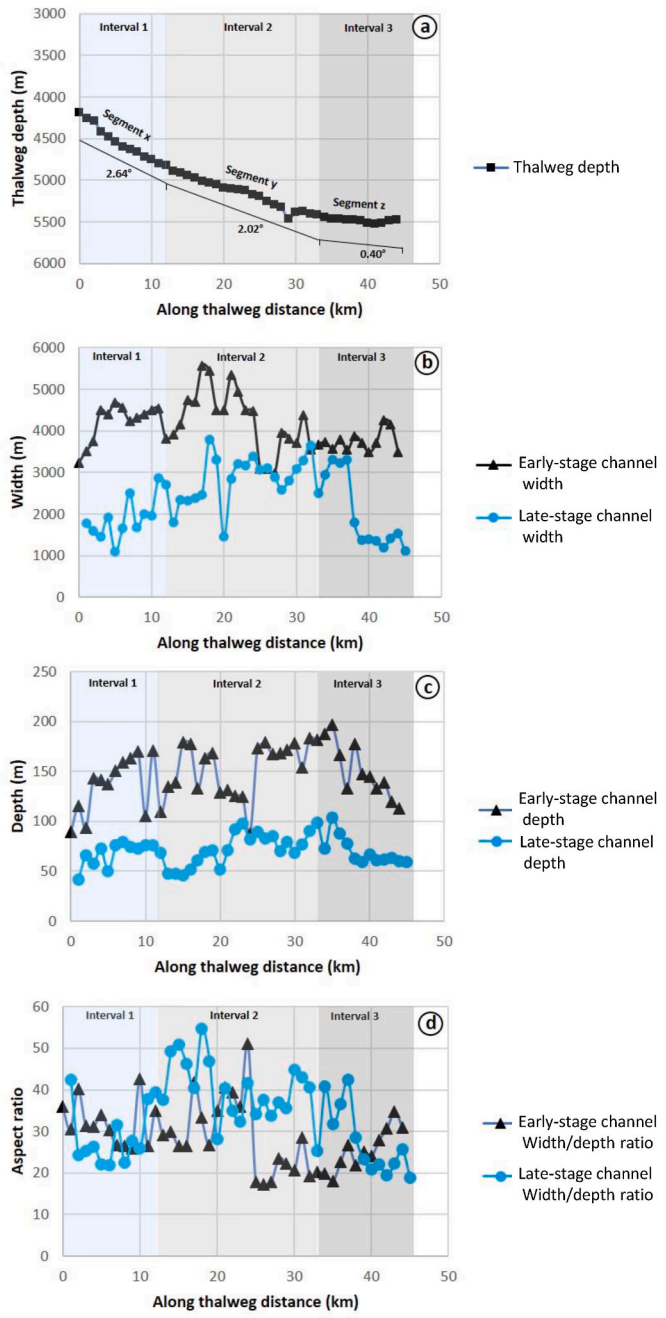

Fig. 11. Quantitative analysis of the submarine channel system. a) Width of early-stage channel and late-stage channel. b) Early-stage channel and late-stage channel depth profile. c) Aspect ratio (width/depth) of the early-stage channel and late-stage channel. d) Depth profile of channel thalweg along the channel.

system within the SU2 in the study area. This encompasses tectonics, relative sea-level fluctuations, fluvial sediment supply, and slope gradient. Here, these factors are examined first in terms of whether and how they might have influenced the evolution of the submarine channel system.

5.1.1. Tectonics

One structural high (Kribi high) was mapped in the study area (Fig. 6). There are highs that are believed to have significant control on the sourcing and distribution of Cretaceous sediments from the onshore to the offshore depocentres. However, these highs have been active during the evolution of the submarine channel system in the Late Cretaceous. The Kribi high lies to the SE of the study area (Fig. 6) and it is a NE-SW trending feature, which has a similar trend to the submarine channel (Le, 2012; SPT/Simon Petroleum and Technology, 1995) (Fig. 9). It comprises a thick Early Cretaceous syn-rift sequence, which is overlain by a Late Cretaceous post-rift sequence (Le, 2012; Loule et al., 2018). Late Cretaceous sediments filled the developing basin, which is bounded by the eroded paleotopographic high to the southeast (Kribi High). Furthermore, the reactivation of some of these structures (e.g., Kribi Campo High, Kribi and Campo Fracture Zones etc.) during the Cretaceous and Tertiary times also affected and promoted the entry and deposition of gravity flow deposits of coarse clastics which represents the primary reservoir targets in the study area (Sterling, 2010; Le, 2012).

Table 2
The result of morphological analysis along the submarine channel system.

Measurements	Intervals		
	Downslope →		
	1 (0–12 km)	2 (12–33 km)	3 (33–44 km)
Channel gradient (°)	2.64	2.02	0.40
Thalweg depth (m)	4188–4820	4820–5463	5417–5522
Early/Late stage Channel width (m)	3224-4677/1094-2865	2879-5573/1452-3802	3483-4260/1115-3300
Early/Late stage Channel depth (m)	89-171/41-79	109-179/45-98	112-197/59-103
Aspect Ratio Early/Late Channel	25-42/21-42	26-51/25-54	18-34/18-42

5.1.2. Relative sea-level fluctuations

It is widely accepted that relative sea-level oscillation can promote the occurrence of submarine channels in deep-water settings (Posamentier, 2001; Posamentier and Kolla, 2003). Seismic based investigations (Posamentier and Kolla, 2003; Niyazi et al., 2018), numerical modellings (Soutter et al., 2021), outcrop analogues (Sprague et al., 2002; Prélat, 2010) and studies focusing on the Pliocene to modern submarine channel systems (Samuel et al., 2003; Chima et al., 2020) showed that lowering sea-level is one of the important mechanisms by which sediments could be transported beyond the shelf break more efficiently, and form turbidity channels even in the distal area of the deep-sea. Although, submarine turbidity channel development during high sea-level were documented in the Congo and Bengal fans, their presence was also linked to increased tectonic activity (Van Weering and Van Iperen, 1984; Weber et al., 1997). In fact, the sea-level fluctuations can act as a switch on the continental shelf, by capturing and storing most of the coarse-grained sediments within the shelf during the period of high sea-level, while by-passing them to the deep basin during sea-level fall and connecting the catchment area to the deep-sea (Posamentier and Kolla, 2003).

An apparent high sea-level can be observed during the late Campanian, which corresponds to the KC-3 horizons (Fig. 2). Interestingly, deep-water fans were documented in this period within SU1 and likely developed due to the rising sea-level (Fig. 5). When the sea-level stands high, the shelf will be submerged and coarse-grained sediments are primarily deposited on the shelf, and only fine-grained materials could be transported to deep waters, forming clay dominated submarine fans (Myers and Milton, 1996; Posamentier and Kolla, 2003; Samuel et al., 2003). As the sediments accumulated in the study area, and sea-level start to drop, coarser materials stored during the previous lowstand (around KC-3) could be transported to deep sea, and those deep-water fans could transit into turbidity channel system (Posamentier and Kolla, 2003; Cross et al., 2009). Due to lower hydraulic pressures and

abundance in coarser grain size sediments, gravity flows during lower sea-level tend to be more erosive and finally could form submarine channels (Catuneanu, 2006). Coincidently, we observed channel incision within SU2 (Figs. 5 and 9), which can be correlated to the lowering sea-level curve of Haq et al. (1987). Since the submarine channels during lowstands are highly erosive and comprise a higher sand proportion (Figs. 8 and 9), it is plausible to suggest that the abundance of coarse-grained sediments available from the shelf and through the fluvial sediment supply during the early stage of sea-level fall, played important role in the formation of the submarine channels. Nevertheless, continuous sea-level drop also could demise the submarine channels, as the coarser materials available on the shelf were consumed by the early-stage channel (Posamentier and Kolla, 2003; Cross et al., 2009). The subsequent channel contains large number of fine-grained materials, and it is no longer as erosive as the early-stage counterpart, since the energy of the turbidity current is directly linked to the sand/mud ratio of the flow (Shanley and McCabe, 1994; Tripsanas et al., 2008). This interpretation also explains the narrower morphology of the late-stage channel comparing to the early-stage channel (Fig. 11).

5.1.3. Fluvial sediment supply

Sediment supply is the material basis for the development of deep-water channel systems (Catuneanu, 2006; Gong et al., 2016). The types and abundance of sediments provided by source area may have had great influence on the formation and characteristics of the deep-water depositional systems in the study area. It is known that following the Santonian tectonic event, a large amount of terrigenous sediment was transported to deep-water basins, forming a widely developed deep-water gravity channel system in the Maastrichtian (SPT/Simon Petroleum and Technology, 1995). During this time, sediment supply from the Sanaga River also played a significant role in the type of infill and the nature of the sediment within the submarine channel systems. Coarse clastic sediments are therefore predicted to have been extensively deposited in the study area, particularly in the vicinity of the Sanaga River (SPT/Simon Petroleum and Technology, 1995). Tracing the conduits that fed the submarine channel system using root-mean-square amplitude slices indicates a transported from the shelf-edge delta systems formed by Sanaga and Nyong Rivers during the depositional stage of the Late Cretaceous (Fig. 9). The infilling of the submarine channel system in this study reflects a deltaic (Sanaga and Nyong) origin of the sediments deposited on the continental shelf

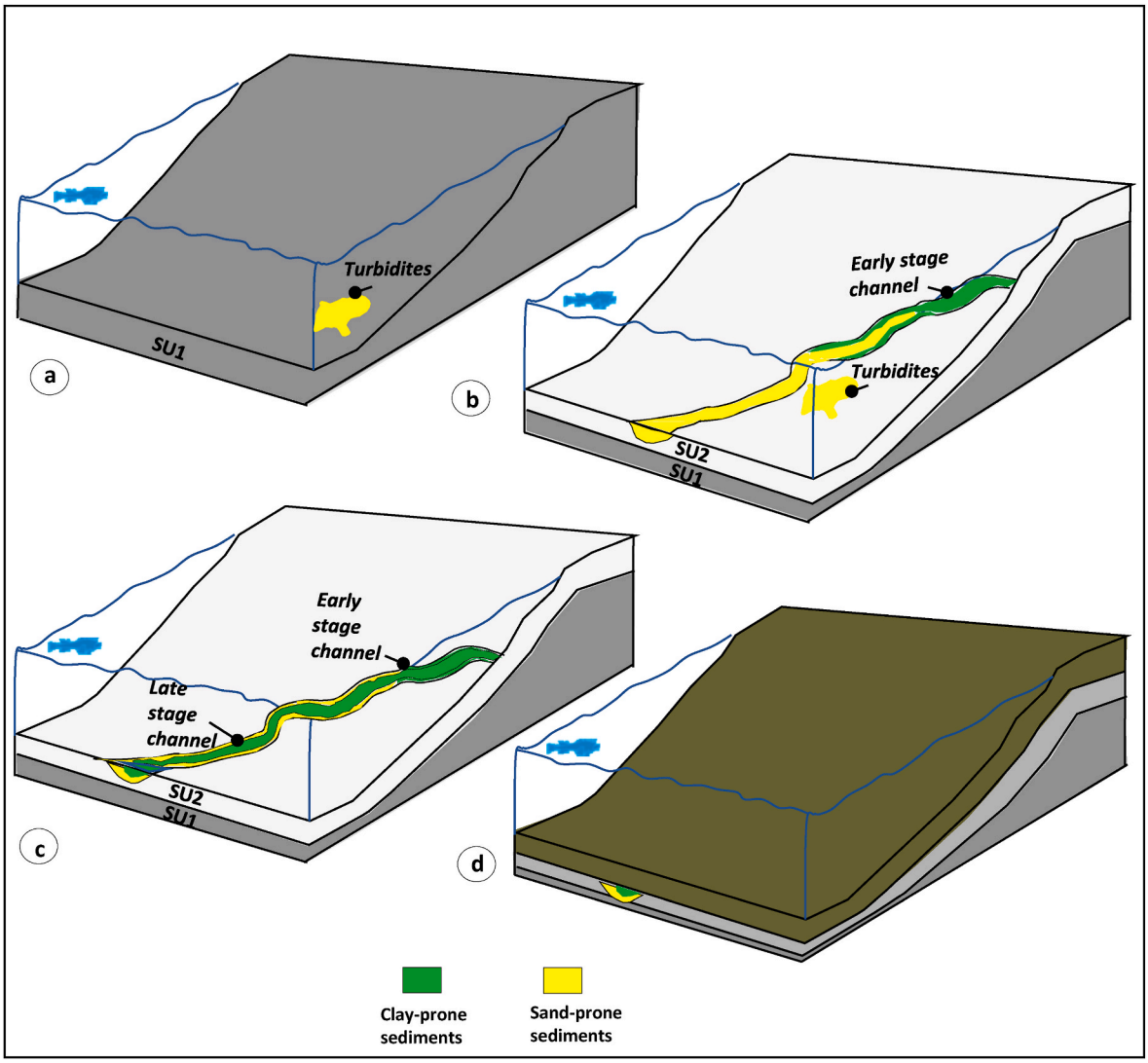

Fig. 12. Diagram of the deposition facies in the study area showing the temporal and spatial evolution of the Late Cretaceous submarine channel. a) Turbidites fan came into being first before the formation of the early-stage of the channel. b) The early-stage channel is characterized by Sand-prone sediments and some Clay-prone sediments. c) The late-stage channel deposit is narrow and is more sinuous characterized by Clay-prone. d) In the final stage, from the Late Cretaceous to the Tertiary, the submarine channel system died out.

margin in the northeast of the study area. The NE-SW trending channels mapped in this study indicate that sediments originate primarily to the northeast (Figs. 9 and 12). This corroborates the interpretation made by Meyers et al. (1996), Iboum Kissaaka et al. (2016), and Yugye et al. (2021).

5.1.4. Paleotopographic gradient

Paleotopographic gradient features appear to have played a key role in controlling the morphology, internal architecture and fills of the submarine channel in the Late Cretaceous (Zhao et al., 2018). The Intervals 1 and 2 were characterized by a strong gradient (2.64° and 2.02°) with a large channel width and shallow depth (Table 2. Fig. 11). However, Interval 3 is characterized by a gentle gradient (0.40°) with a small channel width and large depth. The possible reason for such a difference in morphology over such a short distance could be related to the different palaeotopographic gradients (Fig. 11a). Therefore, the degree of widening is commonly larger than that of deepening with increase in the channel scale. This means that a larger width/depth ratio commonly coincides with a larger-scale channel (Zhao et al., 2018).

The highest amplitudes observed in the map view characterize areas of lower channel gradient, while the lowest amplitude channel amplitude areas are in the upslope to the mid-slope of the channel and characterize the high gradient (Fig. 9). Thus, the amplitude change may reflect a change in lithology from fine to coarse-grained deposits (Sullivan et al., 2000; Morend et al., 2002). In the case of the slope segments x, the low amplitude lithofacies corresponds to fine-grained deposits. On the other hand, when the slope is low (segment z), high amplitude lithofacies indicate deposits of coarse-grained deposits (Figs. 9 and 12). This type of sedimentary submarine channel fill is similar to the indented sedimentary channel fill suggested by Li et al. (2020).

5.2. Evolutionary model for the Late Cretaceous channel system

The local tectonics, sea-level fluctuations, and fluvial sediment supply are likely controls on the occurrence and absence of the submarine channel system in the long term. The paleotopographic gradient is responsible for the morphological evolution of the channel system and the distribution of coarse-grained sediments. The overall formation and development of the studied submarine channel system could be explained by four steps conceptual model (Fig. 12). During the high sea-level at the late Campanian (KC-3), most of the sediments accumulated on the continental shelf and deep-water fans developed at the distal part (Fig. 12a). Following the drop in sea-level, increase of fluvial sediment supply, previously accumulated sediments on the shelf and sourced from the fluvial system were delivered to the deep basin, and formed the Late Cretaceous channel system (Fig. 12b). The differences in the gradient for the topography, on which the channels developed, influenced the distribution of sand-prone sediments. As a result, coarser-grained materials mainly accumulated along the channel at the gentler lower stream (Fig. 12b). Following continuous sea-level fall and the discharge of coarser sediments on the shelf, more fine-grain materials were delivered to the system, decreasing the flow energy, by which only narrower (late-stage) channel could be developed (Fig. 12c). The late-stage channel is also characterized as more mud-prone and less erosive compared to the early-stage channel (Fig. 12c). In the final stage, from the Late Cretaceous to the Tertiary, the study area was submerged by the rapid sea level rise, and then the submarine channel system died out quickly due to the lack of sufficient sediment supply (Fig. 12d).

5.3. Implications for hydrocarbon exploration in deep-water Kribi-Campo sub-basin

Turbidite channel systems are one of the most common types of hydrocarbon reservoirs found along the West Africa margin and elsewhere (Weimer et al., 2000). Therefore, the investigation of these late Cretaceous submarine channels system, have implications for hydrocarbon prospectivity in the deep-water Kribi-Campo sub-basin.

The early-stage channel consists of coarse grain sediments alternating with fine grain sediments rather than being isolated on a basal erosional surface, suggesting multiple barriers and possible thief zones at the base of the channel (Figs. 8 and 9; Mayall et al., 2006). In addition, the late-stage channel is predominantly fine-grained. However, the presence of coarse-grained sediments in the early-stage channel originating from erosive energetic flows may result into good reservoirs in the study area (Loule et al., 2018; Sterling, 2010; Jobe et al., 2011).

Sediment transport models indicate that grain size distribution, as well as slope gradients, are key variables dictating the presence of good reservoir development (McCaffrey and Kneller, 2001; Stevenson et al., 2015). The coarse-grained sediments of the early-stage channel in this study were deposited along the low slope gradients (segment z) and the fine-grained sediments were deposited in the high slope gradients (segment x) (Figs. 9d and 12). As a result, the channel system with gentle gradients and coarse-grained sediments offers the highest potential for hydrocarbon discoveries (McCaffrey and Kneller, 2001; Stevenson et al., 2015).

Another potential application of this study lies in the well-log motif of the submarine channel system where various stages of channel evolution have distinct logs responses (Fig. 8a). The basal coarse-grained lags of the early-stage channel in well W1 show a large kick in GR and display a serrate GR log motif with some blocky/bell-shaped intervals (Well W1 in Fig. 8a). The late-stage channel fills are mainly characterized by a serrate GR motif with some low-amplitude bell-shaped GR intervals (Fig. 8a). The log responses observed in this study is similar to those reported from other slope channel systems (e.g., Fig. 11 of Mayall et al., 2006, Fig. 10 of Li et al., 2021). This suggests that evolutionary stages and associated 2D or 3D reservoir elements of submarine channel systems may be recognized from 1D vertical log patterns or sections.

6. Conclusions

1) Integrated analysis of a high-resolution, 3D seismic reflection dataset and borehole data from the deep-water Kribi-Campo Sub-basin, offshore Cameroon has revealed a submarine channel system that developed during the Late Cretaceous.
2) The submarine channel system recognized in the Late Cretaceous trends approximately NE–SW with a total length of about 56 km and a maximum width and height of 5 km and 197 m respectively within the study area. The submarine channel system is U-shaped and of two parts: (1) the early-stage channel with a linear morphology and: (2) the late-stage channel located within the early channel which is narrower with a sinuous morphology. According to width to depth ratio and variation of erosion bases of the channels, the channel system can be divided into three segments (x, y and z), each of which is characterized by unique internal structure and infilling processes.
3) The development and depositional architecture of the submarine channel system are mainly controlled by the changing interplay of tectonic, sediment supply, relative sea level changes and paleotopographic gradient. The segmentation of the submarine channel system was constrained by paleotopographic gradient of alternating uplifts and depressions. The findings from this study demonstrates that decreasing slope gradient favours coarser-grained deposits primarily along the axis of the channel system, while a strong slope gradient leads to the deposition of fine-grained sediments. The abundant sediments feeding the submarine channel system were transported from the Sanaga and Nyong River source area.
4) Understanding the channel morphology is crucial for facies prediction and efficient development of deep-water channel reservoirs especially as hydrocarbon exploration moves into deeper waters in the study area and elsewhere.

Declaration of competing interest

The authors declare that they have no known competing financial interests or personal relationships that could have appeared to influence the work reported in this paper.

Data availability

The authors do not have permission to share data.

Acknowledgements

The authors are grateful to the National Hydrocarbon Corporation (NHC), Yaoundé (Cameroon) for providing the seismic and well data used in this study for the permission to publish this work. Sam Carmalt at the University of Geneva is thanked for his constructive remarks and revisions that allowed me to improve the grammatical constructions in this manuscript. We are grateful to the associate editor Dr. Damien Do Couto, and two anonymous reviewers, for their helpful suggestions and constructive critiques that have significantly improved this manuscript.

References

Abreu, V., Sullivan, M., Pirmez, C., Mohrig, D., 2003. Lateral accretion packages (LAPs): an important reservoir element in deep water sinuous channels. Mar. Petrol. Geol. 20 (6–8), 631–648.

Ackerman, W.C., Boatwright, D.C., Burwood, B.M., Van Lerberche, D., Bondjo, E., Tamfu, S.F., Ovono, D., 1993. Geochemical analysis of selected hydrocarbon samples in the Douala Basin, Cameroon. Implications for an oil-prone source rock. AAPG Bull. 77 (9), 1604.

Babonneau, N., Savoye, B., Cremer, M., Bez, M., 2010. Sedimentary architecture inmeanders of a submarine channel: detailed study of the present Congo turbidite channel (zaiango project). J. Sediment. Res. 80, 852–866.

Beglinger, S.E., Doust, H., Cloetingh, S., 2012. Relating petroleum system and play development to basin evolution: west African South Atlantic basins. Mar. Petrol. Geol. 30, 1–25. https://doi.org/10.1016/j.marpetgeo.2011.08.008.

Brown, A.R., 2004. Interpretation of Three-Dimensional Seismic Data. American Association of Petroleum Geologists and the Society of Exploration Geophysicists.

Brownfield, M.E., 2016. Assessment of Undiscovered Oil and Gas Resources of the West-Central Coastal Province, West Africa. U.S. Geological Survey, Reston, Virginia, p. 41p.

Brownfield, M.E., Charpentier, R.R., 2006. Geology and Total Petroleum Systems of the West-Central Coastal Province (7203), West Africa: U.S. Geological Survey Bulletin 2207-B, p. 52.

Catterall, V., Redfern, J., Gawthorpe, R., Hansen, D., Thomas, M., 2010. Architectural style and quantification of a submarine channel-levee system located in a structurally complex area: offshore Nile Delta. J. Sediment. Res. 80, 991–1017.

Catuneanu, O., 2006. Principles of Sequence Stratigraphy. Elsevier, Amsterdam.

Chen, H., Lin, C., Zhang, Z., Zhang, D., Li, M., Wu, G., Zhu, Y., Xu, H., Lu, W., Chen, J., 2021. Evolution and controlling factors of the gravity flow deposits in the Miocene sequence stratigraphic framework, the Lower Congo-Congo Fan Basin, West Africa. Petrol. Explor. Dev. 48 (1), 146–158.

Chiang, C.S., Hsiung, K.H., Yu, H.S., Chen, S.C., 2020. Three types of modern submarine canyons on the tectonically active continental margin of shore southwestern Taiwan. Mar. Geophys. Res. 41, 4.

Chima, K.I., Do Couto, D., Leroux, E., Gardin, S., Hoggmasacall, N., Rabineau, M., Granjean, D., Gorini, C., 2019. Seismic stratigraphy and depositional architecture of Neogene intraslope basins, offshore western Niger Delta. Mar. Petrol. Geol. 109, 449–468. https://doi.org/10.1016/j.marpetgeo.2019.06.030.

Chima, K.I., Gorini, C., Rabineau, M., Granjeon, D., Do Couto, D., Leroux, E., Hoggmascall, N., 2020. Pliocene and Pleistocene stratigraphic evolution of the western Niger Delta intraslope basins: a record of glacio-eustatic sea-level and basin tectonic forcings. Global Planet. Change 195 (103355), 1–23. https://doi.org/10.1016/j.gloplacha.2020.103355.

Covault, J.A., Kostic, S., Paull, C.K., Ryan, H.F., Fildani, A., 2014. Submarine channel initiation, filling and maintenance from seafloor geomorphology and morphodynamic modelling of cyclic steps. Sedimentology 61, 1031–1054.

Covault, J.A., Sylvester, Z., Hudec, M.R., Ceyhan, C., Dunlap, D., 2019. Submarine channels 'swept' downstream after bend cutoff in salt basins. Depositional Rec. 6, 259–272.

Cross, N.E., Cunningham, A., Cook, R.J., Taha, A., 2009. Three-dimensional Seismic Geomorphology of a Deep-Water Slope-Channel System: the Sequoia Field, Offshore West Nile Delta, Egypt. AAPG.

Dailly, P., Lowry, P., Goh, Gene, M., 2002. Exploration and Development of Ceiba Field, Rio Muni Basin, Southern Equatorial Guinea. The leading edge, November, pp. 1140–1146.

Deptuck, M.E., Steffens, G.S., Barton, M., Pirmez, C., 2003. Architecture and evolution of upper fan channel-belts on the Niger Delta slope and in the Arabian Sea. Mar. Pet. Geol. 20, 649–676.

Deptuck, M.E., Sylvester, Z., Pirmez, C., O'Byrne, C., 2007. Migration–aggradation history and 3-D seismic geomorphology of submarine channels in the Pleistocene Benin major Canyon, western Niger Delta slope. Mar. Petrol. Geol. 24, 406–433.

Deptuck, M.E., Sylvester, Z., O'Byrne, C., 2012. Pleistocene seascape evolution above a"simple" stepped slope–Western Niger Delta. In: Prather, B.E., Deptuck, M.E., Mohrig, D., Van Hoorn, B., Wynn, R.B. (Eds.), Application of the Principles of Seismic Geomorphology to Continental-slope and Base-Of-Slope Systems: Case Studies from Seafloor and Near-Seafloor Analogues, vol. 99. SEPM Society for Sedimentary Geology, pp. 199–222. https://doi.org/10.2110/pec.12.99.

Di Celma, C., Cantalamessa, G., Didaskalou, P., Lori, P., 2010. Sedimentology, architecture, and sequence stratigraphy of coarse-grained, submarine canyon fills from the Pleistocene (Gelasian-Calabrian) of the Peri-Adriatic basin, central Italy. Mar. Pet.Geol. 27, 1340–1365.

Gamboa, D., Alves, T.M., 2015. Spatial and dimensional relationships of submarine slope architectural elements: a seismic-scale analysis from the Espírito Santo Basin (SEBrazil). Mar. Petrol. Geol. 64, 43–57.

Gamboa, D., Alves, T.M., Cartwright, J., 2012. A submarine channel confluence classification for topographically confined slopes. Mar. Petrol. Geol. 35, 176–189.

Gee, M.J.R., Uy, H.S., Warren, J., Morley, C.K., Lambiase, J.J., 2007. The Brunei slide: agiant submarine landslide on the Northwest Borneo Margin revealed by 3D seismic data. Mar. Geol. 246, 9–23.

Gong, C.L., Steel, R.J., Wang, Y.M., et al., 2016. Shelf-margin architecture variability and its role in sediment-budget partitioning into deep-water areas. Earth Sci. Rev. 154, 2–101.

Hansen, L., Janocko, M., Kane, I., Kneller, B., 2017. Submarine channel evolution, terrace development, and preservation of intra-channel thin-bedded turbidites: Mahin and Avon channels, offshore Nigeria. Mar. Geol. 383, 146–167.

Haq, B.U., Hardenbol, J., Vail, P.R., 1987. Chronology of fluctuating sea levels since the triassic. Science 235, 1156–1167.

Harishidayat, D., Omosanya, K.O., Johansen, S.E., Eruteya, O.E., Niyazi, Y., 2018. Morphometric analysis of sediment conduits on a bathymetric high: implications for palaeoenvironment and hydrocarbon prospectivity. Basin Res. 30, 1015–1041. https://doi.org/10.1111/bre.12291.

Helm, C., 2009. Quantification des flux sédimentaires anciens à l'échelle d'un continent: le cas de l'Afrique au Méso-cénozoïque, vol. 1. Thesis. Univ. Rennes, p. 299.

Huang, Y., 2018. Sedimentary characteristics of turbidite fan and its implication for hydrocarbon exploration in Lower Congo Basin. Petrol. Res. 3, 189–196.

Iboum Kissaaka, J.B., Ntamak-Nida, M.J., Mvondo, F., Fowe Kwetche, P.G., Djomeni Nitcheu, A.L., Abolo, G.M., 2016. Postrift depositional evolution and sequence stratigraphy from offshore subsurface data of the Kribi-Campo sub basin (Cameroon, West African margin). Soc. Explor. Geophys. Am. Assoc. Petrol. Geol. 13, 79–101. https://doi.org/10.1190/INT-2015-0073.1.

Janocko, M., Nemec, W., Henriksen, S., Warchoł, M., 2013. The diversity of deep-watersinuous channel belts and slope valley-fill complexes. Mar. Petrol. Geol. 41, 7–34.

Jobe, Z.R., Lowe, D.R., Uchytil, S.J., 2011. Two fundamentally different types of submarine canyons along the continental margin of Equatorial Guinea. Mar. Petrol. Geol. 28 (3), 843–860.

Jobe, Z.R., Sylvester, Z., Parker, A.O., Howes, N., Slowey, N., Pirmez, C., 2015. Rapid adjustment of submarine channel architecture to changes in sediment supply. J. Sediment. Res. 85, 729–753. https://doi.org/10.2110/jsr.2015.30.

Jolly, B.A., Lonergan, L., Whittaker, A.C., 2015. Growth history of fault-related folds and interaction with seabed channels in the toe-thrust region of the deep-water Niger Delta. Mar. Petrol. Geol. 70, 58–76.

Kane, I.A., Mc Caffrey, W.D., Peakall, J., 2008. Controls on sinuosity evolution within submarine channels. Geology 36 (4), 287–290.

Kolla, V., Posamentier, H.W., Wood, L.J., 2007. Deep-water and fluvial sinuous channels characteristics, similarities and dissimilarities, and modes of formation. Mar. Petrol. Geol. 24, 388–405.

Lawrence, R.S., Munday, S., Bray, R., 2002. Regional Geology and Geophysics of the Eastern Gulf of Guinea (Niger Delta). The leading Edge, pp. 1112–1117.

Le, A.N., 2012. Stratigraphic evolution and plumbing system in the Cameroon margin, West Africa. In: Thesis for the Degree of Doctor of Philosophy. Faculty of Engineering and Physical Science, University of Manchester.

Le, A.N., 2021. Striations at the base of the paleo-fan and channel revealed by 3D seismic data, offshore Cameroon. Indones. J. Geosci. 8, 101–107.

Le, A.N., Huuse, M., Redfern, J., Gawthorpe, R.L., Irving, D., 2014. Seismic characterization of a Bottom Simulating Reflection (BSR) and plumbing system of the Cameroon margin, offshore West Africa. Mar. Petrol. Geol. 68, 629–647.

Li, S., Gong, C., 2016. Flow dynamics and sedimentation of lateral accretion packages insinuous deep-water channels: a 3D seismic case study from the northwestern South China Sea margin. J. Asian Earth Sci. 124, 233–246.

Li, P., Kneller, B., Hansen, L., 2021. Anatomy of a gas-bearing submarine channel-lobe system on a topographically complex slope (offshore Nile Delta, Egypt). Mar. Geol. 437, 106496 https://doi.org/10.1016/j.margeo.2021.106496.

Li, Q., Wu, W., Liang, J., Kang, H., Liu, W., Wang, G., Cai, L., 2020. Deep-water channels in the lower Congo basin: evolution of the geomorphology and depositional environment during the Miocene. Mar. Petrol. Geol. 115, 104260 https://doi.org/10.1016/j.marpetgeo.2020.104260.

Loule, J.P., Jifon, F., Angoua Biouele, S.E., Nguema, P., Spofforth, D., Carruthers, D., Watkins, C., Johnston, J., 2018. An opportunity to re-evaluate the petroleum potential of the Douala/Kribi-Campo Basin, Cameroon. Spec. Top.: Petrol. Geol. 36, 61–70. First break.

Marsset, T., Droz, L., Dennielou, B., Pichon, E., 2009. Cycles in the architecture of the Quaternary Zaïre turbidite system: a possible link with climate. In: Kneller, B.,

Martinsen, O.J., McCaffrey, B. (Eds.), Extern. Controls Deep-Water Depositional Systems, vol. 92. SEPM, Special Publication, pp. 89–106.
Mayall, M., Jones, E., Casey, M., 2006. Turbidite reservoirs-key elements in facies prediction and effective development. Mar. Petrol. Geol. 23, 821–841.
McCaffrey, W., Kneller, B., 2001. Process controls on the development of stratigraphic trap potential on the margins of confined turbidite systems and aids to reservoir evaluation. AAPG Bull. 85 (6), 971–988.
McHargue, T., Pyrcz, M.J., Sullivan, M.D., Clark, J.D., Fildani, A., Romans, B.W., Covault, J.A., Levy, M., Posamentier, H.W., Drinkwater, N.J., 2011. Architecture of turbidite channel systems on the continental slope: patterns and predictions. Mar. Petrol. Geol. 28 (3), 728–743.
Meyers, J.B., Rosendhal, B.R., Groschel-Becker, H., Austin, J.J.A., Rona, P.A., 1996. Deep penetrating MCS imaging of the rift-to-drift transition, offshore Douala and north Gabon basins, West Africa. Mar. Petrol. Geol. 13, 791–835. https://doi:10.1016/0264-8172 (96)00030-X.
Mienlam Essi, M.F., Yene Atangana, J.Q., Abate Essi, J.M., Mbida, Yem, Angoua Biouele, S.E., Nguema, P., Tsimi Ntsengue, C., 2021. Stratigraphical nature of the Top Albian surface, from seismic and wells data analyses, in the south Sanaga area (Cameroon Atlantic margin): palaeogeographical significance and petroleum implications. Mar. Petrol. Geol. 129, 105073 https://doi.org/10.1016/j.marpetgeo.2021.105073.
Mitchell, W.H., Whittaker, A.C., Mayall, M., Lonergan, L., 2021. New models for submarine channel deposits on structurally complex slopes: examples from the Niger delta system. Mar. Petrol. Geol. 129, 105040 https://doi.org/10.1016/j.marpetgeo.2021.105040.
Mitchum Jr., Vail, P.R., Sangree, J.B., 1977. Seismic stratigraphy and global changes of sea level: part 6. In: Stratigraphic Interpretation of Seismic Reflection Patterns in Depositional Sequences: Section 2. Application of Seismic Reflection Configuration to Stratigraphic Interpretation.
Morend, D., Pugin, A., Gorin, G.E., 2002. High-resolution seismic imaging of outcrop-scale channels and an incised-valley system within the fluvial-dominated Lower Freshwater Molasse (Aquitanian, western Swiss Molasse Basin). Sediment. Geol. 149, 245–264.
Mvondo, O.F., 2010. Surrection cénozoïque l'Ouest de l'Afrique à partir de deux exemples : le plateau sud-namibien et la marge nord camerounaise. Thèse de Doctorat, Université de Rennes, p. 324.
Myers, K.J., Milton, N.J., 1996. Concepts and principles of sequence stratigraphy. In: Sequence Stratigraphy. Blackwell Publishing Ltd., pp. 9–41. https://doi.org/10.1002/9781444313710.ch2
Ndonwie Mahbou, E., 2007. Petrophysical Characterization of Petroleum Reservoirs and Source Beds of the Batanga Sub-block, Kribi-Campo Sub-basin, Cameroon. AAPG Annual Convention, Abstract, p. 1p.
Ngo, E.N.J., Ntamak-Nida, M.J., Bisso, D., Mvondo Owono, F., Ngos III, S., Bilong, P., Njandjock Nouck, P., 2018. Depocenters repartition and sequence stratigraphy of the northern part of the Kribi-Campo Sub-basin (Cameroon). Eur. J. Sci. Res. 149, 258–278.
Nguene, F.R., Tamfu, S., Loule, J., Ngassa, C., 1992. Palaeoenvironments of the Douala and Kribi/Campo sub-basins, in Cameroon, West Africa. In: Curnelle, R. (Ed.), Géologie Africaine, 1er Colloque de Stratigraphie et de Paléogéographie des Bassins Sédimentaires Ouest-Africains, 2e Colloque Africain de Micropaléontologie, Libreville, Gabon, 1991, Recueil des Communications: Boussens, pp. 129–139. Elf Aquitaine.
Niyazi, Y., Eruteya, O.E., Omosanya, K.O., Harishidayat, D., Johansen, S.E., Waldmann, N., 2018. Seismic geomorphology of submarine channel-belt complexes in the Pliocene of the Levant basin. Offshore Central Israel. Mar. Geol. 403, 123–128.
Niyazi, Y., Eruteya, O.E., Warne, M., Lerodiaconou, D., 2021. Discovery of large-scale buried volcanoes within the Cenozoic succession of the Prawn Platform, offshore Otway Basin, southeastern Australia. Mar. Petrol. Geol. 123, 104747 https://doi.org/10.1016/j.marpetgeo.2020.104747.
Niyazi, Yakufu, Warne, Mark, Ierodiaconou, Danie, 2020. Hectometer-scale, shallow buried honeycomb-like structures on the continental shelf of the Otway Basin, southeastern Australia. Interpretation 8 (4), SR65–SR81. https://doi.org/10.1190/INT-2020-0039.1.
Normark, W.R., Carlson, P.R., 2003. Giant submarine canyons: is size any clue to their importance in the rock record? Geol. Soc. Am. Spec. Pap. 370, 175–190.
Ntamak-Nida, M.J., Baudin, F., Schnyder, J., Makong, J.C., Komguem, P.B., Abolo, G.M., 2008. Depositional environments and characterisation of the organic matter of thelower mundeck formation (Barremian?-Aptian) of the kribi-campo sub-basin (south Cameroon): implications for petroleum exploration. J. Afr. Earth Sci. 51, 207–219. https://doi.org/10.1016/j.jafrearsci.2008.01.006.
Ntamak-Nida, M.J., Bourquin, S., Makong, J.C., Baudin, F., Mpesse, J.E., Ngouem, C.I., Komguem, P.B., Abolo, G.M., 2010. Sedimentology and sequence stratigraphy from outcrops of the Kribi-Campo Sub-basin: lower Mundeck formation (lower Cretaceous, southern Cameroon). J. Afr. Earth Sci. 58, 1–18. https://doi.org/10.1016/j.jafrearsci.2010.01.004.
Omosanya, K.O., Alves, T.M., 2013. A 3-dimensional seismic method to assess the provenance of Mass-Transport Deposits (MTDs) on salt-rich continental slopes (EspíritoSanto Basin, SE Brazil). Mar. Petrol. Geol. 44, 223–239. https://doi.org/10.1016/j. marpetgeo.2013.02.006.
Pauken, R.J., 1992. Sanaga Sud field, offshore Cameroon, West Africa. In: Halbouty, M.T. (Ed.), Giant Oil and Gas Fields of the Decade 1978–1988, vol. 54. AAPG Bull, pp. 217–230.
Pauken, R.J., Thompson, J.M., Schuman, J.R., Cooke, J.C., 1991. Geology of the Douala basin, offshore Cameroon. AAPG Bull. 75 (3), 651–652.
Peakall, J., Sumner, E.J., 2015. Submarine channel flow processes and deposits: a process-product perspective. Geomorphology 244, 95–120. https://doi.org/10.1016/j.geomorph.2015.03.005.
Picot, M., Droz, L., Marsset, T., Dennielou, B., Bez, M., 2016. Controls on turbidite sedimentation: insights from a quantitative approach of submarine channel and lobe architecture (Late Quaternary Congo Fan). Mar. Petrol. Geol. 72, 423–446.
Posamentier, H.W., 2001. Lowstand alluvial bypass systems: incised vs. unincised. AAPG Bull. 85, 1771–1793.
Posamentier, H.W., Kolla, V., 2003. Seismic geomorphology and stratigraphy of depositional elements in deep-water settings. J. Sediment. Res. 73, 367–388. https://doi.org/10.1306/111302730367.
Posamentier, H., Walker, R.G., 2006. Deep-water turbidites and submarine fans. In: Facies Models Revisited, vol. 84. SEPM Special Publication, pp. 397–520.
Prélat, A., 2010. Evolution, Architecture and Hierarchy of Distributary Deep-Water Deposits: A High-Resolution Outcrop Investigation of Submarine Lobe Deposits from the Permian Karoo Basin. Thesis Ph.D, South Africa.
Qin, Y., Alves, T.M., Constantine, J., Gamboa, D., 2016. Quantitative seismicgeomorphology of a submarine channel system in SE Brazil (Espírito Santo Basin):Scale comparison with other submarine channel systems. Mar. Petrol. Geol. 78, 455–473.
Rabinowitz, P., LaBrecque, J., 1979. The Mesozoic South Atlantic Ocean and evolution of its continental margins. J. Geophys. Res. 84 (B11), 5973–6002.
Reading, H.G., Richards, M., 1994. Turbidite systems in deep-water basin margins classifed by grain size and feeder system. Am. Assoc. Petrol. Geol. Bullet. 78, 792–822.
Robertson, C.G.G., 2015. Petroleum Geological Evaluation: Niger Delta to the Congo Fan. CGG Robertson Multiclient. Report No. AM086.
Samuel, A., Kneller, B., Raslan, S., Sharp, A., Parsons, C., 2003. Prolific deep-marine slope channels of the Nile Delta, Egypt. AAPG Bull. 87, 541–560.
Seiglie, G.A., Baker, M.B., 1984. Relative sea-level changes during the Middle and Late Cretaceous from Zaire to Cameroon (Central West Africa). AAPG Spec. Vol. A166, 81–88.
Shanley, K.W., McCabe, P.J., 1994. Perspectives on the sequence stratigraphy of continental strata. AAPG Bull. 78, 544–568.
Shanmugam, G., 2006. Deep-water Processes and Facies Models: Implications Forsandstone Petroleum Reservoirs, vol. 5. Elsevier.
Shepard, F.P., 1981. Submarine canyons: multiple causes and long-time persistence. AAPG (Am. Assoc. Pet. Geol.) Bull. 65 (6), 1062–1077.
Soutter, E., Kane, I., Hodgson, D.M., Flint, S.S., 2021. Controls on Submarine Canyon Connection to the Shoreline: a Numerical Modelling Approach.
Sprague, A.R., Sullivan, M.D., Campion, K.M., Jensen, G.N., Goulding, F.J., Garfield, T. R., Sickafoose, D.K., Rossen, C., Jennette, D.C., Beaubouef, R.T., Others, 2002. The Physical Stratigraphy of Deep-Water Strata: A Hierarchical Approach to the Analysis of Genetically-Related Stratigraphic Elements for Improved Reservoir Prediction, pp. A167–A168.
SPT/Simon Petroleum and Technology, 1995. Petroleum Geology and Hydrocarbon Potential of Douala basin, Cameroon. (Unpubl. Non-exclusive report).
Sterling Cameroon Limited., 2010. Prospectivity review of the Ntem block (PH-78) in the Douala/Kribi-Campo Basin. (Unpubl. Non-exclusive report).
Stevenson, C.J., Jackson, C.A.-L., Hodgson, D.M., Hubbard, S.M., Eggenhuisen, J.T., 2015. Deep-water sediment bypass. J. Sediment. Res. 85 (9), 1058–1081.
Stow, D.A.V., Mayall, M., 2000. Deep-water sedimentary systems: new models for the21st century. Mar. Petrol. Geol. 17 (2), 125–135.
Su, M., Hsiung, K.H., Zhang, C.M., Xie, X.N., Yu, H.S., Wang, Z.F., 2015. The linkage between longitudinal sediment routing systems and basin types in the northern South China Sea in perspective of source-to-sink. J. Asian Earth Sci. 111, 1–13.
Sullivan, M.D., Jensen, G.N., Goulding, F.J., Jennette, D.C., Foreman, J.L., Stern, D., 2000. Architectural analysis of deep-water outcrops: implications for exploration and production of the Diana Sub-basin, western Gulf of Mexico. In: Weimer, P., Slatt, R.M., Coleman, J., Rosen, N.C., Nelson, H., Bouma, A.H., Styzen, M.J., Lawrence, D.T. (Eds.), Deep-Water Reservoirs of the World. Gulf Coast Section SEPM 20th Bob F. Perkins Research Conference, pp. 1010–1032.
Sylvester, Z., Covault, J.A., 2016. Development of cutoff-related knick points during early evolution of submarine channels. Geology 44, 835–838.
Sylvester, Z., Pirmez, C., Cantelli, A., 2011. A model of submarine channel-levee evolution based on channel trajectories: implications for stratigraphic architecture. Mar. Petrol. Geol. 28, 716–727.
Tamfu, S.F., Batupe, M., Pauken, R.J., Boatwright, D.C., 1995. Geological setting, stratigraphy and hydrocarbon habitat of the Douala Basin, Cameroon. AAPG Bull. 79 (13), 95.
Taner, M.T., 2001. Seismic attributes. CSEG Rec. 26, 48–56.
Tek, D.E., Mcarthur, A.D., Poyatos-Moré, M., Colombera, L., Patacci, M., craven, B., Mccaffrey, W.D., 2021. Relating seafloor geomorphology to subsurface architecture: how mass transport deposits and knick point-zones build the stratigraphy of the deep-water Hikurangi Channel. Sedimentology. https://doi.org/10.1111/SED.12890.
Tripsanas, E.K., Piper, D.J.W., Campbell, D.C., 2008. Evolution and depositional structure of earthquake-induced mass movements and gravity flows: southwest Orphan Basin, Labrador Sea. Mar. Petrol. Geol. 25, 645–662. https://doi.org/10.1016/j.marpetgeo.2007.08.002.
Twichell, D., Nelson, C.H., Kenyon, N., Schwab, W., 2009. The Influence of External Processes on the Holocene Evolution of the Mississippi Fan. External Controls on Deepwater Depositional Systems, vol. 92. Society for Sedimentary Geology Special Publication, pp. 145–157.

Van Weering, T.C.E., Van Iperen, J., 1984. Fine-grained sediments of the Zaire deepsea fan, southern Atlantic Ocean. Geol. Soc. Lond. Spec. Publ. 15, 95e113. https://doi.org/10.1144/GSL.SP.1984.015.01.06.

Weber, M.E., Wiedicke, M.H., Kudrass, H.R., Hübscher, C., Erlenkeuser, H., 1997. Active growth of the Bengal Fan during sea-level rise and highstand. Geology 25, 315–318.

Weimer, P., Slatt, R.M., Coleman, J., Rosen, N.C., Nelson, H., Bouma, A.H., Styzen, M.J., Lawrence, D.T. (Eds.), 2000. Deep-water Reservoirs of the World. Gulf CoastSection SEPM 20th Bob F. Perkins Research Conference.

Weimer, P., Slatt, R.M., Bouroullec, R., 2007. Introduction to the Petroleum Geology of Deep-Water Settings. AAPG/Datapages Tulsa.

Wornardt Jr., W.W., Jory, P., Batupe, M., 1999. Seismic Sequence Stratigraphic Analysis of the Douala Basin, Cameroon. Offshore Technology Conference, Houston, Texas, 1999.

Wu, W., Li, Q., Yu, J., et al., 2018. The central canyon depositional patterns and filling process in east of Lingshui depression, Qiongdongnan basin, northern south China Sea. Geol. J. 53, 3064–3081.

Wynn, R.B., Cronin, B.T., Peakall, J., 2007. Sinuous deep-water channels: genesis, geometry and architecture. Mar. Petrol. Geol. 24 (6–9), 341–387. https://doi.org/10.1016/j.marpetgeo.2007.06.001.

Yugye, J.A., Ngos III, S., Angoua Biouele, S.E., Nkoa Nkoa, P.E., 2021. Seismic stratigraphic interpretation and modeling of offshore synrift and postrift Cretaceous sequences in the Kribi-Campo sub-basin, southern Cameroon. AAPG (Am. Assoc. Pet. Geol.) Bull. 105 (11), 1–20. https://doi.org/10.1306/06092118040.

Zeng, H.L., Ambrose, W.A., 2001. Seismic sedimentology and regional depositional systems in Miocene Norte, lake Maracibo, Venezuela. Lead. Edge 20 (11), 1260–1269.

Zeng, H.L., Backus, M.M., Barrow, K.T., Tyler, N., 1998a. Stratal slicing, part I: realistic 3-D seismic model. Geophysics 63 (2), 502–513.

Zhao, X.M., Qi, K., Liu, L., Xie, T., Li, M.H., Hu, G.Y., 2018. Quantitative characterization and controlling factor analysis of the morphology of bukuma-minor channel on Southern Niger Delta slope. Interpretation 6, 57–69. https://doi.org/10.1190/INT-2017-0147.1.